UNIVERSITEIT VAN PRETORIA
UNIVERSITY OF PRETORIA
YUNIBESITHI YA PRETORIA

MODELLING OF ETHEKWINI HEAT ISLANDS UNDER CLIMATE CHANGE

by

Thizwilondi Robert Maisha

Submitted in partial fulfilment of the requirements for the degree

Philosophy Doctor in Meteorology

In the Faculty of Natural & Agricultural Sciences,

Department of Geography, Geo-Informatics and Meteorology,

Pretoria

July 2025

UNIVERSITEIT VAN PRETORIA
UNIVERSITY OF PRETORIA
YUNIBESITHI YA PRETORIA

DECLARATION OF ORIGINALITY

I, Thizwilondi Robert Maisha declare that the thesis, which I hereby submit for the degree Philosophy Doctor in Meteorology at the University of Pretoria, is my own work and has not previously been submitted by me for a degree at this or any other tertiary institution.

Signature _____

Date _____14 July 2025

UNIVERSITEIT VAN PRETORIA
UNIVERSITY OF PRETORIA
YUNIBESITHI YA PRETORIA

MODELLING OF ETHEKWINI HEAT ISLANDS UNDER CLIMATE CHANGE

Student: Thizwilondi Robert Maisha

Supervisor: Prof. T. A. Ndarana (University of Pretoria)

Co-supervisor Dr. M.M. Bopape (University of Pretoria)

Co-supervisor Prof. F.A. Engelbrecht (University of Witwatersrand)

Department: Department of Geography, Geo-Informatics and Meteorology

Faculty: Faculty of Natural and Agricultural Sciences

University: University of Pretoria

Degree: Philosophy Doctor

SUMMARY

Urbanisation has resulted in the removal of natural surface with artificial surface such as tarred roads and concrete surfaces. This causes more heat storage at the surface, resulting in nighttime temperature difference of average 2°C between urban and rural areas, which impacts climate. This phenomenon is called an urban heat island (UHI's), and negatively affects human health, energy consumption, and the urban environment.

This study investigates the role of urban land surface changes, anthropogenic emissions and urban parameters in the development of UHI over the city of eThekwini, Kwazulu-Natal Province of South Africa (SA). The city is located adjacent to the Indian Ocean, and its proximity to the ocean influences the local climate.

The study applies the Conformal-Cubic Atmospheric Model (CCAM), a climate model developed at the Commonwealth Scientific and Industrial Research Organisation (CSIRO) of Australia. The CCAM is run as a regional model with a stretched grid to provides higher resolution output over the area of interest. CCAM is coupled to an urban climate model (UCM) called the Australian Town Energy Budget (ATEB) via a land surface model (LSM) titled the Community Atmosphere–Biosphere Land Exchange (CABLE), which incorporates

UNIVERSITEIT VAN PRETORIA
UNIVERSITY OF PRETORIA
YUNIBESITHI YA PRETORIA

the 2013 land cover boundary conditions obtained from Moderate Resolution Imaging Spectro-radiometer (MODIS) satellite.

The CCAM is driven by two datasets: (i) CCAM-ERA Interim data, from the European Centre for Medium-Range Weather Forecasts (ECMWF) for the period 2005/6 to 2016; and (ii) Climate Model Intercomparison Project Phase 5 (CMIP5) driven simulations for the periods: 2005/6 to 2016, 2039/40 to 2050, and 2089/90 to 2099. The downscaling was performed in various stages, using both ERAI and CMIP5 driven data, with resolution increasing from 50 km (Africa), 8 km (South Africa) and 1 km (eThekwini). At 1 km, CCAM-CABLE incorporates measured urban parameters provided by the city of eThekwini.

The CCAM analysis indicates that updating the land cover to the 2013 data version and switching on the urban scheme realistically reproduce the orientation of the city and land cover types. CCAM simulated surface and minimum temperatures, and winds using ERAI and CMIP5 driven data effectively reproduced the UHI seen in surface observations and MODIS data. The CCAM simulations indicate that eThekwini experiences the UHI during DJF season, which is evident in minimum and surface temperatures, longwave radiation and sensible heat flux. The model simulations suggest that the city temperature is at most 2°C warmer than the surrounding rural areas.

Projections of minimum and surface temperatures into the near-future indicate that the UHI will persist, will be nearly 1°C higher than in the current climate, and at most 2-4°C higher in the far-future climate. Future projections suggest that the UHI intensity will increase over the city of eThekwini.

An analysis of winds shows that both synoptic scale circulations and mesoscale circulations impact the UHI. Wind analysis shows the presence of sea breeze from 06h00 UTC until around 18h00 UTC, and land breeze after 18h00 UTC until 06h00 UTC.

These results suggest that human activities such as reducing vegetation, increasing artificial surfaces, and building within the city, have contributed to the development of the UHI. However, atmospheric circulations including land and sea breezes regulate the evolution of the UHI.

Different mitigation strategies can be applied to reduce the impact of the UHI in cities, such as increasing water bodies, re-vegetation, and applying high-reflectivity materials. Current

UNIVERSITEIT VAN PRETORIA
UNIVERSITY OF PRETORIA
YUNIBESITHI YA PRETORIA

findings suggest that CCAM could be an important tool for evaluating and understanding the dynamics of the UHI in cities. Further research is needed to validate the model across different cities under various climatic conditions and to test the capability of the model at sub-kilometer scale.

Keywords: city of eThekwini, climate models, updated land cover, surface urban parameters, city climates, urban heat islands, high horizontal resolution.

UNIVERSITEIT VAN PRETORIA
UNIVERSITY OF PRETORIA
YUNIBESITHI YA PRETORIA

AKNOWLEDGEMENTS

I would like to acknowledge and thank the following people for their assistance.

- Prof. Thando Ndarana (University of Pretoria), Prof. Francois Engelbrecht (University of Witwatersrand), and Dr. Mary-Jane Bopape: my supervisors for your encouragement and valuable support.
- Dr. Marcus Thatcher: my co-author and CCAM mentor for your valuable input into this study
- Mr. Yerdashin Padayachi, my former CSIR colleague for your effort in generating the land cover used in this study.
- Dr. Cecilia Molokoane/Masemola, my former CSIR colleague, for your effort in generating the MODIS nighttime land surface temperatures used in this study.
- Mr. Jacobus van der Merwe, my former CSIR colleague for helping with the model technicalities and Linux support.
- Ms. Lerato Mpheshea, my former CSIR colleague for your support and assistance with model data.
- Mr. Lucky Dlamini, Mr. Joe Matsapola, Mr. Musa Mkhwanazi, Mr. Sifiso Mbatha, and Prof. Andries Kruger - South African Weather Service, for assisting with observations datasets including temperatures and winds.
- South African Weather Service (SAWS) - for financially supporting my academic studies and the meteorological observation data and for financially supporting my academic studies.
- The city of eThekwini - for financially supporting the urban heat island modelling research project and urban modelling data
- The Council for Scientific and Industrial Research (CSIR) - for financially supporting my academic studies and providing computing through the Centre for High Performance Computing (CHPC)
- The University of Pretoria (UP) – for financially supporting my academic studies
- The Water Research Commission (WRC) – for financially supporting my academic studies and the research articles.
- The three reviewers, from University of Pretoria, SA-University and International reviewer for their comments and constructive reviews
- Lastly, my family – for the moral support and encouragement during this endeavour

UNIVERSITEIT VAN PRETORIA
UNIVERSITY OF PRETORIA
YUNIBESITHI YA PRETORIA

RELATED PUBLICATIONS AND PRESENTATIONS BY THE AUTHOR

Journal Article:

(i) **Maisha T Robert**, Ndarana Thando, Engelbrecht Francois A, Thatcher Marcus, Bopape M Mary-Jane, Padayachi, Yerdashin, and Masemola, Cecilia; (2023) "Simulation of the eThekwini Heat Island in South Africa", Applied Meteorology and Climatology, 589–609 https://doi.org/10.1175/JAMC-D-21-0231.1

Conference Proceeding:

(i) **Maisha T Robert**, F.A. Engelbrecht., M.M. Bopape., Z. Dedekind, J. van der Merwe and M. Thatcher (2017) "Simulations of present and future climate over eThekwini using the CCAM", South African Society of Atmospheric Sciences (SASAS), University of Venda, Polokwane, September 2017.

(ii) **Maisha T Robert**, Ndarana Thando, Engelbrecht Francois A, Thatcher Marcus, Bopape M Mary-Jane, Padayachi, Yerdashin, and Masemola, Cecilia (2023) "Simulation of the eThekwini Heat Island in South Africa", Centre for High Performance Computing Conference, Skukuza, Kruger National Park, December 2023.

(iii) **Maisha T Robert**, Ndarana Thando, Engelbrecht Francois A, Thatcher Marcus, Bopape M Mary-Jane (2025) "Simulation of current and future temperature of eThekwini, South Africa", International Conference on Southern Hemisphere Meteorology and Oceanography (ICSHMO) 2025, Cape Town International Convention Centre, Cape Town, Western Cape, South Africa, 31 March - 04 April 2025

UNIVERSITEIT VAN PRETORIA
UNIVERSITY OF PRETORIA
YUNIBESITHI YA PRETORIA

TABLE OF CONTENTS

UNIVERSITEIT VAN PRETORIA
UNIVERSITY OF PRETORIA
YUNIBESITHI YA PRETORIA

UNIVERSITEIT VAN PRETORIA
UNIVERSITY OF PRETORIA
YUNIBESITHI YA PRETORIA

UNIVERSITEIT VAN PRETORIA
UNIVERSITY OF PRETORIA
YUNIBESITHI YA PRETORIA

UNIVERSITEIT VAN PRETORIA
UNIVERSITY OF PRETORIA
YUNIBESITHI YA PRETORIA

LIST OF ABBREVIATIONS

ACCESS1-0	Australian Community Climate and Earth System Simulator
AMIP	Atmospheric Model Intercomparison Project
AOGCMs	Atmospheric-Ocean Global Circulation Models
AR5	Fifth Assessment Report
AR6	Sixth Assessment Report
ATEB	Australian Town Energy Budget
AWS	Automatic Weather Stations
A2C	Atmospheric to Computational Fluid Dynamics model
CABLE	Community Atmosphere–Biosphere Land Exchange model
CBD	Central Business District
CCAM	Conformal Cubic Atmospheric Model
CCSM4	Community Climate System Model
CESAR	Cabauw Experimental Site for Atmospheric Research
CHPC	Centre for High Performance Computing
CLUHI	Canopy-level UHI
CMIP3	Coupled Model Intercomparison Project phase three
CMIP5	Climate Model Intercomparison Project Phase Five
CNRM-AROME	National Centre for Meteorological Research-AROME
CNRM-CM5	National Centre for Meteorological Research Coupled Global Climate Model Version Five
COSMO	Consortium for Small-Scale Modeling
CO2	Carbon Dioxide
CORDEX	Coordinated Regional Climate Downscaling Experiment
CORR	Correlation Coefficient
CSIR	Council for Scientific and Industrial Research
CSIRO	Commonwealth Scientific and Industrial Research Organisation
DA	Data Assimilation
DJF	December-January-February
DOE	Department of Energy
DTR	diurnal temperature range
ECMWF	European Centre for Medium Range Weather Forecasting
ERAI	European Centre for Medium Range Weather Forecasting (ECMWF) Interim Reanalysis

UNIVERSITEIT VAN PRETORIA
UNIVERSITY OF PRETORIA
YUNIBESITHI YA PRETORIA

ERA5	European Centre for Medium Range Weather Forecasting (ECMWF) Interim Reanalysis version 5
GCM	Global Climate Model
GEE	Global Earth Engine
GFDL	Geophysical Fluid Dynamics Laboratory
GFDL-CM3	Geophysical Fluid Dynamics Laboratory Coupled Model Version Three
GHG	Global Greenhouse Gases
HKIA	Hong Kong International Airport
IGBP	International Geosphere-Biosphere Programme
IPCC	International Panel on Climate Change
JJA	June, July, and August
JMA	Japan Meteorological Agency
LIDAR	Light Detection and Ranging
LSM	Land Surface Model
LST	Land Surface Temperature
LTGG	Long Term Global Goal
MAE	Mean absolute error
MAM	March, April, and May
MPI-ESM-LR	Max Planck Institute Coupled Earth System Model
MSE	Mean square error
MODIS	Moderate Resolution Imaging Spectro-radiometer
MSL	Mean Sea Level
MSLP	Mean Sea Level Pressure
NCAR	National Centre for atmospheric Research
NCEP	National Centre for Environmental prediction
Mt. Edgecombe	Mount Edgecombe.
NorESM1-M	Norwegian Earth System Model
NRF	National Research Foundation
QA	High-Quality flag (quality assurance)
RCP-4.5	Representative Concentration Pathways 4.5
RCP-8.5	Representative Concentration Pathways 8.5
RMSE	Root Mean Square Error
SA	South Africa
SASAS	South African Society of Atmospheric Sciences

UNIVERSITEIT VAN PRETORIA
UNIVERSITY OF PRETORIA
YUNIBESITHI YA PRETORIA

SAST	South Africa Standard Time
SAWS	South Africa Weather Service
SON	September, October, and November
SAEON	South African Earth Observations Network
SST	sea surface temperatures
SUHI	Surface Urban Heat Island
TDWR	Terminal Doppler Weather Radar
TEB	Town Energy Budget
UCLEM	Urban Climate and Energy Model
UCM	Urban Climate Model
UNFCCC	United Nations Framework Convention on Climate Change
UHI	Urban Heat Islands
UP	University of Pretoria
USA	United States of America
WGI	Working Group I
WITS	University of Witwatersrand
WMO	World Meteorological Organisation
WRC	Water Research Commission
WRF	Weather Research and Forecasting
4DVAR	Four-dimensional variational data assimilation system

UNIVERSITEIT VAN PRETORIA
UNIVERSITY OF PRETORIA
YUNIBESITHI YA PRETORIA

LIST OF FIGURES

UNIVERSITEIT VAN PRETORIA
UNIVERSITY OF PRETORIA
YUNIBESITHI YA PRETORIA

UNIVERSITEIT VAN PRETORIA
UNIVERSITY OF PRETORIA
YUNIBESITHI YA PRETORIA

UNIVERSITEIT VAN PRETORIA
UNIVERSITY OF PRETORIA
YUNIBESITHI YA PRETORIA

UNIVERSITEIT VAN PRETORIA
UNIVERSITY OF PRETORIA
YUNIBESITHI YA PRETORIA

UNIVERSITEIT VAN PRETORIA
UNIVERSITY OF PRETORIA
YUNIBESITHI YA PRETORIA

UNIVERSITEIT VAN PRETORIA
UNIVERSITY OF PRETORIA
YUNIBESITHI YA PRETORIA

UNIVERSITEIT VAN PRETORIA
UNIVERSITY OF PRETORIA
YUNIBESITHI YA PRETORIA

UNIVERSITEIT VAN PRETORIA
UNIVERSITY OF PRETORIA
YUNIBESITHI YA PRETORIA

LIST OF TABLES

UNIVERSITEIT VAN PRETORIA
UNIVERSITY OF PRETORIA
YUNIBESITHI YA PRETORIA

UNIVERSITEIT VAN PRETORIA
UNIVERSITY OF PRETORIA
YUNIBESITHI YA PRETORIA

APPENDIX A

APPENDIX B

UNIVERSITEIT VAN PRETORIA
UNIVERSITY OF PRETORIA
YUNIBESITHI YA PRETORIA

APPENDIX C

UNIVERSITEIT VAN PRETORIA
UNIVERSITY OF PRETORIA
YUNIBESITHI YA PRETORIA

APPENDIX D

UNIVERSITEIT VAN PRETORIA
UNIVERSITY OF PRETORIA
YUNIBESITHI YA PRETORIA

1

UNIVERSITEIT VAN PRETORIA
UNIVERSITY OF PRETORIA
YUNIBESITHI YA PRETORIA

CHAPTER 1:

Introduction

1.1 Background to the study

1.1.1 Climate change, variability, and urbanisation

Currently, at least 50% of the world's population lives in cities (Pokhrel and Lee 2011; Oleson *et al.*, 2011; Fischer *et al.,* 2012; Han *et al.,* 2014; Canton and Dipankar 2024), especially in developed countries (Blake *et al.,* 2011; Chen *et al.,* 2015). The percentage of urbanisation is expected to rise to more than 60% by the year 2050 (Grimmond *et al.,* 2010; Walsh *et al.,* 2013; Estrada *et al.,* 2017; Garuma 2018). Such an increase in urbanisation also applies to the African continent. Half of this population resides in cities (Canton and Dipankar, 2024) along the coast (Pokhrel and Lee, 2011).

The rise in urbanisation leads to an increased demand for infrastructure, water, energy, and transportation (Baklanov *et al.,* 2018; Garuma 2018). These increments will lead to a rise in anthropogenic heating (including includes house-hold, heating from buildings and industries) and concentration of greenhouse gases (GHGs), consequently causing a rise in temperatures (Meehl and Tebaldi 2004; Barriopedro *et al.,* 2011; Blake *et al.*, 2011; Giugni *et al.*, 2015). This temperature increase, evidenced in Walsh *et al.,* (2013) and Nuruzzaman, (2015), will contribute to a surge in extreme weather and climate events, including an increase in the frequency of hot days, heatwaves, droughts, and flood events. The increase in urbanisation strongly influences local meteorology, making cities more vulnerable to meteorological hazards including urban heat island (UHI), urban flash floods and urban air pollution (Estrada *et al.*, 2017; Chen and Dipankar, 2022).

Urbanisation contributes at least 40% of GHG emissions due to high population density and economic activities in cities (Satterthwaite, 2008; Blake *et al.*, 2011). Cities require a huge amount of energy for lighting, heating of buildings, cooling systems as well as for residential use. Additionally energy is needed for mass transportation as there is a large volume of traffic by vehicles (Blake *et al.*, 2011). The amount of energy used in cities contributes at least 70% of the energy used globally

UNIVERSITEIT VAN PRETORIA
UNIVERSITY OF PRETORIA
YUNIBESITHI YA PRETORIA

(Estrada *et al.*, 2017), which is then released into the atmosphere together with fossil fuel burning and vegetation clearance during urbanisation.

Significant amounts of natural vegetation have been cleared during the urbanisation process (Han *et al.,* 2014). This alteration of land use, as noted by Chen *et al.,* (2014), influences the climate by affecting surface reflectivity, surface roughness, as well as hydrological and thermal characteristics (Pokhrel and Lee, 2011; Giugni *et al.,* 2015). Deforestation plays a role in climate modification by inducing changes in solar radiation absorption and moisture transfer (Blake *et al.,* 2011).

The removal of vegetation results in the proliferation of artificial surfaces, particularly tar surfaces that absorb and retain more heat. This change in surfaces contributes to both incoming daytime shortwave and outgoing nighttime longwave radiation being absorbed by buildings and street surfaces (Han *et al.,* 2014), thereby further altering the climate. Such alterations give rise to a night-time temperature differences between cities and rural areas, where city temperatures are at least 2°C higher than in non-urban areas, leading to urban heat islands (UHIs) (Kruger and Shongwe, 2004; Grimmond *et al.,* 2010; Walsh *et al.*, 2013; Chen *et al.,* 2014; Nuruzzaman, 2015; Estrada *et al.,* 2017; Lehoczky *et al.,* 2017; Sannigrahi *et al.,* 2017; Chapman and McAlpine, 2019; Chen and Dipankar, 2022). An increase in urbanisation also results in increased flash flooding and air pollution in urban areas (Arnfield, 2003; Chen and Dipankar, 2022).

Changes in surface roughness within urban environments induce modifications to wind patterns, causing air to decelerate when approaching the city, due to increased friction in urban areas and high roughness (Pokhrel and Lee, 2011; Chen and Dipankar, 2022). Buildings divert wind around cities, and this causes convergence on the downwind side of the city, leading to convection. This type of motion hinders convection within cities, reducing rainfall, and as a result, intensifies the UHI (Han *et al.,* 2014).

UNIVERSITEIT VAN PRETORIA
UNIVERSITY OF PRETORIA
YUNIBESITHI YA PRETORIA

1.1.2 Climate change, city climate and urban heat islands

Climate change has led to an increase in extreme weather events, including rising global temperatures and more frequent heat waves. In addition, previous studies have shown that urbanisation contributes to higher temperature in cities, further influencing local climate patterns (Karl et al., 1993). Research by Kruger and Shongwe (2004), covering the period from 1940 to 1989, revealed a significant rise in average temperature in South Africa (SA) coastal cities.

Hughes and Balling (1996) found that maximum temperatures increased by +0.12°C per decade in urban areas, and minimum temperatures increased by +0.34°C per decade in urban areas during the period 1960-1990. Minimum and annual average surface temperatures also show significant warming trends, mostly for stations located in cities (Kruger and Shongwe, 2004; MacKellar *et al.*, 2014; IPCC, 2023). Stations along the coastal cities have shown a significant decrease in diurnal temperature range (King'uyu *et al.*, 2000). This has been attributed to an increase in minimum temperatures more than maximum temperatures. Kruger and Shongwe (2004) have shown that the number of extremely hot days (maximum temperatures greater than 35°C over a period of at least three consecutive days) has increased in SA cities. Minimum temperatures also show that days with cooler nights have decreased, while warmer nights have increased, particularly for stations along the coastal cities.

In urban areas, various types of micro-climates are experienced, including heat islands, dry islands, moisture islands, air pollution islands, as well as rain islands (Blake *et al.*, 2011; Han *et al.*, 2014). Heat islands are more common during clear nights (Han *et al.*, 2013) in mid-autumn, early winter, summer and spring when conditions are clear and the winds are low (Blake *et al.*, 2011).

In cities, roads and large stationary sources generate heat fluxes that influence the radiation budget, contributing to a type of mesoscale circulation (Grimmond and Oke, 1999). Compared to rural regions, cities have less vegetation, which is often replaced by artificial surfaces. This reduction in vegetation lowers latent heat flux and increases storage heat flux, thereby amplifying anthropogenic heat emissions (Wang

UNIVERSITEIT VAN PRETORIA
UNIVERSITY OF PRETORIA
YUNIBESITHI YA PRETORIA

and Li, 2021). These changes impact the urban energy budget and can intensify the development of the UHI effect.

Urban surfaces differ markedly from rural surfaces, primarily due to their lower reflectivity. This is a result of construction materials such as dark asphalt used in roads, and various roofing materials (Blake *et al.*, 2011; Pokhrel and Lee, 2011). Materials like concrete and asphalt have high heat capacity and thermal conductivity, allowing them to store and release heat more effectively (Pokhrel and Lee, 2011; Ramamurthy *et al.*, 2014; Estrada *et al.*, 2017). Collectively, these factors contribute to higher temperatures in cities compared to surrounding rural areas, enhancing the UHI effect. Additionally, cities emit more longwave radiation than rural or suburban areas. However, due to the complex urban skyline, often characterised by deep street canyons, less amount of longwave radiation is released back into the atmosphere, further trapping heat (Estrada *et al.*, 2017).

Changes from natural to artificial surfaces and the removal of vegetation in cities reduces evapotranspiration and latent heat cooling, thus enhancing the UHI (Estrada *et al.*, 2017). The artificial surfaces have high heat capacity and affect the heat exchange when compared to vegetated surfaces in rural areas (Blake *et al.*, 2011). In cities, both additional atmospheric and heat sources process interact with surface energy balance. This includes aerosols that reduce the amount of incoming radiation reaching the surface, resulting in net cooling, as well as elevated carbon dioxide, which causes an increase in radiative heating (Blake *et al.*, 2011). All these changes result in cities being warmer than rural areas and could lead to an increase in the strength of the UHI.

Urban centres experience enhanced precipitation on the downwind side of cities (Wan *et al.*, 2013). Various explanations exist that link urbanisation with convection in cities. These include sensible heat flux enhancement, UHI-induced convection, the availability of more cloud condensation nuclei, the alteration of urban canopy, disruption of precipitation systems, as well as increased surface roughness (Blake *et al.*, 2011). Coastal cities around the globe have experienced sea level rise as a consequence of climate change (Meehl *et al.,* 2005).

UNIVERSITEIT VAN PRETORIA
UNIVERSITY OF PRETORIA
YUNIBESITHI YA PRETORIA

1.1.3 Impacts of urban heat islands on health

An increase in urban temperature has led to a rise in extreme climate events, such as extreme hot nights and more frequent heatwaves (Meehl and Tebaldi, 2004; Barriopedro *et al.,* 2011; Giugni et al., 2014; Wang and Li 2021). At the same time, the frequency of cold nights and chilly days has declined (Giugni *et al.,* 2014). These climatic shifts, coupled with deterioration air quality (Blake et al., 2011; Estrada et al., 2017), have significantly contributed to increased health risks. Notably, they have been linked to increased mortality rates among elderly individuals over the age of 65 years (Xu *et al.,* 2013; Chen *et al.,* 2015; Garland, *et al.,* 2015; Canton and Dipankar, 2024).

The most vulnerable elders are those with pre-existing medical problems, with women more vulnerable than men (Xu *et al.,* 2013; Garland *et al.,* 2015). Urban areas dominated by old buildings have been subjected to a substantial risk of mortality during heat waves (Meehl and Tebaldi, 2004; Chen *et al.*, 2015; Estrada *et al.*, 2017); this has been attributed to a lack of thermal insulation and lower heat dissipation capacity, which increases indoor temperatures in those buildings (Meehl and Tebaldi, 2004).

Winter temperatures are expected to rise, potentially reducing the energy needed for heating, with a potential increase in UHI intensity (Akbari *et al.*, 2001; Rocklöv *et al.*, 2011; Spinoni *et al.*, 2021). Conversely, higher summer temperatures will increase the air conditioning requirements. This will exacerbate anthropogenic heat sources and contribute to elevated pollution levels, particularly ozone (Blake *et al.,* 2011). Urban areas already suffer from poorer air quality compared to rural and suburban areas, due to urban pollution island effect. The inversion layer formed over the UHI prevents vertical dispersion of pollutants, thus, leading to higher concentration of air pollution, and contributing to the formation of acid rain in the affected areas (Blake *et al.,* 2011).

UNIVERSITEIT VAN PRETORIA
UNIVERSITY OF PRETORIA
YUNIBESITHI YA PRETORIA

1.1.4 Initialisation data for climate models

1.1.4.1 Reanalysis datasets

Climate models utilise reanalysis datasets at various resolutions from different global centres, including National Centres for Environmental prediction (NCEP), the National Centre for atmospheric Research (NCAR), the Department of Energy (DOE), the European Centre for Medium-Range Weather Forecasts (ECMWF), and Japan Meteorological Agency (JMA), among others (Lan et al., 2023). Reanalysis data offer extensive temporal and spatial coverage and can therefore compensate for the lack of surface observations globally (IPCC, 2023; Lan et al., 2023). According to the Sixth Assessment Report (AR6) of Working Group I (WGI) 10 of the IPCC (2023), using multiple source of observational records including reanalysis data that are suitable for evaluating weather and climate phenomena of interest and account for observational uncertainty is fundamental to understanding past regional climate change and assessing regional climate models with high confidence. However, the performance of these models in projecting future climate depends on how well they represent relevant processes, forcings, and boundary conditions used in dynamical downscaling.

These datasets have been improved over time due to rigorous quality control, advancements in modelling and enhanced data assimilation processes (Dee *et al.*, 2011). They have also been widely used for global model validation. Among climate model variables, the mean 2-metre air temperature has been found to be the most accurately reproduced in the ECMWF Reanalysis (ERA-Interim) datasets, demonstrating a consistent correlation above 0.9 and a mean bias ranging from 0.8°C to 1.5°C (Clelland *et al.*, 2024).

Several studies have evaluated the performance of reanalysis data in representing temperature and precipitation, including Lan *et al.*, (2023) and Clelland *et al.*, (2024). For example, in a study conducted over Siberia, ERA-Interim and ERA5 datasets from 2008 to 2018 showed the best performance during summer, with correlation coefficient exceeding 0.97. ERA5 exhibited an average bias of 0.5°C, while ERA-Interim had an average bias of 0.96°C. Reanalysis performance was strongest in

UNIVERSITEIT VAN PRETORIA
UNIVERSITY OF PRETORIA
YUNIBESITHI YA PRETORIA

summer and weakest in winter. These datasets were also more accurate in reproducing temperature maxima. Specifically, ERA-Interim showed an absolute bias of 1.29°C for temperature maxima, while ERA5 demonstrated a significantly lower absolute bias of 0.12°C (Lan *et al.*, 2023; Clelland *et al.*, 2024).

In the current modelling setup, CCAM was initialised using both the ECMWF Interim Reanalysis (ERA-Interim or ERAI) and the CMIP5 RCP 8.5 dataset. ERA-Interim, introduced in 2007 to replace the ERA-40 dataset, provides data from January 1979 until August 2019, after which it was succeeded by ERA5. ERA-Interim has a spatial resolution of 0.5° (~79 km), and a temporal resolution of 6 hours. The dataset was produced using a four-dimensional variational (4DVAR) data assimilation system operating on an hourly cycle (Dee et al., 2011; Lan et al., 2023; Clelland et al., 2024).

ERA-Interim has been widely used to initialise climate models globally and is also considered a reliable alternative to direct global observations (Liu *et al.*, 2018; Clelland *et al.*, 2024). Both ERA-Interim and ERA5 data produce comparable results; however, ERA5 generally yields improved performance. These differences are largely due to the assimilation techniques used, where ERA-Interim applied Cressman interpolation, whereas ERA5 employed two dimensional (2D) optimal interpolation for assimilating station data (Clelland *et al.*, 2024).

1.1.4.2 Climate projection datasets

Global climate projections models (GCMs) use climate projections datasets at various resolutions to simulate the past, current and future climates. In this study, the Coupled Model Intercomparison Project phase five (CMIP5) was applied for the current and future climate projections (Taylor *et al.*, 2012). The CMIP5 experiment was designed to improve our understanding of both historical and future climate behaviour. One of its primary objectives was to investigate why similarly forced models could produce a range of different climate responses.

CMIP5 model simulations were performed by more than 20 modelling groups, utilising more than 50 different models. These simulations were performed using atmosphere–ocean global climate models (AOGCMs), which incorporate the interactions between the atmosphere, land, ocean, sea ice as well as carbon fluxes.

UNIVERSITEIT VAN PRETORIA
UNIVERSITY OF PRETORIA
YUNIBESITHI YA PRETORIA

These models respond to specific time-varying greenhouse gases (GHG's) concentrations, and other climate forces (Taylor *et al.*, 2012).

The dataset used in this study was generated from the long-term integration (on a century time scale) as opposed to the near-term integration (decadal prediction). These long-term experiments build upon those developed under the Coupled Model Intercomparison Project phase three (CMIP3), and include additional simulations aimed at providing a more comprehensive understanding of climate change and variability. CMIP5 model simulations respond to various climate forcings, such as increasing carbon dioxide (CO2) concentrations, and are also designed to project the trajectory of future climate change (Taylor *et al.*, 2012; Yan *et al.*, 2013).

In the long-term experiments, simulations include an Atmospheric Model Intercomparison Project (AMIP) run, a coupled control run, and a historic run that is forced with observed changes in atmospheric composition. These reflect both natural and anthropogenic sources and include dynamic land cover changes. Future projection simulations are forced with specified concentration based on Representative Concentration Pathways (RCP), including RCP4.5 (a low-emission, high-mitigation scenario) and RCP8.5 (a high-emission, low-mitigation scenario) (Riahi *et al.*, 2011; Taylor *et al.*, 2012; Maure *et al.*, 2018a; Muthige *et al.*, 2018). RCP8.5 is widely considered the most realistic "business-as-usual" scenario, given the current trajectory of the GHGs emissions (Maure *et al.*, 2018a).

These model simulations have been used in initiatives such as the Coupled Model Intercomparison Projects (CMIP) phase five (CMIP5) and were integral to the Fifth Assessment Report (AR5) of the International Panel on Climate Change (IPCC). These datasets span the period from 1960 to 2100 (Taylor *et al.*, 2012; Yan *et al.*, 2013).

A range of these model ensembles is available, including the National Centre for Meteorological Research Coupled Global Climate Model, version 5 (CNRM-CM5); the Geophysical Fluid Dynamics Laboratory Coupled Model (GFDL-CM3); the Max Planck Institute Coupled Earth System Model (MPI-ESM-LR); the Norwegian Earth System Model (NorESM1-M); the Australian Community Climate and Earth System Simulator (ACCESS1-0) and the Community Climate System Model (CCSM4), among others.

UNIVERSITEIT VAN PRETORIA
UNIVERSITY OF PRETORIA
YUNIBESITHI YA PRETORIA

However, for the current study, only the first four models were used for downscaling under the RCP8.5 scenario. These simulations were forced with bias-corrected sea surface temperatures (SST's) and sea ice data (Engelbrecht *et al.*, 2011; Muthige *et al.*, 2018; Katzfey *et al.*, 2020). These particular models were selected based on previous studies demonstrating their ability to realistically simulate the current climate of southern Africa (Engelbrecht *et al.*, 2011, 2015a).

It is important to note that both the reanalysis and CMIP data are valuable for climate model downscaling. However, their horizontal resolutions are too low for simulations at numerical weather prediction (1-10 km) and high-resolution urban-scale modelling (~1 km) time scales. As such, these datasets primarily serve as sources of initial and boundary conditions for high-resolution models through dynamical downscaling process. This approach adds significant value in representing regional weather and climate patterns, particularly in areas of complex topography and heterogeneous surface characteristics (IPCC, 2023).

1.1.5 Global climate projections

Global climate change and global warming have led to increased interest in the use of global climate models (GCMs) to project climate patterns across various spatial and temporal scales. Climate models are important tools for studying climate, especially because ground observations are limited in their spatial coverage. These models also enable experimental studies that are not feasible with observations alone, such as projecting future climate scenarios. GCMs are run at a coarse spatial resolution across the entire globe due to computational constraints (Giorgi, 1990; IPCC, 2023).

GCMs simulate large-scale atmospheric circulations in response to global climate forcings, whereas Regional Climate Models (RCM's) or Limited Area models (LAMs) are designed to capture subgrid scale features including complex topography and coastlines (Giorgi, 1990). GCMs have been globally used for weather and climate projections across various time scales, including numerical weather prediction, seasonal forecasting and multi-decadal climate projections (Maisha 2014).

UNIVERSITEIT VAN PRETORIA
UNIVERSITY OF PRETORIA
YUNIBESITHI YA PRETORIA

GCMs have provided essential global climate projections of global climate change. Over Africa, studies have shown that temperatures are expected to rise at a rate at least 1.5 times higher than the global average within the subtropics (Engelbrecht *et al.*, 2015b). This accelerated warming should be considered by the Long-Term Global Goal (LTGG) of United Nations Framework Convention on Climate Change (UNFCCC), which aims to prevent and mitigate the impacts of climate change cross the African continent (Giugni et al., 2014; Engelbrecht *et al.,* 2015;Engelbrecht *et al.,* 2015c).

Additionally, future temperature projections simulated by global models under the A2 scenario indicate that the warming is strongly influenced by increased anthropogenic forcing towards the end of 21st century. However, it appears to be less sensitive to differences in sea surface temperatures (SST) and sea ice forcings, assuming a consistent host model (Engelbrecht *et al.*, 2011, 2015c; Muthige *et al.*, 2018; Katzfey *et al.*, 2020).

Various studies have been conducted at both global and regional time scales. Climate projection studies using Regional Climate Models (RCMs) have been performed across the globe, offering higher spatial resolution than what is achievable with GCMs Chen et al., (2015) conducted future climate change projections using different GCMs over the Central Business District (CBD) of an Australian city. Their findings indicate that increased vegetation cover within the city centre can lead to a reduction in mean summer temperatures. The study also demonstrates that, in a generic urban setting, mean temperatures were projected to be approximately 0.5°C cooler in non-urban areas compared to urban areas.

Thevakaran *et al*., (2016) evaluated downscalings produced by the Conformal-Cubic Atmospheric Model (CCAM) at 50 km over Sri Lanka, using forcing data from CMIP5 global models and ERAI reanalysis. Statistical validation demonstrates that the model was able to reproduce the observed variables, including temperature, winds, and rainfall.

Katzfey et al., (2020) evaluated CCAM at a resolution of 50 km for both current and future climate simulations. They found that the model could not resolve urban climate processes, including the UHI. This finding indicates the need for even higher

UNIVERSITEIT VAN PRETORIA
UNIVERSITY OF PRETORIA
YUNIBESITHI YA PRETORIA

resolution RCMs than those provided in CORDEX simulations (Reason *et al.*, 2006; Caldwell *et al.*, 2009; Maisha, 2014).

Over Africa, a Coordinated Regional Climate Downscaling Experiment (CORDEX) was initiated to provide regional climate projections using RCMs (Maure *et al.*, 2018a; Kruger *et al.*, 2019; Spinoni *et al.*, 2021). Simulations were performed at a horizontal resolution of 0.44° for the two climate periods: (1950-2005, historical) and (2006-2100, future) under Representative Concentration Pathways 8.5 (RCP8.5) scenario (Riahi *et al.*, 2011; Maure *et al.*, 2018a; Kruger *et al.*, 2019; Spinoni *et al.*, 2021).

The simulation results were used to assess the impacts of climate change on projected future temperatures and rainfall over southern Africa, focusing on two global warming levels (i.e. 1.5°C and 2.0°C) relative to pre-industrial conditions. The results indicate that projected temperatures increase over South Africa and some parts of its surrounding countries including Botswana and Namibia, are expected to exceed the global average warming (Maure *et al.*, 2018a).

However, higher resolution model outputs can be obtained through the technique called regional downscaling, in which the output from the GCM is used to drive a high-resolution LAM (Giorgi, 1990; IPCC, 2023)).

1.1.6 Urban climate modelling and urban heat islands

Progress has been made in the development of climate models capable of simulating urban canopy and projecting future climate. These models are called Urban Climate Models (UCM, Thatcher and Hurley, 2012). Such models are coupled to regional atmospheric models and can be used to simulate and investigate the dynamics of urban climate as a result of climate change and global warming. These models can differentiate between various urban classes and simulate urban energy budget, and distinguish between building roofs, walls, and roads (Thatcher and Hurley, 2012; Spinoni *et al.*, 2021). According to the IPCC (2023) report, in urban climate studies that focus on the interplay between UHI effect and regional climate change, the use of a single layer parametrisation scheme is sufficient. Additionally, surface stations

UNIVERSITEIT VAN PRETORIA
UNIVERSITY OF PRETORIA
YUNIBESITHI YA PRETORIA

located in urban areas can provide key information to enhance our understanding of the urban micro-climate and thus improve urban parametrisation.

The intensity and impact of the UHI effect in cities have been studied globally, using either observational data or high-resolution models. In South Africa, the UHI has been inferred from observed temperature records. Kruger and Shongwe, (2004) reported on an increase in urban temperatures, with minimum temperatures rising by at least 0.34°C/decade, higher than the increase observed in rural areas, which is attributed to the UHI effect. Conversely, historical simulations using RCM's have shown that the model underestimated the surface temperature trend by at least 0.05°C/decade (Kruger *et al.,* 2019).

To our knowledge there are currently no urban climate modelling studies conducted in South Africa. However, globally, such studies have been performed applying both observations and high-resolution models which incorporate urban-scale features. The objective of studies include identifying the different mechanisms that lead to the formation of UHI (Wang and Li, 2017; Garuma, 2018).

Urban climate models (UCM's), when coupled to regional atmospheric models (RAMs), can be used to explore the dynamical behaviour of urban climate in response to global warming scenarios and also the impacts of various urban design strategies (Thatcher and Hurley, 2012). These models can assist with urban planning. They were initially developed as slab models, representing the urban environment as a concrete plate with modified roughness length and thermal properties suitable for simulating the urban energy budget (Pokhrel and Lee, 2011; Thatcher and Hurley, 2012; Luhar et al., 2014), but were later modified to incorporate energy budgets from roofs, walls, and roads (Masson 2000; Luhar et al., 2014). As a result of further developments, these models' current settings incorporate all urban parameters, such as heat fluxes, radiation, and anthropogenic emissions. One example of such a model is the Australian Town Energy Budget (ATEB; Masson 2000; Thatcher and Hurley 2012; Luhar *et al.*, 2014; Garuma 2018), which is applied in this study.

Bozonnet (2007) modelled wind flows over the streets of Athens, Greece. The study shows that specific settings of the city's local geography can trigger winds such as sea

UNIVERSITEIT VAN PRETORIA
UNIVERSITY OF PRETORIA
YUNIBESITHI YA PRETORIA

and mountain breezes. These breezes are associated with temperature variations over a short distance and can thus be observed at an urban-scale, whereby cooler winds flow from non-urban areas towards the city centre, and at the same time gradually warming up, as they move inward and rise due to the UHI effect. Similarly, buildings with air-conditioners and condensers mounted on their exterior walls also produce heat and contribute to an increase in UHI intensity (reported in Chapter 2).

Over the city of Melbourne, Australia, Coutts *et al.,* (2007) studied the UHI using various urban classes from highly urban to rural. The study showed significant differences in latent and sensible heat fluxes between rural and urban, as a result of vegetation and water stored in rural areas. All these fluxes influence the UHI intensity.

Wilby (2008) studied the UHI effect over the city of London, defining the UHI intensity as a daily nighttime minimum temperature difference of at least 2-4°C between the two stations, one located within the city and the other in rural area, away from the city. The strength of the UHI has been presented in studies by Grimmond et al., (2011) and Heaviside et al., (2017). Wilby (2008) study also showed that the UHI effect intensifies during both spring and summer.

Fischer et al., (2012) conducted an urban climate study using the Community Climate System Model (CCSM) with an urban canopy model (UCM). The model incorporates various vegetation types, urban surface, anthropogenic heat sources, and air conditioning. Their study showed that during summer, the UHI starts to build up after mid-day and reaches a maximum before sunrise. The study also found that the UHI is latitudinally dependent: it is weaker within tropics, and stronger away from the tropics, at higher latitudes. This is because, in tropical regions, nighttime cooling in non-urban areas is not much greater than in urban areas. This limited cooling is a result of high level of cloud cover, and high tropospheric temperatures and humidity, all of which contribute to increased downward longwave radiation (Fischer et al., 2012).

Likewise, Chen *et al.,* (2014), applied the Weather Research and Forecasting (WRF) coupled to a UCM with a horizontal grid resolution of 1 km to study the UHI over the city of Hangzhou, China, during a heat wave event. Their study found that the UHI is

UNIVERSITEIT VAN PRETORIA
UNIVERSITY OF PRETORIA
YUNIBESITHI YA PRETORIA

more clearly evident in minimum and mean temperatures and is consistent with urban land use characteristics. They also found that the UHI was intensified by a larger urban fraction (higher than 50%) and anthropogenic heating (Chen *et al.*, 2014).

Similarly, Heaviside *et al.,* (2017) studied the UHI over the city of London and found that in large cities, the UHI intensity is of the range 5-10°C. Additionally, studies by Bohnenstengel *et al.,* (2011) and Heaviside *et al.,* (2017) have also revealed that the UHI results in a temperature difference of approximately 4°C between rural areas and cities.

The Australian Town Energy Budget (ATEB) model was applied by Lipson et al., (2017) to study heat conduction through urban materials. They found that storage heat flux density affects atmospheric stability, the boundary layer, and the UHI. This model was further developed and later called the Urban Climate and Energy Model (UCLEM), which makes it conceivable to improve the predictability of the energy demand.

Chapman et al., (2019) evaluated the performance of the CCAM over the city of Brisbane, Australia, to study how urban growth impacts the UHI during the future summer period 2041-2050. The CCAM was run at a high horizontal resolution of 1 km and initialised with the Representative Concentration Pathways (RCPs), RCP8.5, datasets from the Coupled Model Intercomparison Project phase 5 (CMIP5), which include present-day land cover data (Riahi et al., 2011; Taylor et al., 2012; Yan et al., 2013). The study found that the UHI intensity is projected to increase as a result of land cover changes. In the future, rural areas may become urbanised due to increased urbanisation and as a result, may experience the effects of UHI too.

Chen and Dipankar, (2022) studied the urban canopy parametrization over Singapore using an urban Meteorological Service Singapore (uSINGV) model with various grid resolutions. The study found that wind speed gets reduced in cities due to increased friction in urban areas, as a result of higher values of surface roughness. As a result of changes in surface roughness due to urbanisation, air flow is obstructed by buildings and then accelerates in the spaces between these buildings (Pokhrel and Lee, 2011).

UNIVERSITEIT VAN PRETORIA
UNIVERSITY OF PRETORIA
YUNIBESITHI YA PRETORIA

Likewise, there were higher night-time temperatures due to heat trapping by canyons, leading to the UHI. The study also found that in the afternoon, the boundary layer height is highest, due to strongest energy flux on the surface, which helps form a deep boundary layer.

In an urban climate study over Paris, France, Lemonsu *et al.,* (2023) used a high resolution CNRM-AROME. The study confirmed that a high-resolution model incorporating specific urban parameters captured the UHI very well and could therefore be used to study climate impacts at the city scale. The results also showed that the model performed better in urban areas, with a temperature bias less than 1°C in urban areas, which indicates satisfactory performance.

Canton and Dipankar (2024) applied the Consortium for Small-Scale Modeling (COSMO) with an urban canopy parametrization model, TERRA URB, at a horizontal grid resolution of 1.1 km to study UHI and validated it against a network of observations in medium to small size cities over Switzerland, which are populated by more than 70% of the country population. The model output was comparable to observations over cities in Switzerland, with a 2-m temperature bias of 1.32°C over Zurich and 2.93°C over Lugano. In model verification, according to Gordon and Shaykewich, (2000), in their technical report on performance measures for weather services, although subjective, a temperature bias less than 3°C is considered reliable as a measure of accuracy.

A list of urban climate studies, including both reviews and modelling, is shown in Table 1.1. This table illustrates that urban climate modelling has been conducted globally at a high resolution, with an average of 1 km. However, due to their computing demands, such studies are often limited to either numerical weather prediction time scales (up to 72 hours) or short climate predictions (~10 years).

UNIVERSITEIT VAN PRETORIA
UNIVERSITY OF PRETORIA
YUNIBESITHI YA PRETORIA

Table 1.1: A list of high-resolution urban climate modelling studies over global cities

	Authors	Model	Resolution	City
1	Bohnenstengel *et al.*, (2011)	MORUSES	1 km	London, United Kingdom
2	Fischer *et al*., (2012)	CCSM+UCM	0.9375°x1.25°	global simulations
3	Thatcher and Hurley, (2012)	CCAM	1 km	Melbourne, Australian
4	Chen *et al*., (2014)	WRF	1 km	Hangzhou, China,
5	Sharma *et al*., (2016)	WRF	1 km	Chicago metropolitan, USA
6	Lehoczky *et al*., (2017)	MODIS+observations	1 km	Valencia, Spain
7	Lipson *et al*., (2017)	CCAM+UCLEM	1 km	Australian cities
8	Chapman *et al*., (2019)	CCAM+ UCLEM	1km	Brisbane, Australia,
9	Katzfey *et al*., (2020)	CCAM+ UCLEM+CORDEX	50 km	global simulations
10	Chen and Dipankar, (2022)	uSINGV+MORUSES, JULES	2.7 km, 1.5 km & 0.3 k	Singapore
11	Lemonsu *et al*., (2023)	CNRM-AROME.	1 km	Paris, France,
12	Canton and Dipankar (2024)	COSMO+TERRA URB	1.1 km	Switzerland cities

1.1.7 The influence of atmospheric circulations on urban heat island and its modelling

Although the urban heat islands (UHIs) impact coastal cities, their effects are often moderated by atmospheric circulations, including both large-scale systems and mesoscale events such as land and sea breezes (Lee and Shun, 2003; Pokhrel and Lee, 2011; Grachev et al., 2018; Khan et al., 2018), mountain and valley breezes (Pokhrel and Lee, 2011), as well as anabatic and katabatic winds.

Land and sea breezes develop due to differences in the heat capacities of seawater and land along coastlines (Pokhrel and Lee, 2011; Canton and Dipankar, 2024). At night, the land cools more rapidly than the adjacent ocean, creating a mesoscale pressure gradient (Case et al., 2005). This drives cooler, denser air from the land towards the ocean, resulting in the formation of a land breeze (Case, 2002). During summer, onshore advection of cooler air from the ocean to the land lowers land surface temperatures. Conversely, offshore winds from the land to the ocean can lead to warmer conditions over land (Lengoasa, 1988).

During the day, onshore flow in the form of a sea breeze induces advection that helps moderate the daytime temperature increase over land. This results in a weaker pressure gradient, reduced circulation strength, and stable thermal stratification over

UNIVERSITEIT VAN PRETORIA
UNIVERSITY OF PRETORIA
YUNIBESITHI YA PRETORIA

the ocean (Estoque, 1962). These sea breezes play a crucial role in mitigating the impacts of the UHI effect in coastal cities.

Land and sea breezes typically extend vertically up to 1,000 meters during the day, but this depth is reduced to about 200 meters at night (Bastin et al., 2006; Pokhrel and Lee, 2011). Horizontally, the breeze can stretch up to 100 kilometres seaward and approximately 75 kilometres inland (Pokhrel and Lee, 2011). The smooth ocean surface, with its high heat capacity and long-term heat storage, and the land, with its relatively low heat capacity, contribute to a strong diurnal range of sensible heat fluxes (Grachev et al., 2018).

In South Africa (SA), berg winds typically move from the west coast to the east coast, warming as they descend. These westerly winds raise temperatures along the east coast, sometimes resulting in temperature anomalies of up to 4°C above normal. In contrast, when easterly winds dominate, they bring cooling effects, with temperatures falling as much as 4°C below normal (Lengoasa, 1988).

Numerous observational and modeling studies have investigated the dynamics of land and sea breezes globally, as well as their modulation by mesoscale and synoptic-scale events. Case (2002) studied these breezes using observation towers and wind profilers in Florida, USA. Lee and Shun (2003) used Terminal Doppler Weather Radar (TDWR) with a radial velocity resolution of 0.6 degrees to study breezes near Hong Kong International Airport, China.

Pokhrel and Lee (2011) applied the Atmospheric to Computational Fluid Dynamics (A2C) transport and diffusion (t&d) model to simulate breezes over the western peninsula of the city of Incheon, Korea. Their modeling results showed a strong land breeze at 06:00 local time with a maximum speed of 1.5 m/s, weakening between 09:00 and 10:00. This was followed by a sea breeze, which peaked at 2.5 m/s around 15:00 when the surface-air temperature difference reached approximately 15 Kelvin. The sea breeze dissipated between 20:00 and 22:00 as the land breeze re-developed.

Grachev et al. (2017) combined observational data and measurements from a research vessel to study land and sea breezes off the coast of North Carolina, USA.

UNIVERSITEIT VAN PRETORIA
UNIVERSITY OF PRETORIA
YUNIBESITHI YA PRETORIA

Their experiment measured air–sea and land coupling using tower observations and found wind speeds between 4 and 5 m/s during breeze events (Grachev et al., 2017). Similarly, observational studies along the Red Sea recorded average onshore wind speeds of 2 m/s, with a maximum of 7.2 m/s (Khan et al., 2018).

Arrillaga et al. (2018) used observational data from the Cabauw Experimental Site for Atmospheric Research (CESAR) in the Netherlands to examine the effects of land and sea breeze fronts on local turbulence and boundary layer characteristics.

All these studies confirm that land and sea breezes influence the UHI in coastal cities by moderate temperature, sea breezes during the day and land breezes at night.

Table 1.2: A list of high-resolution studies of atmospheric circulations versus land and sea breezes in global cities

	Authors	Model/instrument	Resolution	City
1	Case (2002)	Wind profilers		Florida, USA
2	Lee and Shun (2003)	Terminal Doppler Weather Radar (TDWR)	Doppler radar range 0.6 degree	Hong Kong International Airport, China
3	Bastin *et al.* , (2006)	Méso-NH model, wind profiler, station data	3 km	Rhône Valley, France
4	Pokhrel and Lee (2011)	Atmospheric to Computational Fluid Dynamics model (A2C) transport and diffusion (t&d)	2-4 km	Incheon, Korea
5	Grachev *et al.,* (2017)	R.M. Young sensor, observations		North Carolina, United States of America
6	Lehoczky et al., (2017)	MODIS+observations	1 km	Valencia, Spain
7	Arrillaga *et al.,* (2018)	Observational studies, Cabauw Experimental Site for Atmospheric		Netherlands
8	Khan *et al.,* (2018)	station data,MERRA data	MERRA-50 km	Red Sea, Saudi Arabia

1.1.8 Adaptation and Mitigation strategies for urban heat islands

Although the UHI phenomenon impacts people living in cities, leading to discomfort and fatalities. There are some adaptations and mitigation strategies that can reduce its impacts. These include (i) increasing water bodies in cities, (ii) revegetation in

UNIVERSITEIT VAN PRETORIA
UNIVERSITY OF PRETORIA
YUNIBESITHI YA PRETORIA

cities and (iii) applying highly reflective paints to buildings (Gubler *et al.*, 2021). According to Xu *et al.,* (2013), urban areas with green spaces and cool roofs (Estrada *et al.*, 2017) function as a buffer against the UHI effect and reduce heat stress during heat waves. Planting more trees can lower surface temperatures, reducing heat related mortality (Xu *et al.,* 2013; Estrada *et al.,* 2017). This is due to the absorption of longwave radiation by vegetation and sensible heat from the in-canyon walls and roads within urban areas and the conversion of some of this energy into latent heat fluxes (Thatcher and Hurley, 2012).

In Chen *et al.,* (2015) study, it was discovered that by transforming the CBD into natural forest parkland could result in a maximum cooling potential of 2°C. The study also revealed the rate of change of all temperatures, and that two factors affect the cooling potential of urban vegetation, i.e. (i) vegetation shading and (ii) evapotranspiration. Evapotranspiration was identified as the most dominant effect, as the vegetation shading effect remains constant and depends on the amount of rainfall received (Chen *et al.,* 2015).

When comparing the rate of change of maximum, minimum and average temperatures, there was a variation of around ±20%, with the highest variation seen in the minimum temperature. This discrepancy can be attributed to daily minimum temperatures which occur at night or early morning when there is less or no solar radiation, which is the primary source of urban heat. Evapotranspiration by vegetation acts as a cooling mechanism, making it an important heat sink factor at night and during the early morning hours (Chen *et al.,* 2015). Therefore, transforming urban areas into forest parkland could reduce the number of hot days by as much as 82% to 50% as seen in the case of Melbourne, Australia. The application of urban vegetation has been shown to reduce the severity of the predicted heat stress during hot days (Chen *et al.,* 2015).

1.2 Problem statement

Urbanisation has resulted in an increase in conversion of natural surfaces to artificial surfaces, such as concrete and tarred roads, an increase in buildings, and an increase in emissions due to more road transport in cities. This has led to reduced natural and

UNIVERSITEIT VAN PRETORIA
UNIVERSITY OF PRETORIA
YUNIBESITHI YA PRETORIA

vegetated surface, which result in an increase in surface temperatures over the city, contributing to global warming and the establishment of UHI. According to the IPCC (2023) report, the difference in warming trends between urban areas and their surrounding regions is partly due to urbanisation. This effect is more pronounced in annual mean daily minimum temperatures that are more affected by urbanisation compared to annual mean daily maximum temperatures. Observation studies indicate that this phenomenon is also occurring in South Africa (Kruger and Shongwe, 2004; Kruger *et al.*, 2019).

This study focuses on the city of eThekwini, located over the southeast coast of SA, as depicted in Figure 2.1. Due to increased urbanisation, eThekwini has experienced rising temperatures in recent years. This warming is linked to reduced natural landcover and an increase in buildings, tarred roads, artificial materials and anthropogenic heating sources such as industries, vehicles, and machinery. These factors contributed to intensified UHI effects.

Furthermore, the city's growth has increased demand for resources related to sustainability, heating and transportation, thus placing pressure on city managers to develop more sustainable urban strategies. Compounding the challenge, eThekwini is facing more frequent extreme weather events as a consequence of global warming and rising anthropogenic emissions (Kruger and Shongwe, 2004).

In response, the city of eThekwini commissioned the Council for Scientific and Industrial resolution (CSIR) to lead a project titled "Cool Durban". This initiative was aimed to model the UHI effects across the city and support the development of climate adaptation strategies for informed policy making.

As part of this project, an initial modelling study was conducted at low to medium spatial resolutions (50 km and 8 km). However, these resolutions were insufficient to simulate the development of the UHI effect within the city. Consequently, high-resolution modelling at a horizontal resolution of 1 km was conducted, as it has the capability to accurately reproduce the urban climate and capture the current UHI phenomenon and project its future evolution.

UNIVERSITEIT VAN PRETORIA
UNIVERSITY OF PRETORIA
YUNIBESITHI YA PRETORIA

Urban areas, especially coastal cities, are vulnerable to the impacts of climate change and extreme weather events (Grimmond *et al.,* 2010), such as sea level rise, coastal storms, tropical cyclones as well as UHI. As a result of these impacts, city managers need to develop adaptation and mitigation strategies to reduce the negative impacts of climate change and also UHI. There is a need to study these impacts in order to understand how urban expansion influences the development and sustainability of the UHI, and to derive both adaptation and mitigation strategies to mitigate these impacts to save our planet and life in general. The output from this study will guide urban planners in future city developments in South Africa, Africa, and globally.

1.3 Research aims and objectives

1.3.1 Study aim

The aim of this project is to simulate and analyse the occurrence of urban heat islands (UHIs) over the city of eThekwini during the present climate (2006-2016), the near-future (2040-2050), and the far-future (2090-2099). The study applies the Conformal Cubic Atmospheric Model (CCAM), developed by the Commonwealth Scientific and Industrial Research Organisation (CSIRO) in Australia. CCAM functions as both a global model and a regional climate model (RCM) when operated in stretched grid mode. It is coupled with an urban climate model (UCM), known as the Australian town energy budget (ATEB) model, which resolves realistic urban characteristics as well as land surface features (Thatcher and Hurley, 2012; Luhar *et al.*, 2014; Lipson *et al.*, 2017, 2018; Chapman and Mcalpine, 2019). This coupled model could realistically simulate urban climate dynamics. The model setup also incorporates updated land cover and measured urban parameters, including anthropogenic emissions. This shows improvement compared to the default land surface features applied in the initial setup.

1.3.2 Study objectives

The objectives of the study are as follows:

1.3.2.1. To investigate how the updated land surface parameters incorporated into the ATEB model parameterization scheme has improved the simulation of the UHI over eThekwini during the present climate (2006-2016).

UNIVERSITEIT VAN PRETORIA
UNIVERSITY OF PRETORIA
YUNIBESITHI YA PRETORIA

The first objective was achieved by setting up the CCAM at a high horizontal grid resolution of 1 km with updated land surface features and the measured city parameters within the ATEB model as boundary conditions for the present climate (this is shown schematically in Figure 2.2). The first step was to perform 50 km resolution CCAM downscaling, nudged within European Centre for Medium Range Weather Forecasting (ECMWF) Reanalysis data (ERA-Interim) for the period 2006-2016 as initial conditions. The ERAI data has a horizontal resolution of approximately 79 km. Then 8 km simulations were performed, nudged within the 50 km simulations (with the output of the 50 km simulation providing both the initial and boundary conditions). Lastly, the 1 km setup with the urban scheme of ATEB model was nudged within the 8 km CCAM (with the output of the 8 km simulation providing both the initial and boundary conditions).

This system applies a variable resolution modelling, which is the procedure whereby the model is zoomed into a specific area of interest to provide improved physical and dynamical processes within that area of interest. The 1 km output for the study period (2006-2016) was analysed and compared to the observed meteorological data to evaluate the capability of CCAM to capture the UHI over eThekwini. Variables including outgoing longwave and shortwave radiation, latent and sensible heat fluxes, temperatures, and boundary layer profile were analysed over the city of eThekwini.

The current setup is motivated by the fact that during the initial stages of the project, CCAM was run using default landcover (as shown in Figure 2.3a). This setup resulted in a northwest to southeast orientation of the city, leading to an incorrect representation of the UHI pattern. In this setup, CCAM was first run with the urban scheme switched off, which prevented the model from capturing the dynamic monthly and seasonal variations in vegetation and, consequently, failed to reproduce the UHI. When the urban scheme switched on, the default landcover was still unable to simulate dynamic vegetation changes but managed to reproduce the UHI.

The landcover was then updated with the 2013 version, representing the period from January to December 2013 (shown in Figure 2.3b). When the CCAM was run with the urban scheme switched off, the simulation produced a weak UHI. However, when the

UNIVERSITEIT VAN PRETORIA
UNIVERSITY OF PRETORIA
YUNIBESITHI YA PRETORIA

urban scheme was switched on, the model was able to capture the dynamic monthly and seasonal variations in vegetation, as well as accurately represent the UHI pattern. The preliminary setups, however, do not form part of the final thesis analysis.

1.3.2.2. To investigate how the UHI over the city of eThekwini changed under climate change, as a function of high emission, low mitigation scenario.

The second objective was achieved by setting up the CCAM at 50 km, 8 km, and lastly the 1 km as in objective one. However, for this experiment the reanalysis data was replaced by the four global models. These model's simulations were produced by CCAM downscaling at 50 km as part of the Coupled Model Intercomparison Project phase 5 (CMIP5) (Taylor *et al.*, 2012; Yan *et al.*, 2013), and were forced with the Representative Concentration Pathways (RCPs), RCP8.5, to provide both initial and boundary conditions to both 8 km and 1 km simulations respectively. A schematic representation of the setup is shown in Figure 2.2 (for CCAM-ERAI runs) and also Figure 3.1 (for CCAM-CMIP5 runs). Simulations were conducted for the periods 2006-2016, 2040-2050 ,and 2090-2100. The same variables outlined in objective 1 were evaluated.

1.3.2.3. To investigate the capability of the updated land surface feature within the ATEB model to simulate the UHI and its interactions with atmospheric circulations including land and sea breezes and katabatic winds over the city of eThekwini during the present climate (2006-2016).

The third objective was achieved by setting up the CCAM at 1 km resolution, nudged within the 8 km, with the 8 km nudged within the 50 km simulations, as in objectives 1 and 2. For this objective, the dynamics of the atmospheric circulations, including land and sea breezes, were studied to determine their influence in the development of UHI over the city of eThekwini. Variables including outgoing longwave radiation, shortwave radiation, latent and sensible heat fluxes, temperatures, boundary layer profile, and winds were analysed.

1.4 Research questions

The following research questions were established from the study:

UNIVERSITEIT VAN PRETORIA
UNIVERSITY OF PRETORIA
YUNIBESITHI YA PRETORIA

- Can the CCAM, together with the ATEB model with updated land surface features realistically simulate the development of the UHI over eThekwini under present-day climate?
- If so, how realistically can the CCAM and the ATEB, with updated land surface features, project the future temperature changes and the UHI over the city of eThekwini under climate change?
- Considering the updated land surface features within the ATEB model, how realistic can the CCAM simulate the dynamical interactions of the UHI and atmospheric circulations such as land and sea breezes and katabatic winds?

1.5 Motivation and significance of the study

Due to the high number of mortalities as a result of extreme weather events over the city of eThekwini, this study is relevant to city authorities with regards to climate change:

- The study is of high relevance to city managers and health authorities, as previous and current research have provided evidence that temperatures are expected to rise due to climate change. This increase is likely to intensify the UHI effect, which can also lead to heat strokes and fatalities among elderly individuals over the age of 65.
- The study will assist city managers in developing effective mitigation and adaptation strategies to address projected increase in temperatures, UHIs and heat waves.
- The study will also support disaster management in planning and implementing strategies to mitigate the projected increase in temperatures and UHIs in eThekwini as well as in other global cities.
- The knowledge gained from studying the interactions between land and sea breezes and the UHI will contribute to the design of future buildings that facilitate ventilation, thereby reducing the UHI impacts.
- The knowledge gained from improving the land surface features for future projections will enhance the modelling capabilities of the scientific community at large.

UNIVERSITEIT VAN PRETORIA
UNIVERSITY OF PRETORIA
YUNIBESITHI YA PRETORIA

1.6 Thesis outline

The thesis is structured as follows: Chapter 1 and 5 are written in thesis format. Chapter 1 provides background and introduces the UHI phenomenon along with its causes. Chapter 2, 3, and 4 are presented in the format of journal articles. However, all the references from these chapters have been consolidated and placed at the end of the thesis document.

Chapter 2, which is an already published journal article, addresses Objective 1. Chapter 3 and 4 contain manuscripts for submission to peer-reviewed journals. Chapter 3 addresses Objective 2, while Chapter 4 addresses Objective 3. Chapter 5 concludes the thesis by summarising key findings, drawing conclusions, and providing recommendations based on the study. It is important to note that the headings, tables, and figures in Chapters 2, 3, and 4 have been modified to align with the formatting used in Chapters 1 and 5 and therefore differ slightly from the original journal article formats.

UNIVERSITEIT VAN PRETORIA
UNIVERSITY OF PRETORIA
YUNIBESITHI YA PRETORIA

CHAPTER 2:

Simulation of the eThekwini Heat Island in South Africa

Preface

The work on this chapter is already published in the "Journal of Applied Meteorology and Climatology." The article went through a panel of reviews from three (3) independent, international experts within the field. The citation is provided as follows:

Robert T Maisha, Thando Ndarana, Francois A Engelbrecht, Marcus Thatcher, Mary-Jane M Bopape, Jacobus van der Merwe, Yerdashin Padayachi and Cecilia Masemola (2023) Simulation of the eThekwini Heat Island in South Africa. Journal of Applied Meteorology and Climatology, DOI: https://doi.org/10.1175/JAMC-D-21-0231.1

In this paper, a current climatology of the urban heat island (UHI) is performed over the city of eThekwini for the period 2005/6 to 2016. The CCAM was setup at a horizontal resolution of 1 km. The model was initialised with ERAI data with a grid resolution of 79 km together with measured urban parameters from the city of eThekwini. The CCAM was coupled to an urban model via CCAM-CABLE. The model runs were performed at 50 km (Africa), 8 km (South Africa) and 1 km (over the city of eThekwini). The model output was validated against two observation stations, one within the city (Durban) and the other away from the city (Mt. Edgecombe). Analysis of UHI during various seasons and diurnal range was conducted. Although few or no studies have been performed over SA cities, the current study was motivated by the availability of high-resolution model initialisation data, realistic measured city parameters, and the high-performance computing (HPC) resources.

This article was co-authored by three supervisors (Prof. T. Ndarana, Prof. F.E. Engelbrecht, Dr. Mary-Jane Bopape), one international collaborator (Dr. M. Thatcher) and three former work colleagues (Mr. Jacobus van der Oosthuizen, Ms. Cecilia Molokwane and Mr. Yerdashin Padayachi).

UNIVERSITEIT VAN PRETORIA
UNIVERSITY OF PRETORIA
YUNIBESITHI YA PRETORIA

Simulation of the eThekwini Heat Island in South Africa

Robert T Maisha[a,b], Thando Ndarana[b], Francois A Engelbrecht[c], Marcus Thatcher[d], Mary-Jane M Bopape[b,e], Jacobus van der Merwe[f], Yerdashin Padayachi[f] and Cecilia Masemola[f]

[a]South African Weather Service (SAWS), Weather Research, Pretoria, South Africa

[b]University of Pretoria, Department of Geography, Geoinformatics and Meteorology, Pretoria, South Africa

[c]University of the Witwatersrand, Global Change Institute (GCI), Johannesburg, South Africa

[d]Commonwealth Scientific and Industrial Research Organisation (CSIRO), Aspendale, Australia

[e]South African Earth Observations Network, National Research Foundation, Pretoria, South Africa

[f]Council for Scientific and Industrial Research (CSIR), Smart Places, Pretoria, South Africa

Corresponding author: Robert Maisha:
robert.maisha@weathersa.co.za/trmaisha@gmail.com

Abstract

The study evaluates the performance of the Conformal-Cubic Atmospheric Model (CCAM) in simulating an urban heat island (UHI) over the city of eThekwini, located along the southeast coast of South Africa. The CCAM is applied at a grid length of 1 km resolution with a domain covering eThekwini, in a stretched grid mode. CCAM is coupled with the urban climate model (UCM) called the Australian Town Energy Budget (ATEB). ATEB incorporates measured urban parameters including building characteristics, emissions, and albedo. It also incorporates the land cover boundary conditions obtained from the Moderate Resolution Imaging Spectro-radiometer (MODIS) satellite. The CCAM configuration applied realistically captures the orientation of the city and land cover types. Simulations of meteorological variables such as temperatures and longwave radiation reproduced the spatial distribution and intensity of the UHI. Results show that the UHI is stronger during summer and weaker in all other seasons. The UHI develops due to human factors (e.g., urban expansion, increase in anthropogenic emissions, and additional heating). Because of the city's location along the coast, the UHI simulation could be weakened by atmospheric circulations resulting from land and sea breezes. Mitigation methods such as applying reflective paints and re-vegetation of the city may increase albedo and latent heat fluxes but reduce the sensible heat fluxes and weakens the UHI. However, the UHI may not be completely eliminated since human factors and emissions constantly influence its development.

UNIVERSITEIT VAN PRETORIA
UNIVERSITY OF PRETORIA
YUNIBESITHI YA PRETORIA

Keywords: eThekwini, urban heat island, land cover, urban parameters, surface temperature, radiation

2.1 Introduction

Currently, at least more than 50% of the world's population resides in cities (Oleson *et al.,* 2011; Pokhrel and Lee 2011; Han *et al.*, 2014; Heaviside *et al.*, 2017; Zhang *et al.,* 2022; Barrao *et al.,* 2022; Canton and Dipankar 2024). Due to increasing urbanisation, this number is projected to exceed 60% towards the middle of the 21st century (Walsh *et al.,* 2013; Garuma 2018). Urbanisation growth has led to increased infrastructure demands, such as transport, water, and energy supply (Baklanov *et al.*, 2018; Garuma, 2018; Spinoni *et al.*, 2021). The development associated with urbanisation has resulted in surface modifications from natural to artificial, such as concrete and asphalt surfaces (Pokhrel and Lee, 2011; Ramamurthy *et al.*, 2014; Estrada *et al.*, 2017), and increased heating requirements.

Whilst this may represent progress, one of its consequences is that vegetation cover in cities has been reduced. This has also resulted in increased anthropogenic emissions of greenhouse gases (GHGs) and modified radiative forcing. Urbanisation, with increased GHGs contributes to global warming (Kruger *et al.*, 2019) and may influence climate change, resulting in the development of urban heat islands (UHIs; Nuruzzaman 2015; Lehoczky *et al.,* 2017; Chapman and Mcalpine 2019), whereby night-time urban temperatures are at least 2°C higher than in non-urban areas. Thus, urban growth causes an increase in nighttime temperatures, which results in the development of UHI (Karl *et al.,* 1993; Hughes and Balling 1996; Bohnenstengel *et al.,* 2011; Grimmond *et al.*, 2011; Sharma *et al.,* 2016; Wang and Li 2017; Chen and Dipankar, 2022; Lemonsu *et al*., 2023).

Artificial surfaces found in urban areas absorb shortwave radiation and radiate longwave at the end of the electromagnetic spectrum. This is attributed to the material's storage heat flux density, which is the net flow of heat per unit area, into (out) of the material (Lipson *et al.*, 2017). The situation is reversed in rural areas where vegetation results in a higher albedo, and a larger portion of the incoming shortwave radiation is reflected compared to urban areas.

UNIVERSITEIT VAN PRETORIA
UNIVERSITY OF PRETORIA
YUNIBESITHI YA PRETORIA

Consequently, the heat stored in rural areas during the day is less than the heat stored in urban areas (Baklanov *et al.*, 2018; Garuma 2018; Lehoczky *et al.*, 2017), and thus rural areas do not radiate as much longwave radiation as the urban areas. Since increases in atmospheric temperatures are caused by the absorption of longwave radiation, cities become warmer than rural areas by an average of 2°C compared to the surrounding non-urban areas (Taha, 1997; Bohnenstengel *et al.*, 2011; Walsh *et al.*, 2013; Luhar *et al.*, 2014; Nuruzzaman, 2015; Lehoczky *et al.*, 2017; Baklanov *et al.*, 2018; Garuma, 2018; Chapman and Mcalpine, 2019; Canton and Dipankar, 2024). When the temperature difference between urban and rural areas during night time is highest, this metric is used as a measure of UHI intensity (Heaviside *et al.*, 2017; Zhang *et al.*, 2022).

Wilby (2008) studied UHI intensity and air quality over the city of London. The UHI intensity was defined as the daily minimum temperature difference of at least 2°C between a station within the city and a station in a rural area. An intense nocturnal UHI was defined to occur when the temperature difference between rural and urban exceeds 4°C. The UHI was also found to be higher under clear sky conditions, low humidity, and low wind speed (Wilby, 2008; Heaviside *et al.*, 2017; Zhang *et al.*, 2022), and also high solar irradiance (Gubler *et al.*, 2021).

Heaviside (2017) studied the UHI over the city of London and its impacts on health especially during heat waves. It was found that during an intense UHI, night time temperature difference between urban and rural areas was on average 5-10°C higher, especially in larger cities and this study agrees with Bohnenstengel *et al.,* (2011); Heaviside *et al.*, (2017) and Barrao *et al.,* (2022).

Zhang *et al.,* (2022) studied the UHI intensity over the mountainous city of Chongqing, China, with a focus on the temperature difference between rural and urban stations. The study found nighttime warming in urban areas rather than in rural areas, resulting in a UHI intensity of average of 1.5°C for the mountainous city of Chongqing after 2015. The study also found that urbanisation has a statistically significant influence on daily minimum temperatures. The positive temperature trend is found to be higher during spring and summer months over urban areas.

UNIVERSITEIT VAN PRETORIA
UNIVERSITY OF PRETORIA
YUNIBESITHI YA PRETORIA

Coutts et al., (2007) studied UHI over the city of Melbourne, Australia, using different urban density levels, namely, the central business district, high, medium, low density, as well as rural areas. The study found a significant difference in the latent heat flux between rural and urban areas due to more vegetation cover and water storage in rural areas.

Lemonsu *et al.,* (2023) studied urban climate over Paris, France using a high resolution CNRM-AROME model at a resolution of 2.5 km driven by ERAI reanalysis data. This study showed that higher resolution models capture urban-scale events such as the UHI very well. The study also confirms that high resolution climate models which incorporate specific urban surface processes could be used to diagnose climate and its impacts at the city scale and their evolution in a changing climate. An increase in urbanisation is projected to lead to higher temperature in cities, thus leading to extreme climate events such as hot nights and heatwaves (Meehl and Tebaldi, 2004; Barriopedro et al., 2011; Giugni et al., 2014; Schleussner et al., 2016; Wang and Li 2021), and climate change impacts (Chen et al., 2014; Mirzaei, 2015; Garuma, 2018; Lipson et al., 2018; Chapman and Mcalpine, 2019). The UHI is aggravated by air pollutants from industries, power generation, air-conditioners, and exhaust gases as they increase anthropogenic heating (Yang *et al.*, 2013; Nuruzzaman, 2015; Zhang *et al.*, 2022). The UHI results in compromised health (Barrao *et al.*, 2022; Zhang *et al.*, 2022; Canton and Dipankar, 2024) of the urban population, through exposure to higher temperatures during heat waves, leading to respiratory illness, hospitalisation, and death (Heaviside *et al.*, 2017). Heatwaves also intensify the temperature difference between rural and urban areas during UHI (Estrada *et al.*, 2017; Barrao *et al.*, 2022; Canton and Dipankar, 2024).

Although the strength and spatial distribution of the UHI effect have been studied in various global cities, they have not been modelled for South African cities. Therefore, it is important to study UHI's and the different mechanisms responsible for their formation using both observations and high-resolution atmospheric models set up with urban-scale features (Wang and Li, 2017; Garuma, 2018). Urban climate models (UCMs) are coupled to regional atmospheric models to investigate the dynamics of the urban climate resulting from global emission scenarios and could be used for

UNIVERSITEIT VAN PRETORIA
UNIVERSITY OF PRETORIA
YUNIBESITHI YA PRETORIA

urban planning ((Thatcher and Hurley, 2012; Luhar *et al.*, 2014; Lipson *et al.*, 2017). Initially, UCMs were developed from slab models with urban settings viewed as a concrete plate composed of a modified roughness length and thermal properties (Pokhrel and Lee, 2011; Luhar *et al.*, 2014) suitable for simulating urban energy budget (Thatcher and Hurley, 2012; Spinoni *et al.*, 2021). With advances in technology and innovation, UCMs were further developed, taking into account the energy budget from roofs, roads, and walls (Masson, 2000; Luhar *et al.*, 2014). Currently, these models are built in a manner that incorporates all the urban physical parameters such as heat fluxes, radiation, and anthropogenic emissions, as done in the model applied in this study, the Australian Town Energy Budget (ATEB; Masson 2000; Thatcher and Hurley 2012; Luhar *et al.,* 2014; Garuma 2018).

The UHI existence has been inferred indirectly from observed temperature trends in South Africa. Specifically, observation studies show that temperatures have increased more rapidly in South African cities than in rural areas resulting in the UHI effect (Kruger and Shongwe, 2004). They found a statistically significant warming trend of minimum temperatures by 0.34°C/decade over urban stations. Historical simulations of surface temperatures for the period 1951-2005 using a regional climate model (RCM), based on CORDEX output, Kruger et al., (2019) showed that the model underestimated observed annual minimum temperatures by at least 0.05°C per decade.

Globally, simulations of the UHI with UCMs have been performed in various cities. Bozonnet *et al.,* (2007) modelled winds and natural convection flows over the urban street in Athens. The study found that the specific geographical features of the city can trigger winds, such as sea or mountain breezes. Such breezes are linked to the temperature variations on both micro and urban scales, thus resulting in cooler wind movement from surroundings warming and moving towards cities, thus causing warm air to rise in the city due to the UHI effect (Bozonnet *et al.*, 2007). The UHI reaches its maximum at night when wind velocity is low (Bozonnet *et al.*, 2007), and the UHI gets dispersed during windy days.

UNIVERSITEIT VAN PRETORIA
UNIVERSITY OF PRETORIA
YUNIBESITHI YA PRETORIA

In buildings with air-conditioners and condensers mounted on exterior walls, the condenser produces heat and increases the UHI within the canyons and streets (Bozonnet et al., 2007; Thatcher and Hurley, 2012). Lipson et al., (2017) applied the ATEB to study heat conduction through urban materials. The storage heat flux density of urban materials was found to affect atmospheric stability, boundary layer profile, convection and the UHI effect.

Lipson *et al.,* (2018) developed an integrated building energy demand and urban land surface model called the Urban Climate and Energy Model (UCLEM) to improve the predictability of building energy demand and to study the different impacts of urban planning decisions on current and future climate.

In this study, we apply the Conformal Cubic Atmospheric Model (CCAM) coupled to ATEB. This model functions as both a global model and a regional climate model in stretched grid mode. The CCAM has been applied in many regional climate studies, such as in Sri Lanka (Thevakaran *et al.,* 2016), Vietnam (Nguyen *et al.*, 2014), and South Africa (Engelbrecht *et al.,* 2009; Engelbrecht *et al.,* 2011; Engelbrecht *et a*l., 2015; Garland *et al.*, 2015; Muthige *et al.,* 2018; Engelbrecht *et al.,* 2019).

The ATEB was developed as an urban component of a global climate model, which takes into consideration building and street characteristics (Lipson *et al.*, 2017). It was conceptualised from the Town Energy Budget (TEB) model developed by Masson (2000), but with some customizations for Australia (Lipson *et al.*, 2017). The ATEB is a micro-scale model used to investigate the energy budget within an urban canopy layer (Mirzaei, 2015). In addition to the ability to resolve heat transfer, ATEB includes a planetary boundary layer turbulence closure parameterization (Thatcher and Hurley, 2012; Chen *et al.*, 2015). Because of its spatial scale, ATEB can simulate the urban canopy and separate different energy budget (Ramamurthy *et al.*, 2014; Garuma, 2018), and is able to simulate urban features (Han *et al.,* 2014) such as the UHI (Chen *et al.*, 2011; Garuma, 2018).

The ATEB also considers the diurnal range of temperature within the canyon by including the west and east facing walls. Additionally, ATEB incorporates a big-leaf model, which represents in-canyon vegetation, as well as the parametrisation of air

UNIVERSITEIT VAN PRETORIA
UNIVERSITY OF PRETORIA
YUNIBESITHI YA PRETORIA

conditioners to cater for energy conservation (Thatcher and Hurley, 2012; Luhar *et al.*, 2014; Lipson *et al.*, 2017). Urban parameters are applied to refine the urban surfaces within the UCMs (Garuma 2018) and also influence heat removal from building surfaces (Mirzaei, 2015). Similar types of experiments which incorporate ATEB settings were performed by Luhar *et al.,* (2014) over the city of Basel, Switzerland, and in Brisbane, Australia (Chapman and Mcalpine, 2019). Further developments of the ATEB are described in Lipson *et al.*, (2018).

This study aims to answer the following questions: 1) does the UHI exist over the city of eThekwini? 2) If so, can a climate model accurately simulate a UHI? and 3) how can the improvements in land cover data and measured urban parameters measurements enhance the simulation of the UHI? This research represents the first dynamic study of the UHI over a coastal city of South Africa. The UCM simulation is performed at a high resolution of 1 km and is coupled with a regional climate model (RCM), the CCAM as described in Taha, (1997) and Thatcher and Hurley, (2012).

The study applies the model at a high resolution with the expectation that ingesting the land use at high resolution will result in the model capturing the UHI impacts well to inform adaptation and mitigation strategies. The rest of the paper is outlined as follows: in Section 2 the data, model setup, and methodology applied are discussed, Section 3 focuses on the results, while section 4 presents the discussion and summary and draws conclusions from the study.

2.2 Data and research methods

2.2.1 Study area

The CCAM is applied at a resolution of 1 km over the eThekwini Metropolitan Municipality. The city is located along the southeast coast of the KwaZulu-Natal Province of South Africa, with its centre at 29.86°S and 31.02°E. The city is highly urbanised, especially along the coastline, as depicted in the land cover classification (Figure 2.1). According to the 2013 land cover data from Moderate Resolution Imaging Spectro-radiometer (MODIS), the city of eThekwini is highly urbanised (Figure 2.1). The dataset shows that the city extends in a southwest to northeast direction along the coast, surrounding the port. Beyond the urban area, the dominant

UNIVERSITEIT VAN PRETORIA
UNIVERSITY OF PRETORIA
YUNIBESITHI YA PRETORIA

landcover types are savanna and woody savannas, with relatively few inland water bodies apart from the Indian Ocean located to the east of the city.

The city is classified as a summer rainfall region (Cook *et al.*, 2004). It experiences a warm, fully humid, and hot summer climate (Cfa; Kottek et al., 2006; Engelbrecht and Engelbrecht, 2016), characterised by minimum temperature consistently above 18°C (Kottek *et al.*, 2006). Observation studies (e.g., Kruger and Shongwe, 2004) conducted over the period 1961-2003 at the Durban Weather station (representing the city of eThekwini) indicate a significant increase in the frequency of hot nights. These studies also show a warming trend of 0.1°C/decade for maximum temperature, and 0.346°C/decade for minimum temperature, attributed to urbanisation (Hughes and Balling 1996).

For the historical period 1951-2005, both observational data and multi-model mean of the diurnal temperature range show nighttime warming over coastal areas. This is accompanied by a decrease in the number of cold night days mostly <-2.5%/decade, which has contributed to an increase in day-time warming (Kruger et al., 2019).

Future projections for the period 2025-2095 indicate a warming trend under both Representative Concentration Pathway (RCP4.5 and RCP8.5). However, the warming is stronger and more pronounced with RCP8.5, with the number of hot days increasing approximately +2.5%/decade, including at coastal stations (Kruger *et al.*, 2019).

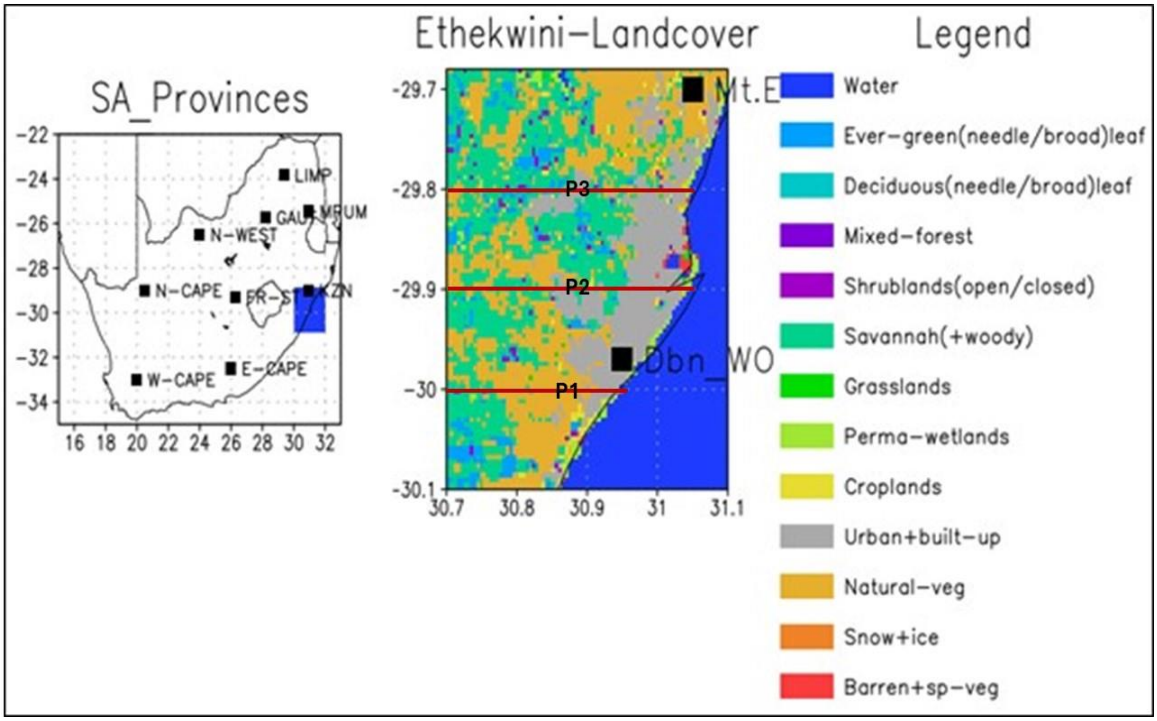

Figure 2.1: The MODIS South African with updated land cover (left) 2013, showing the city of eThekwini municipality on the east coast of Kwazulu-Natal (middle). Both Durban (to the south of the domain, 29.965°S; 30.946°E) and Mt. Edgecombe (to the northeast of the domain, 29.706°S; 31.046°E) stations are plotted. The legend is depicted (right). Urban areas are depicted in grey and are mostly distributed along the coast. Also depicted are the three latitudinal points applied for the vertical cross section.

2.2.2 The model

The CCAM was developed at the Commonwealth Scientific and Industrial Research Organisation (CSIRO) by McGregor (1996). It is both a variable and quasi-uniform resolution model that numerically solves a set of quasi-elastic equations in a terrain-following coordinate system (Engelbrecht *et al.*, 2007a) using a semi-implicit, semi-Lagrangian scheme (McGregor 1996;Reason *et al.,* 2006). The CCAM can be applied seamlessly across different spatial and time scales for both weather and climate simulations (Engelbrecht *et al.*, 2011; Thevakaran *et al.*, 2016; Chapman and Mcalpine, 2019).

[1] https://terra.nasa.gov/about/terra-instruments/modis

UNIVERSITEIT VAN PRETORIA
UNIVERSITY OF PRETORIA
YUNIBESITHI YA PRETORIA

In stretched grid mode, the CCAM is able to produce high-resolution simulations over the areas of interest. The model applies a CSIRO9 mass flux scheme based on the Arakawa mass flux scheme (Arakawa, 2004). It also uses a single-moment cloud microphysics scheme based on Rotstayn (1997). The radiation scheme is based on the Geophysical Fluid Dynamics Laboratory Coupled Model 3 (GFDL-CM3) (Freidenreich and Ramaswamy, 1999). The turbulent mixing scheme is represented by the turbulent kinetic energy as in Hurley (2007).

The CCAM is coupled to a dynamic land-surface model, called the CSIRO Atmosphere Biosphere Land Exchange (CABLE), which provides the boundary conditions to the CCAM (Kowalczyk *et al.,* 1994; Muthige *et al.*, 2018). The CCAM-CABLE incorporates the urban climate model (UCM) called the ATEB model developed by Thatcher and Hurley (2012), which incorporates urban climate processes.

2.2.3 Data collection method

2.2.3.1 Initial and boundary conditions

For this study, a hierarchy of model configurations was developed, with various datasets used. This includes grid lengths of 50 km, 8 km, and 1 km applied respectively, and is shown in Figure 2.2.

a) At a global configuration of 50 km resolution (Figure 2.2, top panel), CCAM is run with initial and lower boundary conditions obtained from the European Centre for Medium Range Forecasting (ECMWF) Interim Reanalysis data (ERAI, Dee *et al.*, 2011; Liu *et al.*, 2018; Clelland *et al.*, 2024). The dataset has a horizontal resolution of 0.75° x 0.75° and a temporal resolution of six hours (Dee *et al.*, 2011; Jones *et al.*, 2017; Liu *et al.*, 2018; Clelland *et al.*, 2024) and is valid for the period 1979-2018. However, for this study, the model is run for the period December 2005 to December 2016. The CCAM is forced at its lower boundary with the ERAI sea-surface temperatures (SST) and sea ice fields (McGregor *et al.,* 2008; Engelbrecht *et al.*, 2009; Dee *et al.*, 2011;Katzfey *et al.*, 2020), while its atmospheric fields are spectrally nudged within the ERAI reanalysis (Thatcher and McGregor, 2009). For this run, CCAM is coupled to CCAM-CABLE at a resolution of 50 km to produce static data such as bathymetry, topography, vegetation, and carbon cycle fields.

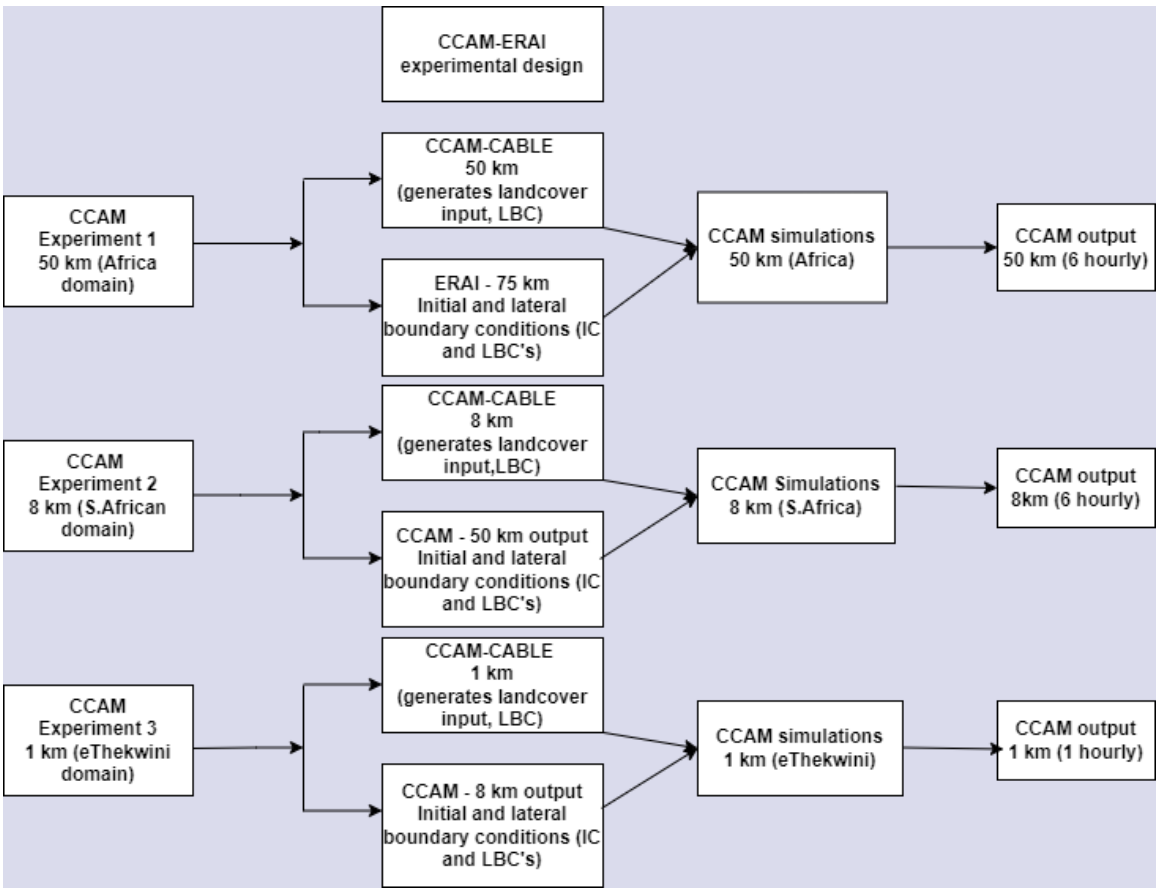

Figure 2.2: The schematic configuration of CCAM runs with ERAI data over Africa at 50 km (top), South Africa at 8 km (middle) and 1 km over eThekwini (bottom) respectively. The output from both the CCAM-CABLE and lower resolution simulations are used as initial and boundary conditions to high resolution model runs.

b) At 8 km resolution (Figure 2.2, middle panel), CCAM is initialised with the 50 km global output. For this configuration, CCAM-CABLE applies lower boundary conditions as in 50 km setting but includes updated land cover data from the high-resolution Moderate Resolution Imaging Spectro-radiometer (MODIS) satellite (https://terra.nasa.gov/about/terra-instruments/modis) which covers South Africa for the period January to December 2013 (Figure 2.1). The MODIS data were mapped to the International Geosphere-Biosphere Programme (IGBP) type 1 description of land cover used by the CCAM-CABLE system. The MODIS data has a horizontal grid spacing of 300 metres.

c) At 1 km resolution (Figure 2.2, bottom panel), CCAM is initialised with the 8 km global output. For this configuration, CCAM-CABLE also applies MODIS updated

UNIVERSITEIT VAN PRETORIA
UNIVERSITY OF PRETORIA
YUNIBESITHI YA PRETORIA

land cover for lower boundary conditions, with measured urban parameters from the city added as they define the class of the city (e.g., low, middle, high, etc.). However, a generic class has been selected and applied (Table 1).

2.2.3.2 Model validation data

For model validation, the model output is validated against two datasets.

(a) Observations from two South African Weather Service (SAWS) automatic weather stations (AWSs), one located within the city, Durban (eThekwini) and the other located away from the city, Mount Edgecombe (Mt.Edgecombe). The Durban station is located at 29.965°S; 30.946°E, at an altitude of 14 metres above mean sea level (MSL). The model height in metres shows the value of 13.99 m, which agrees with the observed station height. Mt.Edgecombe station is located at 29.706°S; 31.046°E, at an altitude of 94 metres above MSL. The model height in metres shows the value of 101,183 m, which is approximately 7m higher than the observed level.

The dataset includes hourly air temperatures and daily minimum and maximum temperatures for the period December 2005 to December 2016. The acquired raw temperature data comprises the daily hourly maximum and minimum temperatures from 01h00 to 24h00 and has been averaged at a monthly interval. The data was quality controlled, and the missing data was not filled. Because of the longitudinal location of the study area, all the results are reported at UTC + 02 hours, which is the South African Standard Time (SAST).

(b) MODIS satellite (MOD11A1.006) nighttime land surface temperature (LST) data with a horizontal grid resolution of 1 km is also used in the study. The dataset is created using a subset of the MOD11A1 products that were downloaded from Google Earth Engine over the city of eThekwini. The LST distribution has an accuracy of approximately 1 Kelvin (K). Before downloading the data, a bitmask was applied to ensure that the images are not contaminated by cloud cover using the Google Earth Engine platform's JavaScript API. This study only applied imagery with a high-quality flag (QA). The MODIS data were averaged for each of the four seasons for the period December 2012 to December 2013.

UNIVERSITEIT VAN PRETORIA
UNIVERSITY OF PRETORIA
YUNIBESITHI YA PRETORIA

2.2.4 Research process

The current CCAM experiment setup over eThekwini is required to simulate complex coupled processes due to the influence of both sea and atmospheric processes and feedback, as well as land cover and topographic features, including UHI effects (Taylor *et al.*, 2012; Yan *et al.*, 2013). For this study, a hierarchy of model configurations was developed. The CCAM was initialised using ERAI dataset at a global resolution of 79 km as described in section 2.2.3.1 above.

(i) Firstly, the CCAM-ERAI setup was applied at a quasi-uniform resolution of approximately 50 km to simulate the present-day climate, following the experimental design of (Horowitz *et al.*, 2017). The CCAM-CABLE, which is coupled to the CCAM, is set up at a resolution of 50 km with a C192 (192 x 192 grid points per panel) centered over Africa (0°S; -25°E), and a Schmidt stretch factor of 0.9523 was applied. The CCAM-CABLE produced static data such as bathymetry, topography, vegetation, and carbon cycle fields. The CCAM-ERAI simulation was performed and produced output at 6-hourly intervals as in 2.2.3.1 (a) above.

(ii) In the second step, the CCAM-CABLE was setup at 8 km over South Africa with updated land cover as described in 2.3.1 (b) above. The use of updated land cover was motivated by the initial test study with default land cover that displayed no dynamic changes in vegetation fraction and no changes in UHI throughout the various seasons. The CCAM-CABLE was set up at a resolution of 8 km with a C192 (192 x 192 grid points centered per panel) centered over southern Africa (-28°S; 25°E;) and a Schmidt stretch factor of 0. 1523. This high-resolution panel spans an area of about 1536 km x 1536 km over southern Africa, with a resolution gradually decreasing outside this region. The CCAM-ERAI output at 50 km resolution global simulations were subsequently used to provide the initial conditions for 8 km simulations, and simulation produced output every six hours.

(iii) Third, for the urban-scale modelling at 1 km, the CCAM-CABLE lower boundary conditions were updated using high-resolution MODIS land cover as in the 8 km setup. The CCAM-CABLE was also updated with measured urban parameters and emissions (Ateb-3) from the city of eThekwini shown in Table 2.1. See also *(e.g.,* Luhar

UNIVERSITEIT VAN PRETORIA
UNIVERSITY OF PRETORIA
YUNIBESITHI YA PRETORIA

et al., 2014; Chapman and Mcalpine 2019) for similar settings. The CCAM-CABLE was set up with a C192 (192*192 grid points centered per panel) centered at (30°S; 30°E) with a Schmidt stretch factor of 0.019.

Table 2.1: The city of eThekwini measured urban (generic) parameters (Ateb-3) and default CCAM parameters (Ateb-1) as well as their differences. The Ateb-3 dataset was used to setup the 1 km CCAM-CABLE.

Units	Ateb-3 (measured)	Ateb-1 (default)	Difference
Building heights (m)	5.86	6.00	-0.14
Height to width	0.24	0.40	-0.16
Vegetation fraction (%)	0.25	0.38	-0.13
Building fraction (%)	0.55	0.45	0.10
Industrial emissions ($W.m^{-2}$)	1.00	0.00	1.00
Traffic emissions ($W.m^{-2}$)	2.62	1.50	1.12
Roof albedo	0.20	0.20	0.00
Wall albedo	0.30	0.30	0.00
Road albedo	0.10	0.10	0.00
Vegetation albedo	0.20	0.20	0.00

Stretching the grid, instead of nesting the higher resolution model within a coarser resolution, helps with avoiding well-known nesting problems such as reflections of atmospheric waves at the lateral boundaries (Engelbrecht *et al.,* 2009). The CCAM-ERAI output at 8 km, generated at six-hourly intervals, was used to provide both the initial and boundary conditions for the high resolution 1 km urban-scale simulation. Measured urban parameters selected are representative of the entire urban area by averaging over factors such as heights and widths of buildings as well as roads. This is because at this resolution, individual buildings and street canyons could not be explicitly resolved, but averaged (Masson, 2000; Chen and Dipankar, 2022). In Garuma (2018), similar types of setups were described, but with 10 different urban classes. At this resolution, the model applied an integration time step of 18 seconds, with 27 vertical levels. In addition, the model applied sigma coordinates with levels

UNIVERSITEIT VAN PRETORIA
UNIVERSITY OF PRETORIA
YUNIBESITHI YA PRETORIA

from 0.9978 up to 0.0045 hPa, and the hourly output was produced to study the UHI over eThekwini.

2.2.5 CCAM validation

2.2.5.1 Statistical analysis applied

In the current studies, at least five statistics were applied in the analysis for validation, but the results focus on bias, root mean square error (RMSE) and Pearson correlation coefficient (r). Bias and RMSE were used to validate the model and observed maximum, minimum temperature and wind speed. The correlation coefficient was used to validate MODIS and model land surface temperature. The equations were applied as follows: let N be the sample size of the simulation (f) and observations (o), where $\bar{f}$ is a mean of the simulation and $\bar{o}$ is a mean for the observed. Bias (equation 2.1) measures the average difference between the model simulation and observations. The mean absolute error (MAE) measures the absolute difference between the model simulation and observations and is a measure of accuracy (equation 2.2). The mean square error (MSE) is a measure of the square of the average difference between the model simulation and observations (equation 2.3). The root mean square error (RMSE), equation (2.4) measures the square root of the mean square error. The Pearson correlation coefficient (CORR, $r_{f,o}$) equation (2.5) was used to measures the strength of the relationship between the model simulation and MODIS land surface temperature, where $r_{fO} \in [-1,1]$. A correlation coefficient of +1 indicates a perfect positive linear relationship; a value of 0 indicates no linear relationship; and a value of -1 indicates a perfect negative linear relationship between the model simulation and MODIS land surface temperature (Gordon and Shaykewich, 2000; Clelland *et al.*, 2024).

$$Bias = \frac{1}{N}\sum_{i=1}^{N}(f_i - o_i) \quad \textbf{(2.1)}$$

$$MAE = \frac{1}{N}\sum_{i=1}^{N}(|f_i - o_i|) \quad \textbf{(2.2)}$$

$$MSE = \frac{1}{N}\sum_{i=1}^{N}(|f_i - o_i|)^2 \quad \textbf{(2.3)}$$

UNIVERSITEIT VAN PRETORIA
UNIVERSITY OF PRETORIA
YUNIBESITHI YA PRETORIA

$$RMSE = \sqrt{MSE} = \sqrt{\frac{1}{N}\sum_{i=1}^{N}(f_i - o_i)^2} \quad \textbf{(2.4)}$$

$$r_{f,O} = \frac{\sum_{i=1}^{N}(f_i - \bar{f})(o_i - \bar{o})}{\sqrt{\sum_{i=1}^{N}(f_i - \bar{f})^2}\sqrt{\sum_{i=1}^{N}(o_i - \bar{o})^2}} \quad \textbf{(2.5)}$$

2.2.5.2 CCAM simulation validation

For the CCAM-ERAI model validation, the station observation dataset described in 2.3.2 (a) are used. Daily hourly averages were calculated over different seasons i.e., summer (December, January, and February-DJF), autumn (March, April, and May-MAM), winter (June, July, and August-JJA) and spring (September, October, and November-SON), using both simulations and observation datasets. The average diurnal cycle was also calculated using both datasets. The monthly average error was calculated between observations and simulated temperatures. The bias (equation 2.1) and root mean square error (RMSE, equation 2.4) were also calculated with reference to Gordon and Shaykewich (2000) for the four seasons separately as well as for the whole year.

The CCAM-ERAI minimum screen temperature was also validated against MOD11A1.006 satellite-derived nighttime LST, as described in 2.3.2 (b). The CCAM-ERAI output was re-gridded to the MODIS grid of 1 km, and spatial correlation coefficients (equation 2.5) were calculated for the four seasons. The extracted temperature data has a similar acquisition period as the MODIS land cover data (Figure 2.1).

2.3 Results

2.3.3 Surface representation over eThekwini

Results presented here are for the urban climate simulations over the city of eThekwini at a horizontal grid spacing of 1 km with updated land cover and measured urban parameters. Figure 2.3 depicts the higher-resolution default (Figure 2.23a) and updated (Figure 2.3b) urban fraction. The updated representation of the surface is more realistic because the simulation is able to identify the correct orientation and

UNIVERSITEIT VAN PRETORIA
UNIVERSITY OF PRETORIA
YUNIBESITHI YA PRETORIA

spatial distribution of the city as shown in the land cover map (Figure 2.1) and the urban fraction (Figure 2.3b).

The model setup with the default land cover data shows higher values of urban fraction spatially distributed in a southeast to a northwest direction (Figure 2.3a). However, in the simulation with updated land cover, the highly urbanised area has a southwest to northeast orientation, with more than 90% urbanised areas located along the coastline. According to Lemonsu et al., (2023), such an area is considered as dense urban.

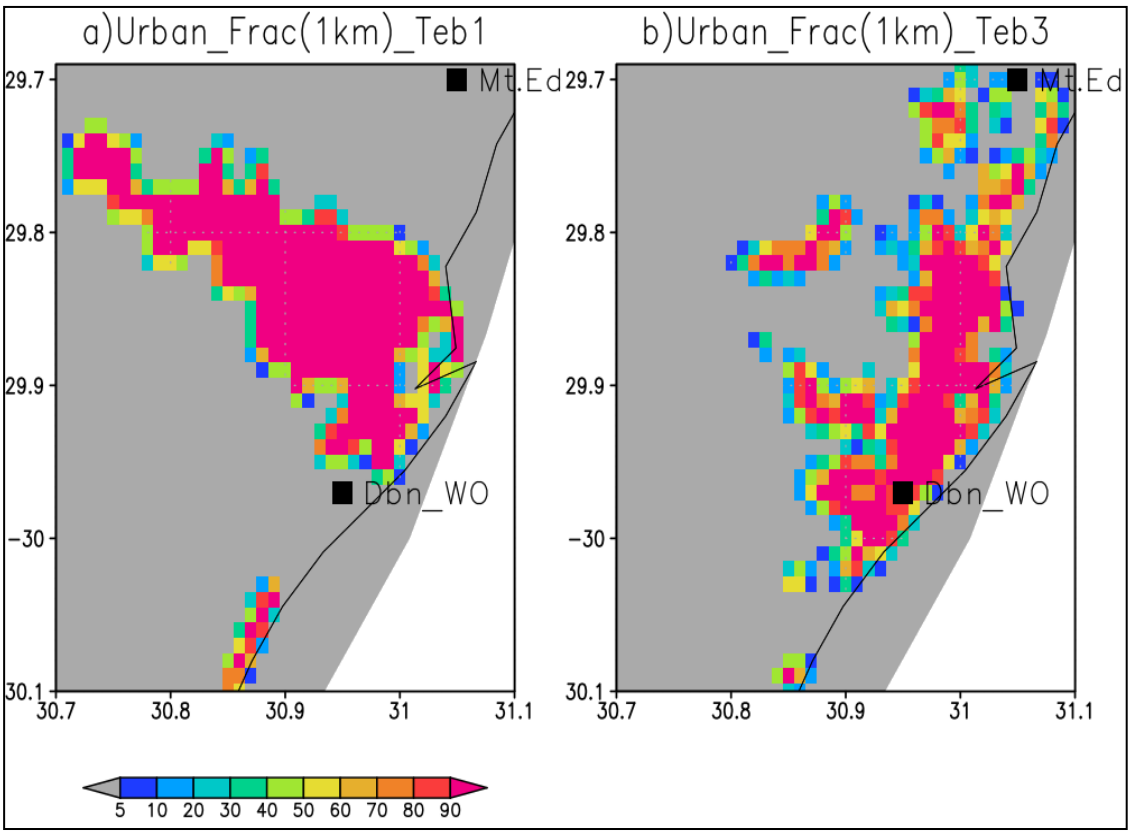

Figure 2.3: The CCAM-CABLE model's 1 km representation of urban fraction for simulation with both the default (left) and updated land cover (right) over the city of eThekwini. Both Durban (to the south of the domain, 29.965°S; 30.946°E) and Mt. Edgecombe (to the northeast of the domain, 29.706°S; 31.046°E) stations are plotted.

This area spans about (30°S-29.8°S=0.2 degree ≈20 km (north to south); and about (30.85°E-31.05°E=0.2 degree≈20 km (west to east) and is depicted in Figure 2.3b. This city is larger than the city of Bern, Switzerland, with dimensions of 10 km *11

UNIVERSITEIT VAN PRETORIA
UNIVERSITY OF PRETORIA
YUNIBESITHI YA PRETORIA

km (Gubler *et al.*, 2021). This model setup is able to capture the dynamic monthly and seasonal variability of vegetation cover (Figure A.1).

2.3.4 Comparison between observed and model simulations

2.3.4.1 Comparison with weather station data for the period 2006-2016

The study applies data from two stations available over the city of eThekwini from the SAWS network, namely Durban Weather Office and Mount Edgecombe. Their locations are shown in Figure 2.3. This observation data was compared to the CCAM-ERAI simulations. Model output data were interpolated to the two stations. Fortunately, at a 1 km resolution, the stations are either located directly on model grid points or remarkably close to the grid points, which facilitates accurate statistical analysis.

a) Monthly analysis

Monthly averages of the observed maximum, minimum and average temperatures were calculated over the 11-year period. Figure 2.4a shows the monthly maximum temperature for the Durban and Mount Edgecombe weather stations. The observed lines for Durban and Mount Edgecombe do not converge at any point throughout the year, with the maximum temperature in Durban being higher.

The CCAM-ERAI simulation captures the intra-annual temperature cycle, however, with some shortcomings. The distinction between the city and rural area is not as clear as in the observations. The Mount Edgecombe maximum temperature is simulated to be higher than in Durban in January, February, and June. The monthly time series indicates that February is, on average, the hottest month, with observed temperatures ranging from 27°C to 29°C. The CCAM-ERAI simulation shows slightly lower variability, with temperatures ranging from 28°C to 28.5°C at the two stations, less than 1°C difference compared to the observations.

The higher temperature during late summer is related to the proximity of the two stations to the Indian Ocean, due to the higher heat capacity of water. July is shown to be the coldest month linked to the southern Hemisphere winter, but with a

UNIVERSITEIT VAN PRETORIA
UNIVERSITY OF PRETORIA
YUNIBESITHI YA PRETORIA

temperature range from 22°C to 23°C for both CCAM-ERAI and observations. There is an increase in temperature from July to December, but with the highest temperature ranging from 25°C to 27°C.

The observed maximum temperature is highest at the urban station (Durban) and is higher than the model throughout all 12 months. The CCAM-ERAI simulated temperature at the urban station is also at least 1°C higher than the observed and CCAM-ERAI simulated temperature at a non-urban station (Mount Edgecombe). This analysis shows that the CCAM-ERAI simulation has underestimated maximum temperature at the urban station and overestimated maximum temperature at non-urban station, but only during summer (DJF) and autumn (MAM).

The analysis of minimum temperature is shown in Figure 2.5b. As with maximum temperature, minimum temperature is highest during February at both stations, and the model captures this. During summer, the lowest minimum temperature was simulated using CCAM-ERAI at a non-urban station, during all months. This temperature is at least 2°C lower than the observed minimum temperature at this station.

At the urban station, the CCAM-ERAI simulation and observed minimum temperatures exhibit a mixed pattern. From March to April, the modelled temperatures are higher than the observed values, while after July, the observed temperatures exceed the modelled temperatures. At the non-urban station, the CCAM-ERAI simulation consistently underestimates the minimum temperature compared to observations, and it also simulates lower temperatures than those observed at the urban station. Additionally, the observed minimum temperature at the non-urban station is higher than that at the urban station. The minimum temperature time series indicates that the model generally underestimates observed temperatures, suggesting an underestimation of both the minimum temperature and the magnitude of the Urban Heat Island (UHI) effect.

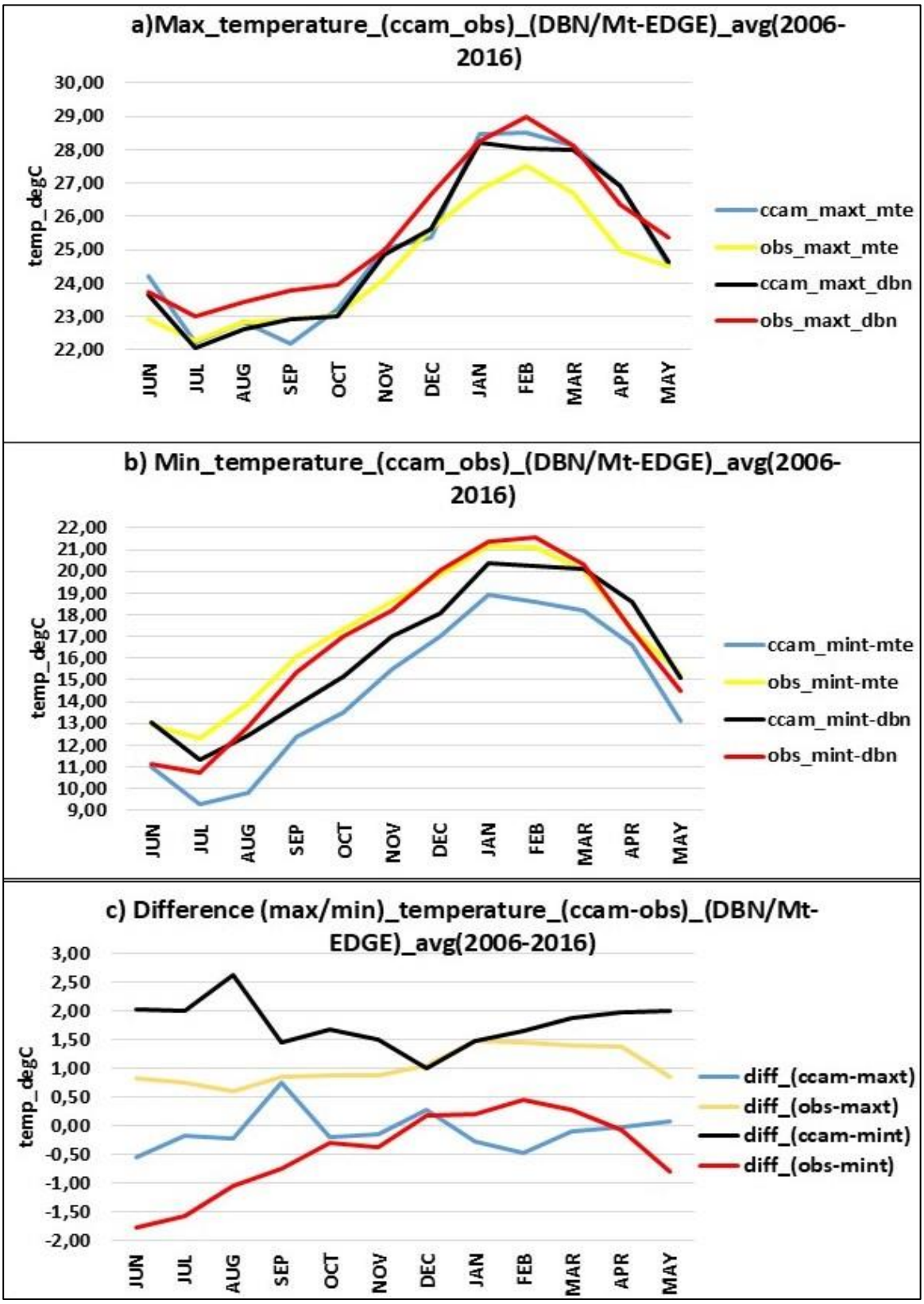

Figure 2.4: Comparison between the monthly observed and the CCAM-ERAI simulated 1 km screen temperatures (maximum, minimum and average) over the Durban and Mount Edgecombe weather stations for the period 2006-2016.

UNIVERSITEIT VAN PRETORIA
UNIVERSITY OF PRETORIA
YUNIBESITHI YA PRETORIA

The difference in model simulations and observations between the urban and non-urban stations is shown in Figure 2.5c. For maximum temperature, the model produces higher values over urban station than non-urban station throughout all months, with values between -0.5 and 0.5°C, with negative values during January, February, and June. However, the observed maximum temperature is higher at the urban station, with values ranging from 0.5 to 1.5°C, and lower values shown during May to August. For minimum temperature, the model produces higher values at the urban station, with values ranging from 1.0 to 2.5°C, as compared to the non-urban station, where higher temperatures values are recorded from January to August.

The minimum observed temperature varies between the two stations, with a positive difference ranging from 0 to 0.5°C between January, April, and December. However, the difference is negative from April to October. These values still show that the urban station is warmer than the non-urban station, which could have enhanced the UHI. This finding is also supported by the IPCC (2023) report on urban climate, which stated that the annual mean daily minimum temperature is more affected by urbanisation than the annual mean daily maximum temperature.

b) Diurnal analysis

The diurnal cycle was also assessed to determine the behaviour of temperature between the model and observations during all seasons at the two stations. All the model output and observations were written out at UTC time before plotting the results (Figure 2.5). Figure 2.5a shows a stronger diurnal range during summer (DJF) and spring (SON) at the two stations than during autumn (MAM) and winter (JJA), with an average range of approximately 6°C. The model temperature is lower at the non-urban station than at the urban station. Results also show a stronger diurnal range at the non-urban station than at the urban station. The autumn diurnal range is also similar to the summer diurnal range, but with a diurnal range higher than 6°C. Lastly, winter diurnal range is weaker, with an average range higher than 8°C.

Results show that during DJF (Figure 2.5a), the observed temperature starts increasing from around 02h00 UTC and reaches the maximum temperature at around 10h00 UTC. This tendency coincides with maximum mixing in a convective boundary

UNIVERSITEIT VAN PRETORIA
UNIVERSITY OF PRETORIA
YUNIBESITHI YA PRETORIA

layer (Efstathiou *et al.*, 2018). The simulated maximum temperature agrees with observation; this also applies to the spring season (Figure 2.5d). The diurnal range at the two stations shows some similarities between the two stations, as they are comparable during all seasons.

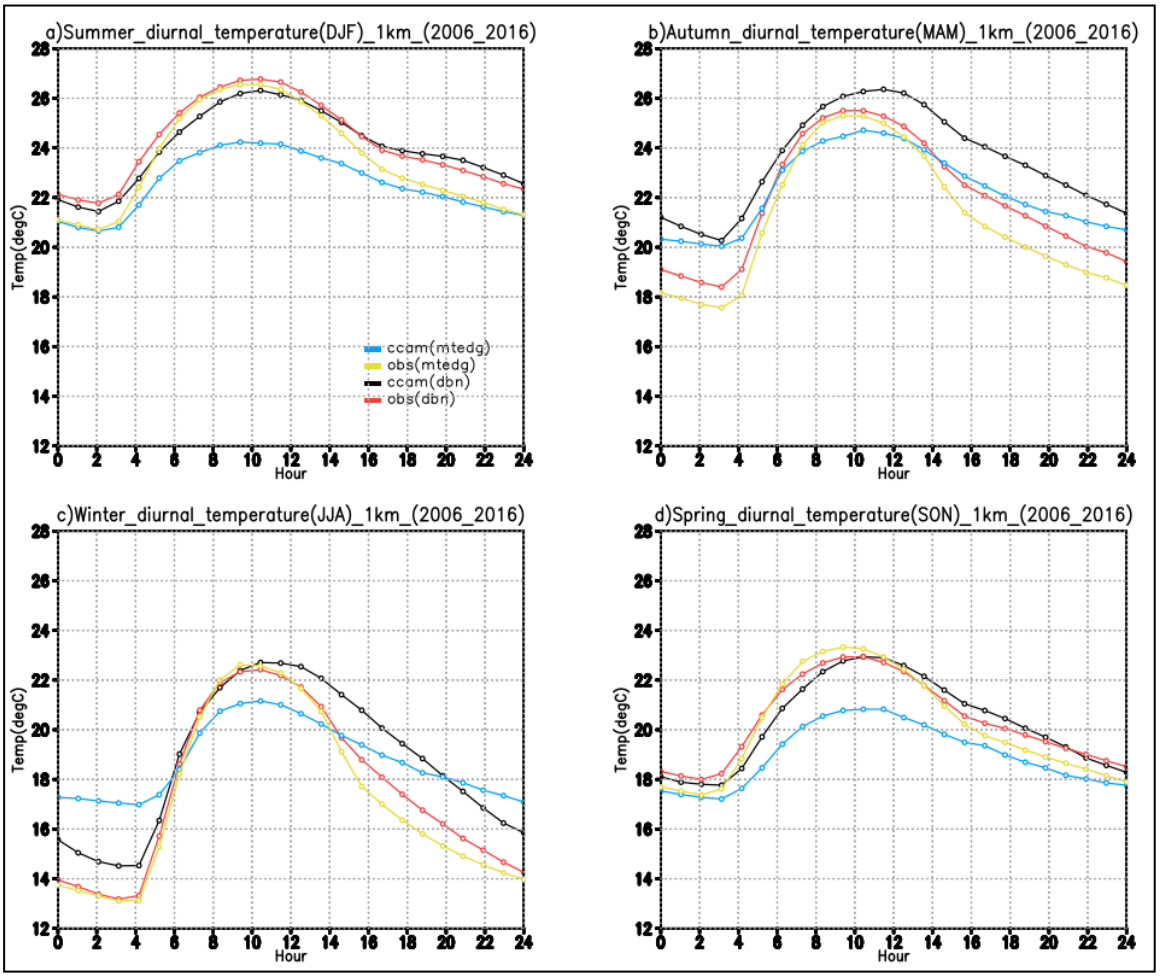

Figure 2.5: Seasonal (DJF, MAM, JJA and SON) diurnal range of air temperature between the observed and the CCAM-ERAI at 1 km simulation over Durban and Mount Edgecombe weather stations for the period 2006-2016.

The stronger summer (DJF) diurnal range provides evidence of the presence of a UHI over the city of eThekwini. The winter (JJA) profile (Figure 2.5c) shows a higher diurnal range, with a range exceeding 8°C, which is twice that of the summer profile. In the early hours (00h00 UTC to 04h00 UTC), the model temperature is higher than observed. From 04h00 UTC to 10h00 UTC, both the model and observation increase and are similar. After 10h00 UTC, the observed temperature decreases faster than the

UNIVERSITEIT VAN PRETORIA
UNIVERSITY OF PRETORIA
YUNIBESITHI YA PRETORIA

model temperature. The reason could be attributed to the radiation scheme's ability to capture the seasonal variation of the UHI.

During the transition seasons, (i) autumn, (Figure 2.5b), the diurnal range for the CCAM-ERAI simulation is nearly 6°C, while the observed range is nearly 8°C. The simulated minimum and maximum temperatures are also higher than the observed temperatures throughout the day. This profile is almost similar to the winter (JJA) profile (Figure 2.5c).

During the transition season (ii) spring, the diurnal temperature ranges from a minimum of around 17°C to a maximum of approximately 23°C, resulting in an average range of 4°C to 5°C (Figure 2.5d). The spring profile is almost similar to the summer profile (Figure 2.5a). This is the season when the UHI starts developing just before it intensifies in summer. When comparing summer and spring, the behaviour of the diurnal range shows similar attributes as in studies by Karl *et al.,* (1993). The autumn and winter profiles are also in strong agreement. The higher heat storage capacity (Bohnenstengel *et al.*, 2011) of buildings, surface materials, and pavements leads to an increased storage heat flux during the day (Ramamurthy *et al.*, 2014). At night, the stored heat is released into the atmosphere as sensible heat, which primarily drives higher nighttime temperatures. The decrease in diurnal range may be attributed to increased cloud cover during both day and night, a lowering of the cloud ceiling, and changes in surface boundary conditions (Karl *et al.*, 1993).

The summary of the validation statistics for Durban and Mt. Edgecombe stations are shown in Table 2.2. For minimum temperature, the bias is mostly negative and low over Durban and negative but high over Mt. Edgecombe. This corresponds to lower RMSE over Durban and higher RMSE over Mt. Edgecombe. This pattern applies to the two stations, except only during MAM where the bias was positive over Durban and negative over Mt. Edgecombe. This result shows that CCAM-ERAI simulation underestimates daytime heat storage and its night time release, which results in more night time cooling, as in the study by Lemonsu *et al.*, (2023). In maximum temperature, the bias is negative and low over Durban, but positive and higher over Mt. Edgecombe.

UNIVERSITEIT VAN PRETORIA
UNIVERSITY OF PRETORIA
YUNIBESITHI YA PRETORIA

Table 2.2: The validation statistics for the Durban and Mount Edgecombe weather stations observations against CCAM-ERAI simulations for the period 2006 -2016.

	Durban		Mt. Edgecombe	
MIN_TEMP	BIAS:	RMSE:	BIAS:	RMSE:
DJF	-0,83	0,93	-2,51	2,53
MAM	1,29	1,39	-1,58	1,70
JJA	-0,44	0,96	-2,99	3,11
SON	-1,69	1,73	-3,55	3,56
All_seasons	-0,42	1,25	-2,66	2,72
MAX_TEMP	Durban		Mt. Edgecombe	
	BIAS:	RMSE:	BIAS:	RMSE:
DJF	-0,68	0,81	0,80	1,14
MAM	-0,10	0,53	1,13	1,39
JJA	-0,61	0,72	0,43	0,75
SON	-0,64	0,73	0,10	0,67
All_seasons	-0,51	0,70	0,62	0,99

However, the bias is also, on average, lower over Durban than over Mt. Edgecombe. This result shows that the model underestimates the minimum temperature at both Durban and Mt. Edgecombe. It also underestimated maximum temperature over Durban but overestimates the maximum temperature over Mt. Edgecombe. These results show that, as in Lemonsu *et al.*, (2023), the model performs better at the urban than at the non-urban station. A bias value less than 1°C indicates very good model performance, and bias is lower in urban areas than in non-urban areas due to that evapotranspiration response of natural areas could be enhanced by rainfall (Lemonsu *et al.*, 2023).

2.3.4.2 Comparison of CCAM-ERAI minimum screen temperature with MODIS LST data for 2012/13

This section investigates whether the modelled nighttime UHI phenomenon is also observed by the MODIS satellite land surface temperature (LST) and if so, its spatial and temporal distribution (Figure 2.6). The CCAM output was first interpolated to the MODIS grid, and then the spatial correlations between observed and simulated

UNIVERSITEIT VAN PRETORIA
UNIVERSITY OF PRETORIA
YUNIBESITHI YA PRETORIA

temperatures were calculated. It is important to note that MODIS provides LST (at the surface) while CCAM simulates screen temperature at a height of ~ 1.5 meters from the surface.

During summer (DJF, Figure 2.6a and b), CCAM-ERAI simulation produced temperatures of dominant values 20-22°C, whereas MODIS produced values of range 22-24°C (circled) over the city, towards the east coastline. However, away from the city, CCAM-ERAI simulation produced temperature of range 12-20°C, whereas MODIS produced values of range 18-22°C. The higher values shown in MODIS is due to that MODIS show temperature produced at the surface, whereas CCAM-ERAI simulation shows temperature values at ~1.5 meters, and is therefore less than MODIS temperature.

Both the CCAM-ERAI screen temperature simulation and MODIS LST correctly reproduce the magnitude and intensity of the UHI, which covers a spatial distribution approximately 20 km*20 km, with an intensity of approximately 2°C temperature difference between rural and urban areas. This agrees with previous studies (Bohnenstengel *et al.*, 2011; Heaviside *et al.*, 2017). These results are consistent with those already presented based on the Durban (eThekwini) station, which reveals that the simulated minimum temperatures are higher than observed, further indicating that this is a general pattern across the entire high-resolution domain. The temperature distribution resembles the spatial distribution of the urban area observed in the land cover distribution (Figure 2.1); whereby higher temperatures are simulated in highly urbanised areas and lower temperatures are simulated away from urbanised areas.

During the autumn (MAM) season, the pattern remains similar to summer, but temperatures are reduced by nearly 2°C to 4°C (Figs. 2.6c and d). The UHI intensity is weakened, with a diurnal range of 2°C, but with higher temperatures along the coastlines and reduced temperatures further inland away from highly urbanised areas.

The winter (JJA) temperature distribution shows a weakening of the UHI but is not completely eliminated. This could be due to anthropogenic heating, which is higher

UNIVERSITEIT VAN PRETORIA
UNIVERSITY OF PRETORIA
YUNIBESITHI YA PRETORIA

in winter due to increased usage of natural gas, coal and electricity for heating (Coutts *et al.*, 2007).

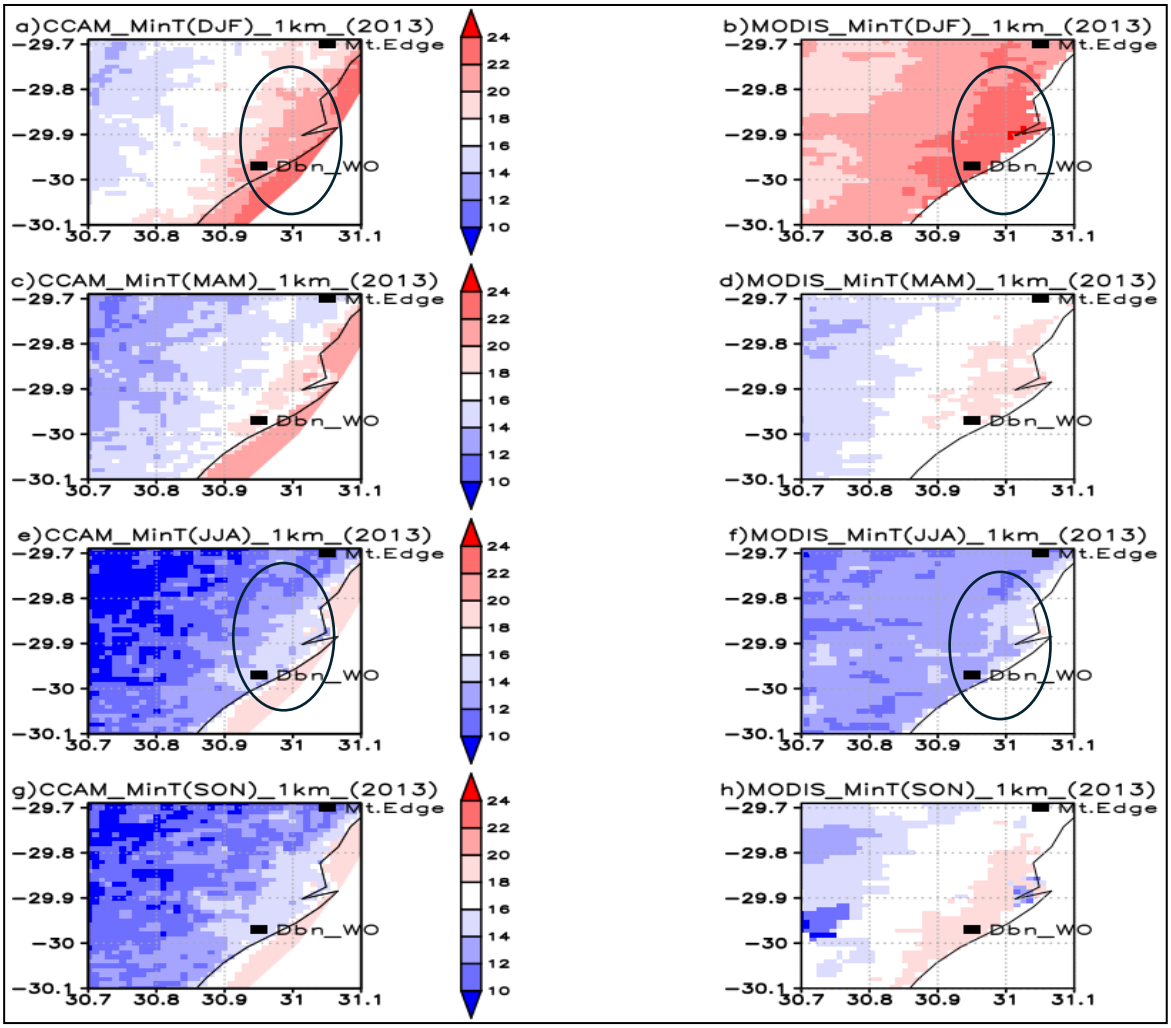

Figure 2.6: The CCAM-ERAI simulated minimum screen temperatures and MODIS representation of nighttime temperatures (LST) over the city of eThekwini for the periods DJF, MAM, JJA and SON, 2012/13. The validation period concurs with the land cover data period. Both Durban (to the south of the domain, 29.965°S; 30.946°E) and Mt. Edgecombe (to the northeast of the domain, 29.706°S; 31.046°E) stations are plotted.

In winter (JJA, Figure 2.6e and f), CCAM-ERAI simulation produced temperatures of dominant values 14-16°C, whereas MODIS produced values of range 14-16°C (circled) towards the east coastline. However, away from the city, CCAM-ERAI simulation produced temperatures of range 8-14°C, whereas MODIS produced values of range 12-14°C.

UNIVERSITEIT VAN PRETORIA
UNIVERSITY OF PRETORIA
YUNIBESITHI YA PRETORIA

During spring (SON), the UHI starts to build up and strengthen; for MODIS, the UHI is almost similar to the one seen in autumn. This observation agrees with studies by (Wilby, 2008), which shows that during spring and summer, the UHI becomes more intense. However, for the CCAM-ERAI screen temperature simulation, the UHI intensity is at most 2°C weaker than during autumn, with less magnitude than in MODIS LST (Figures 2.6g and h). In general, the CCAM-ERAI screen temperature simulated UHI intensity is at most 2°C lower than that of MODIS; this could be due to the CCAM-ERAI simulation underestimating minimum temperature.

The spatial correlation between MODIS and CCAM-ERAI simulated screen temperature distribution were also calculated; summer has the highest correlation (0.90), followed by autumn (0.88), whereas both winter and spring's spatial correlation is 0.62, respectively. This satellite-derived LST provides evidence of the spatial and temporal distribution of the UHI simulated by the CCAM-ERAI minimum screen temperature.

2.3.5 CCAM-ERAI simulation of the UHI over the city of eThekwini

2.3.5.1 UHI seasonal variation from 2005/6 to 2015/16

Improvements in land cover and measured urban settings provide an opportunity to study the temporal and spatial attributes of the UHI. Therefore, in this section, an analysis of seasonal averages of meteorological variables are performed. The screen maximum temperature simulation is displayed in Figure 2.7 and does not reproduce the spatial distribution of UHI seen in the land cover (Figure 2.1) and urban fraction graphs (Figure 2.3).

During summer, the distribution of screen maximum temperatures shows isolated areas with high values ranging between 28°C and 30°C in both urban and rural areas. This also applies to values ranging between 30°C and 32°C in both urban and rural areas. There is a decline in maximum temperatures to lower than 28°C during all three other seasons (autumn, winter, and spring) respectively (Figure 2.7). The non-existence of the UHI in screen maximum temperature confirms that the UHI is a nighttime phenomenon (Chen *et al.*, 2014; Gubler *et al.*, 2021).

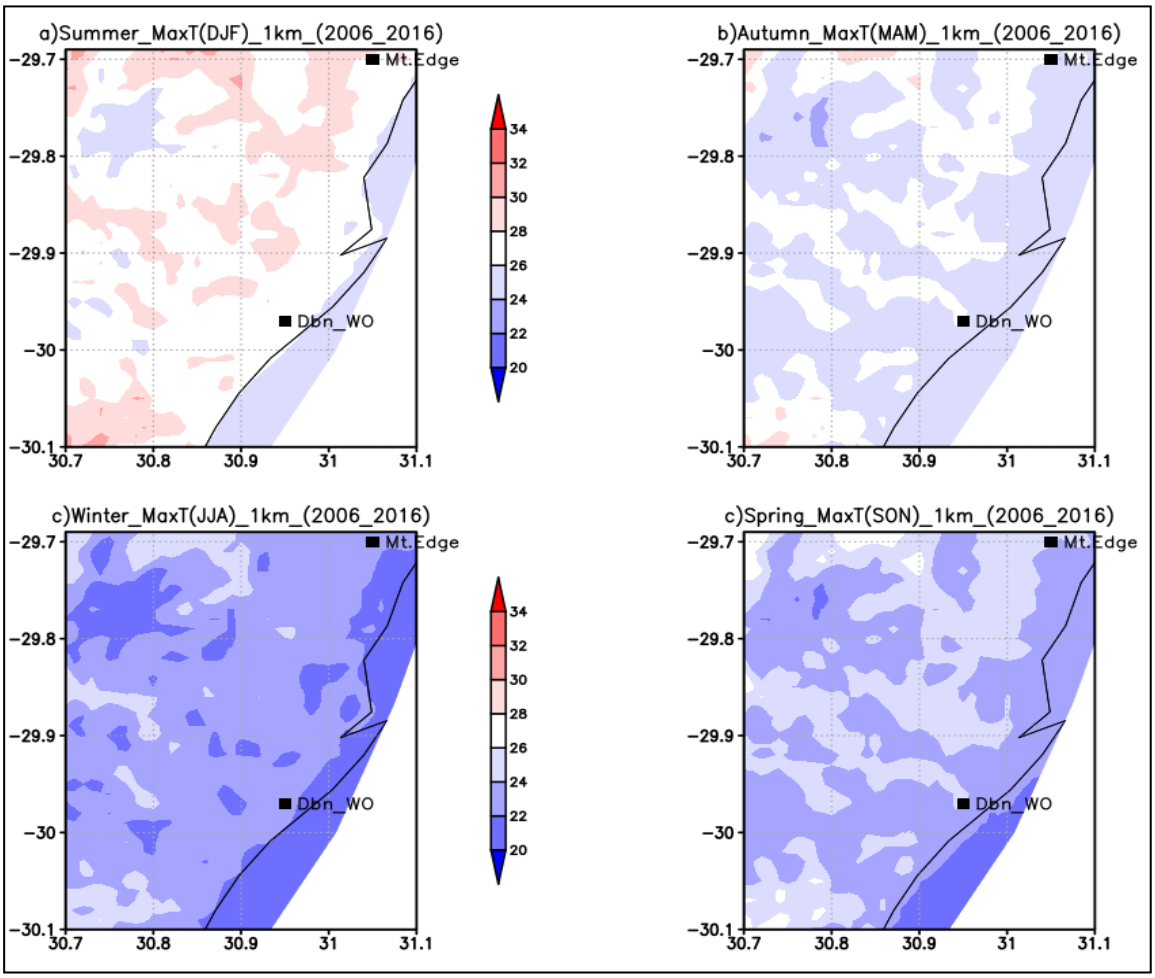

Figure 2.7: The updated CCAM-ERAI 1 km simulated maximum screen temperature over the city of eThekwini for the periods DJF, MAM, JJA and SON, 2005/6 to 2015/16. Both Durban (to the south of the domain, 29.965°S; 30.946°E) and Mt. Edgecombe (to the northeast of the domain, 29.706°S; 31.046°E) stations are plotted.

The CCAM simulated screen minimum temperature is presented in Figure 2.8 and surface temperature in Figure 2.9, respectively. There is a clear difference between the maximum, minimum and surface temperature. The CCAM-ERAI simulated screen minimum and surface temperatures show the presence of the UHI with spatial distribution similar to those of land cover (Figure 2.1) and an urban fraction (Figure 2.3). The existence of the UHI intensity is indicated by the clear difference in screen minimum and surface temperature within the city and away from the city.

The UHI is more clearly simulated during summer, with higher screen minimum temperatures averaging between 18°C and 24°C (Figure 2.8a). During the summer season, the UHI intensity has a range of at most 4°C. During autumn and spring, the

UNIVERSITEIT VAN PRETORIA
UNIVERSITY OF PRETORIA
YUNIBESITHI YA PRETORIA

screen minimum temperatures decrease (Figure s. 2.8b and c), but the UHI remains visible although weakened; its intensity is slightly reduced. The strength of the UHI increases again during spring (Figure 2.8d), which is a transition season, to reach a maximum during the summer months.

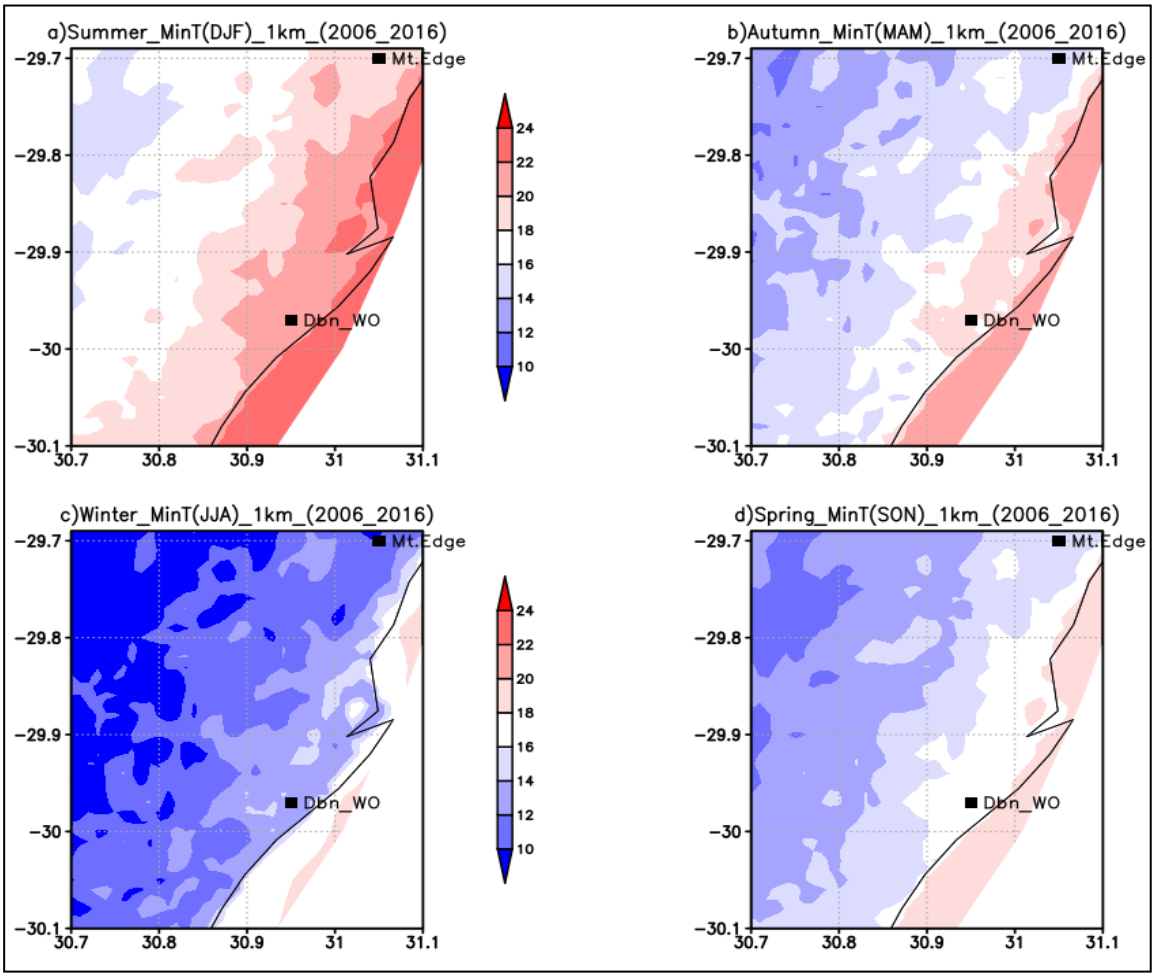

Figure 2.8: The updated CCAM-ERAI 1 km simulated minimum screen temperature over the city of eThekwini for the periods DJF, MAM, JJA and SON, 2005/6 to 2015/16. Both Durban (to the south of the domain, 29.965°S; 30.946°E) and Mt. Edgecombe (to the northeast of the domain, 29.706°S; 31.046°E) stations are plotted.

Observing surface temperatures (Figure 2.9), the UHI is stronger during summer, less strong during the transition seasons, i.e. autumn and spring respectively, and weakened during winter due to its seasonal variation (Sannigrahi *et al.*, 2017). During summer months (DJF), the highest temperature ranges from 30°C to 32°C along the coast and in some other areas with simulated UHIs. During this season, the UHI spatial

UNIVERSITEIT VAN PRETORIA
UNIVERSITY OF PRETORIA
YUNIBESITHI YA PRETORIA

coverage is similar to the distribution of land cover (Figure 2.1) and urban fraction (Figure 2.3), with an intensity of at most 4°C, similar to minimum temperature. As in minimum temperature, the UHI intensity is reduced during autumn and spring. Urban areas are characterised by artificial surfaces with high heat capacity (Akbari *et al.*, 2001; Nuruzzaman, 2015), which strengthens the UHI. It should be noted that the surface is cooler away from the UHI as a result of increased vegetation, with higher latent heat fluxes (Garuma, 2018) and less sensible heat fluxes in highly vegetated areas (Taha, 1997).

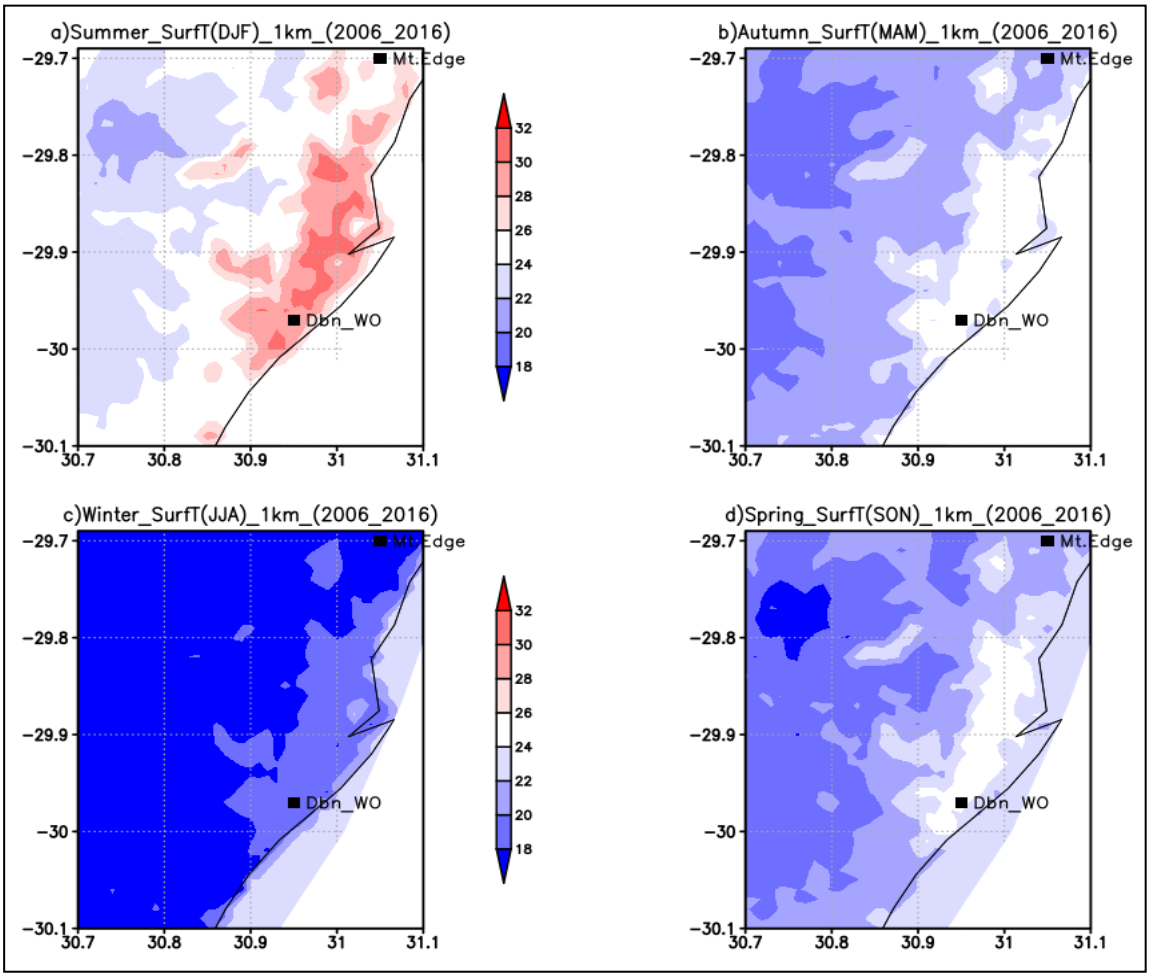

Figure 2.9: The updated CCAM-ERAI 1 km simulated surface temperature over the city of eThekwini during DJF, MAM, JJA and SON for the period 2005/6 to 2015/16. Both Durban (to the south of the domain, 29.965°S; 30.946°E) and Mt. Edgecombe (to the northeast of the domain, 29.706°S; 31.046°E) stations are plotted.

UNIVERSITEIT VAN PRETORIA
UNIVERSITY OF PRETORIA
YUNIBESITHI YA PRETORIA

The UHI is also evident in net longwave radiation at the surface, where a positive value is directed upward (Figure 2.10), with enhanced values in the urban areas during summer, autumn, and spring seasons, respectively.

During summer and spring, net longwave radiation ranges from 70 to 80 W/m^2 within the UHI and is less than 70 W/m^2 away from the UHI. During autumn, these values are further enhanced to values higher than 80 to 90 W/m^2 within the UHI and values less than 80 W/m^2 away from the UHI.

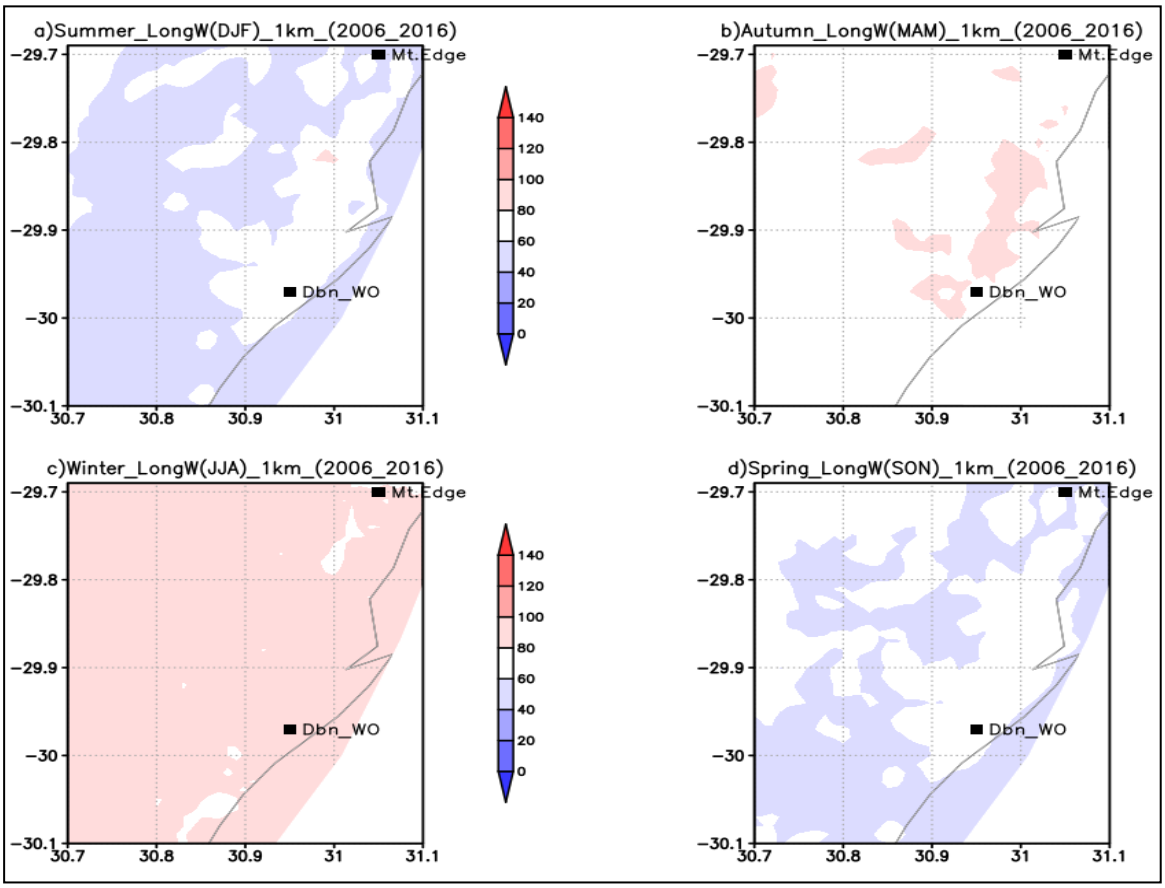

Figure 2.10: The updated CCAM-ERAI 1 km simulated net longwave radiation at the ground (+ve up) over the city of eThekwini for the periods DJF, MAM, JJA and SON, 2005/6 to 2015/16. Both Durban (to the south of the domain, 29.965°S; 30.946°E) and Mt. Edgecombe (to the northeast of the domain, 29.706°S; 31.046°E) stations are plotted.

However, during winter, there is no indication of the UHI, but net longwave radiation values remain high, ranging from 80 to 100 W/m^2. Garuma (2018) attributed higher values of net longwave radiation in cities to both an increased UHI and amplification by pollutants. From this simulation, it is obvious that factors such as high

UNIVERSITEIT VAN PRETORIA
UNIVERSITY OF PRETORIA
YUNIBESITHI YA PRETORIA

urbanisation, low vegetation, anthropogenic heating, and resultant longwave radiation (Figure 2.10) contribute to high minimum and surface temperatures, resulting in the development of the UHI during the summer season.

Vegetation fraction (Figure A.1) was also analysed for the four seasons and compared to urban fraction (Figure 2.3). In summer, it showed that areas located over the city have a vegetation fraction less than 50%, dominated by an urban fraction higher than 90%. As one moves away from the city, the urban fraction is reduced to less than 10%, and vegetation fraction increases to more than 60%. The distribution of vegetation fraction in summer and autumn seasons remains similar. During winter, most parts of the domain have a vegetation fraction of less than 50%, with small areas away from the city having a vegetation fraction ranging from 60 to 70%. This is almost similar to the vegetation distribution during spring, but there is a slight increase in vegetation fraction of 50 to 60% in some areas away from the city.

The distribution of shortwave radiation (Figure A.2) indicates that it is higher in summer over the city, with values exceeding 229 W/m^2. In autumn, shortwave values average 160-180 W/m^2 over the city. In winter, values drop to less than 160 W/m^2 over the city. The amount of shortwave radiation starts to increase again during autumn, leading to radiation ranging from 180 to 200 W/m^2, slightly higher than autumn. However, this distribution does not show the presence of the UHI.

Net radiation (Figure A.3), which is the difference between shortwave and longwave, shows an agreement with longwave radiation (Figure 2.11). In summer, a UHI is depicted, with net radiation averaging 140-60 W/m^2 over the city, indicating that net radiation is trapped within the city. During autumn, winter, and spring, there is no sign of the UHI in net radiation. However, net radiation is reduced in autumn, with the lowest values in winter, averaging less than 60 W/m^2 over the city. Net radiation strengthens again in spring, with average values ranging from 120 to 160 W/m^2 over the city, with no evidence of the UHI. The distribution of longwave, shortwave, and net radiation provides evidence that the UHI is simulated over the city of eThekwini during summer. This effect is driven by human factors such as urbanisation and

UNIVERSITEIT VAN PRETORIA
UNIVERSITY OF PRETORIA
YUNIBESITHI YA PRETORIA

anthropogenic heating which influences the distribution of longwave radiation within urban areas.

The distribution of sensible heat flux (Figure A.4) shows the distribution of the UHI during all four seasons. In summer, sensible heat flux averages 100-140 W/m^2 over the city, contrasting with latent heat flux values of less than 60 W/m^2. Sensible heat is reduced to values of 60-80 W/m^2 during autumn, while latent heat flux remains similar to summer values. Sensible heat flux is further reduced to its lowest values of less than 40 W/m^2 during winter, accompanied by the lowest values of latent heat flux, averaging 40-60 W/m^2.

During spring, sensible heat increases again to average values of 60-100 W/m^2, but latent heat fluxes remain low, with values similar to the summer profile. The distribution of sensible heat flux shows that it is enhanced by anthropogenic heating, as it opposes the distribution of latent heat flux. There is not much increase in latent heat during all seasons, indicating less evaporation, which suggests that there is less water available for evaporation, thus enhancing sensible heat flux. Therefore, these results provide evidence that the UHI is also caused by anthropogenic heating.

2.3.5.2 UHI seasonal diurnal range for 2005/6 to 2015/16

In this section, the analysis focuses on the seasonal diurnal range of surface variables, revealing a 24-hour pattern in meteorological variables over the city. Figure 2.11 illustrates the diurnal range of surface temperatures, boundary layer, net longwave and net shortwave radiation, and latent and sensible heat fluxes.

The surface temperature profile exhibits a similar diurnal range pattern across all seasons (Figure 2.11a), with various strengths. The profiles for summer and autumn are nearly identical and exhibit small variation (less fluctuation) compared to those for winter and spring, respectively. The diurnal temperature range (DTR) for the four seasons is approximated as follows: DJF (black), DTR~5°C (26-21); for MAM (green), DTR~6°C (26-20); for JJA (yellow), DTR~9°C (23-14), and for SON (red), DTR~5°C (23-18).

UNIVERSITEIT VAN PRETORIA
UNIVERSITY OF PRETORIA
YUNIBESITHI YA PRETORIA

Figure 4.12 shows the 24 hours spatial and temporal distribution of surface temperature, longwave radiation, sensible heat fluxes and planetary boundary layer of the CCAM-ERAI driven simulations for DJF period 2005/6-2016. Together, these diurnal ranges indicate that during late hours (after 16h00 UTC), excess heat is not released by the surface, contributing to the UHI effect. Kruger and Shongwe (2004) attributed the negative diurnal temperature trends at stations across South Africa to minimum temperature trends being higher than the maximum temperature trends, due to urbanisation. Additionally Karl *et al.*, (1993) and Hughes and Balling (1996) noted that in South Africa, the temperature diurnal range decreases significantly in spring and increases strongly in autumn, primarily due to an increase in nighttime temperature.

In a modeling experiment by Karl *et al., (*1993), it was found that an increase in gases such as CO_2, sensible heat exchange, and evaporation can reduce the diurnal temperature range, this has been attributed to water vapour feedback. The findings from the current CCAM-ERAI simulated study agree with the previous studies (e.g., Karl *et al.*, 1993; Hughes and Balling, 1996), indicating that increased urbanisation plays a role in reducing the diurnal temperature variation. This is in comparison to contribution of greenhouse gases, seasonal and latitudinal changes in incoming solar radiation, etc. (Karl *et al.*, 1993; Hughes and Balling, 1996).

The daytime variation of the planetary boundary layer height is depicted in Figure 2.11b, whereby the diurnal ranges are similar during all seasons. However, the DJF diurnal range is nearly 100m less than in other seasons, followed by the MAM season's diurnal range. The PBL height ranges from 350 m to 400 m in the morning, to values between 850 m to1000 m in the afternoon, resulting in a range of approximately 600 m to 650 m. This could be due to the total energy flux on the surface, which is strongest in the afternoon, resulting in the deep boundary layer (Chen and Dipankar, 2022). The diurnal range of net longwave radiation on the ground (positive, up) is shown in Figure 2.11c. Its diurnal range is strongest in summer, with the lowest range of 35 W/m^2.

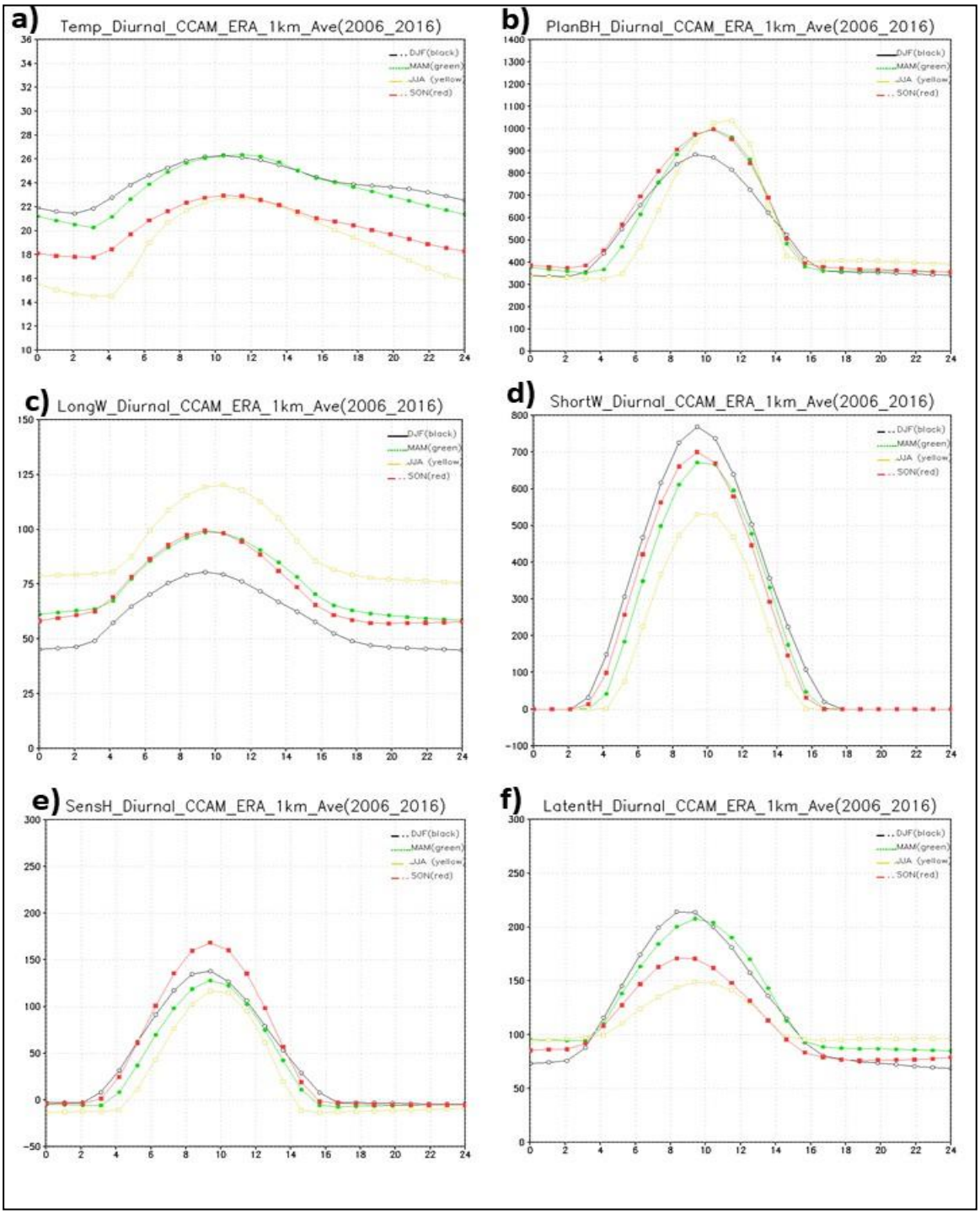

Figure 2.11: The updated CCAM-ERAI 1 km simulated diurnal range of (a) surface temperature, (b) boundary layer profile, (c) net longwave at the ground (+ve; up) and (d) net shortwave radiation at the ground (+ve; down); (e) sensible heat flux and (e) latent heat flux over the city of eThekwini for the periods DJF, MAM, JJA and SON, 2005/6 to 2015/16.

This is followed by the transition seasons, autumn and spring, both with a diurnal range of 40 W/m^2. Winter has the highest diurnal range, with a value of 40 W/m^2. For

UNIVERSITEIT VAN PRETORIA
UNIVERSITY OF PRETORIA
YUNIBESITHI YA PRETORIA

sensible heat fluxes (Figure 2.11e), a strong variation exists during spring, with a range of ±170 W/m^2, followed by summer (±140 W/m^2), autumn, and lastly winter (<130 W/m^2).

For latent heat (Figure 2.11f), the diurnal cycle varies with seasons, showing a strong variation during summer (75-210 W/m^2, range ±135 W/m^2), followed by a less significant variation in autumn (100-200 W/m^2, range 100 W/m^2) and spring (85-170 W/m^2, range 85 W/m^2), and lastly a minor variation in winter (100-150 W/m^2, range 50 W/m^2). Changes in diurnal range have been attributed to increased cloud cover and its changes, which reduce incoming solar radiation during the day, leading to reduced maximum temperature and increased net longwave radiation at night, thereby increasing nighttime temperature and reducing its diurnal range (Easterling *et al.*, 2000). Kruger *et al.,* (2019) found that changes in minimum and maximum temperatures affect diurnal range due to their influence of either local or microscale climate.

All these simulation results confirm the presence of a nighttime UHI over the city of eThekwini during summer, where the ground and building materials hold onto more solar energy during the day (Lipson *et al.*, 2017), instead of releasing it, resulting in a lower rate of radiant cooling at night (Wilby, 2008). Additionally, the availability of anthropogenic heating from air-conditioners increases heat in the cities. However, the existence of atmospheric circulation such as sea breezes could have reduced the strength of the UHI. It is noteworthy that the 2015/16 season experienced the strongest El Ñino over the 11-year period (Blamey *et al.*, 2018). Therefore, there might be a relationship between the UHI and El Ñino, as El Ñino is known to lead to reduced rainfall and almost certainly higher surface temperatures. This comparison demonstrates that the current CCAM-ERAI simulation setup is capable of simulating the urban climate of eThekwini and could be applied in future simulations.

Additionally, the 24 hour spatial and temporal distribution of surface temperature, longwave radiation, sensible heat fluxes and planetary boundary layer alongside wind from CCAM-ERAI driven simulations for the DJF period 2005/6-2016 is shown in Figure 2.12. The surface temperature (Figure 4.12a -d) shows that the UHI starts

UNIVERSITEIT VAN PRETORIA
UNIVERSITY OF PRETORIA
YUNIBESITHI YA PRETORIA

to develop from 13h00 UTC (15h00 SAST) and persists throughout the night and starts to dissipate in the early hours of the morning (06h00 UTC, 08h00 SAST) and vanish by midday.

This observation is consistent with the analysis of the UHI in Karl *et al.*, (1993). A similar spatial and temporal distribution is observed in longwave radiation (Figure 2.12e-h) as well as in the boundary layer (Figure 2.12m-p). However, for sensible heat flux (Figure 2.12i-l), an island of enhanced flux is observed from 13h00 to 18h00 UTC (15h00-20h00 SAST). The distribution of sensible heat flux indicates that less heat is released between 19h00 and 06h600 UTC (21h00-08h00 SAST). Thus, it can be deduced that this heat could have been either stored, thus enhancing the UHI, or converted to latent heat flux.

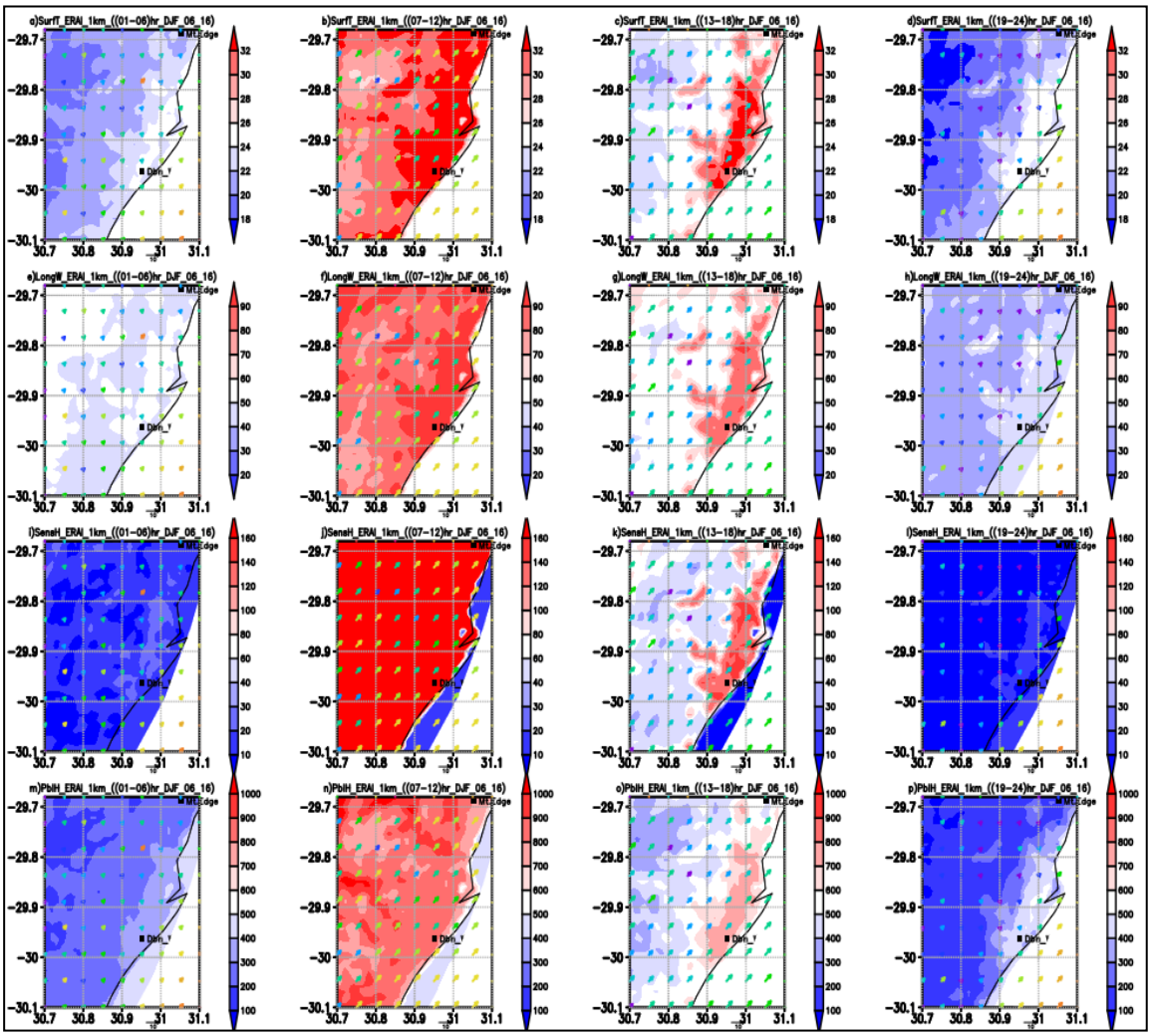

Figure 2.12: The spatial and temporal distribution of (surface temperature, longwave radiation, sensible heat fluxes and planetary boundary layer) versus wind with ERAI driven

UNIVERSITEIT VAN PRETORIA
UNIVERSITY OF PRETORIA
YUNIBESITHI YA PRETORIA

simulations for DJF period 2005/6-2016. Both Durban (to the south of the domain, 29.965°S; 30.946°E) and Mt. Edgecombe (to the northeast of the domain, 29.706°S; 31.046°E) stations are plotted.

2.4 Discussion

In this study, the climate of the UHI during the period 2005 to 2016 is discussed. The UHI was simulated with a CCAM-ERAI setup, coupled to the land surface model, called CABLE. The CCAM-CABLE allows the user to change land cover, with an option of 17 IGBP vegetation classes ranging from water bodies to various land cover types. CABLE includes an option to apply measured urban parameters, such as building characteristics, emission sources, and reflectivity.

In the current study, CCAM-ERAI simulations were performed with updated landcover, where it was found that by updating the land cover to show various land use types, and urban parameters, this influenced the intensity of the UHI. When the model was running with the default land cover, the setup produced the wrong orientation of the city. When the land cover was updated and the urban parameters switched on, there were dynamic changes in vegetation throughout the different seasons, and also dynamical changes in the simulated UHI.

In this study, the CCAM-ERAI simulated urban fraction shows that the city is approximately 90% urban, a level classified as dense urban according to Lemonsu *et al.*, (2023). In this city, vegetation cover is lower and there are more impervious materials, which increases the UHI and its intensity, and this agrees with previous findings, (e.g., Sannigrahi *et al.,* 2017). Therefore, increasing vegetation, ventilation and greening of urban spaces (Heaviside *et al.*, 2017; Zhang *et al.*, 2022) improves the development of daytime boundary layers since they alter the surface energy balance (Sharma *et al.*, 2016), cools the urban space and increase evapotranspiration. Additionally, green and cool roofs and pavements help mitigate the effects of the UHI (Estrada *et al.*, 2017).

In cities, sensible heat and heat storage dominates in summer, and latent heat is small, which influences the UHI (Coutts *et al.*, 2007). More vegetation within the canyon (in-canyon vegetation) helps reduce urban temperatures, as vegetation absorbs both

UNIVERSITEIT VAN PRETORIA
UNIVERSITY OF PRETORIA
YUNIBESITHI YA PRETORIA

longwave radiation and sensible heat fluxes from roads and walls, thereby increasing latent heat (Thatcher and Hurley, 2012).

In this study, the albedo from roofs, walls and roads is similar to the default albedo (0.2). Previous studies have shown that darker materials cause an increase in surface temperatures in cities (Taha, 1997; Synnefa *et al.*, 2006; Nuruzzaman, 2015), with temperatures nearly 2°C higher than in rural areas (Taha, 1997; Garuma, 2018; Chapman and Mcalpine, 2019). The application of lighter and brighter colours increases the albedo to values higher than 0.25, which could therefore reduce temperatures by at most 4°C in cities (Taha, 1997; Synnefa *et al.*, 2006; Garuma, 2018), thereby eliminating the UHI and reducing energy demand for both heating and cooling (Spinoni *et al.*, 2021).

The city is located on the east coast of South Africa and is bounded by the warm Indian Ocean. Previous studies have shown that the proximity of cities to water bodies such as lakes and the ocean results in the development of sea or lake breezes, which act as UHI mitigating factors (Sharma *et al.*, 2016; Canton and Dipankar, 2024). This study has found that the UHI has an intensity of range 2-4°C, whereas in large cities, the UHI intensity could range from 5-10°C (Grimmond *et al.*, 2011; Heaviside *et al.*, 2017). Therefore, the ocean could have played a role in reducing the UHI intensity over the city of eThekwini.

The study shows that the CCAM-ERAI simulation is able to capture the spatial and temporal distribution of the UHI by reproducing the time series of seasonal variation of temperatures over both non-urban and urban stations in the eThekwini municipality. The results also indicate that the highest average monthly temperature is observed and simulated in February. The proximity to the Indian ocean is also thought to have modulated the temperature over the city of eThekwini. The observed temperature is higher in the urban station during summer, with a range 0-0.5°C for minimum temperature and 0.5-.5°C for maximum temperature, respectively.

The diurnal range is strongest during summer, especially at the urban station compared to the non-urban station, with an average range of 6°C. This variation is almost similar to the one in spring before the UHI strengthens again. During July, the

UNIVERSITEIT VAN PRETORIA
UNIVERSITY OF PRETORIA
YUNIBESITHI YA PRETORIA

temperature is the lowest, as the city receives the lowest radiation. The diurnal range in winter is the weakest, with an average of 8°C or more, and is almost similar to the autumn profile. Still, an urban station shows higher values compared to the non-urban station.

The comparison between CCAM-ERAI simulation and MODIS data also shows that during summer, the UHI intensity is on average 4°C between urban and rural areas. The UHI intensity is reduced during all other seasons, although MODIS temperature is warmer than CCAM-ERAI simulation. Likewise, the highest correlation was found between MODIS and simulated minimum temperatures in summer.

The CCAM-ERAI simulation of maximum temperatures did not provide any evidence of a UHI. The reason could be that daytime temperatures are dependent on the amount of received shortwave radiation. Also, the convective boundary layer or turbulent exchange in the near-surface layer during the day contributes to the dissipation of the UHI (Zhang *et al.*, 2022).

The current CCAM-ERAI climate simulations of surface parameters such as temperature (minimum and surface), longwave radiation, and boundary layer profile provide evidence of the existence of the UHI over the city of eThekwini. The magnitude of the area covered by the UHI stretches about 20 km (west to east) and 20 km (south to north) and is similar in distribution to land cover and areas which are more than 80% urbanised.

In the minimum temperature simulation, the UHI intensity shows its dominance during summer, where city temperature is on average 4°C higher than in rural areas. This is in agreement with findings in (Wilby, 2008). This pattern is also shown in surface temperature, but with a slightly different intensity pattern shown in minimum temperature. This is indicated by the more intense UHI shown away from the ocean, which could be due to the effects of land and sea breeze that have diluted the UHI closer to the coastline. The UHI is then weakened during autumn and spring and is almost non-existent during the winter season. The UHI is oriented in a southwest to northeast direction, most distinguished along the coastal area, and resembles the distribution of both the land cover and the urban fraction.

UNIVERSITEIT VAN PRETORIA
UNIVERSITY OF PRETORIA
YUNIBESITHI YA PRETORIA

The UHI also follows the pattern depicted by the longwave radiation, especially during summer. This is the result of shortwave radiation being trapped by urban structures as longwave radiation and not released at night. The distribution of longwave radiation has led to an increase in both surface and minimum temperatures, with the UHI intensity of urban temperatures nearly 4°C higher than in rural areas (Grimmond *et al.*, 2011; Heaviside *et al.*, 2017), which also agrees with studies by (e.g. Taha 1997; Garuma 2018). Away from urban areas, there is an increase in vegetation and a reduction in artificial materials, thereby reducing both surface and minimum temperatures. There is also increased evapotranspiration, and trees absorb more carbon dioxide. Large tree canopies help in reducing heat as they intercept light (Nuruzzaman 2015), thereby reducing the UHI.

An analysis of the diurnal range of various meteorological variables such as temperature, boundary layer, longwave and shortwave radiation, sensible and latent heat fluxes confirm the strength of the UHI. In summer, the diurnal range of temperature, boundary layer, longwave radiation, and sensible heat fluxes are strongest.

From this study, human factors contributed to the development of the UHI. The distribution of longwave radiation was identified (Coutts *et al.*, 2007), whereby an increase (decrease) in radiation was found to enhance (reduce) the development and strength of the UHI. Additionally, regional atmospheric circulations could have played a role in enhancing the UHI. Blamey et al., (2018) indicated that the El Niño climate pattern, characterised by unusually warm ocean waters, dominated the South African weather during the year 2015/16. It impacts moisture transport over the region, whereby the weakening of onshore moisture flow over the south Indian Ocean contributes to dry conditions (Blamey *et al.*, 2018). Additionally, man-made factors, including urban expansion and increased anthropogenic heating within the city, influenced the spatial and temporal distribution of the UHI (Coutts *et al.*, 2007; Wang and Li, 2017). This is also attributed to the difference in observed warming trends in cities compared to the surrounding areas as a result of increased urbanisation, leading to increased minimum and surface temperatures (IPCC,2023).

UNIVERSITEIT VAN PRETORIA
UNIVERSITY OF PRETORIA
YUNIBESITHI YA PRETORIA

These simulations have shown that an increase in both spatial and temporal resolution improved the spatial distribution of the UHI. On average, the formation of a UHI was not strong, with an average of 4°C. Heaviside et al., (2017) and Bohnenstengel *et al.,* (2011) have shown that in larger cities, the UHI intensity is between 5 and 10°C, but also in extreme cases. This could be due to the location of the city, which is situated along the east coast of SA, adjacent to the warm Indian Ocean. In this case, mesoscale circulation could result in the development of sea breezes. Such circulations are dominant mesoscale systems over coastal areas and are responsible for the dilution of the UHI (Taha, 1997; Pokhrel and Lee, 2011; Lehoczky *et al.*, 2017; Arrillaga *et al.*, 2018). Additionally, water bodies provide evaporation and reduce surface temperatures. Taha (1997) indicated that in higher latitudes, the UHI reduces energy demand for heating compared to lower latitudes since UHI increases lead to higher demand for cooling systems.

The current study has shown that the CCAM-ERAI simulation is able to reproduce the UHI over eThekwini as it captures the spatial and temporal distribution of the UHI. The UHI resulted from factors such as increased urbanisation, increased greenhouse gas emissions, reduced vegetation in cities, as well as climatic conditions (Nuruzzaman 2015). The current study has also proven that the CCAM system could be used as a tool to model urban climate at any geographical location around the globe and at any time scale. The current model configuration and results, therefore, support earlier findings by Reichler and Kim (2008) who attributed climate model performance to developments such as (i) more realistic model parametrisation; and (ii) higher resolution.

According to previous studies, increased urbanisation leads to an increase in the Bowen ratio, as sensible heat fluxes increase (due to strong surface heating) compared to latent heat fluxes, which is attributed to a reduction in surface moisture (Coutts *et al.*, 2007), as well as the replacement of natural vegetation by artificial surfaces (Ramamurthy *et al.*, 2014; Estrada *et al.*, 2017). This has also resulted in the enhancement of the UHI.

UNIVERSITEIT VAN PRETORIA
UNIVERSITY OF PRETORIA
YUNIBESITHI YA PRETORIA

The current study is essential because the occurrence of UHI in cities has a catastrophic impact on human lives. Therefore, this kind of study assists city planners when developing modern cities, enhancing researchers' understanding of how atmospheric circulations impact city climates. The UHI is due to man-made factors such as an increase in urbanisation and anthropogenic emissions. Therefore, numerical and climate modellers could use this study to understand that radiation parameters and emissions from cities, as well as urban modification including removal of natural surfaces, are important in physical parametrisation.

In this study, there were some limitations, listed as follows: (i) The study area has limited observation stations and incomplete data, which limit the study's scope. (ii) CABLE was set up with measured urban parameters, making it capable of producing the realistic orientation of the city and the dynamic change of vegetation within cities. Therefore, not having the required and latest land cover data impacts on the results of urban modelling studies, as it would not reproduce the realistic UHI. In Africa, this dataset is, however, not easily accessible except from large global centres. Therefore, in this study, we attempted to obtain this measured data, customise it for the CCAM-CABLE to read, and prepare surface parameters. (iii) Another limitation is that the UCM allows for only one class of urban parameter to represent the entire grid during simulations. Therefore, due to the complexity of urban-scale simulation, large computing resources are required to successfully complete the model runs. (iv) The urban model study requires large computing resources, and for countries without such resources, it has a detrimental effect on high-resolution modelling studies.

From the current studies, the realistic simulation of the UHI with ERAI provides an opportunity to run the model at high resolution and project the future occurrence of UHI using CMIP5/6 data. Such future projections will be used to assist disaster management with the dissemination of information on extreme weather and climate events over the cities. However, it is important for the modellers to update the land cover and urban parameters to realistically simulate city climate in the future.

UNIVERSITEIT VAN PRETORIA
UNIVERSITY OF PRETORIA
YUNIBESITHI YA PRETORIA

2.5 Conclusion

The study aimed to evaluate the performance of the CCAM-ERAI set up at a resolution of 1 km in simulating the UHI over the city of eThekwini during the current climate from 2006 to 2016. The CCAM setup at 1 km was coupled to a land surface model (CCAM-CABLE), which considers updated landcover and measured urban parameters.

During the simulations, the urban scheme was turned on. These two changes allowed for a realistic simulation of the UHI. (i) The updated land cover data helped capture the true seasonal variability of vegetation compared to the default setup, which showed no such variability. (ii) The measured urban parameters, instead of a generic option, allowed for a realistic simulation of UHI intensity. An overestimation of these values could have resulted in an overestimation of the UHI intensity, particularly in medium or highly urbanised areas.

All these parameters show the true spatial distribution of the city, located along the warm east coast of South Africa, as compared to the default setup. The city is located at approximately 29.9°S, which is remarkably close to the subtropical high-pressure belt (30°S). The urban fraction shows that the city is more than 80% urbanised and covers an area of around 20 km by 20 km.

The monthly variation of temperature shows that CCAM-ERAI simulation underestimates maximum temperature by at most 2°C and over-forecast minimum temperature by nearly 3°C when compared to observation. An analysis of temperature diurnal range shows that it is strong in summer, with a range between maximum and minimum value around 6°C due to UHI intensity.

The comparison between CCAM-ERAI simulated temperature and MODIS temperature values show the UHI intensity at most 4°C higher in urban areas than rural areas during summer. This is in agreement with previous studies such as (Grimmond *et al.*, 2011; Heaviside *et al.*, 2017). The UHI intensity is reduced in autumn and winter but starts growing during spring, which agrees with a study by Zhang et al., (2022).

UNIVERSITEIT VAN PRETORIA
UNIVERSITY OF PRETORIA
YUNIBESITHI YA PRETORIA

The CCAM-ERAI climate simulations show no UHI in daytime maximum temperature as this is a nighttime event. The UHI is shown in minimum and surface temperature during summer, with its intensity being at most 4°C. The UHI intensity is also seen in longwave radiation during summer, with a difference of at most 10 W/m^2 between urban and rural areas. The UHI spatial distribution is similar to the urban fraction and land cover distribution. The UHI also exists during both autumn and spring, but with reduced intensity. However, it gets reduced during the winter season.

This study shows that both shortwave and longwave radiation play a role in the development, spatial distribution, and intensity of UHI. Since a shortwave is received at the surface during the day, where it is absorbed in cities. During nighttime, longwave radiation is released back into the atmosphere. However, this study shows that longwave radiation is only reduced in rural areas and is retained by urban surfaces, including roads and buildings, in cities. The combination of longwave radiation and anthropogenic heating raises the surface temperature and increases the intensity of UHI. In this study we can conclude that changes in land cover and urban parameters have assisted in simulating and identifying the UHI over the city of eThekwini.

Results of this study will further assist the municipality in deriving strategies to mitigate the impacts of climate change and also for modern urban design. This includes the use of material with high reflectivity or emissivity as they promote cooler surfaces (Taha, 1997;Synnefa *et al.*, 2006), green spaces, and water features (Wilby, 2008; Heaviside *et al.*, 2017; Zhang *et al.*, 2022). For example, the use of reflective coating could reduce the white concrete tile surface temperature by 4°C during hot summer and 2°C during the night (Synnefa *et al.*, 2006).

Future research studies will include (i) simulation of the projected urban climate of eThekwini and the occurrence of UHI under enhanced anthropogenic emissions using the different emission scenarios data from the IPCC's report, and (ii) assessing the influence of atmospheric flow dynamics such as land and sea breezes on the distribution of a UHI. We also recommend that similar studies be conducted over

UNIVERSITEIT VAN PRETORIA
UNIVERSITY OF PRETORIA
YUNIBESITHI YA PRETORIA

other South African cities to help the government with its implementation of the District Development Model.

UNIVERSITEIT VAN PRETORIA
UNIVERSITY OF PRETORIA
YUNIBESITHI YA PRETORIA

Postface

The current chapter analysed the current climate's occurrence of the UHI over the city of eThekwini. The CCAM was initialised with ERAI data. The model boundary conditions applied was from the MODIS land cover data and measured urban parameters from the city of eThekwini. The objective for this study was to assess the capability of the CCAM-ERAI simulation in modelling the UHI given the updated land cover and the measured urban parameters. Firstly, observed maximum and minimum temperatures were compared with modelled temperature at an urban station (Durban) and non-urban station (Mt. Edgecombe). These comparisons show that the model underestimated maximum temperature and overestimated minimum temperature. When compared with MODIS-LST, there was strong correlation between model and observed, with highest correlation during DJF and lowest correlation during JJA, with similar correlation scores during MAM and SON. The UHI was simulated in variables such as surface and minimum temperature. In both temperatures the UHI was clearly simulated during summer (DJF). It was weakened during transition seasons, autumn (MAM) and spring (SON). The CCAM-ERAI simulated UHI dissipated during winter (JJA) seasons. The study shows that the UHI was caused by man-made factors (the distribution of longwave radiation) and anthropogenic heating (seen in sensible heat fluxes). The UHI simulated shows strong agreement with the urban fraction distribution.

This study has shown that when CCAM-ERAI simulation was bounded with measured parameters, it could realistically simulate the current occurrence and evolution of UHI over the city of eThekwini. In the next chapter, the CCAM together with updated land cover and measured urban parameters are used to simulate the future occurrence of the UHI until the end of the 21st century. However, for these simulations, CCAM is initialised with RCP 8.5 from the CMIP5 project.

UNIVERSITEIT VAN PRETORIA
UNIVERSITY OF PRETORIA
YUNIBESITHI YA PRETORIA

CHAPTER 3:

Simulation of current and future temperature of eThekwini, South Africa

Preface

In the previous chapter, the study demonstrated that the CCAM is capable of simulating the Urban Heat Island (UHI) during the current climate period. The study detailed in this chapter is planned to be published in an accredited Journal under the title "**Simulation of current and future temperature of eThekwini, South Africa."** In the current chapter, CCAM projections of future climate during the near-future (2039/40-50), and far-future (2089/90-99) climate periods are evaluated using the period (2005/6-16) as the present-day reference period. As in the previous chapter, the CCAM is set up at a horizontal resolution of 1 km, with updated land cover and measured urban parameters. It is initialised using output from CCAM downscalings of the global climate models (GCMs) participating in the Coupled Model Intercomparison Project Phase Five (CMIP5), driven by the representative concentration pathway scenario (RCP8.5) and ERAI data but for the current climate. The datasets applied are CNR8.5, GFD8.5, MPI8.5 and NOR8.5, incorporating changes in urban expansion and emissions throughout the 21st century. In the experimental design, CCAM was first downscaled to 8 km over South Africa with CMIP5 input at a global resolution of 50 km. In the second setup, CCAM was run at a resolution of 1 km over the city of eThekwini with input from the 8 km downscalings.

UNIVERSITEIT VAN PRETORIA
UNIVERSITY OF PRETORIA
YUNIBESITHI YA PRETORIA

Simulation of current and future temperature of eThekwini, South Africa

Robert T Maisha[a,b], Thando Ndarana[b], Francois A. Engelbrecht[c], Marcus Thatcher[d], Mary-Jane M. Bopape[a,e]

[a]University of Pretoria, Department of Geography, Geoinformatics and Meteorology, Pretoria, South Africa

[b]South African Weather Service (SAWS), Weather Research, Pretoria, South Africa

[c]University of the Witwatersrand, Global Change Institute (GCI), Johannesburg, South Africa

[d]Commonwealth Scientific and Industrial Research Organisation (CSIRO), Aspendale, Australia

[e]South African Earth Observations Network, National Research Foundation, Pretoria, South Africa

Corresponding author: Robert Maisha,
robert.maisha@weathersa.co.za/trmaisha@gmail.com

Abstract

Changes in land cover and anthropogenic warming in cities has led to urban areas becoming warmer than the surrounding non-urban areas. This phenomenon has led to urban temperatures being at most 2°C higher than non-urban areas, resulting in the development of the urban heat island (UHI). To simulate the current and future occurrence of the UHI over the city of eThekwini, the Conformal-Cubic Atmospheric Model (CCAM) was configured at a resolution of 1 km with updated land cover and measured urban parameters. The CCAM was initialised with (i) the output from the global climate models (GCMs) participating in the Coupled Model Intercomparison Project Phase Five (CMIP5) driven by the representative concentration pathway 8.5 (RCP8.5) and (ii) European Centre for Medium Range Weather Forecasting (ECMWF) Interim Reanalysis (ERAI) data. The model output was compared against the observations from two stations in the areas, which showed that temperatures are higher in urban areas compared to the surrounding non-urban areas. The simulations showed that the summertime UHI is most clearly seen in night-time minimum and surface temperature over eThekwini.

During the current climate summer, defined as the period from December 2005 to December 2016, the UHI is observed in all CMIP5 simulations, urban temperature up to 2°C higher than

UNIVERSITEIT VAN PRETORIA
UNIVERSITY OF PRETORIA
YUNIBESITHI YA PRETORIA

those in non-urban areas. Surface temperature ranges from 26 to 30°C within the UHI and less than 26°C away from the UHI. Similarly, minimum temperature ranges from 20 to 24°C within the UHI and less than 20°C away from the UHI.

During the near-future summer, defined as 2039-2050, surface temperature is projected to change to an average range of 1 to 2°C higher compared to the current summer climate, while in the far-future summer, period 2089-2099, surface temperature is expected to increase to an average range of 2 to 4°C higher than the current climate, and the UHI is expected to become more intense, as anthropogenic emissions continue to contribute to global warming.

Keywords: land cover, urban heat island, measured urban parameters, minimum and surface temperature

3.1 Introduction

The city of eThekwini is located in a warm climatic zone over the eastern coast of South Africa, (i.e. Ndarana *et al.*, 2021). The city is highly urbanised along the coastline. Urbanisation has led to significant land-use changes, with natural vegetation being replaced by artificial materials such as concrete surfaces and low reflectivity materials (Pokhrel and Lee, 2011; Ramamurthy *et al.*, 2014; Estrada *et al.*, 2017). This phenomenon is observed in similar settings worldwide (Chen *et al.*, 2015; Nuruzzaman, 2015; Sannigrahi *et al.*, 2017; Katzfey *et al.*, 2020; Zhang *et al.*, 2022). These artificial materials and buildings absorb incoming shortwave solar radiation and re-radiate it as longwave radiation, which warms the atmosphere, particularly during the night (Parker, 2010; Nuruzzaman, 2015). This differential heating between the urban and rural areas causes urban temperatures to be at most 2°C higher than those in surrounding rural areas. The urban areas where this difference is 2°C higher compared to non-urban areas is defined as an urban heat island (UHI; IPCC, 2007;Walsh *et al.,* 2013; Chen *et al.,* 2015; Nuruzzaman, 2015; Sannigrahi *et al.,* 2017; Chapman *et al.,* 2019; Katzfey *et al.*, 2020; Barrao *et al.*, 2022; Parker 2010; Canton and Dipankar, 2024). This has also been shown in Chapter 2 (Maisha *et al.*, 2023).

The night time UHI intensity vary with cities, with temperature difference between urban and non-urban ranging from 2 to 4°C, and can be as high as 10°C, depending on

UNIVERSITEIT VAN PRETORIA
UNIVERSITY OF PRETORIA
YUNIBESITHI YA PRETORIA

the size of the city, urban morphology, land use and weather conditions (Wilby, 2008; Parker, 2010; Heaviside *et al.*, 2017; Dirksen *et al.*, 2020; Barrao *et al.*, 2022; Zhang *et al.*, 2022). The high temperature difference occurs mostly at night when the outgoing longwave radiation is absorbed by urban structures and artificial surface materials during the day as shortwave radiation is hardly released (Arnfield, 2003; Barrao *et al.*, 2022), thus enhancing the UHI effect.

The UHI is most pronounced during calm and clear nights (Parker, 2010) due to surface changes in albedo, emissivity, thermal conductivity, higher anthropogenic heat emissions, a decrease in evapotranspiration in urban surfaces, and complex surface, and flow between tall buildings (Chen *et al.,* 2014; Chapman et al., 2019; Katzfey *et al.,* 2020;Parker 2010).

Various urban modelling studies have been conducted globally using climate models with spatial resolutions ranging from low to high. These models incorporate an urban-scale component to better represent local processes. One example is the CCAM, a seamless modelling system applicable across various time scales, from short-range forecasts to century-scale projections, and spatial scales, from global processes down to urban-scales dynamics. The system can be used either as a global circulation model (GCM) or a regional climate model (RCM) using a stretched grid configuration(Dedekind *et al.*, 2016a; Katzfey *et al.*, 2020).

At low resolution, Katzfey *et al.,* (2020) evaluated the impact of urban areas on the performance of the Conformal Cubic Atmospheric Model (CCAM), using a horizontal resolution of 50 km to model the canopy-level UHI (CLUHI) during both current and future climates. This study shows that globally, areas with higher urban fractions and higher anthropogenic emissions are characterised by higher sensible heat flux, higher minimum temperature and UHI. The above-mentioned study shows that global circulation models (GCMs) can simulate both current and future city climates, although at this coarse resolution, urban climate processes, including the UHI, cannot be resolved.

However, higher resolution modelling can improve the performance of these models since they reduce the model dependence on parametrization, such schemes include

UNIVERSITEIT VAN PRETORIA
UNIVERSITY OF PRETORIA
YUNIBESITHI YA PRETORIA

cloud microphysics, cumulus parametrisation and radiation schemes (Reichler and Kim, 2008), and therefore resolve UHI processes. Such studies include Fischer *et al.,* (2012), who conducted an urban study by applying a Community Climate System Model (CCSM) coupled to an urban canopy model (UCM) that incorporates various vegetation types, urban surface, anthropogenic heat sources, and air conditioning. Their simulation of the UHI in summer showed that the UHI starts to build up during the second half of the day and reaches a maximum before sunrise. The UHI was also found to be latitudinally dependent, weaker in tropics, and stronger from sub-tropics to higher latitudes (Fischer *et al.*, 2012).

Chen *et al.,* (2014) applied the Weather Research and Forecasting (WRF) model coupled with a UCM at a horizontal resolution of 1 km to study the UHI over the city of Hangzhou during a heatwave event. The UCM was configured with Moderate Resolution Imaging Spectro-radiometer (MODIS) updated land cover data, including various land use classifications. The study found that the UHI was reproduced in both minimum and mean temperatures compared to maximum temperature and was consistent with urban land use characteristics. Additionally, the study showed that the UHI was intensified by a larger urban fraction and anthropogenic heating, leading to the conclusion that anthropogenic heating should be included in urban climate modelling since its increase with urbanisation resulted in increased temperature within the city.

Chapman *et al.,* (2019) applied CCAM to study how urban growth and land use changes influence the UHI over the city of Brisbane, Australia, for the summer period 2041-2050. CCAM was configured at an urban scale with a horizontal resolution of 1 km, using both controlled and urban growth landcover scenarios under RCP8.5 climate pathway. The study found that changes in landcover due to urbanisation increases the temperature, resulting in an increase in UHI effect. Zhang *et al.,* (2022) studied the UHI over the mountainous city in China. The study shows that urbanisation influences the UHI, with a statistically significant warming in mean annual daily minimum temperatures at most 1.5°C higher within the city compared to non-urban areas.

UNIVERSITEIT VAN PRETORIA
UNIVERSITY OF PRETORIA
YUNIBESITHI YA PRETORIA

Climate modelling studies, especially at high resolution, are limited on the African continent due to the extensive computational resources needed to produce these simulations. This study analyses the effects of landcover changes and realistic urban parameters on the UHI over the eastern coastal city of eThekwini, South Africa, under both present-day and projected future climate conditions. Simulations in this study are forced with high-resolution land cover data and measured urban parameters, as in Chapman *et al.,* (2019).

The simulations presented in this chapter, follows simulation performed during current climate (Chapter 2), which showed that simulations of the UHI are possible over cities by means of high-resolution models, measured emissions, land feature parameters, and supercomputing power.

This chapter aims to demonstrate that the use of MODIS land cover data, and measured urban parameters used as boundary conditions, and changes in land cover data in RCP8.5 from CMIP5, which incorporates urban expansion and changes in anthropogenic heating, can be explored to project the UHI over the coastal city of eThekwini, into the future. Additionally, the chapter aims to illustrate that the current modelling system, which incorporates measured urban parameters, enables urban-scale modelling, and can be evaluated in this context.

The outline of the paper is as follows: Section 1 describes an introduction to the study; Section 2 describes the data and methodology applied; Section 3 validates the model performance and provides further analyses of the results; Section 4 discusses the results; and Section 5 presents the conclusions to the study.

3.2 Data and Methodology

3.2.1 The Conformal Cubic Atmospheric Model

The study applies the CCAM, developed at the Commonwealth Scientific and Industrial Research Organization (CSIRO) in Australia (McGregor, 1995; *McGregor et al.,* 2008). The model configuration has been described in the previous chapter but is briefly reported here for convenience. CCAM is a nonhydrostatic model, whose dynamical core is solved using a semi-implicit, semi-Lagrangian method (McGregor,

UNIVERSITEIT VAN PRETORIA
UNIVERSITY OF PRETORIA
YUNIBESITHI YA PRETORIA

1996; Engelbrecht *et al.,* 2009; Engelbrecht *et al.*, 2015; Dedekind *et al.,* 2016). Its physics schemes and parametrisations include mass-flux cumulus convection and the Geophysical Fluid Dynamics Laboratory (GFDL) scheme for both longwave and shortwave radiation parametrisation schemes (see also Dedekind et al., *2016)*. Detailed information on the CCAM physics is also detailed in Chapman *et al.,* (2019).

Various modelling studies have utilised the CCAM system, including simulations of rainfall over South Africa (Dedekind *et al.*, 2016a; Bopape *et al.*, 2022); projections of tropical cyclones over the Indian Ocean (Muthige *et al.*, 2018), using sea surface temperature (SST) and sea ice and RCP8.5 data as boundary conditions (Engelbrecht *et al.*, 2011; Riahi *et al.*, 2011; Katzfey *et al.*, 2020). The CCAM has also been used for urban modelling in various cities, such as Melbourne, Australia and other global cities (Luhar *et al.*, 2014; Lipson *et al.,* 2017, 2018; Chapman et al., 2019).

In this study, the CCAM is applied as a regional model at a higher horizontal resolution of 1 km using a stretched grid mode over the city of eThekwini (Figure 2.1). When used as a regional climate model (RCM), CCAM can be run at higher resolutions, allowing for improved representation of land use changes (IPCC, 2023) and enhanced simulation of interactions between sea and atmospheric circulation (Taylor *et al.*, 2012; Yan *et al.*, 2013).

To simulate urban-scale climates, CCAM is coupled with the Australian town energy budget (ATEB) urban climate model (UCM) (Thatcher and Hurley 2012; Luhar *et al.*, 2014; Lipson *et al.*, 2017, 2018; Chapman *et al.*, 2019) through the CSIRO Atmosphere Biosphere Land Exchange (CABLE) model, as described in Kowalczyk *et al.*, (2006) and Wang *et al.,* (2006). The updated version of ATEB is called urban climate and energy model (UCLEM, Lipson *et al.*, 2018; Katzfey *et al.*, 2020) and has been upgraded to represent heat transfer processes in the external and internal urban environment, taking into account human behaviours related to energy use (Lipson *et al.*, 2018).

3.2.2 Urban climate model

The ATEB model applied is a prognostic meteorological model that combines both urban canopy and mesoscale climate modelling. It parameterises both latent heat and

UNIVERSITEIT VAN PRETORIA
UNIVERSITY OF PRETORIA
YUNIBESITHI YA PRETORIA

sensible heat fluxes within the building canyons, the atmosphere, and the surface beneath urban areas (Thatcher and Hurley, 2012; Luhar *et al.*, 2014; Lipson *et al.*, 2017, 2018; Chapman and Mcalpine, 2019). The model also parameterises both shortwave and longwave radiation and comprises a big-leaf energy budget to represent urban vegetation more accurately (Chen *et al*., 2010; Thatcher and Hurley, 2012; Han *et al.,* 2013; Garuma, 2017). Additionally, it incorporates a planetary boundary layer scheme for turbulence closure parameterization (Thatcher and Hurley, 2012; Chen *et al*., 2015).

Most of the features and parameters of the ATEB model are described in studies such as Masson, (2000), Thatcher and Hurley, (2012), Mirzaei, (2015) and Garuma, (2017). The model applies high resolution measured land cover and urban parameters described in the methodology section in Chapter 2. Due to the higher resolution simulation demand, ATEB models are applied only when there are adequate computational resources available (Garuma, 2017). The land cover and urban parameters data used are listed in the downscaling methodology in section 3.2.4 below.

3.2.3 Data

In this section, simulations of the current and future UHI effect over the city of eThekwini using the CCAM (Engelbrecht *et al.,* 2007; McGregor, 1996; McGregor *et al.*, 2008; Dedekind *et al.*, 2016) are described. The model was forced with four GCM simulations of the CMIP5 Project (Taylor *et al.,* 2012;Yan *et al.*, 2013) and the Assessment Report 5 (AR5) of the International Panel on Climate Change (IPCC, 2007; Taylor *et al.,* 2012; Monerie *et al.,* 2020). The four GCMs applied from CMIP5 data are as follows (i) the National Centre for Meteorological Research Coupled Global Climate Model, version 5 (CNRM-CM5); (ii) the Geophysical Fluid Dynamics Laboratory Coupled Model (GFDL-CM3); (iii) the Max Planck Institute Coupled Earth System Model (MPI-ESM-LR); and (iv) the Norwegian Earth System Model (NorESM1-M). These models were initially downscaled to a globally horizontal resolution of 0.5°.

These models were downscaled as part of Coordinated Regional Climate Downscaling Experiment (CORDEX) over of the globe, including South Asia and Africa, and South

UNIVERSITEIT VAN PRETORIA
UNIVERSITY OF PRETORIA
YUNIBESITHI YA PRETORIA

Africa (Thevakaran *et al.*, 2016; Maure *et al.*, 2018a; Muthige *et al.*, 2018; Kruger *et al.*, 2019; Spinoni *et al.*, 2021). A detailed description of these models and their resolutions is described in Thevakaran *et al.,* (2016). An important feature of the downscaling process is that the model was forced with bias corrected SSTs and sea ice data from four GCMs. The bias was computed by subtracting the Reynolds (1988) SST climatology (1961–2000) from the corresponding GCM output for each month, consistently applied throughout the entire simulation period (1961–2099). By performing such a procedure, it ensures that the climatology of the SST applied as lower boundary forcing is the same as that of Reynolds SST (Thatcher and McGregor, 2009; Dedekind *et al.*, 2016; Muthige *et al.*, 2018).

These four models were selected randomly, and forced with the RCP8.5 emission scenario, which represents a high-emission, low mitigation pathway (Riahi *et al.,* 2011; Garland et al., 2015; Maure *et al.*, 2018a; Muthige *et al.*, 2018). This scenario assumes a growing population and economy with slow improvements in the energy sector, and leading to an increase in energy demand by a factor of three and an increase in radiative forcing up to 8.5 W/m^2 by the end of the 21st century (Riahi *et al.*, 2011; Kruger *et al.*, 2019; Spinoni *et al.*, 2021). The choice to use RCP8.5 data was motivated by the fact that it takes into consideration significant warming, as compared to RCP4.5 scenario, where radiative forcing stabilises at 4.5 W/m^2 towards the end of 2100 (Riahi *et al.*, 2011; Thomson *et al.*, 2011; Kruger *et al.*, 2019).

During the initial phase of the Cool Durban project, the model was first tested using both RCP4.5 and RCP8.5 data for the periods, 2030's, 2050's and 2060's. The model was run with the urban scheme switched on at both 8 km and 1 km resolution. At 8 km, the UHI could not be simulated with either RCP4.5 or RCP8.5 model outputs. However, at 1 km resolution, the UHI simulated was weak for RCP 4.5 but stronger for RCP8.5. Therefore, the RCP8.5 data, which represent the higher-emission scenario, was adopted to maximize the signal in the UHI development, characteristics, and impact under climate change that may not be discernible under RCP4.5 (Maisha *et. al.,* 2017).

UNIVERSITEIT VAN PRETORIA
UNIVERSITY OF PRETORIA
YUNIBESITHI YA PRETORIA

The CMIP5 data provides more realistic and time varying external forcing at an inter-annual time scale (Taylor *et al.*, 2012; Yan *et al.*, 2013). This forcing includes anthropogenic greenhouse gases, aerosols, and land-use (Taylor *et al.*, 2012; Yan *et al.*, 2013; Muthige *et al.*, 2018). This study specifically applies only RCP8.5 data because the interest is on high emission scenarios (Riahi *et al.*, 2011; Maure *et al.*, 2018a; Muthige *et al.*, 2018) and how climate change impacts the development and progression of the UHI. For the current climate (2006-2016), the study also applied the CCAM customised ERAI (Dee *et al.*, 2011; Balsamo *et al.,* 2015) data, with a horizontal resolution of 0.75° (Uppala *et al.*, 2005), downscaled to 1 km over the city of eThekwini. Therefore, the output of the CCAM-CMIP5 runs is compared with CCAM-ERAI simulations (from Chapter 2, Maisha *et al.*, 2023) and station observations data, but only for the current climate before analysing the results for the near-future and far-future climates.

3.2.4 Methods of downscaling

The CMIP5 data (Taylor *et al.*, 2012; Yan *et al.*, 2013) was used for the periods 2006-2016, 2040-2050, and 2090-2100, defined as present day, near future and far future climates, respectively. A continuous simulation from 2006 to 2100 was not feasible due to the computational resources required, as the Centre for High Performance Computing (CHPC) resources are shared among various modelling groups across the entire African continent.

Each set of experiments was run for 11 successive years: December 2005 to December 2006, December 2039 to December 2050, and December 2089 to December 2099, where possible, in parallel (see Figure 3.1 for the flow chart). At a resolution of 50 km (2005-2006), 264 processors were reserved, and the ERAI experiment took a total of 66 hours (~3 days) to complete. A summary of the experiments with the number of nodes, total run hours, and days, is provided in Table 3.1.

UNIVERSITEIT VAN PRETORIA
UNIVERSITY OF PRETORIA
YUNIBESITHI YA PRETORIA

Table 3.1: A table of experimental design, the number of nodes applied, a total number of hours and days to complete the ERAI and CMIP5 runs.

Decade	experiment	nodes	experiment	hours	days
2005-2015	ERAI	264	1*50 km	66	2,75
	ERAI, CNR8.5, GFD8.5, MPI8.5, NOR8.5	288	5*8 km	1320	55
	ERAI, CNR8.5, GFD8.5, MPI8.5, NOR8.5	432	5*1 km	2640	110
2039-2050	CNR8.5, GFD8.5, MPI8.5, NOR8.5	288	4*8 km	1056	44
	CNR8.5, GFD8.5, MPI8.5, NOR8.5	432	4*1 km	2112	88
2089-2099	CNR8.5, GFD8.5, MPI8.5, NOR8.5	288	4*8 km	1056	44
	CNR8.5, GFD8.5, MPI8.5, NOR8.5	432	4*1 km	2112	88
Total amnount of resources used					
	experiment	nodes	experiment	total hours	total days
	ERAI	264	1*50 km	66	2,75
	ERAI, CNR8.5, GFD8.5, MPI8.5, NOR8.5	288	5*8 km	3432	143
	ERAI, CNR8.5, GFD8.5, MPI8.5, NOR8.5	432	5*1 km	6864	286

At a resolution of 8 km, a total of 288 processors were applied, with each experiment taking 264 hours to compete. Therefore, for the five experiments, (i.e. four CMIP5 and one ERAI runs) it took a total of 3432 hours (143 days) to complete all the experiments.

At a horizontal resolution of 1 km, a total of 432 processors were applied, with each experiment taking a total of 528 hours to compete. Thus, for the five experiments, (i.e. four CMIP5 one ERAI runs) it took 6864 hours (286 days) to complete all the experiments (Table 3.1).

The CMIP5 experiment design is outlined as follows:

a) In the first experiment, CCAM simulations were conducted at a horizontal resolution of 8 km centered over South Africa and forced with the output from four GCMs downscaled globally to 50 km resolution and model setup was centered over Africa. The CCAM-CABLE was configured at a resolution of 8 km with a C192 (192*192) grid points) centered over southern Africa (-28°S; 25°E) and a Schmidt stretch factor of 0.1523 (refer to Figure 3.1, top flowchart).

UNIVERSITEIT VAN PRETORIA
UNIVERSITY OF PRETORIA
YUNIBESITHI YA PRETORIA

The CCAM-CABLE model generated static data such as bathymetry, topography, vegetation, and carbon cycle fields were used as boundary conditions. A detailed explanation of the CCAM-CABLE is found in Kowalczyk *et al.*, (2006) and Wang et al., (2006). The CABLE was updated using MODIS satellite land cover data over South Africa for the year 2013. This data is illustrated in Figure 2.1, providing details for the city of eThekwini. The city is located on the east coast of SA, with urban and built-up areas presented in detail. This dataset was selected because it provides a realistic distribution of the urban areas globally (Katzfey *et al.*, 2020). This high-resolution panel covers an area of approximately 1536 km*1536 km over southern Africa, with the resolution gradually decreasing outside this region. This configuration produces output at six (6) hourly intervals.

b) In the second experiment focusing on urban climate modelling, the CCAM was configured and run at a horizontal resolution of 1 km centered over eThekwini (also known as the Durban; Walsh *et al.,* 2013), located in the Kwazulu-Natal Province of South Africa (Figure 3.1, bottom flowchart). The CCAM-CABLE model was configured at 1 km resolution with a C192 (192*192 grid points centered per panel) located at (30°S; 30°E) with a Schmidt stretch factor of 0.019. The lower boundary conditions of the CCAM-CABLE were updated using high-resolution MODIS land cover data, as used in the 8 km configuration. Additionally, the CCAM-CABLE was updated with measured urban parameters and emissions from the city of eThekwini, following similar settings as described in studies by Luhar *et al.,* (2014) and Chapman and Mcalpine (2019).

The high resolution measured urban parameters applied were provided by the city of eThekwini and were measured using Light Detection and Ranging (LIDAR). These parameters include average building heights (5.86 metres), building height-to-width ratio (0.24 metres), vegetation fraction (0.25%), building fraction (0.55%), industrial emissions (1.00 $W.m^{-2}$), traffic emissions (2.62 $W.m^{-2}$), roof albedo (0.2 $W.m^{-2}$), wall albedo (0.3), road albedo (0.1) and vegetation albedo (0.2) (see detailed Table 2.1, Ateb-3). Some of the variables applied in this study are similar to those applied in a study by Katzfey *et al.*, (2020). The ATEB model includes eight urban types (Thatcher and Hurley, 2012), but in modelling studies only one urban class is

UNIVERSITEIT VAN PRETORIA
UNIVERSITY OF PRETORIA
YUNIBESITHI YA PRETORIA

selected at a time, which is representative of the entire urban area, and incorporates urban parameters for buildings, walls, roads, and albedo (Thatcher and Hurley, 2012; Garuma, 2017). This is because individual buildings and street canyons in urban areas could not be explicitly resolved, but their effects are instead aggregated (Masson, 2000; Chen and Dipankar, 2022). Garuma (2017) described a similar type of experiment but with 10 different urbanisation classes. Similar to Katzfey *et al.*, (2020), there is no change in the measured parameters over the entire climate period of simulation. The CCAM 1 km configuration produces output at an hourly interval.

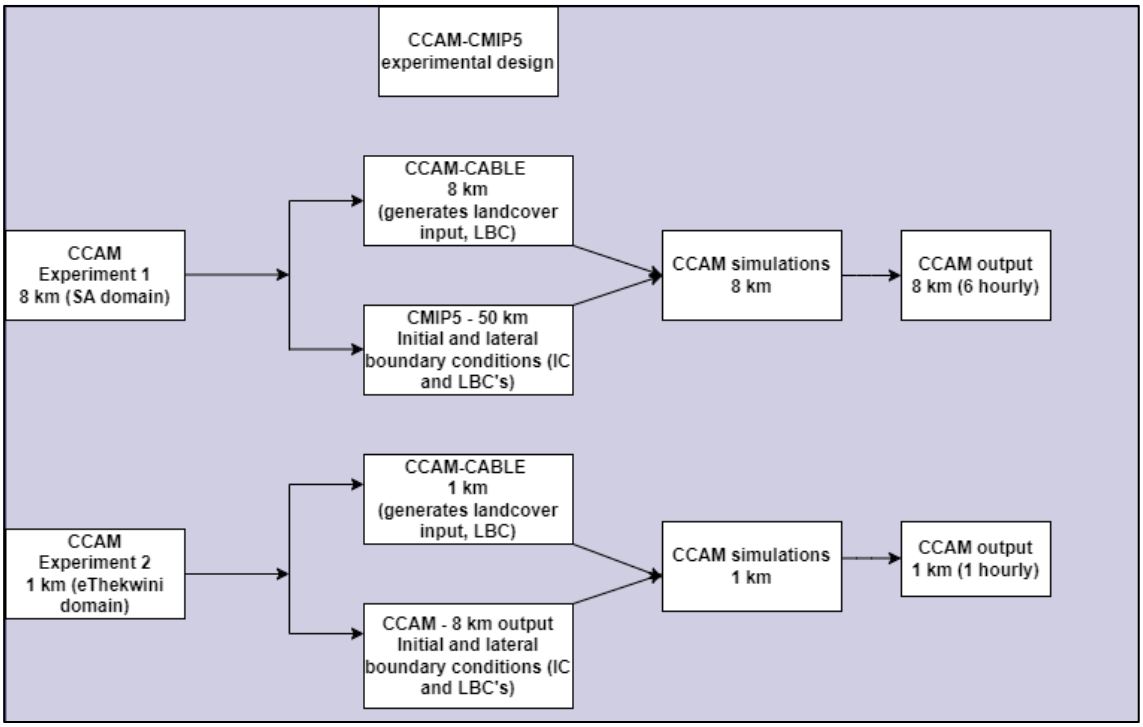

Figure 3.1: The schematic configuration of CCAM runs with CMIP5 data over South Africa at 8 km (top) and 1 km over eThekwini (bottom) respectively. The output from both the CCAM-CABLE and lower resolution simulations are used as initial and boundary conditions to high resolution model runs.

3.2.5 CCAM validation

The 1 km model output from both the RCP8.5 and the ERAI simulations (Dee *et al.*, 2011; Riahi *et al.*, 2011; Balsamo *et al.*, 2015) were only validated against observations during the current climate (2006-2016). The first observations consisted of 1 km MODIS satellite nighttime Land Surface Temperature (LST) data for

UNIVERSITEIT VAN PRETORIA
UNIVERSITY OF PRETORIA
YUNIBESITHI YA PRETORIA

the period December 2012 to December 2013. This study of the UHI using surface temperature is considered a surface urban heat island (SUHI) study (Barrao *et al.*, 2022). Although both the CCAM runs and MODIS data are at 1 km resolution, they do not share similar grid points. Therefore, the CCAM output was first linearly interpolated to the MODIS grid, and the spatial correlation (equation 2.5) between the model and observations was calculated.

The second set of observational data used in the study was obtained from two South African Weather Service (SAWS) weather stations. The first station is Durban, located at the southern parts of the domain (latitude 29.965°S; and longitude 30.946°E), and the second station is Mt Edgecombe, located at the north-eastern parts of the domain (latitude 29.706°S; and longitude 31.046°E), as shown in Figure 2.1. This data spans the period from December 2005 to December 2016. The variables verified against the model are hourly temperatures (for diurnal range), daily maximum and minimum temperatures, and monthly averages. For validation purposes, the model temperatures (both maximum and minimum) are compared to temperatures measured at the screen level, which is approximately 2 metres above the ground.

3.3 Results

3.3.1 Model validation

The CCAM output was validated against MODIS LST and SAWS station observations. For convenience, the GCMs runs are shortened as follows: CNRM-CM5 (CNR8.5); GFDL-CM3 (GFD8.5); MPI-ESM-LR (MPI8.5); and NOR-ESM1-M (NOR8.5). Model validation statistics such as bias (equation 2.1) and root mean square error (RMSE, equation 2.4) are applied for the current climate period (2006-2016). Although simulations were performed for December to February (DJF), March to May (MAM), June to August (JJA), and September to November (SON), the analysis mainly focuses on DJF and to a lesser extent JJA season, as analysed in Chapter 2.

3.3.1.1 CCAM validation against MODIS satellite data

The CCAM simulated minimum temperature simulations forced with ERAI (Dee *et al.*, 2011; Balsamo *et al.*, 2015), CNR8.5, GFD8.5, MPI8.5, and NOR8.5 are compared with MODIS nighttime LST for the period December 2012 to December 2013 (Figure 3.2).

UNIVERSITEIT VAN PRETORIA
UNIVERSITY OF PRETORIA
YUNIBESITHI YA PRETORIA

a) Seasonal variations

During the summer (DJF) season, the UHI is clearly depicted in both MODIS satellite data and all CCAM simulations (Figure 3.2). Simulations with MPI8.5 shows the best agreement with MODIS, although MODIS is, on average, at most 2°C warmer than MPI8.5. The difference could be attributed to MODIS showing the SUHI observed at the surface (Barrao *et al.*, 2022), as opposed to the air temperature simulated by the CCAM. The other simulations are comparable and generally 2°C cooler than MODIS, while MPI8.5 is warmer than all the models, even over the ocean.

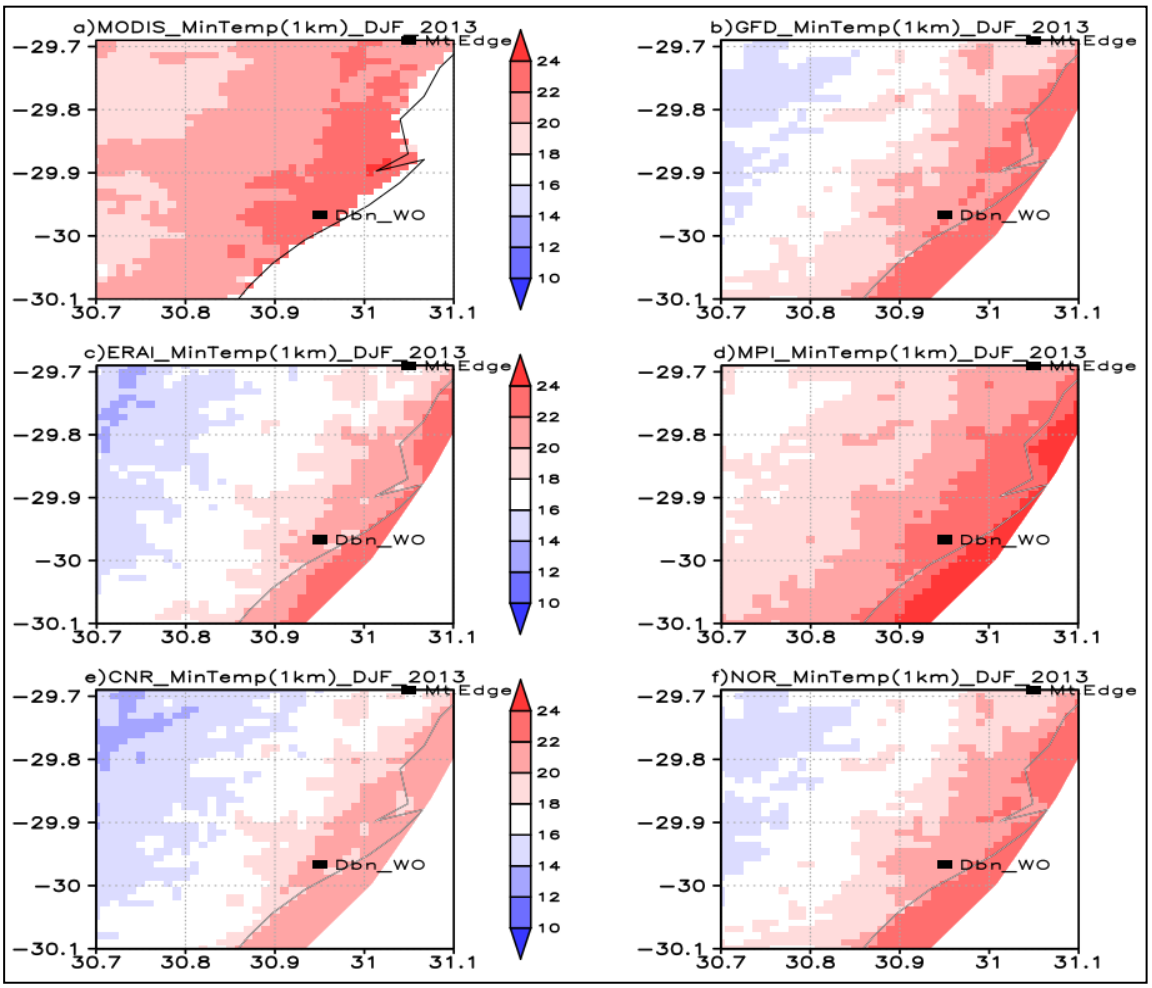

Figure 3.2: The CCAM minimum screen temperature versus MODIS nighttime LST over the city of eThekwini for the period DJF 2012/13. The panel represents MODIS (left-top), GFD8.5 (right-top), ERAI (middle- left), MPI8.5 (middle-right), CNR8.5 (bottom- left) and NOR8.5 (bottom-right). This is in comparison with the updated 2013 landcover data applied in the setup of the CCAM-CABLE used to provide initial and boundary conditions. Both Durban (to

UNIVERSITEIT VAN PRETORIA
UNIVERSITY OF PRETORIA
YUNIBESITHI YA PRETORIA

the south of the domain, 29.965°S; 30.946°E) and Mt. Edgecombe (to the northeast of the domain, 29.706°S; 31.046°E) stations are plotted.

During the two transition seasons, autumn (Figure B.1), and spring (Figure B.2), the strength of the UHI varies. In autumn, the UHI starts to weaken just before it disappears during the winter season. As the spring season approaches, the UHI starts to develop and reaches maximum intensity in summer.

In winter (Figure 3.3), MODIS temperature is still higher than all the model simulations but is closer to the MPI8.5 simulation. Larger parts of the city show a temperature of range of 14 -18°C and are at most 2°C warmer than the other simulated temperatures.

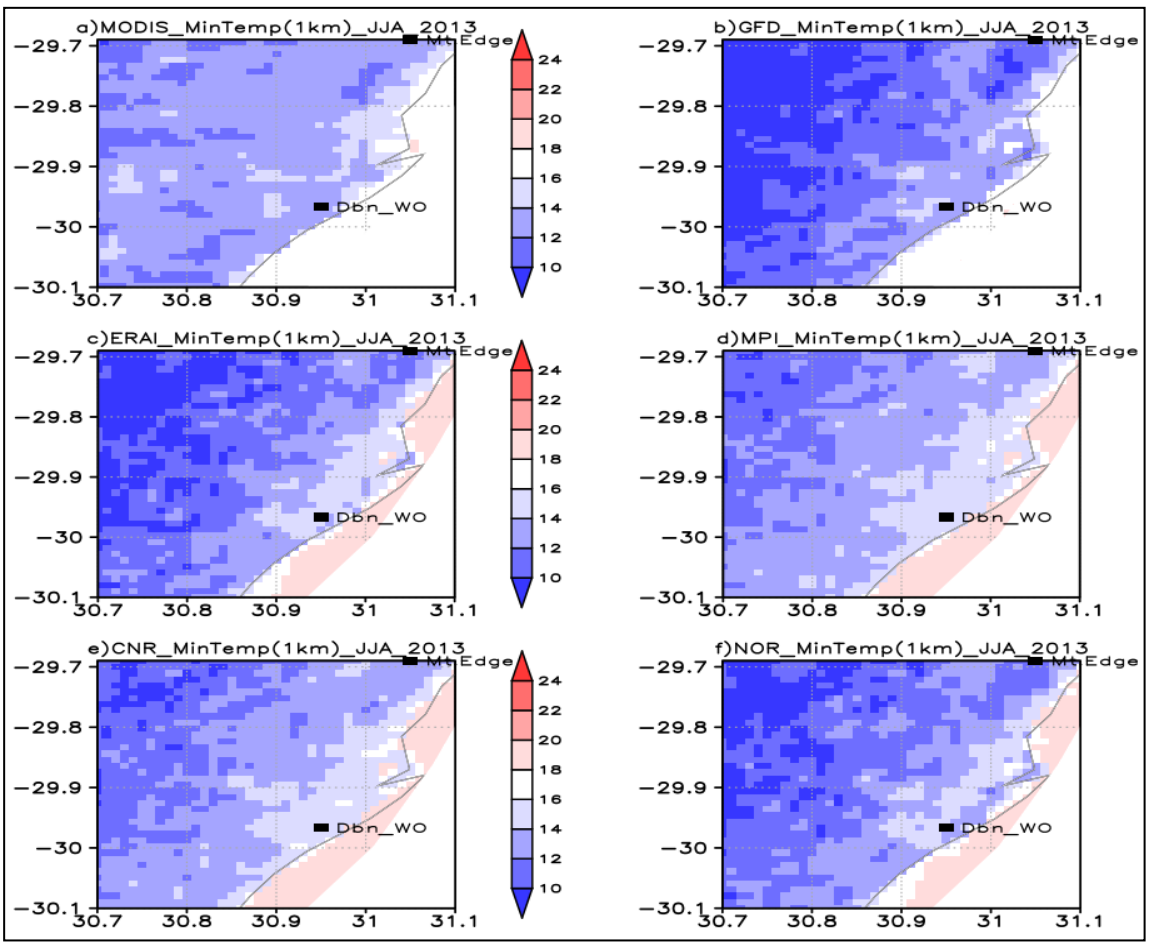

Figure 3.3: The CCAM minimum screen temperature versus MODIS nighttime LST over the city of eThekwini for the period JJA 2012/13. The panels represent MODIS (left-top), GFD8.5 (right-top), ERAI (middle-left), MPI8.5 (middle-right), CNR8.5 (bottom-left) and NOR8.5

(bottom-right). Both Durban (to the south of the domain, 29.965°S; 30.946°E) and Mt. Edgecombe (to the northeast of the domain, 29.706°S; 31.046°E) stations are plotted.

Although the models show some variability, CNR8.5 and GFD8.5 exhibit better agreement. This could be due to the fact that the initialisation data for the two models have similar characteristics.

b) Spatial correlations

The spatial correlations were also calculated between MODIS and CCAM simulations, shown in Figure 3.4. During summer (DJF), the spatial correlation is extremely high among all the simulations and MODIS data, ranging from 0.89 to 0.9. This is followed by MAM with a range of 0.87 to 0.91. The spatial correlation is lowest during winter, with a range of 0.61 to 0.63. During spring, the correlations improved to a range of 0.62 to 0.74.

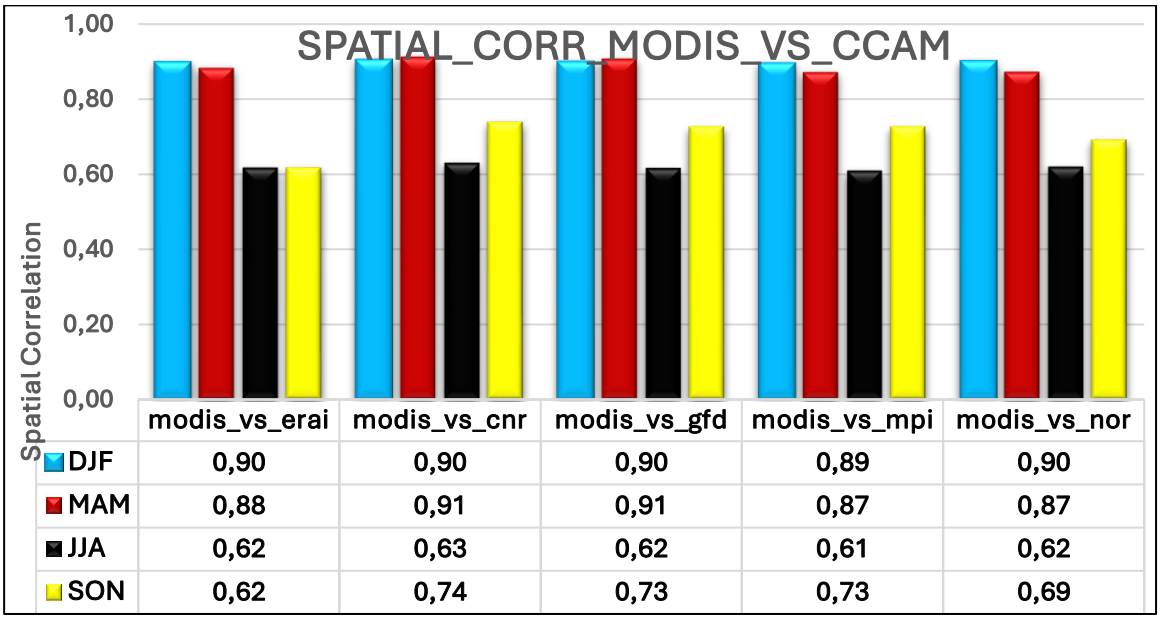

	modis_vs_erai	modis_vs_cnr	modis_vs_gfd	modis_vs_mpi	modis_vs_nor
DJF	0,90	0,90	0,90	0,89	0,90
MAM	0,88	0,91	0,91	0,87	0,87
JJA	0,62	0,63	0,62	0,61	0,62
SON	0,62	0,74	0,73	0,73	0,69

Figure 3.4: The spatial correlations between CCAM minimum screen temperature simulations with ERAI, CNR8.5, GFD8.5, MPI8.5 and NOR8.5 versus MODIS nighttime land surface temperature (LST) over the city of eThekwini for the period DJF, MAM, JJA and SON 2012/13. The validation period aligns with the applied land cover data period.

From these comparisons, high positive correlations are found in summer between all the CCAM simulations and MODIS, with minor differences between ERAI, CNR8.5,

UNIVERSITEIT VAN PRETORIA
UNIVERSITY OF PRETORIA
YUNIBESITHI YA PRETORIA

GFD8.5, MPI8.5, and NOR8.5 runs. This statistic shows that the CCAM captured the spatial distribution of temperature observed in MODIS-LST very well. Similar conclusions were reached in a study over Sri Lanka by Thevakaran *et al.,* (2016), although comparisons were made between ERAI and CMIP5 model runs. Their study found that when CCAM is forced with CNR8.5 and GFD8.5, it produces better scores for rainfall, but almost perfect score (0.99) for temperature. In the current study, CNR8.5 and GFD8.5 produced better scores for all seasons.

3.3.1.2 CCAM validation with station data

a) Monthly variation

Figure 3.5 shows the simulated maximum and minimum temperatures compared with SAWS observations at Durban (urban) and Mt. Edgecombe (non-urban) stations for the 10-year present-day simulated period from December 2005 to December 2016. The highest maximum temperature is observed in February at both stations, while the lowest temperature is observed in July (see Figure 3.5a and 3.5b). At the Durban station, the observed temperature was higher than the model simulations during both February and July.

The intra-annual variability of simulated maximum temperature compares well with observations. The results show that CCAM underestimates the maximum temperature when forced with CMIP5 data, except from September to December. For Mt Edgecombe, there is a better agreement between the observation and CCAM simulations forced with ERAI. This suggests that the shortcomings in the CCAM simulations are also linked to shortcomings in the forcing models. The reason for this underestimation could be either due to absorbed shortwave radiation or upward sensible heat flux (Chen *et al*., 2014).

For minimum temperature, shown in Figures 3.6c and 3.6d, the observed temperature is lower than in all RCP8.5 simulations for the Durban station, while the ERAI run was closer to the observations. For Mt. Edgecombe, the observed minimum temperature is higher than CMIP5 and ERAI runs during all months. These simulations show mixed results for maximum and minimum temperature at the two stations. Thevakaran *et al.,* (2016) found that the CCAM overestimates temperature

UNIVERSITEIT VAN PRETORIA
UNIVERSITY OF PRETORIA
YUNIBESITHI YA PRETORIA

in a study over Sri Lanka. However, studies by Engelbrecht *et al.*, (2011) and Katzfey *et al.*, (2020) have shown that CCAM provides satisfactory simulations of rainfall and temperature distributions.

For the current study, minimum temperature is overestimated at the urban station (Durban) and is underestimated at non-urban station (Mt. Edgecombe). This underestimation at Mt.Edgecombe agrees with a study by Kruger *et al.*, (2019). As in maximum temperature, the highest values are simulated and observed during February and the lowest during July, respectively. These comparisons between the model and observations indicate that model simulations at higher resolution (1 km) captured monthly/seasonal temperatures well as they are closer to the observations. As in Chapter 2, these comparisons provide confidence in the use of CCAM for simulations of the occurrence of UHI during current and future climate.

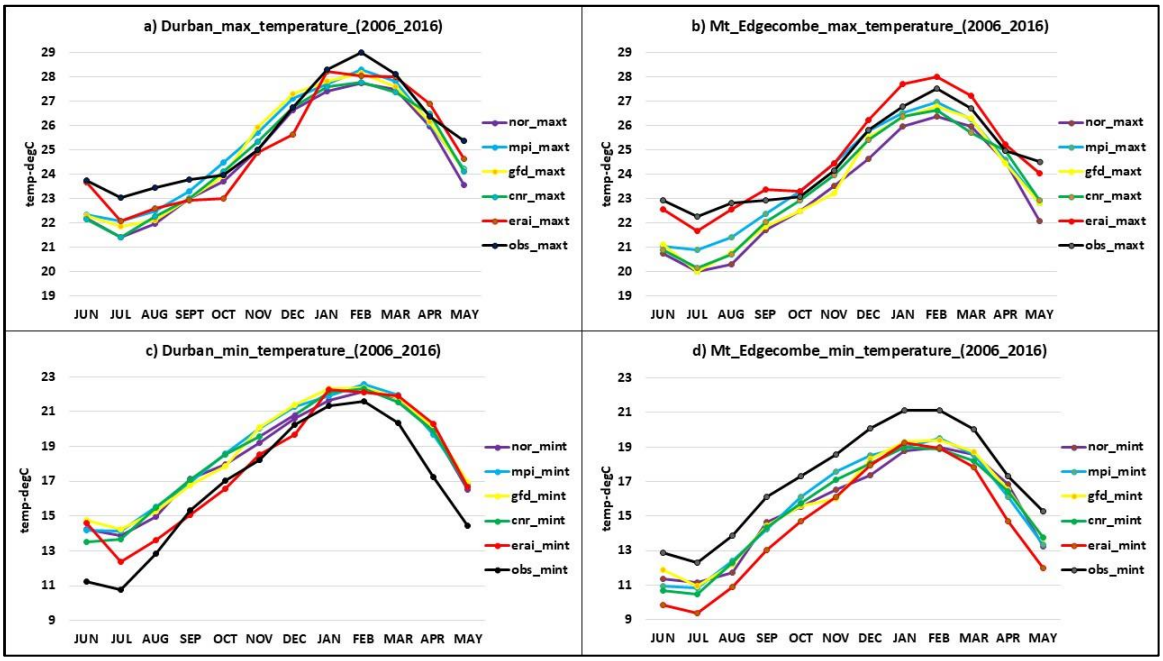

Figure 3.5: The CCAM simulation of monthly variation of maximum and minimum temperature with ERAI and representative concentration pathway 8.5 (RCP8.5) and observations for the period 2006-2016. Similar analyses were conducted in Chapter 2, but with ERAI data only.

UNIVERSITEIT VAN PRETORIA
UNIVERSITY OF PRETORIA
YUNIBESITHI YA PRETORIA

b) Diurnal range

Figures 3.6 and 3.7 show the diurnal range of modelled temperature at the two observation stations, Durban, and Mt. Edgecombe for the current climate period 2005-2016.

During DJF (Figure 3.6a and Figure 3.7a, top-left panels), the ERAI diurnal range shows strong agreement with station observations. The minimum value starts slightly lower than 22°C and rises to a maximum of slightly higher than 26°C at 10h00 UTC. The temperature then starts to decrease and reaches a minimum value of average of 22°C and lower after 24 hours. The diurnal range during summer is stronger and has a maximum range of 5°C. There is also strong agreement between observed and CMIP5 output, especially between 03h00 and 10h00 UTC. From 00h00 to 03h00 UTC, all the CMIP5 temperature values are less than observed by a value less than 2°C, and this also applies after 12h00 UTC. The spatial distribution of the temperature shows a spread of values less than 1°C, but from 06h00 to 12h00 UTC. When comparing urban and non-urban stations, temperatures show higher average values in urban than non-urban station, indicating the influence of artificial materials in urban areas, which raises the temperature more than in non-urban station.

In summer (DJF), at the urban station (Durban), minimum values average between 20 and 22°C, while maximum values range between 26 and 28°C. At a non-urban station (Mt. Edgecombe), minimum values are slightly lower, averaging between 20 and 21°C, with maximum values between 26 and 28°C. However, during the early hours (00h00-02h00 UTC), the temperature spread is ~2°C at Durban station and around 1°C at Mt. Edgecombe. This indicates greater heat retention at the Durban station, which enhances the UHI effect.

Additionally, during the day, both ERAI and observations at Durban station show higher temperatures than CMIP5 outputs. These high temperatures persist and do not drop, but remain higher than 22°C. In contrast, at Mt.Edgecombe, the CMIP5 and ERAI diurnal range are more consistent with each other. This pattern provides evidence of a detectable UHI effect at the urban station compared to the non-urban station.

UNIVERSITEIT VAN PRETORIA
UNIVERSITY OF PRETORIA
YUNIBESITHI YA PRETORIA

During MAM (see Figures 3.6b and Figure 3.7b, top-right panels), ERAI values are warmer than observation during all hours. The diurnal temperature range in ERAI is stronger (6°C) at the urban station, while it is weaker for observation (~8°C). However, ERAI and all the CMIP5 temperature values are on average less than 1°C higher than observed, except between 14h00 and 20h00 UTC.

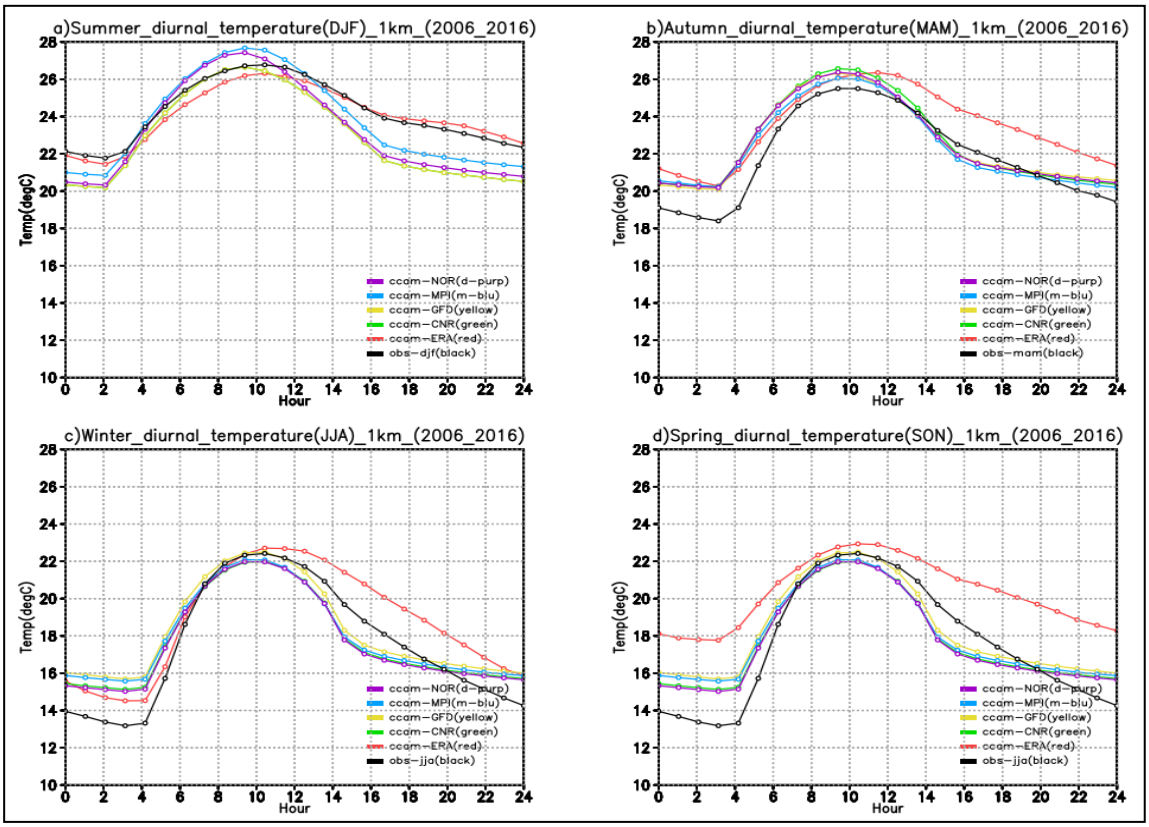

Figure 3.6: The CCAM simulation of diurnal temperature range, using ERAI and representative concentration pathway 8.5 (RCP8.5) as well as observations for DJF, MAM, JJA and SON for the period 2006-2016 over Durban weather station. It should be noted that in (a) CNR8.5 (green) overlaps with NOR (purple), in (b) GFD8.5 (yellow) overlaps with MPI8.5 (blue), in (c) CNR8.5 (green) overlaps with NOR8.5 (purple) and in (d) CNR8.5 (green) overlaps with NOR8.5 (purple).

In the non-urban station, the observed temperature is lower than CMIP5 and ERAI simulations in the urban station. On average, the urban station temperature is slightly higher than the non-urban station, and the diurnal cycle is similar between observation and all the CCAM runs.

UNIVERSITEIT VAN PRETORIA
UNIVERSITY OF PRETORIA
YUNIBESITHI YA PRETORIA

During JJA (see Figure 3.6c and Figure 3.7c, bottom-left panels), the diurnal range is also slightly similar to the autumn (MAM) profile. This applies to both urban and non-urban stations, respectively. After 10h00 UTC, ERAI is much warmer than observation and CMIP5 runs, resulting in the diurnal range at most 8°C for an urban station. In a non-urban station, CMIP5 and ERAI profiles are similar, and the observed temperature is lower during the early and late hours of the day. This difference could be due to artificial materials and anthropogenic heating in urban areas.

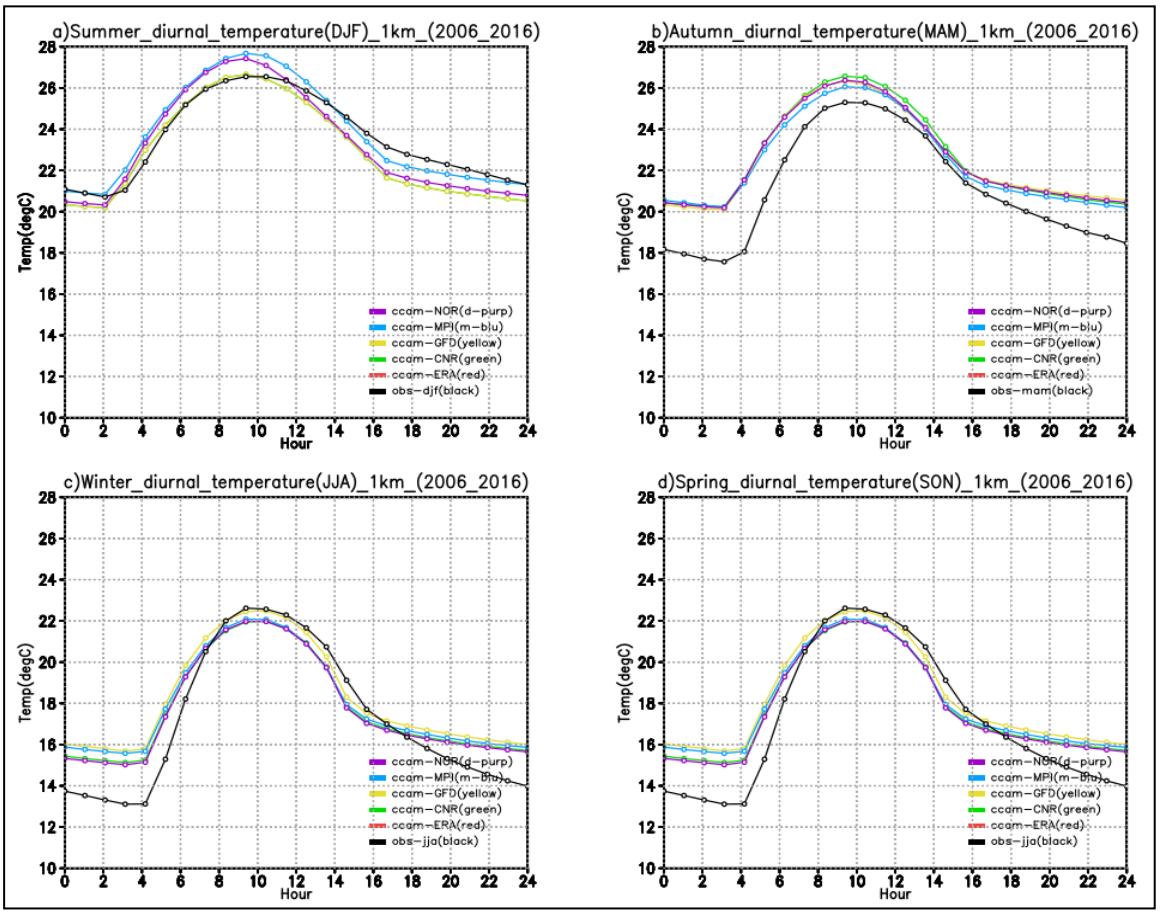

Figure 3.7: The CCAM simulation of diurnal temperature range using ERAI and representative concentration pathway 8.5 (RCP8.5) as well as observations for DJF, MAM, JJA and SON for the period 2006-2016 over Mt. Edgecombe Weather station. It should be noted that in (a) CNR8.5 (green) and ERAI (red) overlap with other profiles, in (b) GFD8.5 (yellow) and ERAI (red) overlap with other profiles, in (c) CNR8.5 (green) and ERAI (red) overlap with other profiles and in (d) CNR8.5 (green) and ERAI (red) overlap with other profiles.

UNIVERSITEIT VAN PRETORIA
UNIVERSITY OF PRETORIA
YUNIBESITHI YA PRETORIA

During SON (see Figures 3.6d and Figure 3.7d, bottom right panels), the diurnal range of both ERAI shows temperature higher than CMIP5 and observation, especially for the urban station. In the non-urban station, the SON profiles are almost similar to the JJA profiles. The spread of the diurnal range is higher and stronger at the urban station as compared to the non-urban station.

c) Verification statistics

The CCAM verification statistics for the period 2006–2016 are shown in Tables 3.2, 3.2, 3.4 and 3.4 respectively for the Durban and Mt.Edgecombe stations, following Gordon and Shaykewich (2000). Values of minimum temperature bias are shown in Table 3.2. Results show that bias varies with seasons and among models. During DJF, there is a positive bias in all CMIP5 runs for Durban and a negative bias for Mt. Edgecombe.

Table 3.2: The CCAM bias statistics for minimum temperature for simulations with ERAI and representative concentration pathway 8.5 (RCP8.5) against observations at the urban station (Durban) and non-urban station (Mt. Edgecombe) for DJF, MAM, JJA, and SON for the period 2006-2016.

Durban		BIAS_MINT			
	obs_vs_erai	obs_vs_cnr	obs_vs_gfd	obs_vs_mpi	obs_vs_nor
DJF	-0,8	1,8	1,0	0,9	0,4
MAM	1,3	6,8	2,3	2,1	2,1
JJA	-0,4	-0,9	3,1	3,0	2,8
SON	-1,7	-1,2	1,4	1,7	1,2
All_Seasons	-0,4	1,7	1,9	1,9	1,6
Mt_Edgecombe		BIAS_MINT			
	obs_vs_erai	obs_vs_cnr	obs_vs_gfd	obs_vs_mpi	obs_vs_nor
DJF	-2,5	-2,1	-1,8	-1,8	-2,4
MAM	-1,6	-1,4	-1,2	-1,5	-1,3
JJA	-3,0	-1,9	-1,4	-1,6	-1,6
SON	-3,6	-1,6	-2,0	-1,4	-1,8
All_Seasons	-2,7	-1,8	-1,6	-1,6	-1,8

In Durban, NOR8.5 and MPI8.5 have smaller bias (less than 1°C) than for both CNR8.5 and GFD8.5 runs. At Mt. Edgecombe, GFD8.5 and MPI8.5 have a similar bias of -1.8°C, whereas CNR8.5 and NOR8.5 have higher negative bias (less than -2°C). During MAM, the bias is also positive and comparable for the Durban station (with CNR8.5 having

UNIVERSITEIT VAN PRETORIA
UNIVERSITY OF PRETORIA
YUNIBESITHI YA PRETORIA

the highest bias), whereas bias is negative for all model runs at Mt. Edgecombe station.

During JJA and SON, the temperature bias at the Durban station is generally positive and consistent across most simulations, except for the CNRM RCP8.5 run, which shows a negative bias. In contrast, all simulations show a negative bias at the Mt. Edgecombe station. Comparisons with ERAI run shows that the CCAM simulations underestimated the minimum temperature at both Durban and Mt. Edgecombe stations.

However, the overall bias scores reveal that CCAM tends to overestimate minimum temperature at the urban (Durban) station, an outcome which is consistent with previous studies, such as Thevakaran et al., (2016). Conversely, the model underestimated minimum temperature at Mt. Edgecombe (non-urban) station.

The minimum temperature RMSE scores are also shown in Table 3.3. During DJF, RMSE scores are lower in Durban (except for CNR8.5) and higher in Mt. Edgecombe. However, during MAM, the RMSE scores are similar in Durban and Mt. Edgecombe, except for the CNR8.5 run.

Table 3.3: The CCAM RMSE for minimum temperature for simulations with ERAI and representative concentration pathway 8.5 (RCP8.5) against observations at the urban station (Durban) and non-urban station (Mt. Edgecombe) for DJF, MAM, JJA, and SON for the period 2006-2016.

UNIVERSITEIT VAN PRETORIA
UNIVERSITY OF PRETORIA
YUNIBESITHI YA PRETORIA

		RMSE_MINT			
Durban	obs_vs_erai	obs_vs_cnr	obs_vs_gfd	obs_vs_mpi	obs_vs_nor
DJF	0,9	3,1	1,4	1,4	1,1
MAM	1,4	7,1	2,6	2,4	2,4
JJA	1,0	2,0	3,6	3,3	3,1
SON	1,7	1,9	1,9	2,0	1,8
All_Seasons	1,3	2,2	2,5	2,4	2,2
Mt_Edge		RMSE_MINT			
	obs_vs_erai	obs_vs_cnr	obs_vs_gfd	obs_vs_mpi	obs_vs_nor
DJF	2,5	2,5	2,2	2,3	2,7
MAM	1,7	2,2	2,1	2,4	2,2
JJA	3,1	2,8	2,7	2,4	2,5
SON	3,6	2,2	3,7	2,1	2,3
All_Seasons	2,7	2,4	3,3	2,3	2,4

During JJA, the RMSE scores are higher in Durban and Mt. Edgecombe. During SON, the RMSE scores are slightly lower in Durban than in Mt. Edgecombe. Comparison of observations with ERAI shows a lower bias for Durban compared to Mt. Edgecombe. The overall scores (all seasons) show that RMSE is slightly comparable but lower in Durban and higher in Mt. Edgecombe.

The maximum temperature bias at both urban and non-urban stations is shown in Table 3.4. DJF bias scores are negative at both urban station (Durban) and nonurban station (Mt. Edgecombe), except for ERAI, which is positive at Mt. Edgecombe. Bias remains negative during MAM, except for NOR8.5 at the Durban station and ERAI at Mt. Edgecombe. The bias is also mostly negative for JJA and SON in all CMIP5 runs at the two stations but is positive for ERAI at Mt. Edgecombe.

Table 3.4: The CCAM bias for maximum temperature for simulations with ERAI and representative concentration pathway 8.5 (RCP8.5) against observations at the urban station (Durban) and non-urban station (Mt. Edgecombe) for DJF, MAM, JJA, and SON for the period 2006-2016.

UNIVERSITEIT VAN PRETORIA
UNIVERSITY OF PRETORIA
YUNIBESITHI YA PRETORIA

Durban		BIAS_MAXT			
	obs_vs_erai	obs_vs_cnr	obs_vs_gfd	obs_vs_mpi	obs_vs_nor
DJF	-0,7	-0,5	-0,3	-0,3	-0,7
MAM	-0,1	1,7	-0,7	-0,6	-0,9
JJA	-0,6	-1,8	-1,3	-1,1	-1,5
SON	-0,6	-2,3	0,0	0,2	-0,3
All_Seasons	-0,5	-0,7	-0,5	-0,4	-0,9
Mt_Edgecombe		BIAS_MAXT			
	obs_vs_erai	obs_vs_cnr	obs_vs_gfd	obs_vs_mpi	obs_vs_nor
DJF	0,8	-0,6	-0,5	-0,3	-1,1
MAM	1,1	-0,9	-0,9	-0,8	-1,2
JJA	0,4	-2,1	-2,0	-1,5	-2,3
SON	0,1	-0,4	-0,9	0,0	-0,8
All_Seasons	0,6	-1,0	-1,1	-0,7	-1,3

The maximum temperature bias is negative for the CMIP5 runs and is mostly lower at the urban station compared to the nonurban station. These results are comparable to the results achieved in a study by Thevakaran et al., (2016) over Asia.

The RMSE scores for maximum temperature for both stations are also shown in Table 3.5. The scores are comparable and less than 2°C at both the Durban and Mt. Edgecombe stations during DJF season. For MAM, the RMSE is still comparable to DJF but slightly less for Durban when compared to Mt. Edgecombe. The JJA scores are slightly lower in Durban compared to Mt. Edgecombe but higher than during the DJF and MAM seasons.

Table 3.5: The CCAM RMSE for maximum temperature for simulations with ERAI and representative concentration pathway 8.5 (RCP8.5) against observations at the urban station (Durban) and non-urban station (Mt. Edgecombe) for DJF, MAM, JJA, and SON for the period 2006-2016.

UNIVERSITEIT VAN PRETORIA
UNIVERSITY OF PRETORIA
YUNIBESITHI YA PRETORIA

		RMSE_MAXT			
Durban	obs_vs_erai	obs_vs_cnr	obs_vs_gfd	obs_vs_mpi	obs_vs_nor
DJF	0,8	1,8	1,2	1,5	1,4
MAM	0,5	2,1	1,3	1,2	1,6
JJA	0,7	2,1	1,7	1,5	1,8
SON	0,7	2,5	1,3	1,1	1,0
All_Seasons	0,7	1,4	1,4	1,3	1,5
Mt_Edge		RMSE_MAXT			
	obs_vs_erai	obs_vs_cnr	obs_vs_gfd	obs_vs_mpi	obs_vs_nor
DJF	1,3	1,6	1,5	1,3	1,7
MAM	1,4	1,7	1,8	1,6	2,0
JJA	0,8	2,5	2,7	2,0	2,8
SON	0,7	1,3	2,5	1,1	1,4
All_Seasons	1,0	1,8	2,4	1,5	2,02

Likewise, during SON, RMSE scores are comparable at both Durban and Mt. Edgecombe, except for CNR8.5, which is higher in Durban than in Mt. Edgecombe, and GFD8.5, which is higher in Mt. Edgecombe than Durban. Comparison with ERAI runs show lower RMSE in Durban and Mt. Edgecombe compared to CMIP5 runs. The overall scores show that RMSE is higher in Mt. Edgecombe compared to the Durban station. Detailed comparisons of stations data against ERAI runs were performed in Chapter 2, and this analysis shows variability associated with model input data.

The current statistical analysis indicates that CCAM underestimated maximum temperature at both urban and non-urban stations, with biases ranging between -2°C and 2°C. At the non-urban station (Mt. Edgecombe), the model has overestimated minimum temperatures. In contrast, results for the urban station (Durban) are mixed but remain within the same bias range of -2°C and 2°C.

These findings are consistent with a climate change study by Chapman et al., (2019), which reported similar patterns across stations in Brisbane, Australia. The RMSE is used as an indicator of overall model error, as discussed by Gordon and Shaykewich, (2000). In this analysis, the average RMSE is less than 3°C, suggesting that CCAM demonstrates satisfactory performance in simulating temperature extremes.

UNIVERSITEIT VAN PRETORIA
UNIVERSITY OF PRETORIA
YUNIBESITHI YA PRETORIA

3.3.2 CCAM simulations and climate projections with ERAI and CMIP5 data

In this section, CCAM simulations are analysed for three climate periods: the current (2006-2016), the near-future (2040-2050), and the far-future (2090-2099) climate, respectively. Although simulations were performed for all seasons (DJF, MAM, JJA, and SON) and averaged over 10 years, the UHI is a summer event, so only the DJF season is analysed. In applying RCP8.5 data, we were motivated by the fact that RCP8.5 data takes into consideration warming, as compared to RCP4.5 data, which shows that radiative forcing stabilised at 4.5 W/m^2 towards the end of 2100 (Riahi *et al.*, 2011; Thomson *et al.*, 2011; Maure *et al.*, 2018a; Muthige *et al.*, 2018).

3.3.2.1 CCAM simulations and validation during the climate periods 2006-2016, 2040-2050 and 2090-2099

During the current climate, CCAM simulations with CNR8.5, GFD8.5, MPI8.5, NOR8.5, and ERAI are compared. However, in analysis for the near-future and far-future climates, only CMIP5 runs are compared, as ERAI reanalysis data are only available for the current climate. For ease of analysis, the city eThekwini, and thus the UHI is dominantly located to the east of the 30.9°E longitude of the simulation domain.

a) Minimum temperature

Figure 3.8 presents the simulation of DJF minimum temperatures for the current climate, near-future, and far-future periods. The city and the UHI are predominantly located to the east of the 30.9°E longitude, along the coastal city of eThekwini. During the current climate, the simulations clearly display a broader spatial and temporal distribution of minimum temperature, along with a distinct UHI effect (Figure 3.8, left panels). Its strength varies across different models, however, all CMIP5 models show strong agreement, with elevated minimum temperatures averaging around 20°C within the city. This highlights the presence of the UHI to the east of 30.9°E longitude. In contrast, temperature drops below 20°C to the west of this longitude, outside the UHI-affected zone. These findings are consistent with the study by Chen et al. (2014), which reported that the UHI effect is evident in both mean and minimum temperatures and is closely aligned with the distribution of urban land cover.

UNIVERSITEIT VAN PRETORIA
UNIVERSITY OF PRETORIA
YUNIBESITHI YA PRETORIA

The simulated change in minimum temperature for the near-future climate is illustrated by shading in Figure 3.8 (middle panels). The results show a slight increase in the spatial distribution of average temperatures, with a rise of approximately 1-2°C across the entire domain. This increase varies with the four CMIP5 models, with GFD8.5 and NOR8.5 showing an increase of nearly 2°C, followed by CNR8.5 and lastly MPI8.5, with an increase of 1°C. This increase is similar to the changes seen in maximum temperature (Figure B.1).

In the near future, the actual minimum temperature, which depicts the UHI, is shown as contours in the middle panel of Figure 3.8. These contours indicate that areas with temperatures higher than 20°C have shifted slightly to the west of the 30.9°E longitude. This westward shift suggests a slight intensification of the UHI, with an average increase of approximately 2°C within the UHI. Overall, the minimum temperature increases by about 1-2°C across the domain, depending on the specific CMIP5 simulation.

Similarly, changes in minimum temperature for the far-future climate, relative to the current climate, are shown in shading in Figure 3.8 (right panels). These results show an increase of temperature by nearly 2-4°C compared to the near-future climate. However, this increase varies with CMIP5 models, with GFD8.5 showing a greater increase in the spatial distribution of higher temperatures by nearly 4°C compared to the current climate. Simulations with CNR8.5 and MPI8.5 show similar changes, with an increase of about 3°C compared to the near-future climate. In contrast, NOR8.5 shows the smallest change, with an increase of around 2°C. These simulations show that CMIP5 models exhibit internal variabilities.

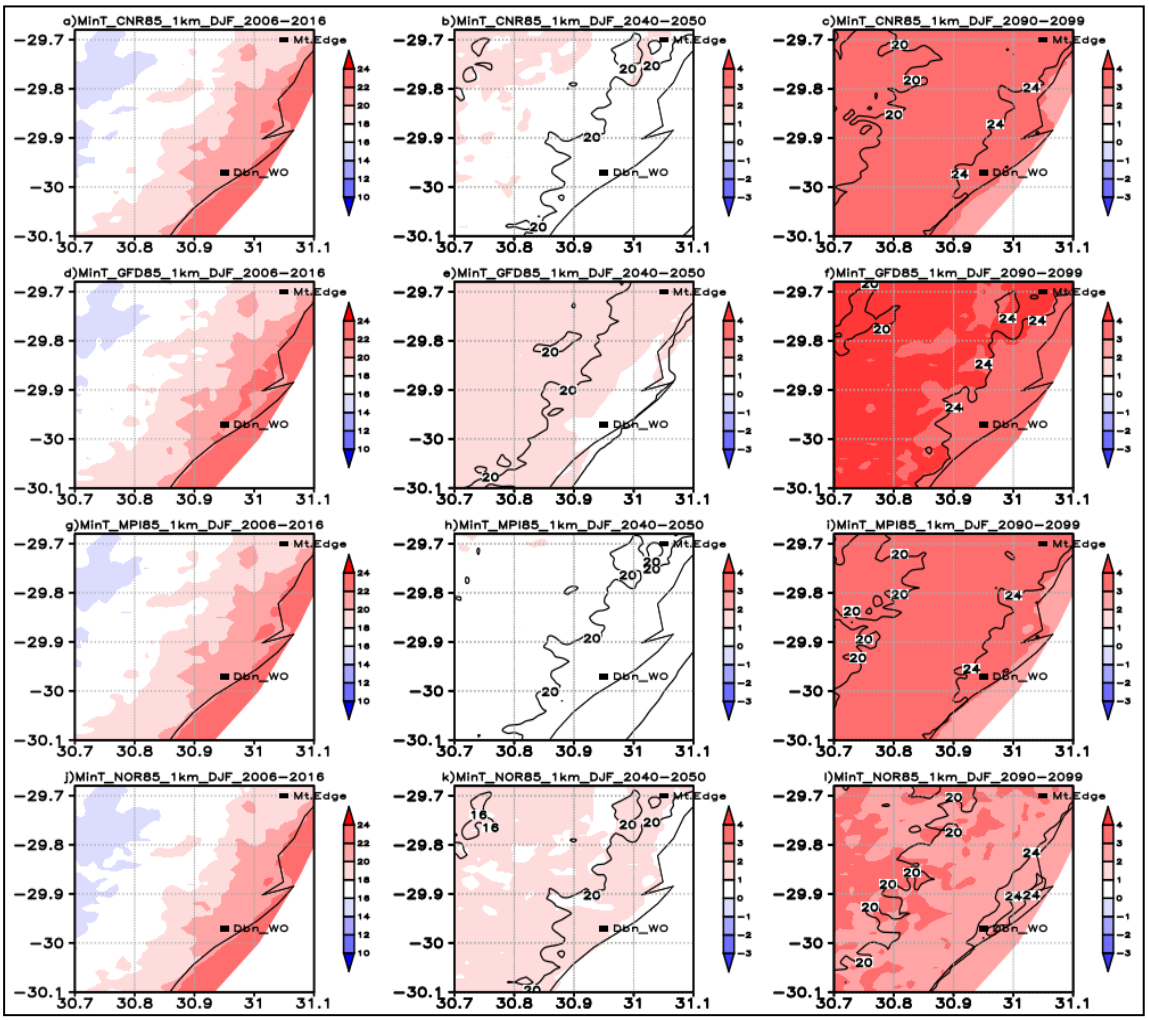

Figure 3.8: The CCAM simulation of minimum temperature with four RCP8.5 scenarios for the DJF period (2006-2016) and changes for the period (2040-2050) and (2090-2099) relative to (2006-2016) baseline. Changes from current to the near -future ((2040-2050) minus (2006-2016)) and from current to the far-future ((2090-2099) minus (2006-2016)) are shaded, whereas the near-future (2040-2050) and far-future (2090-2099) minimum temperature are contoured. Both Durban (to the south of the domain, 29.965°S; 30.946°E) and Mt. Edgecombe (to the northeast of the domain, 29.706°S; 31.046°E) stations are plotted.

The actual minimum temperature simulations for the far-future climate are shown as contours in Figure 3.8 (right panels). The contour of the UHI (as in the right panel) shows its spread, with the 20°C temperature contour having increased to at least 24°C, and the 20°C contour shifting from 30.9°E to longitude 30.7°E. These CMIP5 simulations indicate an average temperature increase of approximately 4°C, over the UHI, thus intensifying the UHI effects by nearly 4°C compared to the current and near-future climates.

UNIVERSITEIT VAN PRETORIA
UNIVERSITY OF PRETORIA
YUNIBESITHI YA PRETORIA

These results show that CMIP5 models exhibit internal variabilities. Similar to the minimum temperature patterns, the UHI contour (as shown in the middle panel) shows its spatial spread. Areas with average temperatures of 20°C have increased to at least 24°C, contributing to a strengthening of the UHI by nearly 4°C compared to the current and near-future climates.

The CMIP5 RCP8.5 scenario represents a low mitigation, high emission pathway (Riahi *et al.*, 2011; Taylor *et al.*, 2012). It suggests that due to climate change, temperatures will increase and spread over larger areas over South Africa affecting both urban and rural, as confirmed in Maure *et al.*, (2018a). This increase in minimum temperature is expected to intensify the UHI effect. Future projections of higher minimum temperatures in cities due to increased urbanisation have been confirmed in the IPCC (2023) report, which indicates that the resulting warming could be comparable to the broader global warming signal.

b) Surface temperature

The simulated surface temperature during the current climate shows a detailed spatial distribution of the SUHI over the city of eThekwini (Figure 3.9, left panels). Due to the presence of the UHI, temperature values range from 26 to 30°C over the UHI (to the east of the 30.9°E longitude). In contrast, temperature values drop below 26°C to the west of the 30.9°E longitude, further away from the city. This pattern is persistent across all the CMIP5 simulations, although GFD8.5 shows some small, isolated islands of temperatures exceeding 30°C. This is consistent with the study by Chen et al., (2014), which showed higher intensity of the UHI in surface temperatures (SUHI) compared to the UHI shown in two metres temperatures. This difference is due to urban land categories with urban fraction higher than 95%. These simulations show that the UHI dominates areas of high urban fraction, which also agrees with a study by Katzfey et al., (2020).

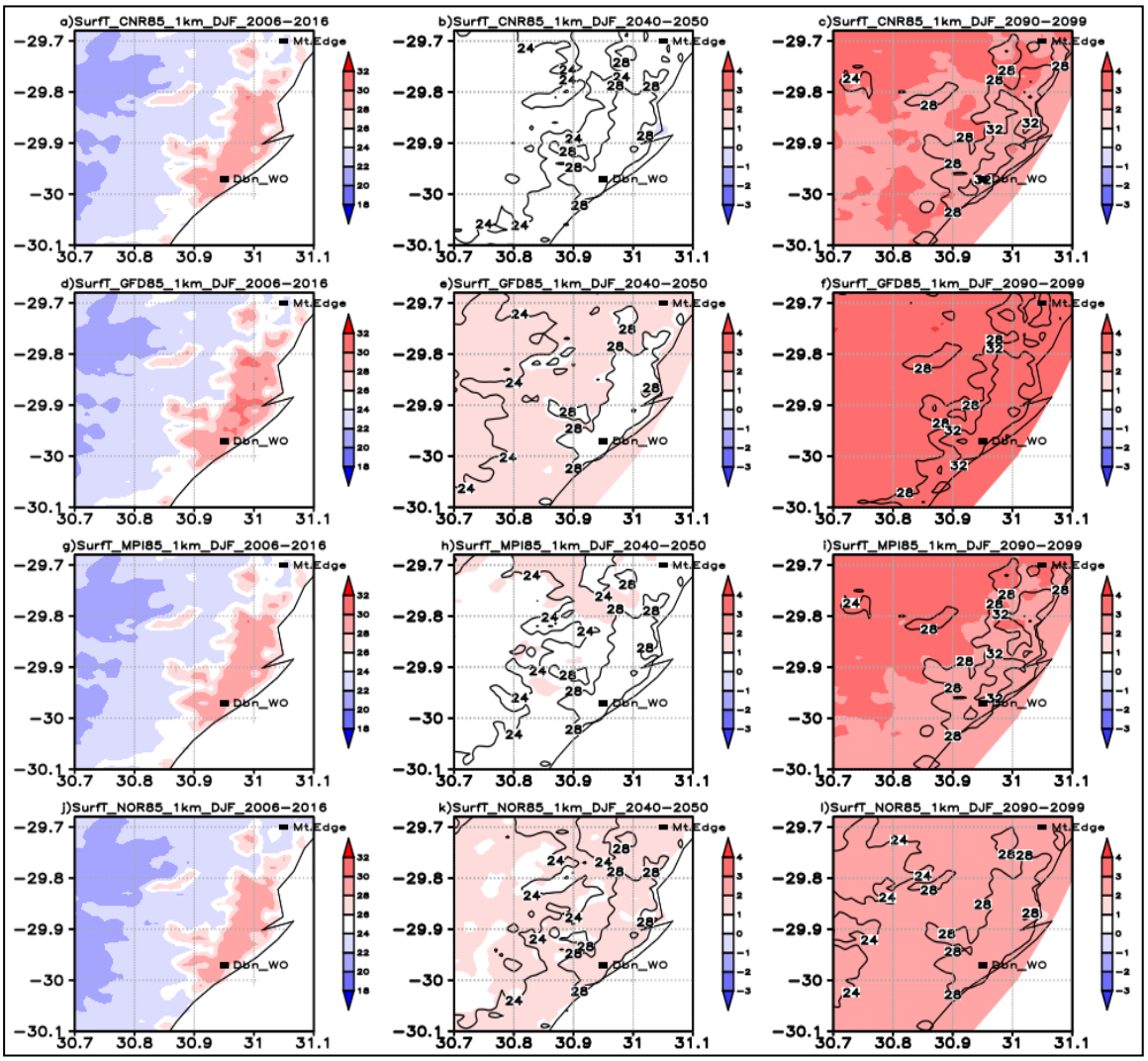

Figure 3.9: The CCAM simulation of surface temperature with four RCP8.5 scenarios for the DJF period (2006-2016) and changes for the period (2040-2050) and (2090-2099) relative to (2006-2016) baseline. Changes from current to the near -future ((2040-2050) minus (2006-2016)) and from current to the far-future ((2090-2099) minus (2006-2016)) are shaded, whereas the near-future (2040-2050 and far-future (2090-2099) surface temperature are contoured. Both Durban (to the south of the domain, 29.965°S; 30.946°E) and Mt. Edgecombe (to the northeast of the domain, 29.706°S; 31.046°E) stations are plotted.

Changes in surface temperature during the near-future climate (Figure 3.9, middle panel, shaded) show an average increase of 1-2°C compared to the current climate. This trend is consistent for both maximum and minimum temperatures. Although the magnitude of change varies amongst different CMIP5 models, GFD8.5 and NOR8.5 project an average increase of 2°C, while CNR8.5 and MPI8.5 project a smaller

UNIVERSITEIT VAN PRETORIA
UNIVERSITY OF PRETORIA
YUNIBESITHI YA PRETORIA

increase of approximately 1°C compared to the current climate. The distribution of the SUHI, shown in contours, shows temperatures exceeding 28°C within the city (middle panel), and temperature below 28°C in the surrounding rural areas. These simulations indicate that the 26°C temperature contour has shifted westward of the 30.9°E longitude, leading to an average increase in UHI intensity of approximately 2°C.

Changes seen in surface temperature in the far-future climate (Figure 3.9, right panels, shaded) are also similar to changes seen in minimum temperature (Figure 3.8). The increase has spread to larger areas of the domain. All CMIP5 simulations show an increase in temperature by an average of 3°C compared to the current and near-future climate. The GFD8.5 simulation shows strongest changes, followed by CNR8.5 and MPI8.5, with NOR8.5 showing the least spread of 2°C over the simulation domain.

The distribution of the SUHI, shown in contours, indicates a spread in areas of temperature range of 28-32°C within the city. However, the NOR8.5 simulation shows no changes in SUHI compared to the near-future climate, with average temperature around 28°C. In contrast, CNR8.5, GFD8.5 and MPI8.5 simulations show a stronger UHI effect, with an average temperature of approximately 32°C, representing an increase of 4°C from the near-future climate. These results highlight the internal variability among the four CMIP5 simulations when downscaled using the CCAM.

c) Maximum temperature

During the current climate period, simulation of maximum temperature does not reproduce the UHI (Figure B.3, left panel, shaded), which agrees with the study by Chen *et al.*, (2014). This could be due to daytime turbulent mixing from the convective boundary layer, which removes heat from the surface (Parker, 2010; Luhar *et al.*, 2014; Krishnamurthy *et al.*, 2021; Sedlar *et al.*, 2022). Higher maximum temperatures, averaging 26-30°C, were simulated in urban areas along the coast, (to the east of the 30.9°E longitude), with temperatures less than 26°C simulated away from urban areas. This applies to all CMIP5 simulations, respectively.

UNIVERSITEIT VAN PRETORIA
UNIVERSITY OF PRETORIA
YUNIBESITHI YA PRETORIA

Changes in maximum temperature from the current to the near-future climate (Figure B.3, middle panel, shaded) do not clearly indicate the presence of a UHI. However, they do show a slight spatial increase in average temperature by approximately 1°C across CNR8.5, MPI8.5 and NOR8.5 model simulations. In contrast, the GFD8.5 simulation shows pronounced warming, with an average increase of 2°C across the entire simulation domain.

Changes in maximum temperature in the far-future climate show an increase of 2-4°C over eThekwini (Figure B.3, right panel, shaded). However, this increase varies among CMIP5 model simulations, reflecting internal model variability. The CNR8.5, MPI8.5 and NOR8.5 simulations project temperature increases of 2-3°C, while only GFD8.5 simulation shows a large increase of up to 4°C, which is on average 1°C higher than all the other CMIP5 simulations. Notably, none of the far-future simulations display a clear UHI signal.

d) Longwave, shortwave, and net radiation

(i) Longwave radiation

The CMIP5 simulated longwave radiation is presented in Figure 3.10. These simulations indicate that, within the UHI (east of the 30.9°E longitude), an average of 60 to 80 W/m^2 of longwave radiation is emitted into space (Figure 3.10, left panels). The amount of longwave radiation released varies among the CMIP5 models, with CNR8.5 and GFD8.5 showing more radiation released compared to MPI8.5 and NOR8.5.

Changes in the emitted longwave radiation in the near-future climate (Figure 3.10, middle panel, shaded) shows a negative change for CNR8.5 and GFD8.5. These two model simulations indicate a decrease in longwave radiation released into the atmosphere, with an average reduction of less than 10 W/m^2 compared to the current climate levels, which range from 70 to 90 W/m^2. In contrast, the MPI8.5 and NOR8.5 simulations show positive changes, with an increase in longwave radiation being emitted into space.

UNIVERSITEIT VAN PRETORIA
UNIVERSITY OF PRETORIA
YUNIBESITHI YA PRETORIA

Changes in the emitted longwave radiation in the far-future climate (Figure 3.10, right panel, shaded) show negative changes. There is an average decrease in all CMIP5 models. This is almost similar to the changes seen CNR8.5 and GFD8.5 during the near-future climate. These changes could be attributed to the modified city surface which absorb longwave radiation as compared to its release into space. The projected longwave radiation shows a slight decrease throughout the entire domain, with an average of 40 W/m^2, which is slightly less than 60 W/m^2 simulated during the current climate. These suggest that, in a warming climate, more longwave radiation may be absorbed rather than emitted, thereby enhancing the urban heat island (UHI) effect in the future.

(ii) Shortwave radiation

The distribution of shortwave radiation is depicted in Figure B.4 and contrasts with that of longwave radiation, as shortwave radiation does not capture the variation associated with the UHI. During the current climate period (Figure B.4, left panels, shaded), all CMIP5 simulations are consistent, showing shortwave radiation values ranging from approximately 200 W/m^2 in areas away from the city to values exceeding 220 W/m^2 over the city.

Simulated changes in shortwave radiation during the near-future climate (Figure B.4, middle panels, shaded) show negative changes in the CNR8.5 and GFD8.5 simulations, while MPI8.5 and NOR8.5 display positive changes. This reflects variability in the boundary forcings applied across the CMIP5 models. Despite these differences, the contoured simulations of shortwave radiation show a slight overall increase over the city, with average values rising from approximately 200 to 220 W/m^2.

Changes in simulated shortwave radiation during the far-future climate (Figure B.4, right panels, shaded) show negative changes in the CNR8.5, GFD8.5 and NOR8.5 simulations, while MPI8.5 shows a slight positive change. Both CNR8.5 and GFD8.5 show a consistent decrease in shortwave radiation from the near-future to the far-future climate. The transitions from positive values in the near-future to negative values in the far-future for both MPI8.5 and NOR8.5 simulations indicate a reversal in

UNIVERSITEIT VAN PRETORIA
UNIVERSITY OF PRETORIA
YUNIBESITHI YA PRETORIA

trend. These patterns highlight the variability among CMIP5 model projections for future shortwave radiation.

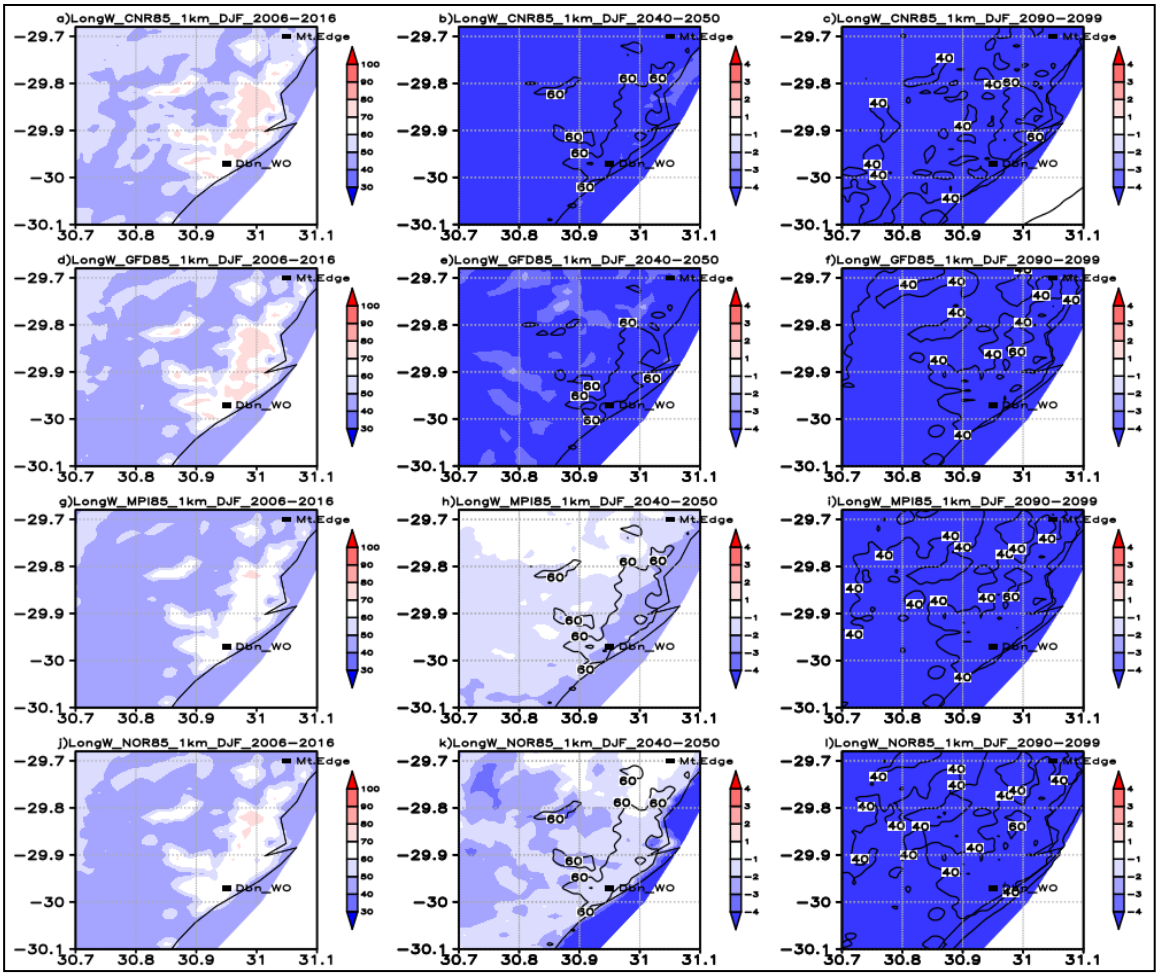

Figure 3.10: The CCAM simulation of longwave radiation with four RCP8.5 scenarios for the DJF period (2006-2016) and changes for the period (2040-2050) and (2090-2099) relative to (2006-2016) baseline. Changes from current to the near -future ((2040-2050) minus (2006-2016)) and from current to the far-future ((2090-2099) minus (2006-2016)) are shaded, whereas the near-future (2040-2050 and far-future (2090-2099) longwave radiation are contoured. Both Durban (to the south of the domain, 29.965°S; 30.946°E) and Mt. Edgecombe (to the northeast of the domain, 29.706°S; 31.046°E) stations are plotted.

(iii) Net radiation

The CMIP5 simulation of net radiation for all climate periods is shown in Figure B.5. Net radiation is defined as the difference between shortwave and longwave radiation. All the CMIP5 simulations reproduced the UHI observed in both minimum and

UNIVERSITEIT VAN PRETORIA
UNIVERSITY OF PRETORIA
YUNIBESITHI YA PRETORIA

surface temperatures. In the UHI region (to the east of the 30.9° longitude), net radiation values exceed 120 W/m^2 over the city and fall below 120 W/m^2 in surrounding rural areas, away from the city. These results are consistent with the patterns of longwave radiation (Figure 3.10).

Changes in net radiation into the near-future climate show variability across CMIP5 simulations (Figure B.5, middle panel, shaded). The GFD8.5 simulation indicates a decrease in net radiation, with values dropping below -6 W/m^2 over the entire domain. In contrast, the CNR8.5 simulation shows positive changes, with an average increase of 2 W/m^2 over the city, and negative changes less than -2 W/m^2 in surrounding areas. However, positive changes are observed in both MPI8.5 and NOR8.5, with NOR8.5 showing more positive changes than MPI8.5. Additionally, the actual net radiation values are projected to increase from 140 W/ m^2 (current climate) to values higher than 160 W/m^2 over the city (middle panel, contoured), with lower values away from the city.

Changes in net radiation into the far-future climate also exhibit variability across the CMIP5 simulations (Figure B.5, right panel, shaded). Both the CNR8.5 and NOR8.5 simulations show more negative changes compared to the previous climate periods, with values falling below-2 W/m^2 within the city, and even more negative changes in surrounding areas. The GFD8.5 simulation similarly shows negative changes, averaging between 2 to -2 W/m^2 within the city, with greater decreases outside the urban area. However, these changes are less pronounced than those observed during the near-future climate period. Among the simulations, only MPI8.5 shows positive changes, with values exceeding 2 W/m^2 within the city and even higher increases in areas outside the city.

The actual net radiation values in CMIP5 simulations show some variation (Figure B.5, right panel, contoured). No significant increase in net radiation is observed in CNR8.5, GFD8.5 and MPI8.5 simulations, suggesting that the UHI effect remains similar to that in previous periods. In contrast, the NOR8.5 simulation shows a slight decrease in net radiation during the far-future period, indicating a weakened UHI effect.

UNIVERSITEIT VAN PRETORIA
UNIVERSITY OF PRETORIA
YUNIBESITHI YA PRETORIA

e) Sensible heat flux

Sensible heat flux has also been analysed to explore the influence of anthropogenic heating and changes from natural surfaces to artificial ones. As shown in Figure 3.11 (left panel), sensible heat flux is highest within the city (to the east of the 30.9° longitude), with average values ranging from 80 to120 W/m^2, and decreases in areas outside the city. This variation could be attributed to artificial materials, reduced evapotranspiration, and higher air temperature (Katzfey *et al.*, 2020). This pattern is shown in all four CMIP5 simulations. This spatial pattern is consistently observed across all four CMIP5 simulations, which are in agreement with findings from previous studies (Taha 1997; Chen *et al.*, 2014; Chapman *et al.,* 2019).

Changes in sensible heat flux in the near-future climate show some variability across the CMIP5 simulations (Figure 3.11, middle panel, shaded). The CNR8.5 simulation exhibits smaller positive changes within the UHI and more pronounced negative changes outside the UHI. In contrast, the GFD8.5 simulation shows a negative change within the UHI, and positive changes in surrounding areas. Both MPI8.5 and NOR8.5 display modest positive changes within the city and stronger positive changes outside the urban area.

The actual sensible heat flux simulations are shown as contours in Figure 3.11 (middle panel). All CMIP5 simulations indicate average values ranging from 40 to 80 W/m^2 within the UHI, located to the right of the 30.9° longitude, and lower values observed in areas outside the city. These results suggest that urban areas experience increased sensible heat flux, likely due to reduced latent heat flux resulting from fewer water bodies and limited surface moisture availability.

Changes in sensible heat flux in the far-future climate (Figure 3.11, right panel, shaded) show a slight decrease in GFD8.5, MPI8.5 and NOR8.5 simulations, with average values less than 40 W/m^2 in areas outside the UHI. In contrast, the CNR8.5 displays a shift from negative to positive changes, with average values around 20 W/m^2, observed across both urban and non-urban areas (Figure 3.11, right panel).

UNIVERSITEIT VAN PRETORIA
UNIVERSITY OF PRETORIA
YUNIBESITHI YA PRETORIA

The changes in these model-simulated variables indicate that the urban heat island (UHI) effect is projected to intensify during summer in both the near-future and far-future periods. The simulation of UHI shows that currently non-urban areas may experience temperature increases of up to 2-3°C. This warming is primarily attributed to anthropogenic forcings, including urban expansion and land surface modifications.

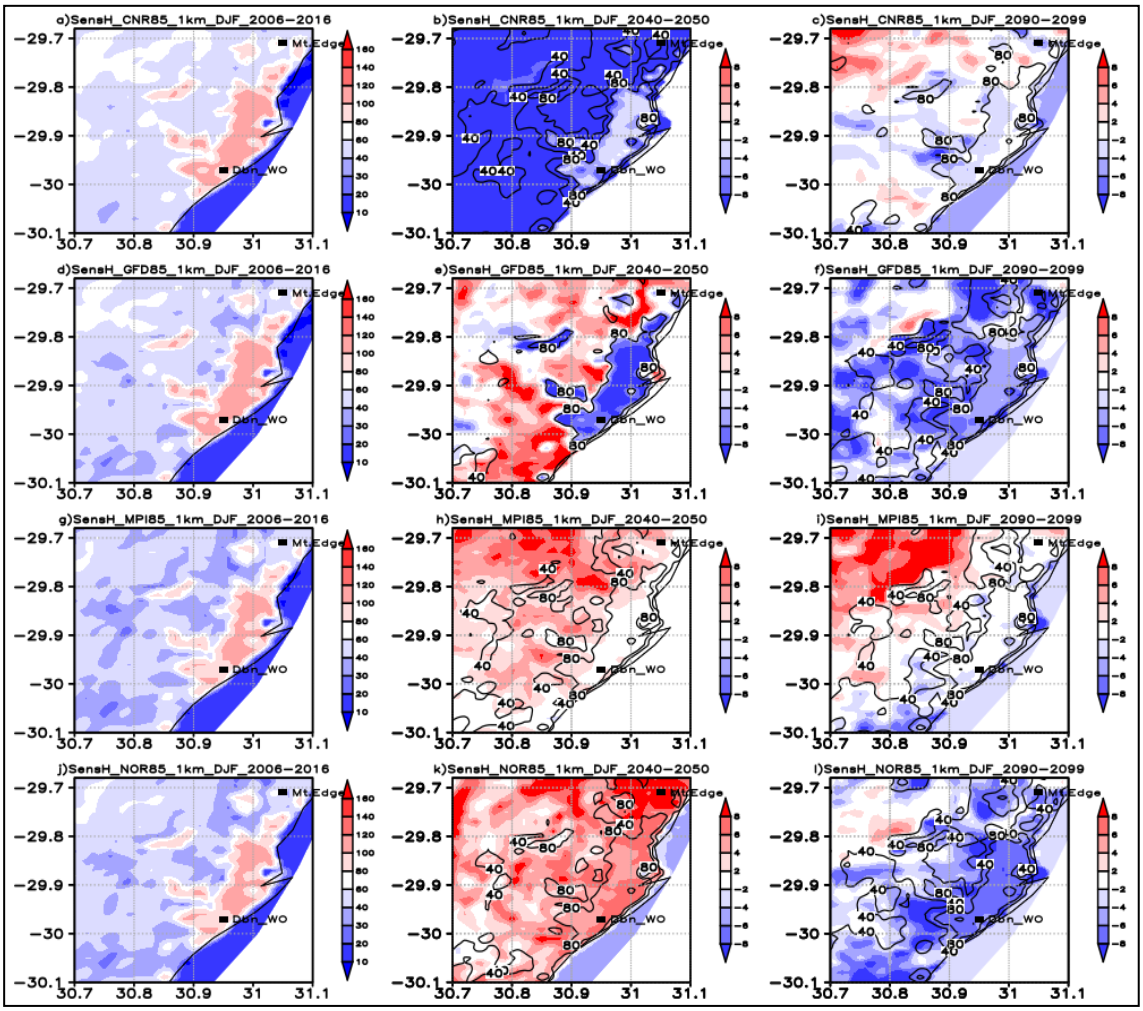

Figure 3.11: The CCAM simulation of sensible heat flux with four RCP8.5 scenarios for the DJF period (2006-2016) and changes for the period (2040-2050) and (2090-2099) relative to (2006-2016) baseline. Changes from current to the near-future ((2040-2050) minus (2006-2016)) and from current to the far-future ((2090-2099) minus (2006-2016)) are shaded, whereas the near-future (2040-2050 and far-future (2090-2099) sensible heat flux are contoured. Both Durban (to the south of the domain, 29.965°S; 30.946°E) and Mt. Edgecombe (to the northeast of the domain, 29.706°S; 31.046°E) stations are plotted.

UNIVERSITEIT VAN PRETORIA
UNIVERSITY OF PRETORIA
YUNIBESITHI YA PRETORIA

3.3.2.2 CCAM simulations of diurnal range during the climate periods 2006-2016, 2040-2050 and 2090-2099

The areal average was computed for the region covering the city of eThekwini. The diurnal range, averaged over the city for the current climate period (2006–2016), was analysed along with its projected changes for the near-future (2040–2050) and far-future (2090–2099) climates. During the current climate period, the diurnal ranges from the CNR8.5, GFD8.5, MPI8.5, and NOR8.5 models were compared with the ERA-Interim (ERAI) diurnal range.

a) Surface temperature

The 24-hourly diurnal range of surface temperature during summer (DJF) and winter (JJA) seasons is shown in Figure 3.12. The DJF daily range (Figure 3.12a) shows strong agreement among all CMIP5 models, including ERAI, with minimum values ranging from just above 20°C to 21°C, and maximum values of range from above 26°C to 28°C, resulting in an average diurnal range of average 8°C (20-28°C). During the early hours, 00–02h00 UTC, the temperature remains constant probably due to minimum values not dropping much from the previous day. Similarly, after 17h00 UTC, the temperature drops very slowly to values seen at 00h00 UTC.

For winter (JJA), Figure 3.12d, shows that both minimum and maximum temperatures are relatively low. Minimum values range between 15°C and 16°C, while maximum values generally reach up to 22°C, except for ERAI which shows a higher average maximum value of 25°C. This results in an average diurnal range of approximately 7°C (15-22°C) for most CMIP5 models, except for ERAI, which has the highest diurnal range of nearly 10°C (Figure 3.12d). This suggests that ERAI simulates higher maximum temperature values compared to all the CMIP5 model runs.

Changes in diurnal range from current to the near-future summer (DJF) climate period excludes ERAI run, which is only available during the current climate. The diurnal range shows a similar pattern between different RCP8.5 runs (Figure 3.12b). There is a slight increase in minimum temperature values which averages around 22°C, and maximum values averaging around 28°C, leading to the strength of the diurnal

UNIVERSITEIT VAN PRETORIA
UNIVERSITY OF PRETORIA
YUNIBESITHI YA PRETORIA

range averaging around 6°C (22-28°C) in comparison to the current climate. The changes show a rise in minimum temperature values by nearly 2°C from the current climate, with initial values ranging from 20-21°C to values slightly less than 22°C at 00h00 UTC. This result indicates the increase of temperatures from the current to the near-future climate.

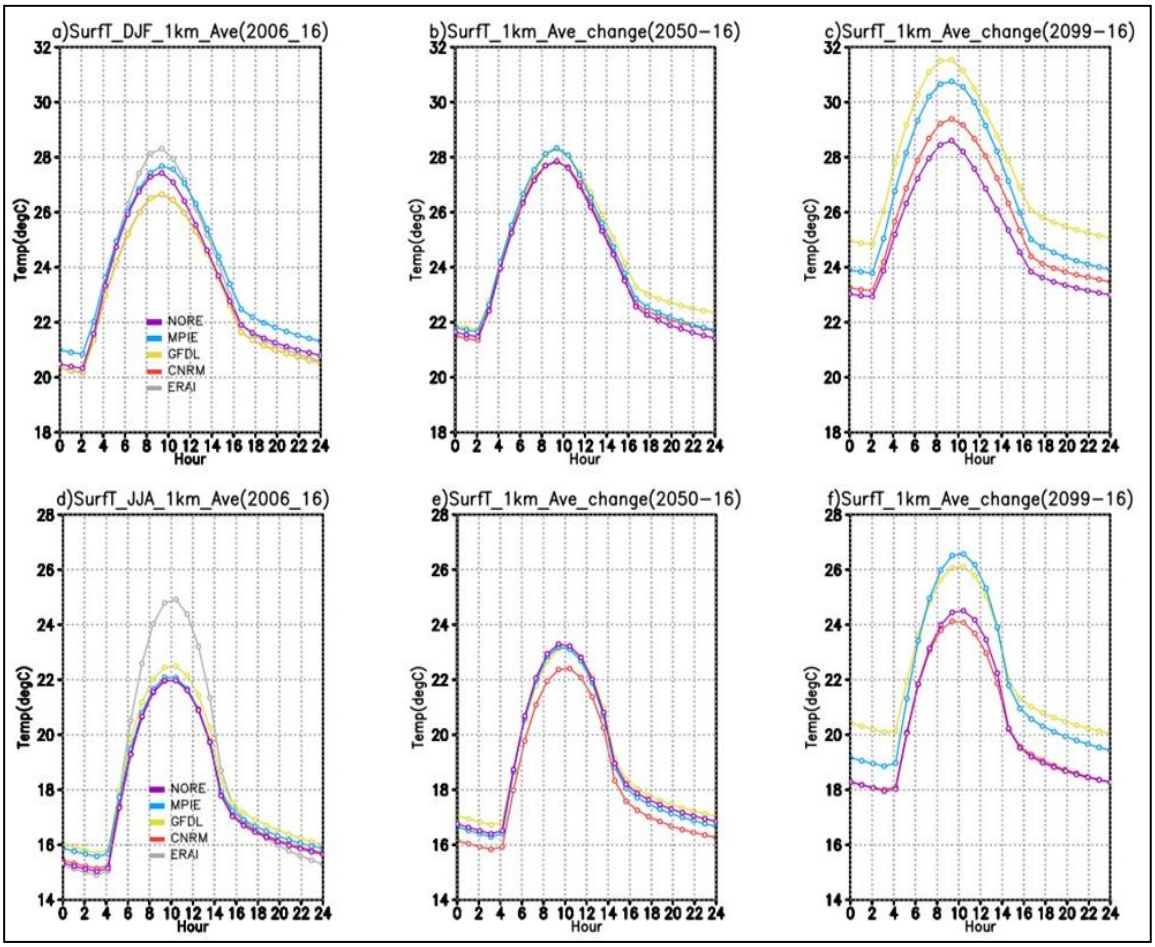

Figure 3.12: The CCAM diurnal range of surface temperature with ERAI and RCP8.5 simulations for summer (DJF) and winter (JJA) period 2006-2016 and changes in diurnal range during the climate periods 2039/40-2050 and 2089/90-2099 respectively.

Changes in winter (JJA) temperature (Figure 3.12d) show an increase from minimum values below 16°C, to slightly above 16°C on average, while maximum values rise from an average around 22°C to just above 22°C during the near-future climate (Figure 3.12e). This indicates a slight increase in minimum values and weakening in the diurnal range, which averages around 6°C in all the CMIP5 simulations.

UNIVERSITEIT VAN PRETORIA
UNIVERSITY OF PRETORIA
YUNIBESITHI YA PRETORIA

Figure 3.12c illustrates the changes in the diurnal range of surface temperature from the current to the far-future summer (DJF) climate period (2090-2099). The surface temperature diurnal ranges show a wider spread within RCP8.5 simulations, with minimum values ranging from 23°C to 25°C, and maximum values ranging from just above 28°C to values slightly below 32°C. This results in an average diurnal range between approximately 5.5°C (23-28.5°C) and 6.5°C (25-31.5°C). This spread among the model simulations may be attributed to inter-model variability. Overall, the diurnal range during the far-future climate is slightly higher than in the current climate (Figure 3.12a) and near-future (Figure 3.12b) summer climate. These simulations indicate an average increase of less than 2°C in the near-future and up to 4°C in the far-future summer climate.

Changes in diurnal range during winter (Figure 3.12f) in the far-future climate show an increase in minimum values from an average 16°C and slightly higher during the near-future climate, to an average of 18°C and higher during the far-future climate. The maximum values have increased from an average higher than 22°C to an average higher than 24°C during the far-future climate. This increase represents a warming of winter temperature by an average of 2°C compared to the current and near-future climate as well as the summer temperatures (Figure 3.12c), winter temperatures also show spread among the CMIP5 runs, with MPI8.5 and GFD8.5 showing the most warming.

b) Longwave and net radiation

As in surface temperature, the diurnal range of longwave radiation is shown in Figure 3.13. The current climate (Figure 3.13a) summer (DJF) diurnal range is wider (from 02h00 UTC to 16h00 UTC). The CMIP5 simulations show minimum values of range 40-45 W/m^2 and maximum values of range 65-70 W/m^2, leading to an average diurnal range of 30 W/m^2. However, ERAI diurnal range is slightly higher, a minimum value of 45 W/m^2 and a maximum of 80 W/m^2, resulting in an average diurnal range of 35 W/m^2. The increase in diurnal range in summer could be due to a greater increase in minimum temperatures compared to maximum temperature. This is also

UNIVERSITEIT VAN PRETORIA
UNIVERSITY OF PRETORIA
YUNIBESITHI YA PRETORIA

an indication that the boundary layer takes longer to become cooler and stably stratified from the previous day mixing.

During the current climate winter season (JJA; Figure 3.13d), the diurnal range of outgoing longwave radiation exhibits greater variability. In the CMIP5 simulations, minimum values range from 65 to 70 W/m^2, while maximum values range from 85 to 95 W/m^2, resulting in an average diurnal range of at most 25 W/m^2. In contrast, ERAI shows higher values for both minimum and maximum, with a diurnal range of approximately 40 W/m^2(values ranging from 120 to 80 W/m^2), which is nearly twice that of the CMIP5 simulations.

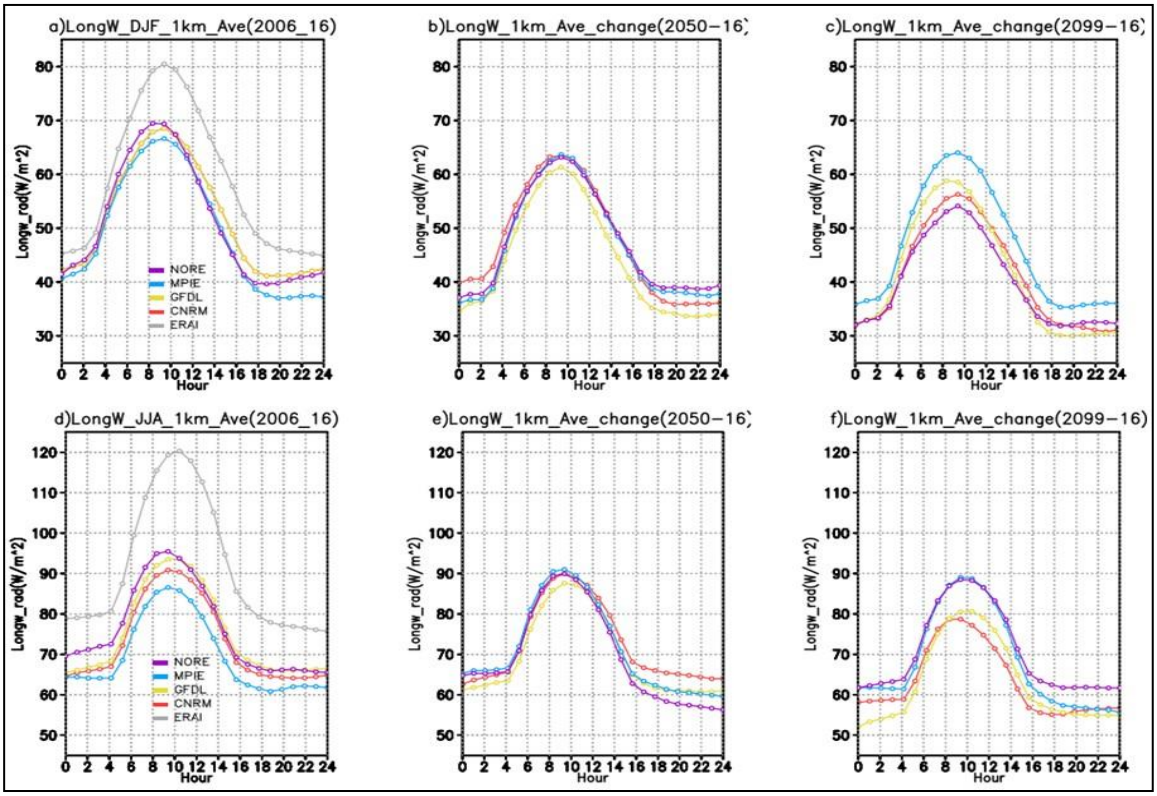

Figure 3.13: The CCAM diurnal range of longwave radiation with ERAI and RCP8.5 simulations for summer (DJF) and winter (JJA) period 2006-2016 and changes in diurnal range during the climate periods 2039/40-2050 and 2089/90-2099 respectively.

Changes in diurnal range during summer (DJF) from the current to the near-future climate (Figure 3.13b) shows a decrease in the diurnal range to an average of 20 W/m^2, compared to approximately 30 W/m^2 in the current climate. However, the initial values at 00h00 UTC average around 40 W/m^2, the final values at 24h00 UTC

UNIVERSITEIT VAN PRETORIA
UNIVERSITY OF PRETORIA
YUNIBESITHI YA PRETORIA

average around 60 W/m^2, indicating a slight decrease compared to the current climate.

This results in an average diurnal range of approximately 30-35 W/m^2. The apparent increase in the diurnal range suggests that, although shortwave radiation has not significantly increased, the variability in longwave radiation has intensified. This implies that more heat is being retained within the boundary layer, with less being released, thereby contributing to a warming effect.

During winter (JJA) in the near-future climate (Figure 3.13e), initial values of outgoing longwave radiation have slightly increased compared to summer, with minimum values averaging around 65 W/m^2, as opposed to the summer average of 40W/m^2. However, when compared to the current winter, there is little to no changes in spread, the current winter shows minimum values averaging between 65 and 80 W/m^2. Maximum values average around 90 W/m^2 in the near future, with less variability compared to the current climate. As a result, the diurnal range shows no spread relative to the current climate and averages around 25 W/m^2, which is almost similar to summer values. This indicates that only outgoing longwave radiation has increased in winter while the diurnal variability has remained largely unchanged.

In the far-future climate (Figure 3.13c), during the summer (DJF) season, the minimum values of outgoing longwave decrease to averages slightly above 30 W/m^2 and below 40 W/m^2, This suggests that more heat is retained near the surface than released into the atmosphere, indicating a strengthening of the UHI effect. Meanwhile, maximum values decreased to below 60 W/m^2 in most simulations, except for MPI8.5 which shows a higher maximum average of 75 W/m^2. As a result, the diurnal range remains nearly the same as in the near-future summer, averaging around 25 W/m^2, However, both the minimum and maximum values are higher compared to the current summer, reinforcing the trend of increased heat retention.

During winter (JJA) in the far-future climate (Figure 3.13f), the minimum value of outgoing longwave radiation increases from values lower than 40 W/m^2, observed in summer, to minimum values averaged around 60 W/m^2 except for GFD8.5, which has a slightly lower minimum value above 50 W/m^2. Compared to the near-future winter

UNIVERSITEIT VAN PRETORIA
UNIVERSITY OF PRETORIA
YUNIBESITHI YA PRETORIA

climate, these minimum values have slightly decreased. Maximum values, on the other hand, have increased from the near-future winter average of 90 W/m^2 to a range of 80-90 W/m^2. Compared to the far-future summer, maximum values have slightly increased, from a range of 55-65 W/m^2 to 80-90 W/m^2. As a result, the winter diurnal range shows more spread, varying between 20 and 30 W/m^2, and is comparable to both the far-future summer and near-future winter values. This indicates that during winter, less radiation is retained by urban surfaces and buildings compared to summer, resulting in more heat being released into the atmosphere.

The simulation of the diurnal range provides evidence that in the far-future climate, summer will experience more heating, leading to an increase in stored longwave radiation and anthropogenic heating, thereby strengthening the UHI. Likewise, in winter, more longwave radiation will be stored by buildings than released into the atmosphere, and anthropogenic heating will result in the strengthening of the UHI within the city. The two transitional seasons, autumn (MAM) and spring (SON), mark the beginning of either the strengthening (SON) or weakening (MAM) of the UHI, respectively.

3.4 Discussion

The study evaluates the simulations of the UHI during the current (2006-2016), near-future (2040-2050), and far-future (2090-2099) climates over the city of eThekwini. The CCAM simulations were conducted at a horizontal resolution of 1 km using both ERAI and CMIP5/RCP8.5 input data (Riahi *et al.*, 2011; Taylor *et al.*, 2012). The objective of the study was to investigate how the UHI effect over the city of eThekwini will change under climate change, under high emission, low mitigation scenario. This study was motivated by the fact that during the initial runs, CCAM-CABLE was set up with default land cover and RCP8.5 data. In those initial runs, CCAM simulations showed no dynamic changes in vegetation, which affected the temporal and spatial distribution of UHI even when the urban scheme was switched on. However, when the land cover and urban parameters were updated, simulations showed dynamical changes in vegetation and the correct spatial and temporal distribution of UHI.

UNIVERSITEIT VAN PRETORIA
UNIVERSITY OF PRETORIA
YUNIBESITHI YA PRETORIA

The CCAM simulations were validated using MODIS nighttime (LST) data for the period December 2012 to December 2013 and SAWS station temperature observations for the period December 2005 to December 2016. Model validation against MODIS data shows the intensity and magnitude of the UHI, with temperatures ranging from 2-4°C, higher within the city during DJF and lower temperatures away from the city. This agrees with some previous studies on the intensity of UHI including (Heaviside *et al.*, 2017; Barrao *et al.*, 2022; Maisha *et al.*, 2023). The ERAI simulations and the four RCP8.5 minimum temperature scenarios show a similar pattern but with varying strength. During DJF, MPI8.5 shows a stronger UHI and is comparable to MODIS but higher than ERAI and other CMIP5 simulations.

An analysis of spatial correlations for the period January to December 2013 shows variabilities, with high correlation between MODIS, CMIP5, and ERAI data during DJF (0.9). This correlation is slightly reduced during MAM (0.89), SON (0.61-0.73), and is lowest during JJA (>0.61).

Model validation against station-observed maximum and minimum temperatures reveals variability in the monthly distribution between the observations, ERAI, and CMIP5 simulations.

During the DJF season, the observed maximum temperature at Durban station is higher than simulated temperature, while at Mt. Edgecombe, the observed maximum temperature falls within the range of simulations. In contrast, the observed minimum temperature at Durban station is lower than simulated values, whereas at Mt. Edgecombe, it is higher than simulated minimum temperatures. However, temperature varies during other seasons, including MAM, JJA, and SON. Simulated minimum temperature shows variation during all months, with station-observed and ERAI data lower than all CMIP5 simulations.

The model's validation of diurnal temperature range was also analysed comparing station observation, ERAI, and the CMIP5-driven CCAM simulations over the period from December 2005 to December 2016. Results show notable temporal variation during the DJF season. The CCAM simulated temperatures are slightly lower than station observations during the early morning hours (00h00-04h00 SAST) and reach

UNIVERSITEIT VAN PRETORIA
UNIVERSITY OF PRETORIA
YUNIBESITHI YA PRETORIA

their maximum earlier than observed. Additionally, the CCAM-CMIP5 simulations exhibit a faster cooling rate compared to observations. This pattern of diurnal range observed during DJF is also observed during all other seasons though with some differences. On average, the observed diurnal range during DJF is approximately 5°C, while the CCAM simulations show a range between ~4°C and ~7°C. Similar variability in the diurnal range is observed across all seasons.

Validation statistics show that, at the Durban station, the CMIP5 simulations over-predict minimum temperature, with a positive bias averaging less than 2°C (Table 3.1), and an RMSE also averaging below 2°C, except for CNR8.5 with higher RMSE exceeding 3°C (Table 3.2). In contrast, the CMIP5 simulations under-predict maximum temperature, with a negative bias of less than -1°C (Table 3.3), and RMSE below 2°C (Table 3.4).

At the Mt. Edgecombe station, the CMIP5 simulations show a negative bias for minimum temperature, averaging less than -3°C (Table 3.1), with an RMSE averaging below 3°C (Table 3.2). The simulations also display a negative bias for maximum temperature, averaging less than -1°C (Table 3.3), except for ERAI, which shows positive bias of less than 1°C, and an RMSE averaging below 2°C.

These results indicate that the CCAM simulations driven by CMIP5 data tend to underpredict both maximum and minimum temperatures at the non-urban station (Mt.Edgecombe) station, while at the urban (Durban) station, they overpredict minimum temperatures and underpredict maximum temperatures.

This model performance, supported by observational data, provides confidence in the use of CCAM and CMIP5 data for simulating future temperature projections and assessing the Urban Heat Island (UHI) effect over the city of eThekwini. However, the inclusion of additional observational measurements would further strengthen the justification for conducting such studies.

After the CMIP5 simulations validation, the UHI projections were performed using ERAI and four CMIP5 datasets for the current, near-future and far-future climates. Variables including temperature (maximum, minimum and surface) as well as

UNIVERSITEIT VAN PRETORIA
UNIVERSITY OF PRETORIA
YUNIBESITHI YA PRETORIA

longwave, shortwave, and net radiation, and sensible heat flux were analysed. During the current climate, simulations show that the UHI is more dominant during summer (DJF) over the city of eThekwini. This is depicted in both the minimum and surface temperatures. However, there is no indication of the UHI in maximum temperature simulations, as confirmed in studies by Chen *et al.*, (2014) and Katzfey *et al.*, (2020).

During the near-future climate, the spatial distribution, and the strength of the UHI increased by an average of 1-2°C. This is shown in the distribution of both the minimum and surface temperature simulations. These simulations have also indicated that the UHI will spread to other seasons during the near-future climate. This could be due to an increase in anthropogenic heating, greenhouse gases and the expansion of the city.

During the far-future climate simulations, the UHI intensifies by an average between 3 to 4°C. The UHI is also expected to spread during the MAM season. The spread of UHI shown in minimum and surface temperature has resulted in an increase in maximum temperature over the domain. This finding agrees with previous studies including Chen *et al.*, (2014), which shows a UHI in both minimum and mean temperature over Hangzhou city in China. As in the city of Brisbane, the city of eThekwini is close to the Indian ocean, which moderates urban temperatures compared to rural temperatures (Chapman *et al.,* 2019). This could be due to higher sensible heat flux in urban areas, resulting in increased UHI. This study shows that urbanisation leads to the intensification of the UHI, and is in agreement with the study by Chen et al., (2014). An increase in anthropogenic emission and summer heating also leads to an increase in UHI. However under a warming climate, the need for winter heating will be reduced (Katzfey *et al.*, 2020).

An analysis of diurnal range shows that during the current climate; the diurnal range is higher during DJF and is reduced during other seasons. In the near-future climate, the diurnal range also shows a similar pattern to the current climate, but with an increase in minimum values by an average of 1 to 2°C for DJF, with a slight decrease during all other seasons. This pattern also applies to the far-future climate, but with

UNIVERSITEIT VAN PRETORIA
UNIVERSITY OF PRETORIA
YUNIBESITHI YA PRETORIA

an increase in minimum values by an average of ± 3°C during DJF and MAM, a decrease during JJA, and a slight increase during SON.

This study has shown that man-made factors determined the development of UHI: (i) the distribution of longwave radiation, and (ii) anthropogenic heating. Although there are no changes in shortwave radiation, longwave radiation shows some changes during the current, near-future and far-future climates. In the future climate, outgoing longwave radiation shows a decrease, which indicates more absorption by urban surfaces. This could result in an increase in net radiation (net difference between shortwave and longwave), thus intensifying the UHI.

An investigation of the boundary layer settings presents an opportunity to study the UHI into the future. The land cover and observed surface parameters were kept constant in this study. However, the UHI intensified into the future. This is attributed to changes in boundary forcings such as greenhouse gas emissions within RCP8.5 data. An increase in UHI resulted in an increase in variables such as maximum, minimum, and surface temperature, as well as planetary boundary layer. This could be attributed to a rise in greenhouse gases, i.e., CO_2, in the future leading to a rise in temperatures.

The IPCC (2023) report confirms that future increases in urbanisation are expected to lead to higher minimum temperatures, reflecting a global warming signal associated with urban development. This trend also contributes to the increased frequency and intensity of extreme climate events, including heatwaves. In cities, the removal of vegetation and increased drainage systems lead to more water being collected and removed from cities, resulting in less water available for evaporation. Together with longwave radiation, more heat gets trapped (Chen *et al.*, 2014), resulting in high values of net all-wave radiation due to radiation trapping, which increases the UHI. These simulations also show an increase in sensible heat flux, which could be due to the removal of vegetation as a result of urban expansion, further increasing the UHI (Taha, 1997; Pokhrel and Lee, 2011; Ramamurthy *et al.*, 2014; Estrada *et al.*, 2017; Chapman and Mcalpine, 2019).

UNIVERSITEIT VAN PRETORIA
UNIVERSITY OF PRETORIA
YUNIBESITHI YA PRETORIA

The UHI has a negative impact on climate and human life. Therefore, it is necessary to apply mitigating factors to reduce its impacts since it cannot be entirely removed. This includes increasing water bodies and re-vegetating cities. The availability of water bodies, such as the ocean, as well as increased vegetation, reduces the UHI effect (Theeuwes *et al.*, 2012; Nuruzzaman, 2015). This is because vegetation reduces UHI by increasing evapotranspiration (Chen *et al.,* 2015; Nuruzzaman 2015; Chapman et al., 2019). Similarly, using high albedo materials and green roofs reduces the effects of UHI and is considered an effective mitigation strategy to reduce surface and air temperatures, and therefore reducing the UHI effect (Taha, 1997; Chen *et al.*, 2015; Nuruzzaman, 2015; Estrada *et al.*, 2017).

This study has demonstrated that as a seamless system, the CCAM is adaptable to use any available global data including ERAI, ERA5 and any CMIP5 and CMIP6 dataset. The code is also adaptable to any global city as shown in this study and other cited studies.

3.5 Conclusion

In this chapter, various CCAM simulations were conducted for three climate periods. The CCAM was configured at a horizontal resolution of 1 km over the city of eThekwini, utilising both ERAI and RCP8.5 downscaled data of the CMIP5 project. The model was set up using updated land cover and measured urban parameters provided by the city of eThekwini.

Initial test simulations using default land cover showed no seasonal changes in vegetation, which affected the spatial and temporal distribution of UHI. However, when the land cover was updated, dynamical changes in vegetation were observed in various seasons, with the highest vegetation cover during summer season.

Model validation against MODIS temperature data revealed that the intensity of the UHI is in the range of 2-4°C higher within the city during DJF and diminishes during other seasons. Simulations with MPI8.5 are comparable to MODIS, but higher than ERAI simulation.

UNIVERSITEIT VAN PRETORIA
UNIVERSITY OF PRETORIA
YUNIBESITHI YA PRETORIA

The spatial correlation coefficient is 0.9 for all CMIP5 model simulations against MODIS during summer and is reduced to values slightly higher than 0.6 during winter. Model validation against station observations shows a similar monthly distribution pattern during all months. However, for maximum temperature, observations are slightly higher than CMIP5 simulations, resulting in negative bias at the two stations, whereas for minimum temperature, the observed temperatures are lower than CMIP5 simulations at an urban station, and higher than CMIP5 simulations at a non-urban station.

The CCAM simulations during current, near-future, and far-future climates indicate that the UHI is more pronounced during summer (DJF), with an intensity ranging from 2 to 4°C. The UHI is evident in minimum temperature and SUHI in surface temperature, but not in maximum temperature. It is also reflected in longwave radiation and sensible heat flux. There are indications that the UHI will expand into autumn (MAM) and spring (SON) in the future, driven by climate change and increased anthropogenic heating.

The analysis of diurnal range of meteorological variables, such as temperature, longwave radiation, and sensible heat flux, reveals that the UHI has a stronger influence during summer and diminished in other seasons, being weakest in winter. However, this diurnal range is projected to strengthen during the near-future and far-future climate periods.

This chapter highlights the persistence of the effects of the UHI over the coastal city of eThekwini during the current and future climates, respectively. Simulations suggest that the UHI will intensify into the future due to anthropogenic factors unless some mitigation and adaptation strategies are implemented. These strategies include revegetation, creating green spaces, and using high-reflective materials and increasing the water bodies. Further studies include a study of how the dynamics and atmospheric circulations by sea and land breeze influence the development, spatial and temporal distribution of the UHI over the coastal city of eThekwini.

UNIVERSITEIT VAN PRETORIA
UNIVERSITY OF PRETORIA
YUNIBESITHI YA PRETORIA

Postface

In this chapter, CCAM runs with both CMIP5, and ERAI were analysed to evaluate its capability to simulate the UHI and its variability during the current, near-future and far-future climates. The output of CCAM was compared to both MODIS nighttime temperature and station observations. During summer (DJF), validation against MODIS data shows that MODIS data is highly comparable to MPI8.5 simulated UHI, but with MODIS temperature higher than MPI8.5 and all other CCAM runs. However, CNR8.5 simulated the least strong UHI, whereas GFD8.5, NOR8.5 and ERAI simulated the most comparable UHI over eThekwini. In winter (JJA), the UHI disappears, but with minimum temperature variability observed amongst the CMIP5, ERAI and MODIS temperature. Still MODIS temperature is slightly higher and comparable to MPI8.5. The minimum temperature simulated by CNR8.5, GFD8.5, NOR8.5 and ERAI is still comparable. The correlation statistics show the highest correlations during DJF, which averages 0.9, followed by MAM (~0.88), SON (~0.7), and the lowest correlations during JJA, which average 0.62. However, this varies slightly amongst the CMIP5, and ERAI runs.

When comparing monthly variability between CCAM runs and station observations, it is shown that February recorded the highest temperature, and July recorded the lowest temperature. This is seen at both Durban and Mt. Edgecombe stations. It is also shown that CCAM overestimates minimum temperature at Durban station and underestimates minimum temperature at Mt. Edgecombe. The CCAM slightly overestimates maximum temperature at both stations. This is confirmed in both the bias and RMSE statistics. The diurnal range of temperature during summer (DJF) and autumn (MAM) is slightly similar and strong at the two stations. However, it is weaker and slightly similar during winter (MAM) and spring (SON) at the two stations.

Analysis of changes in the magnitude and intensity of the UHI was analysed in surface variables. In both minimum and surface temperature, the UHI is slightly similar during the current climate, but will change slightly in the near-future climate, and changes show variability going into the far-future climate. This study shows that the UHI is reproduced in CCAM-downscaled CMIP5 runs over the city of eThekwini.

UNIVERSITEIT VAN PRETORIA
UNIVERSITY OF PRETORIA
YUNIBESITHI YA PRETORIA

CHAPTER 4:

The influence of the atmospheric circulation patterns on the variability of the eThekwini heat islands

Preface

In the previous chapter, CCAM was run forced with both CMIP5 model simulations and ERAI data to assess its performance in simulating the current and provide future climate projections. In the current chapter, the CCAM present day (2005/6-2016) simulations are analysed to evaluate the influence of the atmospheric circulation on the variability of the urban heat island over the city of eThekwini. First, wind (speed and direction) and diurnal cycle are analysed at the two stations, Durban (urban) and Mt. Edgecombe (non-urban), to see if land and sea breeze occurred. Wind speeds are analysed on a monthly and seasonal time scale to assess their variability. Then, the verification statistics are compared at the two stations for the model's accuracy. Analysis of surface variables is then conducted at the two stations to validate the UHI. Next, the 24 hours spatial and temporal distribution of UHI is conducted over the domain to determine the onset and cessation of the land and sea breeze phenomenon. Lastly, the latitudinal cross section is applied to investigate the horizontal penetration of land and sea breeze into the interior of the domain, and conclusions are drawn.

This work has been planned for submission to an accredited Journal with details as follows:

Robert T Maisha, Thando Ndarana, Francois A. Engelbrecht, Marcus Thatcher, Mary-Jane M. Bopape **(2025) The influence of the atmospheric circulation patterns on the variability of the eThekwini heat islands, Climate Dynamics,**

The second, third and fifth authors are my supervisor, and the fourth author is the external collaborator who assisted in developing the code, assisting with setting up the land cover and urban parameters for the model runs.

UNIVERSITEIT VAN PRETORIA
UNIVERSITY OF PRETORIA
YUNIBESITHI YA PRETORIA

The influence of the atmospheric circulation patterns on the variability of the eThekwini heat islands

Robert T Maisha[a,b], Thando Ndarana[b], Francois A. Engelbrecht[c], Marcus Thatcher[d], Mary-Jane M. Bopape[a,e]

[a]University of Pretoria, Department of Geography, Geoinformatics and Meteorology, Pretoria, South Africa

[b]South African Weather Service (SAWS), Weather Research, Pretoria, South Africa

[c]University of the Witwatersrand, Global Change Institute (GCI), Johannesburg, South Africa

[d]Commonwealth Scientific and Industrial Research Organisation (CSIRO), Aspendale, Australia

[e]South African Earth Observations Network, National Research Foundation, Pretoria, South Africa

Corresponding author: Robert Maisha,
robert.maisha@weathersa.co.za/trmaisha@gmail.com

The influence of the atmospheric circulation patterns on the variability of the eThekwini heat islands

Abstract

In this study, the Conformal-Cubic Atmospheric Model (CCAM) is run with a grid length of 1 km, allowing for detailed simulations of the occurrence of urban heat island (UHI) over the city of eThekwini, in KwaZulu Natal, South Africa. In this study the UHI is linked with atmospheric circulation such as land and sea breeze for the purpose of understanding the development mechanisms. The simulated winds are validated against observations from two South African Weather Service stations, and the diurnal range of modelled variables such as temperature, radiation and heat fluxes are analysed, both within and away from the city. The 24-hour spatial distribution of atmospheric variables is analysed, and the horizontal and vertical wind diurnal cycle are analysed over three latitudinal points to investigate the behaviour of land and sea breeze. The diurnal range in the observed wind speed and direction indicate the presence of both land and sea breeze and also synoptic-scale systems at both Durban and Mt. Edgecombe stations. Between 00h00 and 04h00 and again from 18h00 to 00h00 UTC, the wind direction indicates the presence of land breeze circulations along with the influence of synoptic-scale systems. In contrast, from 04h00 to 18h00 UTC, the wind direction reflects the development of a sea breeze at both Durban and Mt. Edgecombe stations.

UNIVERSITEIT VAN PRETORIA
UNIVERSITY OF PRETORIA
YUNIBESITHI YA PRETORIA

The surface temperature, longwave radiation, sensible heat fluxes and boundary layer show strong diurnal and spatial variability and UHI within the city. The longitudinal cross-section of vertical winds shows mixing as a result of land and sea breeze. The existence of land and sea breeze helps to dilute the UHI effects over eThekwini. The boundary layer within the city is found to be highly disturbed, due to the influence of urban structures as well as the UHI.

4.1 Introduction

Urbanisation has led to a higher number of the world's population living in cities (Canton and Dipankar, 2024), and more than half of this population resides within 50 km of the coastlines (Pokhrel and Lee, 2011). This has resulted in land surface changes, including the replacement of natural vegetation by artificial surfaces, leading to changes in albedo and thermal conductivity, as well as higher anthropogenic heat emissions, and a decrease in evapotranspiration in urban areas (Pokhrel and Lee, 2011; Chen *et al.*, 2014; Ramamurthy *et al.*, 2014; Estrada *et al.*, 2017). As a result, cities experience nighttime temperatures that are at most 2°C higher than non-urban areas, a phenomenon called an urban heat island (UHI). The nighttime build-up of UHI results from the rural-urban contrast in daytime heat storage and heat release from the ground at night (Oleson *et al.*, 2011; Fischer *et al.*, 2012; Barrao *et al.*, 2022). The intensity of the night time UHI, i.e. the difference between the urban and surrounding rural temperature could range from 2 to 4°C and depends on the size of the city, land type, and weather conditions (Bohnenstengel *et al.*, 2011; Heaviside *et al.*, 2017; Barrao *et al.,* 2022).

The UHI occurs mostly during clear sky conditions, low humidity, and low wind speed (Wilby, 2008; Heaviside *et al.*, 2017; Zhang *et al.*, 2022), and also high solar irradiance (Gubler *et al.*, 2021), the UHI dissipates at high wind speed (Parker, 2010; Barrao *et al.*, 2022). Bush *et al.,* (2020) have shown that numerical model parametrisation of physical processes such as radiation and microphysics (slow processes), and atmospheric boundary layer turbulence, cloud, and surface coupling (fast processes), are the main drivers of atmospheric circulation. They affect both maximum and minimum temperature distribution and contribute to UHI formation and its evolution (Bush et al., 2020).

UNIVERSITEIT VAN PRETORIA
UNIVERSITY OF PRETORIA
YUNIBESITHI YA PRETORIA

The climate in coastal area is influenced by different mesoscale meteorological phenomena due to temperature difference between the land and sea, which result in land and sea breezes (Lee and Shun, 2003; Pokhrel and Lee, 2011; Grachev *et al.*, 2018; Khan *et al.*, 2018), large-scale atmospheric flow, and mountain and valley breeze resulting from the orography (Pokhrel and Lee, 2011). These land and sea breezes have an influence on the existence of the UHI's. According to Parker, (2010), a coastal city affected by land and sea breeze may sometimes experience a weaker UHI compared to an inland city, whereas a city in mountainous areas is influenced by katabatic winds (Tyson and Preston-Whyte, 2000).

The air quality of coastal cities is influenced by local meteorology, with both sea and land breezes playing a key role in the transport of air pollutants along the coast (Pokhrel and Lee, 2011; Khan *et al.*, 2018). Sea breezes occur at either a local scale, with a range of 100 metres to 10 kilometres or at a mesoscale, with a range of 10 kilometres to 100 kilometres (Khan *et al.*, 2018). The vertical depth of breezes vary with time, with their depth reaching up to 1000 metres during the day (sea breeze), and is reduced to 200 metres at night (land breeze)(Bastin *et al.*, 2006; Pokhrel and Lee, 2011). A boundary layer develops with a height up to 1200 metres during the day and 200 metres at night (Pokhrel and Lee, 2011; Chen and Dipankar, 2022). This occurs due to a strong updraft at the front of the sea breeze, where the pressure gradient generates boundary layer separation (Bastin *et al.*, 2006). The horizontal scale varies between locations, with seaward penetration averaging up to 100 kilometres and landward penetration up to 75 kilometres (Pokhrel and Lee, 2011).

During offshore flow (land breeze), the sensible heat flux is negative, which is associated with a stable boundary layer (Grachev *et al.*, 2018). In contrast, during onshore flow (sea breeze), wind speeds can average 2.0 m/s, with a highest wind speed value of 7.2 m/s (Khan *et al.*, 2018). These winds (and their direction) influence the sensible heat fluxes, making it positive, representing an unstable boundary layer.

Estoque (1962) showed that sea breezes result from synoptic-scale systems and thermal stratification. The study further showed that during the daytime sea breezes, the largest vertical velocity is located at the sea breeze front, whereas during

UNIVERSITEIT VAN PRETORIA
UNIVERSITY OF PRETORIA
YUNIBESITHI YA PRETORIA

nighttime offshore flow (land breeze), large-scale prevailing winds cause advection of warmer air from land to the ocean (Barriopedro *et al.*, 2011; Maisha, 2014). During daytime onshore flow, advection reduces and removes higher temperature over the land's atmosphere, leading to a weaker pressure gradient with weaker circulation (Estoque, 1962). In Estoque (1962) study, the prevailing winds were found to influence the movement of sea breezes towards the land, with a range of up to 32 km, while offshore flow extends less than 18 km from the shoreline. However, in the current study, the range may differ. During both these circulations, the prevailing winds influence the temperature field, with intense vertical circulation resulting in adiabatic warming in the descending regions along the coastlines (Estoque, 1962).

Case (2002) found that, at night, the land cools faster when compared to the adjacent ocean due to higher heat capacity of water (Akbari *et al.*, 2001; Blake *et al.*, 2011; Nuruzzaman, 2015; Grachev *et al.*, 2018), resulting in the development of mesoscale pressure system. Cooler and dense air moves away from the land (high pressure) towards the ocean (low pressure), resulting in the development of land breeze. This land breeze results in a shift of winds from an onshore flow to an offshore flow during the early hours of the night, typically from 05h00-06h00 UTC (07h00-08h00 SAST) (Case, 2002). Consequently, velocity and the height reached result in land breeze being weaker than the sea breeze, since the amount of heat generated by the surface during land breeze is weaker than the heat required by the sea breeze. As a result, onshore (sea breeze) wind speed greater than 5 m/s prevents the formation of land breeze (Case, 2002).

Land breezes form due to the thermal contrast over land, contrasting with the thermally driven nighttime events. Temperature is higher over the land before the land breeze, dropping significantly afterwards. Some stations experience slight temperature increase due to land breezes, especially when not affected by onshore winds and located adjacent to water bodies (Case, 2002). Land breezes typically begin 0 to 6 hours after sunset, with most events occurring within 0 and 2 hours. Their vertical depths vary; deep land breezes extend up to 150 metres, showing a sharp transition from onshore (sea breeze) to offshore (land breeze) flow, and stronger offshore wind speeds. Weaker land breezes have a more gradual or shallow transition

UNIVERSITEIT VAN PRETORIA
UNIVERSITY OF PRETORIA
YUNIBESITHI YA PRETORIA

and a vertical depth of less than 150 metres. In the early afternoon, sea and valley breezes interact, as observed by Case (2002), aligning with each other.

Lee and Shun (2003) studied the impacts of sea breeze interactions at Hong Kong International Airport (HKIA) using Terminal Doppler Weather Radar (TDWR). Their observations indicate that sea breezes occur during fine weather, with low cloud cover ranging from 1 to 4 octas. Additionally, daytime air temperature rises 3°C higher than the sea surface temperature.

Although the above studies illustrate the global observational studies of land sea breezes, both land and sea breezes have been studied using dynamic models. Pokhrel and Lee, (2011) studied land and sea breezes over the coastal areas of Incheon, Korea, using a three-dimensional A2C flow model with Computational Fluid Dynamics (CFD) capabilities. The study showed the diurnal range of the 10-metre wind speed, which demonstrates the direction of the land and the sea breezes. During land breeze (recorded at 05h00 local time), the maximum wind speed averages ~1m/s, while during sea breeze (recorded at 03h00 pm local time), the maximum wind speed averages ~1.7 m/s. Additionally, during sea breeze, wind speed doubles the amount observed during land breeze. Changes from sea to land breeze occurred between 8 and 9 pm, whereas changes from land to sea breeze occurred from 9 to 10 am.

Arrillaga *et al.,* (2018) studied the atmospheric circulations and found that the presence of land and sea breezes front collapses the UHI in cities and also breaks down the nighttime surface inversion in non-urban areas. Grachev *et al.,* (2018) studied the boundary layer interaction between air, sea, and land interaction over the coastal area of North Carolina using data from meteorological towers. The study shows that during onshore flow (sea breeze), the boundary layer becomes either stable or mostly unstable, whereas offshore flow (land breeze) leads to a stable boundary layer as warm air moves over cooler sea surface. As a result, sea breezes reduce the UHI effect during the day, whereas at night, land breezes strengthen the UHI effect.

To the authors knowledge, during this study, there were fewer, or no modelling studies conducted on how atmospheric circulation such as land and sea breezes

UNIVERSITEIT VAN PRETORIA
UNIVERSITY OF PRETORIA
YUNIBESITHI YA PRETORIA

influence the UHI over coastal cities of South Africa. However, climate studies have primarily focussed on the temperature warming trends (Jury, 2013; Kruger and Sekele, 2013; Kruger *et al.*, 2019) and the effects of urbanisation on the UHI phenomenon (Kruger and Shongwe, 2004). Additional motivation came from the availability of realistic land cover data, urban observational parameters, sufficient computational resources, and a high-resolution urban-scale model capable of simulating the urban heat island (UHI) effect as well as both land and sea breezes (IPCC, 2023).

High-resolution simulations are desirable because they reduce and eliminate the model's dependence on parametrizations (Reichler and Kim, 2008). To our knowledge, this is one of the first projections of its kind over South Africa and Africa as a region. The current chapter is outlined as follows: Section 2 describes the data methodology applied in the study. Section 3 presents the analysis of the model output and its comparison with observational data. Section 4 presents the discussion of the findings, while Section 5 offers a summary and the conclusion of the study.

4.2 Methodology

4.2.1 Study area

The city of eThekwini is highly urbanised and is situated within Kwazulu-Natal Province of South Africa (see Figure 2.1). The urban area is situated to the east of 30.9^0E and south of 29.9^0S (shaded in grey), with less vegetation cover over the urban areas. The dominant land cover includes natural vegetation, savannah, and grasslands with less barren land in the city of eThekwini (depicted in red).

The city is bounded to the east by the Indian Ocean, depicted in blue. Figure 2.1 is based on the MODIS land cover for the year 2013, chosen for its realistic representation of urban areas worldwide (Katzfey *et al.*, 2020). The city of eThekwini is more than 90% urban (Figure 2.1, grey shading) and also shown in urban fraction (Figure 2.3b), with a higher urban fraction oriented in a southwest to northeast direction. This is in contrast to the default model land cover, which shows the city oriented in a southeast to northwest direction (shown in Figure 2.3a). The urban

UNIVERSITEIT VAN PRETORIA
UNIVERSITY OF PRETORIA
YUNIBESITHI YA PRETORIA

fraction decreases from 90% to10% when moving away from the city towards non-urban areas (Figure 2.1).

4.2.2 CCAM Regional downscaling

The study applies the Conformal-Cubic Atmospheric Model (CCAM), which is a global model that can run at both global scale with quasi-uniform resolution, and a regional scale with variable resolution giving the highest resolution over the area of interest (McGregor, 1996; McGregor *et al.*, 2008; Engelbrecht *et al.*, 2015a; Dedekind *et al.*, 2016b). For this study, it is coupled to an urban climate model (UCM) called Australian Town Energy Budget (ATEB, (Masson, 2000; Thatcher and Hurley, 2012; Luhar *et al.*, 2014; Lipson *et al.*, 2017, 2018; Chapman and Mcalpine, 2019). In this study, the CCAM is initially set up at a horizontal resolution of 50 km across Africa, with its output nudged to the 8 km settings run over South Africa. The 8 km output is then nudged to the 1 km setup for urban climate modelling (UCM), centred over eThekwini. The CCAM is applied at a stretched grid mode for 8 km and 1 km to provide higher resolution over South Africa and eThekwini, respectively. The high resolution setup assists in capturing the complex interaction between the ocean, land and atmospheric circulation (Taylor *et al.*, 2012; Yan *et al.*, 2013).

4.2.3 CCAM global input data

The CCAM is forced with two global datasets: first, the European Centre for Medium Range Weather Forecasting (ECMWF) Interim Reanalysis (ERAI) and second, simulations from four Global Climate Models (GCMs) that participated in the Coupled Model Intercomparison Project Phase Five (CMIP5) which were used for the International Panel on Climate Change (IPCC) Assessment Report Five (AR5) (Maure *et al.*, 2018b; Kruger *et al.*, 2019).

These models are: (i) the National Centre for Meteorological Research Coupled Global Climate Model, version 5 (CNRM-CM5); (ii) the Geophysical Fluid Dynamics Laboratory Coupled Model (GFDL-CM3); (iii) the Max Planck Institute Coupled Earth System Model (MPI-ESM-LR); and (iv) the Norwegian Earth System Model (NorESM1-M). A description of the GCMs origin and their spatial resolution is summarised in

UNIVERSITEIT VAN PRETORIA
UNIVERSITY OF PRETORIA
YUNIBESITHI YA PRETORIA

Thevakaran et al., (2016). The model runs were forced with the Representative Concentration Pathway 8.5 (RCP8.5) emission scenario which is a high-emission and low-mitigation scenario (Riahi *et al.*, 2011; Maure *et al.*, 2018a; Muthige *et al.*, 2018; Kruger *et al.*, 2019). The CMIP5 dataset resolution was an improvement over phase 4 (i.e. CMIP4), the model physics were updated, and they described prognostic aerosols, atmospheric chemistry, dynamic vegetation, as well as the carbon cycle (Taylor *et al.*, 2012; Yan *et al.,* 2013). The CMIP5 data also include sea surface temperature (SST) and sea ice data obtained from integration of previous atmosphere-ocean coupled models (AOGCMs) used in previous CMIP phases (Taylor *et al.*, 2012; Yan *et al.*, 2013; Katzfey *et al.*, 2020). Each model was run for the same current climate period, from December 2005 to December 2016.

4.2.4 CCAM urban input data

At a high resolution of 1 km, the study applies measured urban (generic) parameters, i.e. average building heights (5.86 metres), building height-to-width ratio (0.24 metres), vegetation fraction (0.25%), building fraction (0.55%), industrial emissions (1.00 $W.m^{-2}$), traffic emissions (2.62 $W.m^{-2}$), roof albedo (0.2 $W.m^{-2}$), wall albedo (0.3), road albedo (0.1) and vegetation albedo (0.2). This information was supplied by the city of eThekwini and was derived from Light Detection and Ranging (LIDAR) measurements (see also Table 2.1). These parameters were updated in the model to enhance the realism of the representation. However, the ATEB-3 measured urban parameters remain static throughout the simulations, whereas the vegetation exhibits seasonal (dynamic) variation.

4.2.5 Methods of analysis

The UHI is analysed during the summer season (December-January-February, (DJF)) period 2006-2016, since the UHI is more visible and persistent in summer compared to other seasons over the city of eThekwini. This was demonstrated in the simulation of the UHI using ERAI data presented in Chapter 2 (Maisha *et al*., 2023). Firstly, DJF 24 hours diurnal range of the atmospheric variables such as wind speed, outgoing longwave radiation, shortwave radiation, net radiation, latent and sensible heat fluxes, temperatures, and boundary layer diurnal range is analysed to observe the strength of the UHI and when it starts developing and dissipating. Secondly, the

UNIVERSITEIT VAN PRETORIA
UNIVERSITY OF PRETORIA
YUNIBESITHI YA PRETORIA

diurnal range of the same variables is analysed at two stations, one within the city, Durban Weather Office (DBN), (latitude -29.97; longitude 30.95) and another away from the city, Mt. Edgecombe; (latitude -29.97; longitude 30.95).

The locations of the two stations are shown in Figure 2.1. Durban is situated at an elevation of 14 metres above mean sea level (MSL), while Mt. Edgecombe is at an elevation of 94 metres above MSL. Information regarding the station data is provided in Section 2.2.3.2, which covers model validation data. Lastly, the longitudinal vertical cross-section of vertical winds (omega) and horizontal winds (u and v-components) are mapped at three latitudes: (-30^{o}S; -29.9 ^{o}S and -29.8 ^{o}S). They are used to observe the extent to which the land and sea breeze penetrate into the study domain and interact with the UHI. These locations are labelled P1, P2 and P3, respectively, in Figure 2.1.

4.2.6 Verification statistics

In the current study, the data applied for verification is from two weather stations discussed with previous chapters, one within the city, namely Durban Weather Office, and another away from the city, namely Mt. Edgecombe. The dataset includes wind speed and direction.

4.3 Results

4.3.1 The model validation against observations

The simulated wind speed is validated against observations from the two weather stations, Durban, and Mt. Edgecombe, for the period 2006 to 2016. For validation, the study considers monthly time series, diurnal range, wind rose, bias and root mean square error (RMSE).

4.3.1.1 The diurnal range of wind speed

a) **Investigating land and sea breeze**

Wind speed data were averaged at hourly intervals over a 24-hour period for the DJF seasons from 2006 to 2016. The data were collected from two weather stations: the Durban station, located southwest of the city and the simulation domain, approximately 1.76 km from the Indian Ocean coastline (Figure D.1); and the Mt.

UNIVERSITEIT VAN PRETORIA
UNIVERSITY OF PRETORIA
YUNIBESITHI YA PRETORIA

Edgecombe station, located northeast of the city and the simulation domain, approximately 4.63 km from the Indian Ocean coastline (Figure D.2).

Analysis of the model output in Chapter 2 and Chapter 3 shows that the UHI effect is evident in both station data and simulations produced by the CCAM. The UHI is also detectable in MODIS LST data. It is most prominent during DJF season, with the highest temperatures and UHI intensity occurring during February. Therefore, February was selected for wind analysis, as it is representative of the DJF season (Figure D.1).

The analysis illustrated in Figure 4.1 aimed to investigate the capability of the updated land surface feature within the ATEB model to simulate the UHI and its interactions with atmospheric circulations, These include the presence of sea and land breezes, as well as katabatic winds (mountain and valley breeze), over the city of eThekwini during February for the period 2006 to 2016.

(i) Daytime sea breeze and anabatic winds (04h00 and 18h00 UTC)

Both Durban and Mt. Edgecombe stations are located to the southwest and northeast of the simulation domain, respectively (Figure 2.1). At these stations, sea breeze and large-scale atmospheric scale circulations are represented by wind direction ranging from 45^{o} (north-easterly) to 225^{o} (south-westerly) during daytime period, from 04h00 UTC (06h00 SAST) to 18h00 UTC (20h00 SAST). At Durban station, the dominant wind direction is approximately 135^{o} (south-easterly), while at Mt. Edgecombe, it is around 90^{o} (easterly).

At the Durban station, daytime wind analysis (Figure 4.1 (a) and (b), blue lines) shows that wind speed begins to increase from an average of 4 m/s at 04h00 UTC (06h00 SAST), with wind direction shifting from approximately 180^{o} (southerly) to around 230^{o}(south-westerly). Wind speed reaches a peak average of 7.6 m/s at 11h00 UTC (13h00 SAST), with wind direction averaging around 200^{o} (south south-westerly).

After this peak, wind speed gradually decreases, reaching an average of 4.5 m/s at 18h00 UTC (20h00 SAST). During this period, wind direction varies from

UNIVERSITEIT VAN PRETORIA
UNIVERSITY OF PRETORIA
YUNIBESITHI YA PRETORIA

approximately 200° (south-south-westerly) to 0° (northerly), indicating a transition from see breeze to land breeze, which occurs between 14h00 UTC (16h00 SAST) and 16h00 UTC (18h00 SAST).

The secondary wind speed and direction diurnal range at Durban station (orange line, Figure 4.1 (a) and (b)) is broadly similar to the primary wind speed diurnal range (blue line), but with variable wind direction (Figure 4.1 (b), orange line). Between 06h00 UTC (08h00 SAST) and 12h00UTC (14h00 SAST), wind direction shifts from approximately 150° (south-south-easterly) to about 20° (~north-north-easterly). This pattern suggests the influence of anabatic winds or large-scale circulations. From 12h00 UTC (14h00 SAST) to 18h00 UTC (20h00 SAST), the wind direction changes again from 0° (northerly) to approximately 200° (south-southwesterly) at around 15h00 UTC (17h00 SAST) and then reverses back to 20°(~north-north-easterly) by 18h00 UTC (20h00 SAST).

The wind speed and direction diurnal range at the Mt. Edgecombe station is shown in Figure 4.2. At this station, the wind speed diurnal pattern is broadly similar to that observed at Durban station; however, wind speed at Mt. Edgecombe is roughly half those at Durban.

During the daytime period from 04h00 UTC (06h00 SAST) to 18h00 UTC (20h00 SAST), wind speed increases to an average maximum of around 5 m/s (blue line). The dominant wind direction (blue curve) shows a shift from approximately 100 ° (~easterly) to approximately 200° (south south-westerly) between 04h00 UTC (06h00 SAST) and 08h00 UTC (10h00 SAST).

After 08h00 UTC (10h00 SAST), the wind direction shifts again from around 200° (south south-westerly) to approximately 50° (north-easterly) and remains generally northeasterly until 15h00 UTC (7h00 SAST). After 15h00 UTC (17h00 SAST), the wind direction changes once more turning to approximately 220° (south-westerly) and remaining so until 18h00 UTC (20h00 SAST).

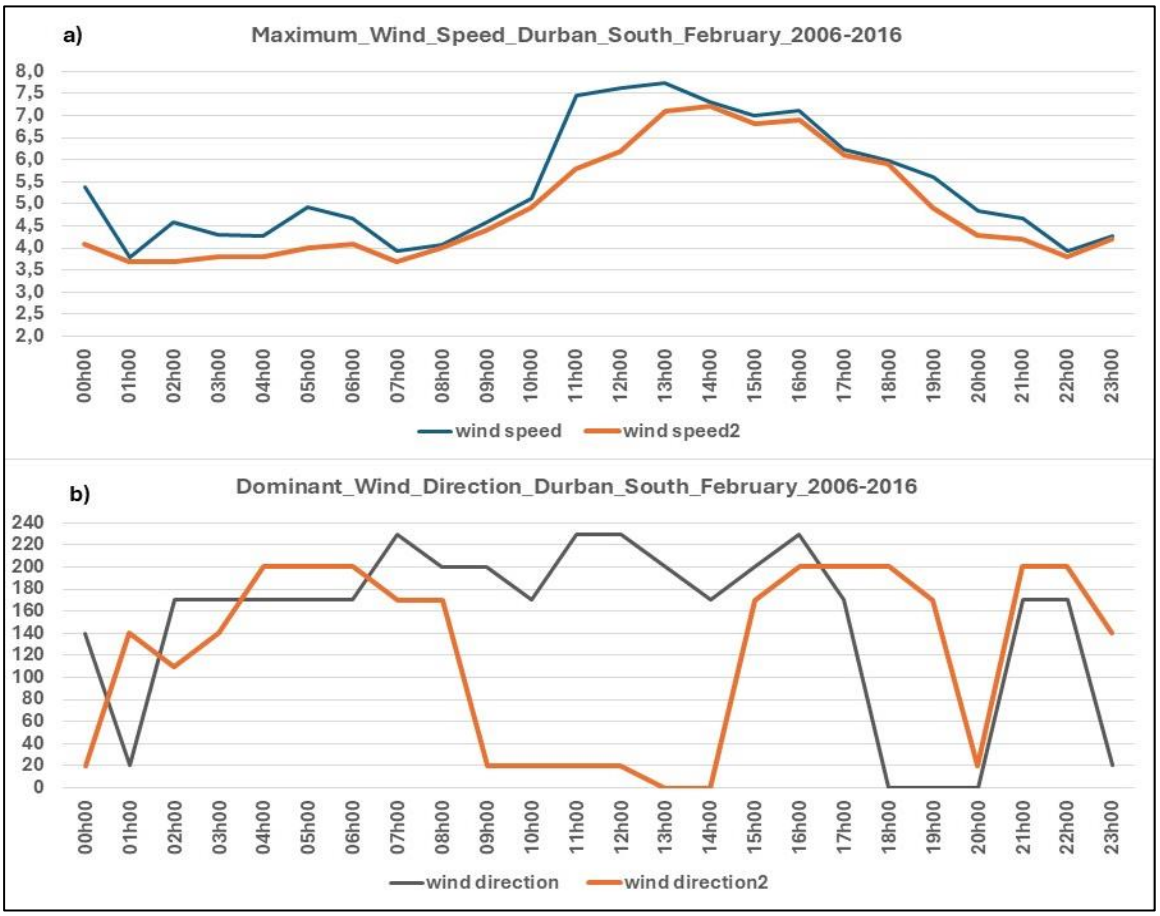

Figure 4.1: The diurnal range of maximum over Durban weather station (wind) speed, (b) wind direction for the period DJF 2006 -2016.

The secondary curve (orange line) indicates that during the day, Mt. Edgecombe experiences wind directions that are generally opposite to those of the primary wind direction curve (blue line). From 04h00 UTC (06h00 SAST) to 15h00 UTC (17h00 SAST), the wind direction represented by the orange line varies in opposite to the blue curve, with dominant winds shifting from approximately 40 ^{o} (north-easterly) to around 200^{o} (~south south-westerly) and then returning to approximately 40^{o} (north-easterly). Between 15h00 UTC (17h00 SAST) and 20h00 UTC (22h00 SAST), the blue and orange curve nearly aligned, with wind direction changing from around 40 ^{o} (north-easterly) to between 200 to 220^{o} (south-westerly).

From this analysis, one can deduce that the wind speed curves observed during the day indicate that both Durban (blue line) and Mt. Edgecombe (orange line) experience sea breeze, accompanied by synoptic-scale circulations, including

UNIVERSITEIT VAN PRETORIA
UNIVERSITY OF PRETORIA
YUNIBESITHI YA PRETORIA

anabatic winds. Additionally, the presence of Durban's secondary wind pattern (orange line) and Mt. Edgecombe's (blue line) further supports this interaction between local and larger-scale wind systems.

(i) Nighttime land breeze and katabatic winds (18h00 and 04h00 UTC)

Land breeze and large-scale atmospheric circulations are represented by wind directions averaging between 2225° (south-westerly) and 45° (north-easterly) during the nighttime period, from 18h00 UTC (20h00 SAST) to approximately 04h00 UTC (06h00 SAST). At the Durban station, (Figure 4.1a) during land breeze conditions, the dominant wind direction averages 315° (north-westerly), while at the Mt. Edgecombe station, it averages around 90° (easterly).

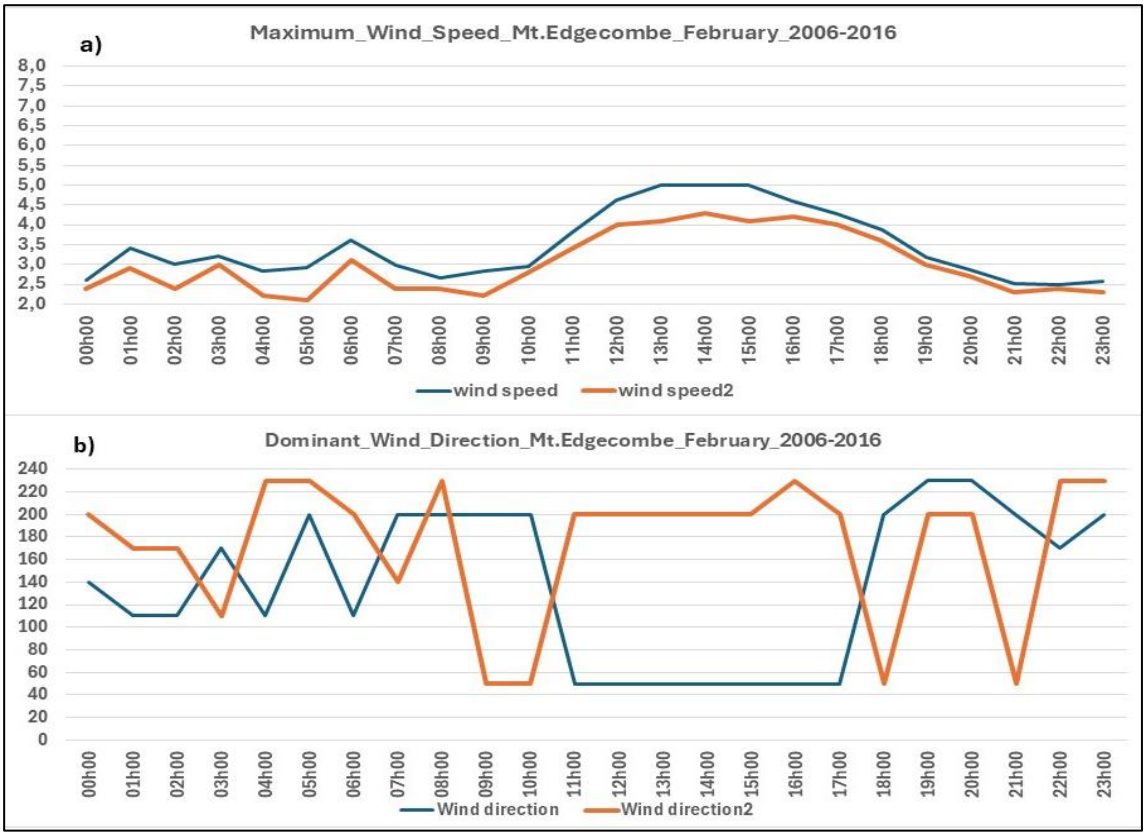

Figure 4.2: The diurnal range of maximum over Mount Edgecombe weather station (wind) speed, (b) wind direction for the period DJF 2006 -2016.

From this analysis, it is evident that at the Durban station (Figure 4.1, blue line), between 18h00 UTC (20h00 SAST) and 04h00 UTC (06h00 SAST), wind speeds

UNIVERSITEIT VAN PRETORIA
UNIVERSITY OF PRETORIA
YUNIBESITHI YA PRETORIA

average between 4.5 m/s and 5 m/s, with a slight decrease to around 4 m/s at 23h00 UTC (01h00 SAST). During this period, wind direction shifts from approximately 0° (northerly) between 18h00 UTC (20h00 SAST) and 20h00 UTC (22h00 SAST), to an average of about 170° (southerlies) between 20h00 UTC (22h00 SAST) and 22h00 UTC (00h00 SAST) (Figure 4.1a, blue lines).

The second diurnal wind direction range curve at Durban station (orange line) shows that from 18h00 UTC (20h00 SAST) to 21h00 UTC (23h00 SAST), the two wind direction patterns are nearly identical. However, they begin to diverge again during the early morning hours, from 00h00 UTC (02h00 SAST) to 05h00 UTC (07h00 SAST).

During nighttime at Mt. Edgecombe (blue line), from 00h00 to 04h00 UTC (02h00 to 06h00 SAST) and from 18h00 to 04h00 UTC (20h00 to 06h00 SAST), maximum wind speeds average between 2.0 m/s and 3.5 m/s. In contrast, at Durban station, wind speeds average between 3.5 m/s and 5 m/s.

The wind direction at Mt. Edgecombe (blue line) varies from 50° (north-easterly) to 230° (south-westerly) between 15h00 UTC (17h00 SAST) and the following morning at 06h00 UTC (08h00 SAST). The secondary curve (orange line) exhibits greater variation during this period. As in the daytime diurnal range curves, these results show that both stations, Durban (blue line) and Mt. Edgecombe (orange line) experienced nighttime land breeze, large-scale atmospheric systems, and katabatic winds.

This wind analysis shows the presence of both sea and land breezes at the Durban station (Figure 4.1) and Mt. Edgecombe station (Figure 4.2), which could have contributed to the strengthening of the nighttime UHI effect, as observed in surface and minimum temperatures, longwave radiation and sensible heat flux. This is evident in the reduction of wind speed from a maximum of around 8 m/s during the day to a maximum of 4 m/s from 18h00 UTC (20h00 SAST) until the following morning at Durban station. At Mt. Edgecombe, the wind pattern is similar, but lighter than those observed at Durban station.

UNIVERSITEIT VAN PRETORIA
UNIVERSITY OF PRETORIA
YUNIBESITHI YA PRETORIA

b) **Validation of winds using wind rose**

Wind roses were created for data at monthly intervals from January 2006 to December 2016 (Figures 4.3 and 4.4). An analysis of DJF wind rose shows similarities for December, January, and February; therefore, only the February wind rose is presented and discussed (Figure 4.3). Similarly, the JJA diurnal cycles look similar, and therefore the July diurnal cycle is analysed (Appendix D.3 and D.4). It should be noted that the Durban AWS was moved in July-August 2014, the Durban AWS was moved, and therefore only Mt. Edgecombe data stretched from January 2006 to December 2016

(ii) Daytime sea breeze and anabatic winds (04h00 and 18h00 UTC)

At the Durban station (Figure 4.3a), which is located to the southern part of the domain, the wind rose for February shows that between 04h00 and 18h00 UTC, the dominant and strong winds are primarily from north-northeast (3-5 m/s, 5%) and northeast (5-8 m/s, 10%). Winds from the south-southwest to southwest also occur (~5%), with average speeds of 5-8 m/s. Additionally, winds with speeds of 3-5 m/s contribute approximately 5% of winds in the area (Figure 4.3a).

Due to its location in the southern part of the domain, the Durban station experiences dominant winds blowing from the southwest to southeast, as well as from the north to northwest. This wind pattern confirms the influence of large-scale circulation, with sea breezes playing a lesser role. This is consistent with the diurnal range in wind speed observed at the Durban station, as shown in Figure 4.1a.

However, at Mt Edgecombe (Figure 4.3b), the dominant winds are east-northeasterlies (ENE), with wind speeds of 1.5-3.3 m/s, (~5%), 3-5 m/s (~10%), and 5-8 m/s, (~4%). Easterly winds are also common, with speeds of 1.5-3.0 m/s (~7%) and 3-5 m/s (~5%). These are followed by southwesterlies (SW) of strength 3-5 m/s (~5%), and south-southwesterlies (SSW), at 3-5 m/s (~5%) as well as variable winds of speed 1.5-3.0 m/s (5%). This wind distribution supports the observed diurnal range at Mt. Edgecombe (Figure 4.2b). The dominance of these wind patterns suggests that the Mt. Edgecombe station, located ~4.63 km from the coast, is

UNIVERSITEIT VAN PRETORIA
UNIVERSITY OF PRETORIA
YUNIBESITHI YA PRETORIA

primarily influenced by large-scale circulation and, to a lesser extent, sea breezes during the day.

Considering the location of the Durban station, which is situated to the southwest of the city of eThekwini (Figure 2.1), the dominant wind direction during the day indicates an onshore flow (sea breeze). This pattern may be attributed to atmospheric circulation associated with a low-pressure system, typically located over the interior of the country during summer and a high-pressure system generally situated over the west Indian ocean (Tyson and Preston-Whyte, 2000).

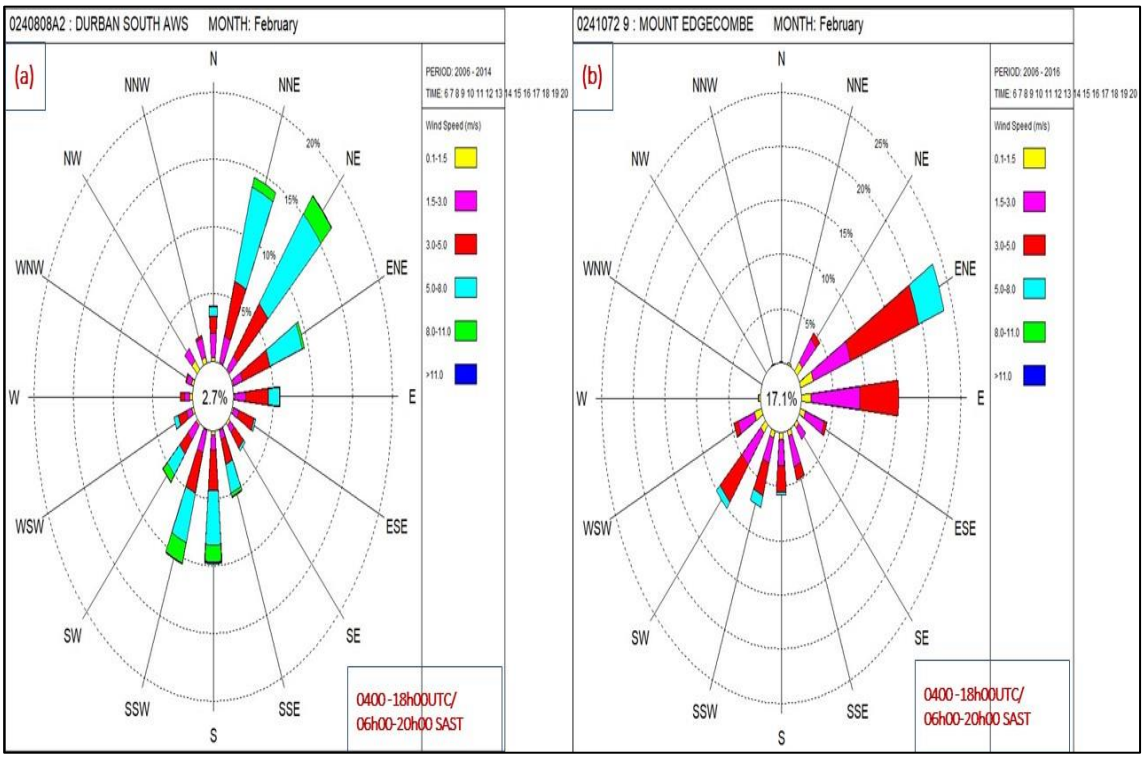

Figure 4.3: The wind rose showing diurnal range of winds (speed and direction in metres per seconds (m/s) over (a) Durban (b) Mt. Edgecombe Weather stations during February (representing DJF) period 2006-2016. The panels represent wind roses between 04h00 and 18h00 UTC (06h00 to 20h00 SAST).The percentage contribution of the wind direction is represented in circles at 5%, 10%,15%, 20% and 25% respectively, with the inner circle representing calm winds (less than 1.5 m/s). The wind direction of which the winds come from is represented by the spokes (arrows).

UNIVERSITEIT VAN PRETORIA
UNIVERSITY OF PRETORIA
YUNIBESITHI YA PRETORIA

(iii) Night-time land breeze and katabatic winds (18h00 to 04h00 UTC)

The wind rose for the time period from 18h00 to 04h00 UTC (Figure 4.4a and Figure 4.4b) indicates that the dominant wind direction at the Durban station is from south-southwest to northeasterly (Figure 4.4). By considering southwesterlies to northerly, it is shown that a land breeze occurs at night, with average wind speed of strength (0.1-1.5 m/s, less than 5%), and wind speed of strength (1.5-3.0 m/s, up to 10%). At Mt. Edgecombe (Figure 4.4d), the dominant winds are northeasterlies to east-northeasterlies and southwesterlies to west-southwesterlies. These winds are of average strength (0.1-1.5 m/s, 5%), and winds of strength (1.5-3.0 m/s, 10%). When comparing Durban and Mt. Edgecombe stations, Durban is located along the coast and experiences pronounced land and sea breeze, whereas Mt. Edgecombe is situated slightly further inland, and experiences weaker land and sea breeze effects.

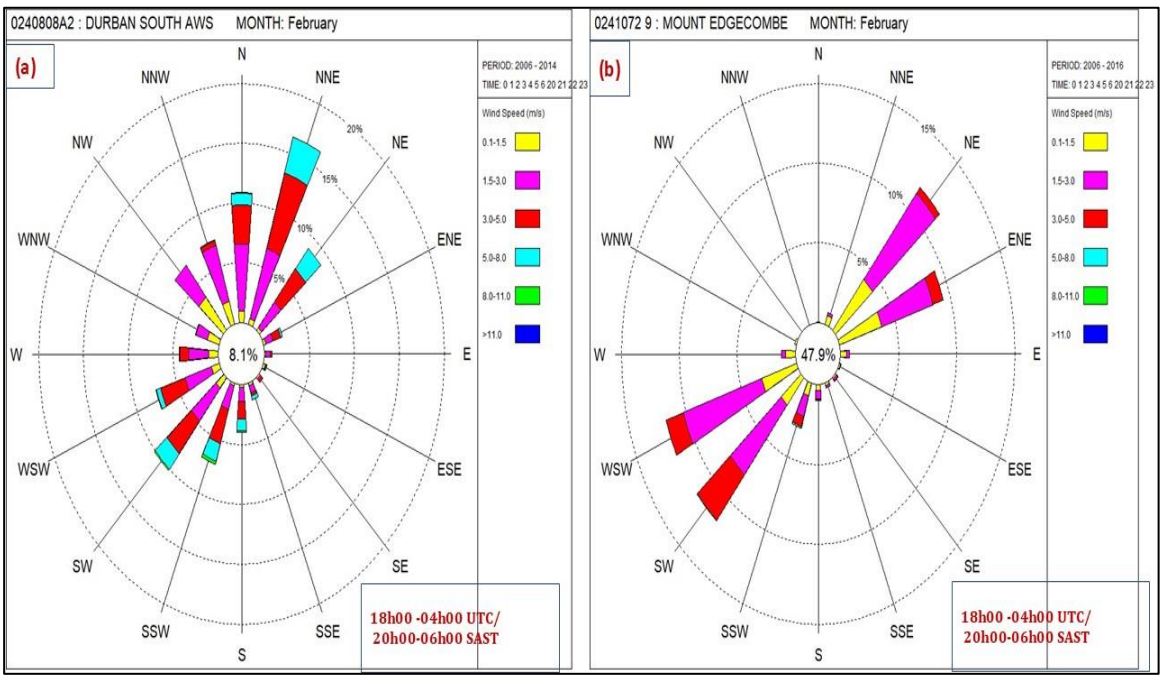

Figure 4.4: The wind rose showing diurnal range of winds (speed and direction in metres per seconds (m/s) over (a) Durban (b) Mt. Edgecombe weather stations during February (representing DJF) period 2006 -2016. The panels represent wind roses between 18h00 and 04h00 UTC (20h00 and 06h00 SAST).The percentage contribution of the wind direction is represented in circles at 5%, 10%,15%, 20% and 25% respectively, with the inner circle representing calm winds (less than 1.5 m/s). The wind direction of which the winds come from is represented by the spokes (arrows).

UNIVERSITEIT VAN PRETORIA
UNIVERSITY OF PRETORIA
YUNIBESITHI YA PRETORIA

An analysis of wind roses at the two stations was also conducted for the winter period (July) (Appendix D.3 and D.4). As in February, the Durban station shows similar wind strength at both 04h00 and 18h00 UTC, as well as during the overnight period from 18h00 and 04h00 UTC (see Appendix D.4). The land and sea breeze patterns are again evident at the Durban station. At Mt. Edgecombe, a similar wind pattern to that observed in February is also present during July, although the land and sea breeze signals remain weaker at this station.

4.3.1.2 Verification of wind speed

a) **The monthly variation of wind speed**

The average monthly wind speed from the CMIP5 driven CCAM simulations are presented as line graphs in Figure 4.5, alongside the observed averages, and the ERAI driven CCAM simulations for both the urban station (Durban) and non-urban (Mt. Edgecombe) stations. The observed annual pattern is similar for both stations with lower wind speeds in the cooler months of May, June, and July. The winter months over land are characterised by a continental high-pressure system, which may explain the lower wind speeds. The ERAI driven simulation shows an opposite pattern, with stronger winds during winter and weaker winds from October to December. This is followed by February and March, which show lower wind speed values for Durban.

For Durban, the CCAM-CMIP5 driven simulations do not show a clear intra-annual cycle. There is no clear change from January to August with lower values for September to December. For the rural station, the winds are simulated to be stronger in the winter months, although with a shorter season compared to ERAI driven simulation, which also indicates intense winds in winter. The CMIP5 driven simulations are comparable to one another across all months with the exception of GFD8.5, which shows some unusually high values in November at both the urban and non-urban stations.

These simulations indicate that the model struggles to reproduce station-observed winds at a seasonal timescale, especially when compared to its performance in simulating temperatures, as validated in Chapter 3.

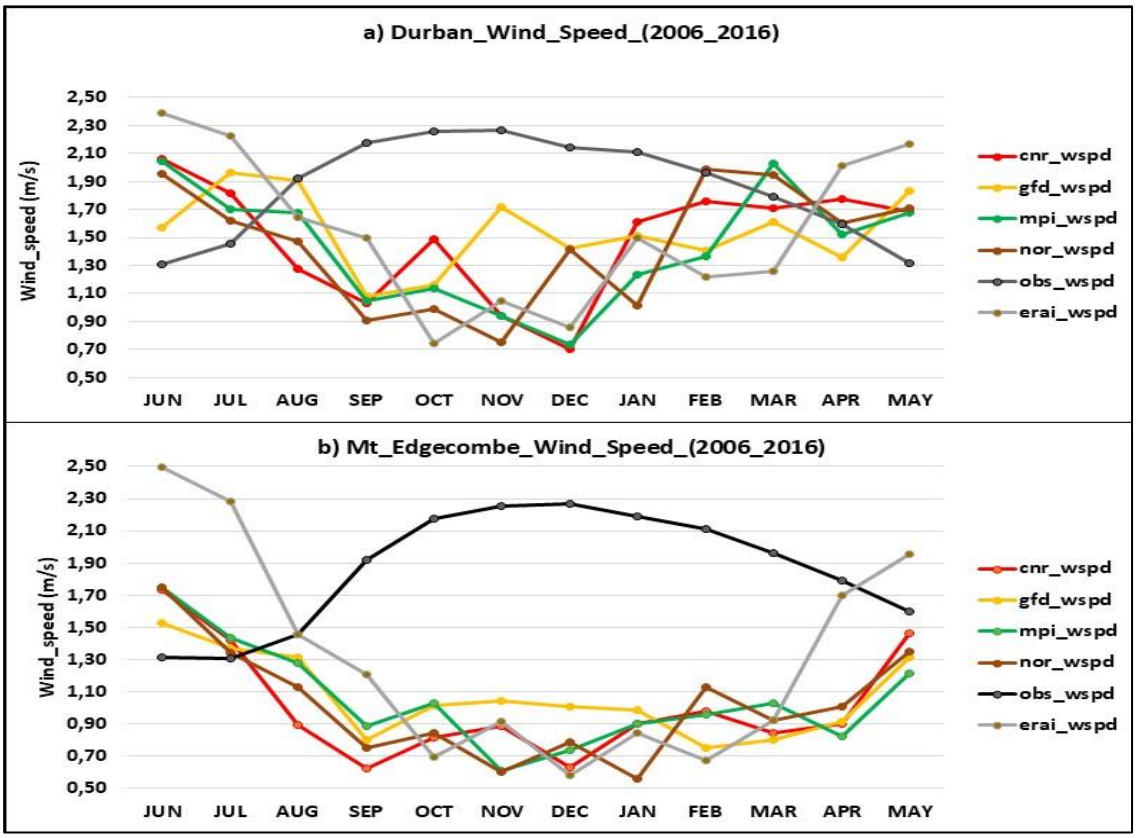

Figure 4.5: A comparison of the average monthly wind speed over an urban station (Durban) and non-urban station (Mt. Edgecombe) for both CMIP5 runs, and ERAI runs against station observed wind speed.

The two stations are located in a coastal region where two types of mesoscale circulations are dominant, (i) systems that are forced by surface inhomogeneity, such as land and sea breezes and (ii) systems that are induced by synoptic scale circulations. As a result, ultra-high model simulations at sub-kilometer resolution may be necessary to accurately reproduce the observed winds behaviour.

b) The verification statistics of wind speed

Tables 4.1 and 4.2 show wind speed bias and RMSE for both the Durban and Mt. Edgecombe stations. During summer (DJF), the bias is negative at both Durban and Mt. Edgecombe stations, with a smaller bias over Durban compared to Mt. Edgecombe across all CMIP5 runs.

Table 4.1: The validation statistics (bias) over (i) Durban and (ii) Mt. Edgecombe weather stations for the period 2006-2016. Statistics were computed between observations and

UNIVERSITEIT VAN PRETORIA
UNIVERSITY OF PRETORIA
YUNIBESITHI YA PRETORIA

CCAM-CMIP5 driven simulations (CNR8.5, GFD8.5, MPI8.5 and NOR8.5) and ERAI driven CCAM simulations.

Durban	BIAS_Wind_Speed (m/s)				
	obs_vs_erai	obs_vs_cnr	obs_vs_gfd	obs_vs_mpi	obs_vs_nor
DJF	-0,9	-0,7	-0,6	-1,0	-0,6
MAM	0,2	0,2	0,0	0,2	0,2
JJA	0,5	0,2	0,3	0,2	0,1
SON	-1,1	-1,1	-0,9	-1,2	-1,3
All_Seasons	-0,3	-0,4	-0,3	-0,4	-0,4
Mt_Edgecombe	BIAS_Wind_Speed (m/s)				
	obs_vs_erai	obs_vs_cnr	obs_vs_gfd	obs_vs_mpi	obs_vs_nor
DJF	-1,4	-1,2	-1,2	-1,2	-1,2
MAM	0,0	-0,5	-0,6	-0,5	-0,5
JJA	0,5	-0,2	-0,2	-0,1	-0,2
SON	-1,3	-1,5	-0,7	-1,4	-1,5
All_Seasons	-0,5	-0,9	-0,6	-0,8	-0,8

The wind speed bias is comparable between CMIP5, and ERAI driven simulations. During autumn (MAM) season, the bias is positive and consistent over Durban station, whereas it is negative for CMIP5 driven simulations at Mt. Edgecombe station, except for the ERAI driven simulation. In winter (JJA), the bias is also positive over Durban station in both CMIP5, and ERAI driven simulations, while it remains negative at Mt. Edgecombe station for all CMIP5 driven simulations. The bias is also negative and minimal at Durban station, but slightly higher at Mt. Edgecombe station.

An analysis of RMSE (Table 4.2) shows that during DJF, the RMSE is comparable and less than 1.5 m/s for all the CMIP5 and ERAI driven simulations at both urban and non-urban stations.

During autumn (MAM) and winter (JJA), the RMSE is reduced to values less than or equal to 1 m/s at Durban and Mt. Edgecombe stations. In spring (SON), RMSE values increased to above 1 m/s in all CMIP5, and ERAI driven simulations, except for GFD8.5, which recorded a value of 3.4 m/s. Overall statistics indicate larger errors at a non-urban station compared to an urban station. Comparable results were observed in temperature verification statistics for these same stations as reported in Chapter 2.

UNIVERSITEIT VAN PRETORIA
UNIVERSITY OF PRETORIA
YUNIBESITHI YA PRETORIA

Table 4.2: The validation statistics (RMSE) over (i) Durban and (ii) Mt. Edgecombe weather stations for the period 2006-2016. Statistics were computed between observations and CMIP5 runs (CNR8.5, GFD8.5, MPI8.5 and NOR8.5) and ERAI data

Durban	RMSE_Wind_Speed (m/s)				
	obs_vs_erai	obs_vs_cnr	obs_vs_gfd	obs_vs_mpi	obs_vs_nor
DJF	1,2	1,3	1,1	1,3	1,1
MAM	0,8	0,9	0,9	0,6	0,9
JJA	1,0	1,0	0,8	0,8	0,7
SON	1,3	1,4	1,4	1,3	1,5
All_Seasons	1,1	1,1	1,1	1,0	1,1
Mt_Edgecombe	RMSE_Wind_speed (m/s)				
	obs_vs_erai	obs_vs_cnr	obs_vs_gfd	obs_vs_mpi	obs_vs_nor
DJF	1,5	1,4	1,3	1,3	1,4
MAM	0,8	0,9	0,9	0,8	0,8
JJA	1,0	0,8	0,8	0,8	0,8
SON	1,4	1,6	3,4	1,5	1,6
All_Seasons	1,2	1,2	2,0	1,1	1,2

This analysis demonstrates that incorporating urban parameters into CCAM-CABLE and activating the urban scheme improves model performance especially in urban areas compared to simulations with the urban scheme switched off.

4.3.2 CCAM simulations and the link to atmospheric circulations

4.3.2.1 Diurnal range of the UHI within and away from the city

An analysis of the diurnal range of the UHI is presented for both CCAM-ERAI reanalysis and the four CCAM-CMIP5 driven simulations (CNR8.5, GFD8.5, MPI8.5 and NOR8.5) over the city of eThekwini. The analysis focuses on two locations: one within the city, Durban (DBN), and one outside the city, Mt. Edgecombe (MtE). Durban station is located to the southwest and Mt. Edgecombe station is located to the northeast of Durban, and is dominated by natural vegetation, as shown in Figure 2.1.

a) Surface temperature

Comparisons of surface temperature between an urban area, Durban (Figure 4.6a, c) and non-urban area, Mt. Edgecombe (Figure 4.6b, d) reveals some variability. During summer, the diurnal range of surface temperature in urban area (Durban, Figure

UNIVERSITEIT VAN PRETORIA
UNIVERSITY OF PRETORIA
YUNIBESITHI YA PRETORIA

4.6a) is stronger (difference between maximum and minimum value is smaller) than in non-urban area (Mt. Edgecombe, Figure 4.6b), where the difference between maximum and minimum value is higher (weaker variation). In Durban, the temperature remains around 22˚C between 00h00 and 02h00 UTC, then increases to a maximum average of 32˚C, resulting in a diurnal range of 10˚C (32-22˚C). This variation could be attributed to the UHI effect, which existed (is present) during the night. In contrast, Mt. Edgecombe experiences a slight drop in temperature from 20˚C to 18˚C between 00h00 and 02h00 UTC, indicating the absence of UHI in non-urban areas. After 02h00 UTC, temperature rises to a maximum between 30˚C and 33˚C, resulting in a weaker diurnal range (>12˚C). However, there is variability among the models, especially in non-urban area (Mt. Edgecombe).

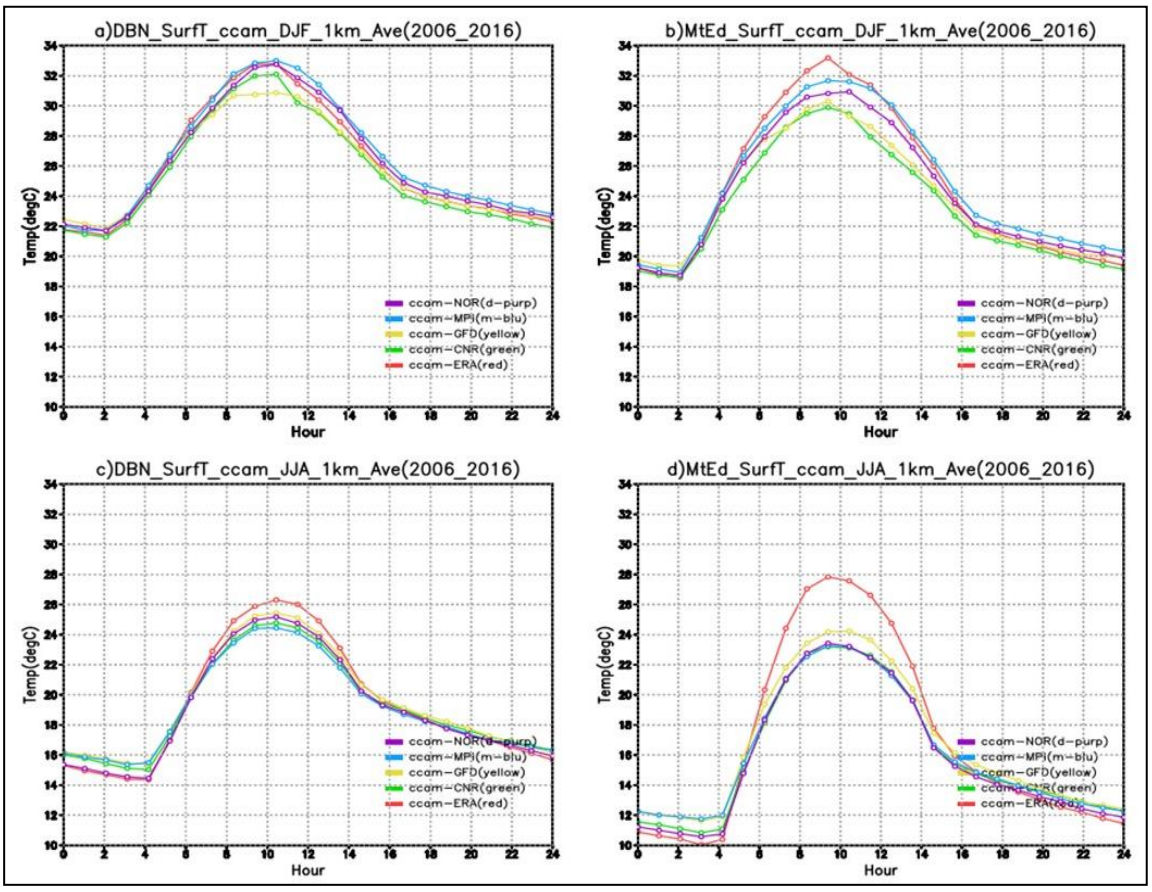

Figure 4.6: The CCAM-CMIP5 driven simulations of diurnal range of surface temperature with ERAI driven simulations and representative concentration pathway 8.5 (RCP8.5) for DJF and JJA over Durban Weather Office and Mt. Edgecombe for the period 2006-2016

UNIVERSITEIT VAN PRETORIA
UNIVERSITY OF PRETORIA
YUNIBESITHI YA PRETORIA

The CCAM-CMIP5 simulations indicate that surface temperature is higher in urban areas (Durban), especially the maximum values, compared to non-urban areas (Mt. Edgecombe), except for CCAM-ERAI run, which shows maximum temperatures higher than 32˚C just before 10h00 UTC (11h00 SAST). The elevated temperatures in cities lead to a stronger diurnal range, compared to non-urban areas and is attributed to factors such as reduced vegetation, increased artificial materials such as concrete and asphalt, as well as increased anthropogenic heating (Pokhrel and Lee, 2011; Ramamurthy *et al.*, 2014; Estrada *et al.*, 2017). The increased diurnal range in cities is due to a faster rate of increase in minimum temperatures compared to the slower rise in maximum temperatures, as observed in non-urban areas (Katzfey *et al.*, 2020).

In winter (JJA, Figure 4.6c and d), temperatures are lower, but the diurnal range remains stronger in urban areas (Durban) and weaker in non-urban areas (Mt. Edgecombe). This contrast highlights the significant diurnal range difference between urban and non-urban areas.

However, the diurnal range of temperature (Figure 4.6) shows similarities to the observed diurnal range of wind speed (Figure 4.2), suggesting that temperature distribution may be influenced by wind patterns. At night, an analysis of winds reveals that at both stations, the dominant winds are from the land (land breeze), whereas during the day, dominant winds come from the ocean (sea breezes). The sea breeze helps reduce daytime maximum temperatures, whereas land breeze acts to reduce temperatures over the land at night. However, due to the presence of buildings and artificial surfaces, more heat is retained than can be released, as a result, weaker land breezes are not effective in reducing night-time temperatures over the city, thus resulting in a slight reduction of the UHI.

b) Shortwave radiation

An analysis of shortwave radiation at both the urban (Durban) and non-urban (Mt. Edgecombe) stations are presented in Figure 4.7. Compared to surface temperature (Figure 4.6), the figure shows no significant difference in the shortwave radiation between urban and non-urban areas across all the CMIP5 simulations. This is expected since an equal amount of shortwave radiation is received irrespective of

UNIVERSITEIT VAN PRETORIA
UNIVERSITY OF PRETORIA
YUNIBESITHI YA PRETORIA

urban/non-urban surface. The shortwave's radiation diurnal range displays an increase from a minimum of 0 W/m^2 to a maximum of approximately 700 W/m^2 at around 10h00 UTC (12h00 SAST) during summer. This radiation then decreases to a minimum at around 16h00 UTC (18h00 SAST). However, the GFD8.5 model shows a slightly stronger diurnal range, but this is observed only in Durban. All other simulations exhibit strong agreement. The JJA diurnal cycles (Figure 4.7c and d) indicate that there is no significant difference in the diurnal range of shortwave radiation between urban and non-urban areas across all the CMIP5 simulations, since a similar amount of radiation is received at both urban and rural areas.

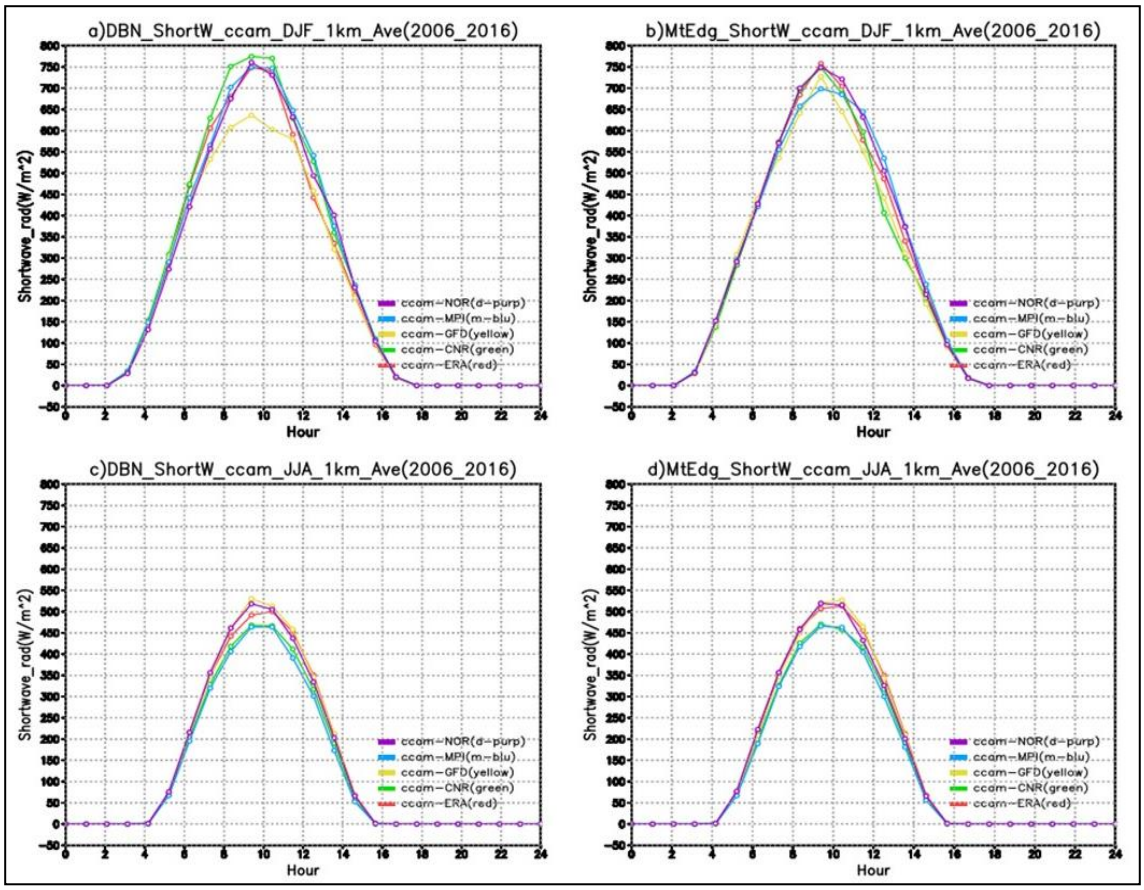

Figure 4.7: The CCAM simulation of diurnal range of shortwave radiation with ERAI and representative concentration pathway 8.5 (RCP8.5), CMIP5 driven simulations for DJF and JJA over Durban Weather Office and Mt. Edgecombe for the period 2006-2016

UNIVERSITEIT VAN PRETORIA
UNIVERSITY OF PRETORIA
YUNIBESITHI YA PRETORIA

c) Longwave radiation

An analysis of longwave radiation (Figure 4.8) shows higher values over Durban compared to Mt. Edgecombe, indicating that more radiation is stored in cities than is released back to space. However, results also show almost similar diurnal range (maximum-minimum values) at both Durban and Mt. Edgecombe. In Durban, the minimum value is around 40 W/m^2 and the maximum value ranges from 70 W/m^2 to 100 W/m^2. In contrast, at Mt. Edgecombe, the minimum value is averaged at 35 W/m^2 and the maximum value is averaged from 70 W/m^2 to 100 W/m^2.

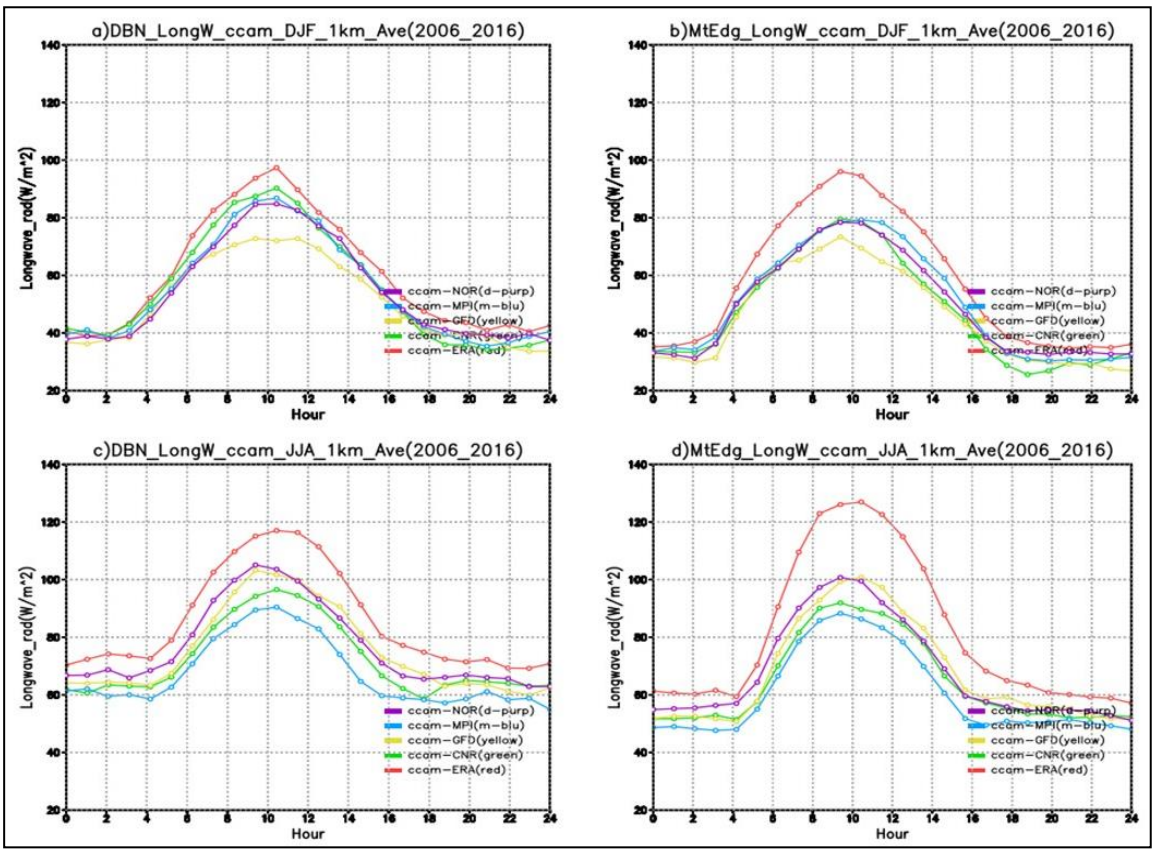

Figure 4.8: The CCAM simulation of diurnal range of longwave radiation with ERAI and representative concentration pathway 8.5 (RCP8.5) driven simulations for DJF and JJA over Durban and Mt. Edgecombe Weather Office for the period 2006-2016

Thus, the diurnal range is slightly small (stronger) at Durban station compared to Mt. Edgecombe. Notably, the ERAI driven simulations exhibit larger diurnal range than all the CMIP5 driven simulations. The difference between ERAI and CMIP5 simulations could be due to that ERAI is a reanalysis and considered globally as

UNIVERSITEIT VAN PRETORIA
UNIVERSITY OF PRETORIA
YUNIBESITHI YA PRETORIA

observed data whereas the CMIP5 simulations are low mitigation driven emission scenarios. This result suggests that due to urbanisation, more radiation is stored within cities resulting in a stronger diurnal range (less diurnal range) in urban areas compared to areas away from urban areas. The JJA diurnal cycles reveal variability in longwave radiation between models, with higher radiation being emitted in urban areas compared to non-urban areas. This suggests a distinct contrast in longwave radiation between urban versus non-urban areas (Figure 4.8c and d).

d) Net radiation

An analysis of the diurnal range in net radiation is presented in Figure 4.9. The figure reveals both similarities and differences between Durban and Mt. Edgecombe. From 00h00 to 02h00 UTC, minimum values are slightly similar over both Durban and Mt. Edgecombe. The negative values indicate the absence of incoming shortwave radiation at night, as net radiation is the difference between incoming shortwave radiation and outgoing longwave radiation. However, from 02h00 to 24h00 UTC, the summer diurnal range is also quite similar, but with slightly higher maximum values at Durban compared to Mt.Edgecombe. The GFD8.5 model, however, displays a slightly lower maximum value compared to the other CMIP5 model simulations.

Among all the radiation outputs, only longwave radiation indicates the presence of the UHI effect. The JJA diurnal range of net radiation (Figure 4.9c and d) exhibit similar patterns between urban and non-urban stations, amongst all the CMIP5 simulations. The diurnal range of net radiation is also similar to that of shortwave radiation (Figure 4.7c and d). This could be because net radiation is influenced by both shortwave and longwave radiation.

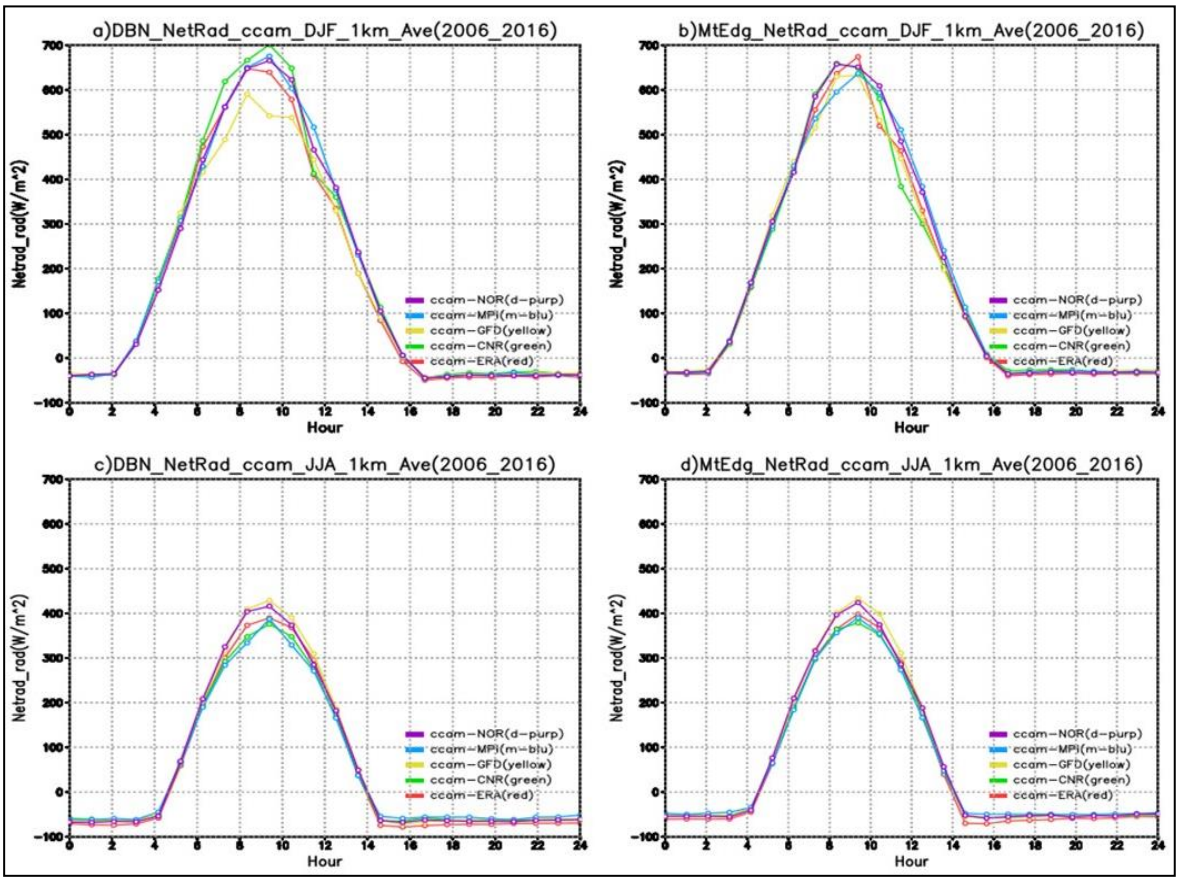

Figure 4.9: The CCAM simulation of diurnal range of net radiation with ERAI and representative concentration pathway 8.5 (RCP8.5) driven simulations for DJF and JJA over Durban and Mt. Edgecombe Weather Office for the period 2006-2016

e) Planetary boundary layer height

The diurnal range of the planetary boundary layer height is illustrated in Figure 4.10. In the morning (00h00-04h00 UTC), minimum values vary between Durban and Mt. Edgecombe. In Durban (Figure 4.10a), the minimum value is initially higher, with an average of approximately 300 metres and the maximum height reached is approximately 700 metres amongst some of the CMIP5 model simulations (GFD8.5, MPI8.5 and NOR8.5), with a maximum around 800 m for CNR8.5. The stronger (smaller) boundary layer could have been influenced by the strong mixed layer within the city. Notably, only the CNR8.5 simulation shows higher maximum value over Durban compared to all other CMIP5 model simulations, with a maximum around 800 m. At Mt. Edgecombe, the minimum values range around 100 to 200 metres, and the maximum values average from 700 to less than 900 metres, resulting in a weaker

UNIVERSITEIT VAN PRETORIA
UNIVERSITY OF PRETORIA
YUNIBESITHI YA PRETORIA

(larger) diurnal range compared to Durban. The maximum height in non-urban areas exceeds that in urban areas, which may be attributed to free convection in non-urban areas opposed to a more disturbed boundary layer in urban areas (Bozonnet *et al.,* 2007).

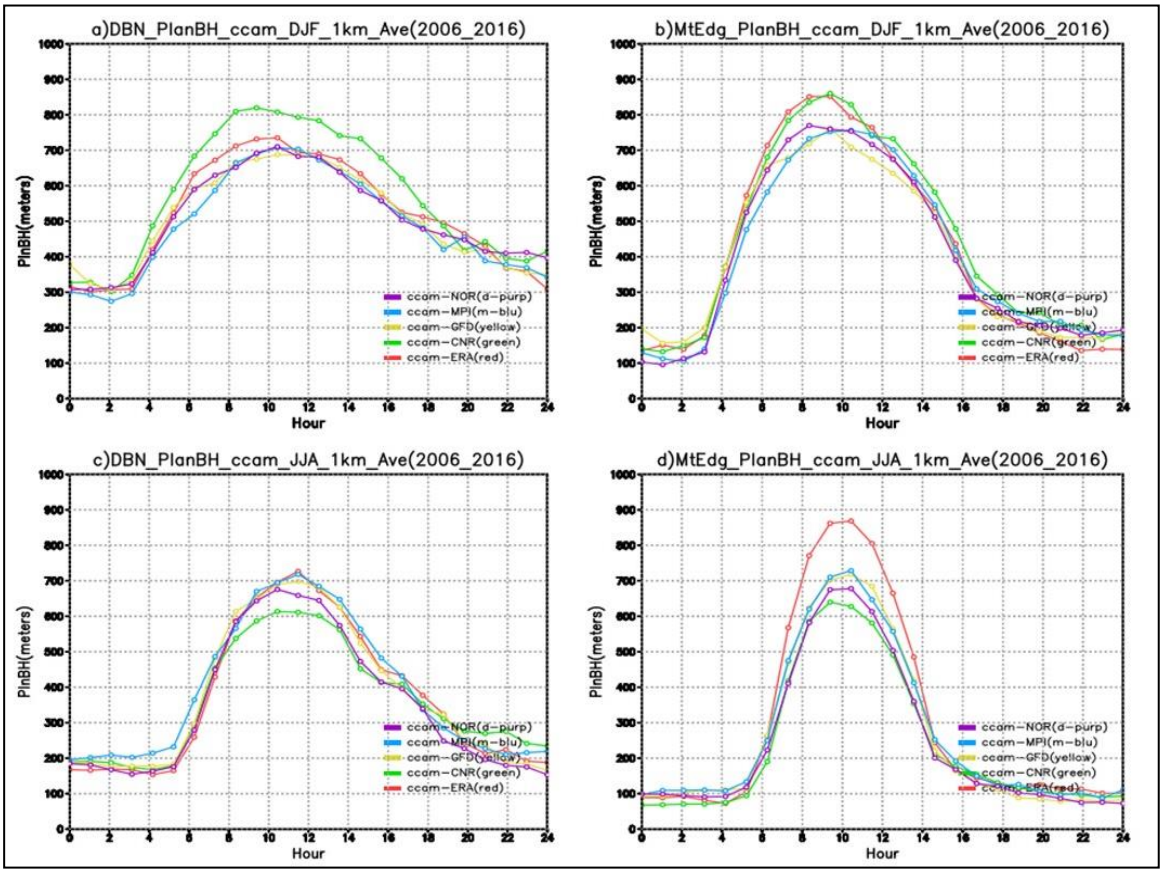

Figure 4. 10: The CCAM simulation of diurnal range of planetary boundary layer with ERAI Reanalysis and representative concentration pathway 8.5 (RCP8.5) driven simulations for DJF and JJA over Durban and Mt. Edgecombe Weather Office for the period 2006-2016.

After 16h00 UTC, the boundary layer remains highly convective over Durban but weakens in Mt. Edgecombe. According to literature, the average boundary layer height reaches up to 1200 metres during the day and decreases to 200 metres at night (Pokhrel and Lee, 2011; Chen and Dipankar, 2022). However, this pattern is not observed in Durban but is nearly observed in Mt. Edgecombe. This difference could be attributed to a disturbed convective boundary layer (Bozonnet *et al.*, 2007) in Durban, and potentially influenced by sea breeze or large-scale circulations. During

UNIVERSITEIT VAN PRETORIA
UNIVERSITY OF PRETORIA
YUNIBESITHI YA PRETORIA

the day, sea breeze reduces the higher temperatures over the land, which in turn reduces the boundary layer height, whereas at night, land breeze removes higher temperatures over the land, thus leading to a more stable boundary layer.

Although the JJA diurnal range (Figure 4.10c and d) of the boundary layer is lower than the DJF diurnal range, the urban diurnal range (Durban) remains more convective compared to the non-urban diurnal range shown over Mt. Edgecombe.

f) Sensible heat fluxes

The diurnal range of the sensible heat fluxes in Durban and Mt. Edgecombe during summer (Figure 4.11), reveals some variability. In Durban, the minimum value is around 0 W/m^2 from 00h00 to 03h00 UTC, rises to a maximum value of range 180-240 W/m^2.

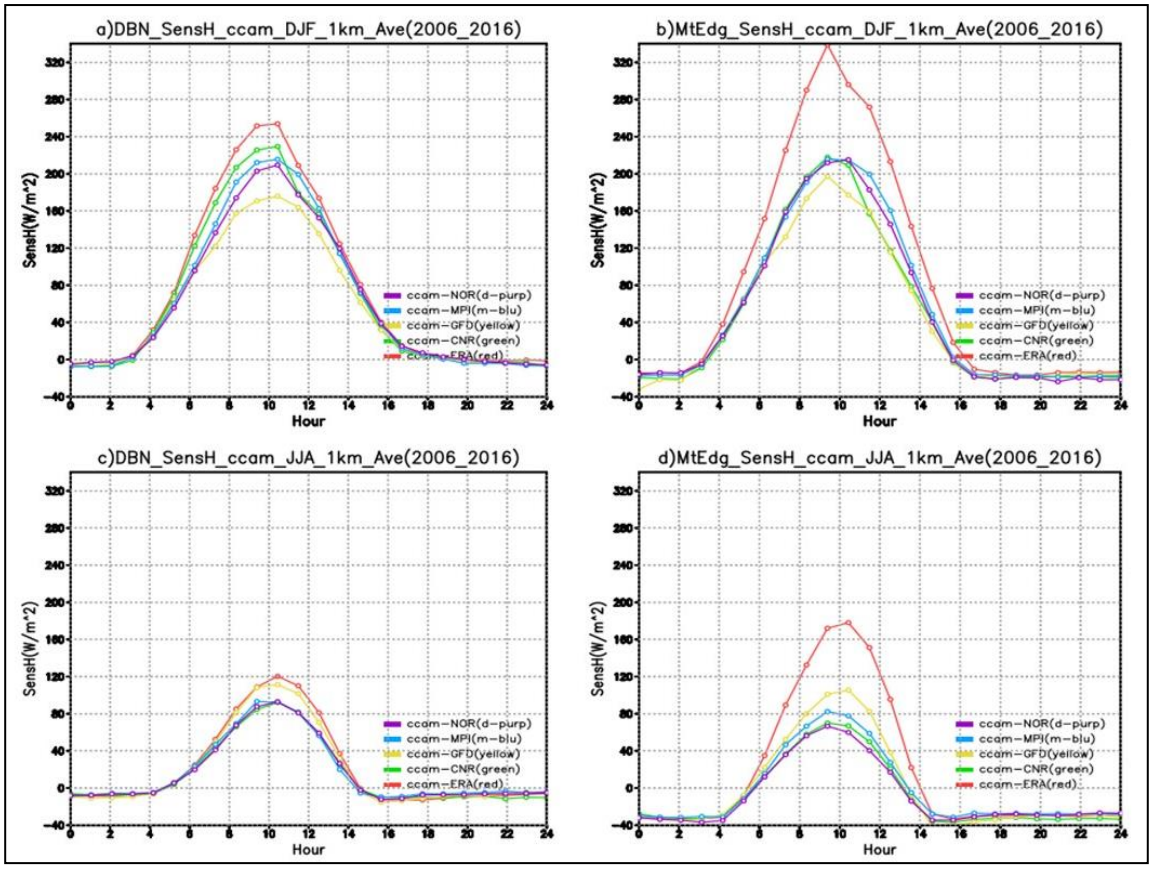

Figure 4. 11: The CCAM simulation of diurnal range of sensible heat flux with ERAI and representative concentration pathway 8.5 (RCP8.5) driven simulations for DJF and JJA over Durban and Mt. Edgecombe Weather Office for the period 2006-2016

UNIVERSITEIT VAN PRETORIA
UNIVERSITY OF PRETORIA
YUNIBESITHI YA PRETORIA

This is higher compared to Mt. Edgecombe, where the minimum value is on average less than 0 W/m^2 during the same period, reaching a maximum value around 200 W/m^2 for all CMIP5 simulations except for ERAI with a maximum higher than 320 W/m^2. After midday, the values drop again in Durban to an average around 0 W/m^2, whereas for Mt. Edgecombe, the values drop to values less than 0 W/m^2. The negative value of sensible heat flux could be due to the presence of natural vegetation and water bodies in non-urban areas, which result in higher latent heat fluxes compared to sensible fluxes.

This analysis indicates that urban areas, with more artificial materials and buildings and fewer water bodies, experience higher sensible heat fluxes than non-urban areas. Conversely, non-urban areas, with fewer artificial materials, show reduced sensible heat fluxes. The JJA diurnal cycle of sensible heat flux (Figure 4.11c and d) indicates that less sensible heat flux is released during this season for both urban and non-urban station, but urban areas still exhibit higher and variable heat flux compared to non-urban areas. It can also be noted that ERAI shows larger diurnal range in a non-urban area compared to an urban area.

g) Latent heat fluxes

Compared to sensible heat fluxes (Figure 4.11), during summer, the latent heat fluxes values are lower in Durban compared to Mt. Edgecombe (Figure 4.12). In Durban, the minimum value is averaged around 40 W/m^2, and the maximum value ranges from around 180 to around 230 W/m^2, resulting in a diurnal range of ranging from around 120 W/m^2 and higher. ERAI values are slightly lower than all CMIP5 simulations, while CNR8.5 values are slightly higher than all the simulations.

In Mt. Edgecombe, the minimum value is averaged around 0 W/m^2, and the maximum value exceeds 320 W/m^2 for all CMIP5 driven simulations runs, with ERAI driven simulations maximum value around 240 W/m^2 thus leading to a diurnal range higher than 320 W/m^2 for CMIP5 simulations and around 240 W/m^2 for ERAI simulation. This difference may be attributed to limited water bodies in urban areas, which reduces evaporation and latent heat fluxes and increases sensible heat flux. In

UNIVERSITEIT VAN PRETORIA
UNIVERSITY OF PRETORIA
YUNIBESITHI YA PRETORIA

contrast, non-urban areas with more vegetation and water bodies experience enhanced evaporation and higher latent heat fluxes.

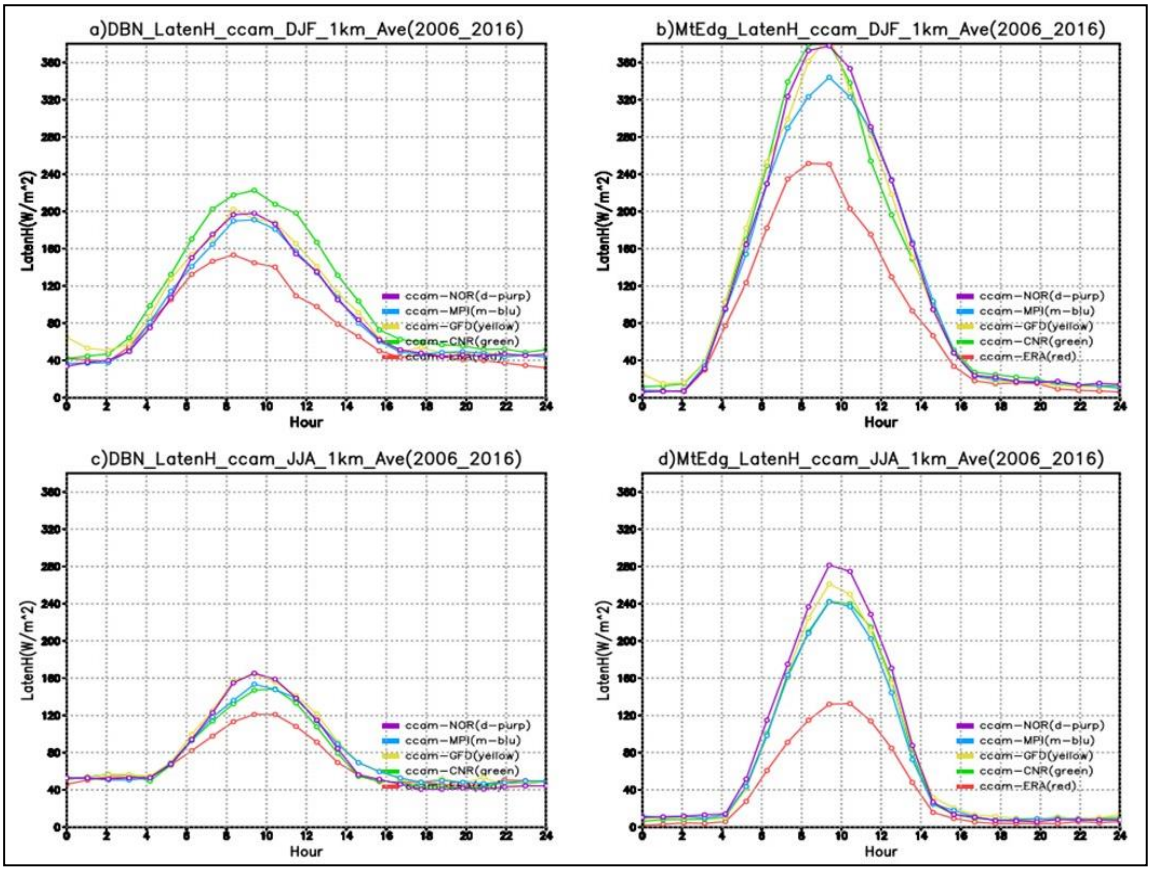

Figure 4. 12: The CCAM simulation of diurnal range of latent heat flux with ERAI and representative concentration pathway 8.5 (RCP8.5) driven simulations for DJF and JJA over Durban and Mt. Edgecombe Weather Office for the period 2006-2016.

The JJA latent heat diurnal cycle (Figure 4.12c and d) demonstrates stronger diurnal range in urban areas compared to non-urban areas. In Durban, minimum values range around 40 W/m^2 and maximum values ranging around 160 W/m^2 for CMIP5 simulations and around 120 W/m^2 for ERAI, thus leading to a diurnal range from 80 W/m^2 for ERAI to 120 W/m^2 for CMIP5 simulations. In Mt. Edgecombe, minimum values range just above 0 W/m^2 and maximum values range above 240 W/m^2, whereas ERAI has maximum value just above 120 W/m^2, and is almost half of the CMIP5 simulations. The diurnal range is thus around 120 W/m^2 for ERAI and around 240 W/m^2 for CMIP5 simulations. Despite this variation, latent heat fluxes are lower

UNIVERSITEIT VAN PRETORIA
UNIVERSITY OF PRETORIA
YUNIBESITHI YA PRETORIA

in urban areas than in non-urban areas, primarily due to fewer water bodies in urban areas.

This analysis shows that temperatures were higher within the city compared to areas away from the city. There are similarities between the diurnal range of temperature and wind speed, an indication that temperature distribution may have been influenced by wind patterns. Additionally, radiation, the boundary layer and sensible heat flux could have been affected by winds. During the day, sea breezes likely contributed to reduced temperature and longwave radiation over the city, thus also reducing the strength of the boundary layer and sensible heat fluxes. At night, sea breezes were weaker, and they may not be able to remove higher temperatures over the city, resulting in more energy being stored as longwave radiation, thus, leading to the strengthening of the UHI over the city.

4.3.2.2 The spatial and temporal variation of the UHI

This section examines the spatial and temporal variation of atmospheric variables, including temperature, radiation (outgoing longwave, shortwave, and net radiation), planetary boundary layer, and sensible heat flux over a 24-hour period for the current climate. The analysis is organised into four six-hourly periods: (01h00 to 06h00), (07h00 to 12h00), (13h00 to 18h00) and (19h00 to 24h00) UTC hours. The objective is to determine the onset and dissipation time for the UHI effect. Fischer et al., (2012) demonstrated in their urban climate study that UHI begins to develop after mid-day and reaches its maximum at dawn. This study builds on the results of previous studies by analysing the spatial and temporal variation of the UHI.

a) Surface temperature

The spatial and temporal distribution of temperature between ERAI (Figure 4.13) and CMIP5 driven simulations (Figure 4.14) is analysed. The surface temperature analysis reveals lower temperatures from 00h00 to 06h00 UTC, with maximum values reaching up to 26°C within the city and dropping to values below 22°C in non-urban areas. The higher temperature values within the city may be due to the residual effects of the previous nighttime UHI effect. Between 07h00 and 12h00 UTC,

UNIVERSITEIT VAN PRETORIA
UNIVERSITY OF PRETORIA
YUNIBESITHI YA PRETORIA

temperatures increase, reaching over 32°C in the UHI-affected coastal city, while temperatures away from the city peak around 26 °C. This rise in temperature could be attributed to increased longwave radiation trapped by buildings and anthropogenic heating within the city.

From 13h00 to 18h00 UTC, the temperature maximum begins to drop, falling to values below 32°C within the city and decreasing further away from the city. Between 19h00 and 24h00 UTC, temperatures continue to drop, with maximum values falling below 26°C in the UHI-affected coastal city and decreasing even further away from the city.

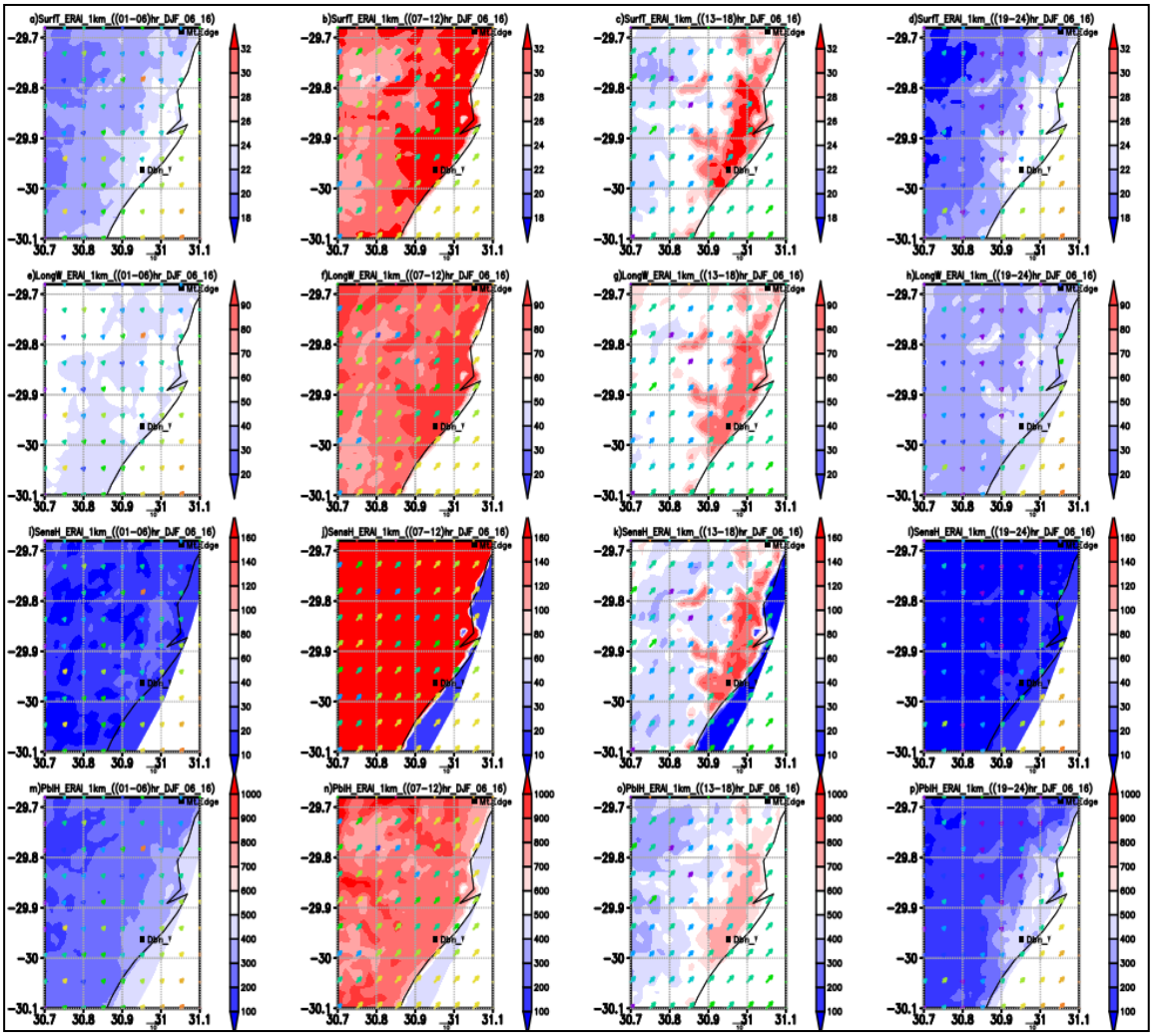

Figure 4.13: The spatial and temporal distribution (i) surface temperature (top row, left to right, (a:01h00-06h00); (b:07h00-12h00); (c:13h00-18h00); (d:19h00-24h00) UTC), (ii) longwave radiation (second row, left to right, (e:01h00-06h00); (f:07h00-12h00); (g:13h00-

UNIVERSITEIT VAN PRETORIA
UNIVERSITY OF PRETORIA
YUNIBESITHI YA PRETORIA

18h00); (h:19h00-24h00) UTC), (iii) sensible heat fluxes (third row, left to right, (i:01h00-06h00); (j:07h00-12h00); (k:13h00-18h00); (l:19h00-24h00) UTC) and (iv) planetary boundary layer (bottom row, left to right, (m:01h00-06h00); (n:07h00-12h00); (o:13h00-18h00); (p:19h00-24h00) UTC)) versus wind with ERAI driven simulations for DJF period 2005/6-2016. Both Durban (to the south of the domain, 29.965°S; 30.946°E) and Mt. Edgecombe (to the northeast of the domain, 29.706°S; 31.046°E) stations are plotted.

When comparing the (01h00-06h00) cycle with the (19h00-24h00) cycle, one would expect cooler temperatures during the early morning hours (01h00-06h00) than in the late evening (19h00-24h00) hours. However, the opposite is observed, indicating that the UHI effect results in warmer temperatures within the city during the (01h00-06h00) period.

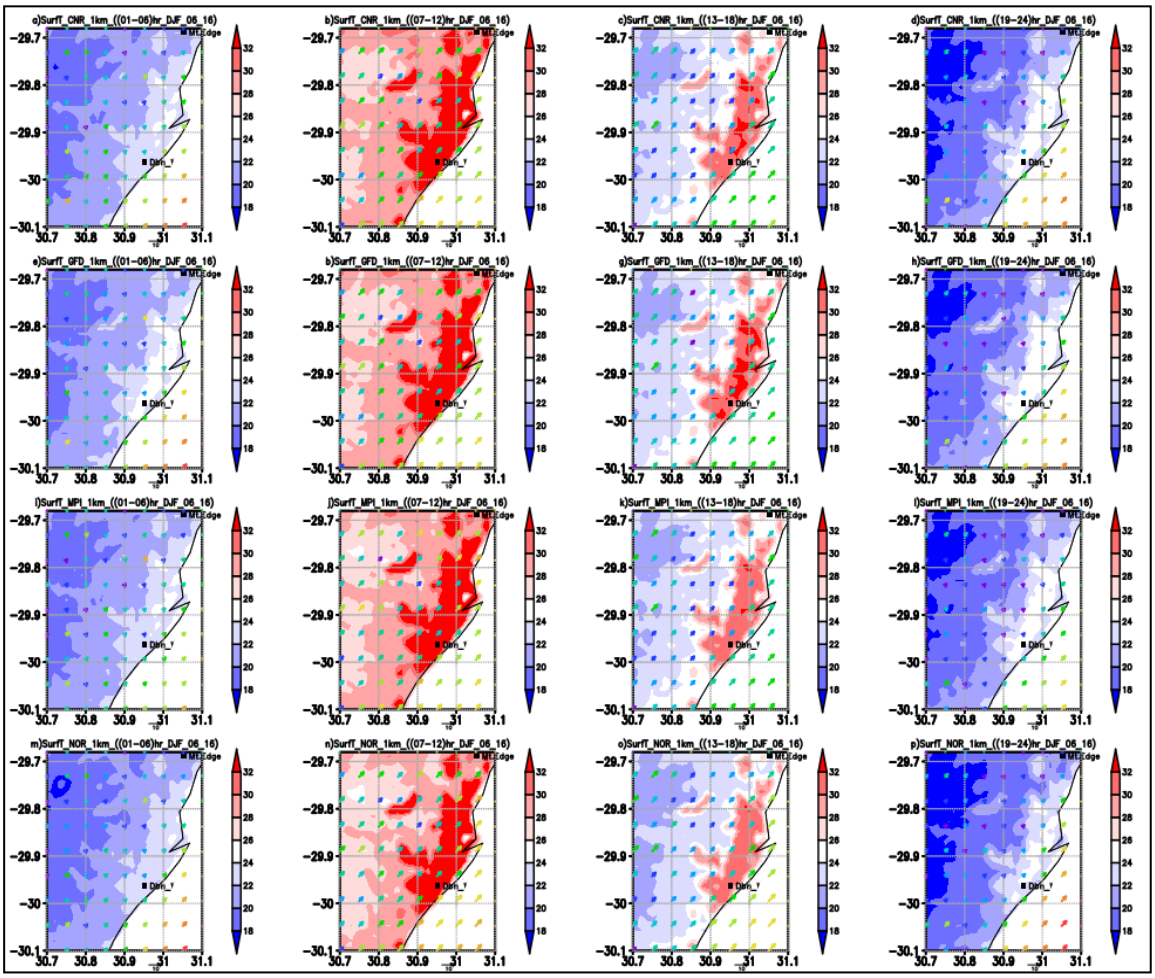

Figure 4.14: The spatial and temporal distribution of surface temperature versus wind with *CMIP5* driven simulations for DJF period 2005/6-2016. Left row (01h00-06h00); second row (07h00-12h00); third row (13h00-18h00); fourth row (19h00-24h00) UTC). First column:

UNIVERSITEIT VAN PRETORIA
UNIVERSITY OF PRETORIA
YUNIBESITHI YA PRETORIA

CNR simulations; second column: GFD simulations; third column: MPI simulations; fourth column: NOR simulations. Both Durban (to the south of the domain, 29.965°S; 30.946°E) and Mt. Edgecombe (to the northeast of the domain, 29.706°S; 31.046°E) stations are plotted.

The UHI pattern and its intensity in ERAI simulations of surface temperature, longwave radiation and boundary layer (Figure 4.13) are consistent with all MPI8.5 driven simulations (Figure 4.14) across all the periods, although with some slight variability.

An analysis of horizontal winds is however complex compared to the observed winds at the two stations (Figure 4.3). During the early hours, from 01h00 to 06h00 UTC, winds are very weak both over the ocean and over the land (Figure 4.13 a-d), with the wind rose indicating the presence of land breezes during this period. These land breezes are responsible for the removal of higher temperatures over the land, resulting in a weaker UHI. From 07h00 to 12h00 UTC and from 13h00 to 18h00 UTC, wind speed increases to an average around 10 m/s and are from the southwest (SW). These winds are shown to be sea breezes in the wind rose.

Although these winds may be stronger, the building structures within the city make it difficult for sea breezes to reduce higher temperatures over the city, thus resulting in sustained higher temperatures. Between 19h00 and 24h00, there is a decrease in wind speed to a pattern observed from 01h00-06h00 UTC. This change is due to a shift in wind pattern from sea breeze to land breeze during this time of the day.

The winds plotted at the two stations (Figure 4.3) show that model simulations are in agreement with the observations; however simulated winds are weaker than observed. This disparity could be due to the model's resolution of 1 km, which may struggle to capture the observed winds. It could also be attributed to the dominance of synoptic scale systems over mesoscale systems, given the proximity to the ocean.

b) Longwave radiation

In the analysis of outgoing longwave radiation for ERAI (Figure 4.13, second row) and CMIP5 driven simulations (Figure 4.15), positive values represent upward radiation, while negative values indicate downward radiation at the ground. From 01h00 to

UNIVERSITEIT VAN PRETORIA
UNIVERSITY OF PRETORIA
YUNIBESITHI YA PRETORIA

06h00 UTC, the ERAI driven simulations show some evidence of the UHI effect at the surface, whereas the CMIP5 driven simulations do not. Specifically, ERAI driven simulation exhibits a maximum value of less than 60 W/m^2 (Figure 4.13), while all CMIP5 driven simulations show values below 50 W/m^2 (Figure 4.15), with no apparent UHI effect. During this period, most of the radiation is absorbed by buildings and only a small amount is slightly released back into the atmosphere, with remnants of the previous night's UHI still present.

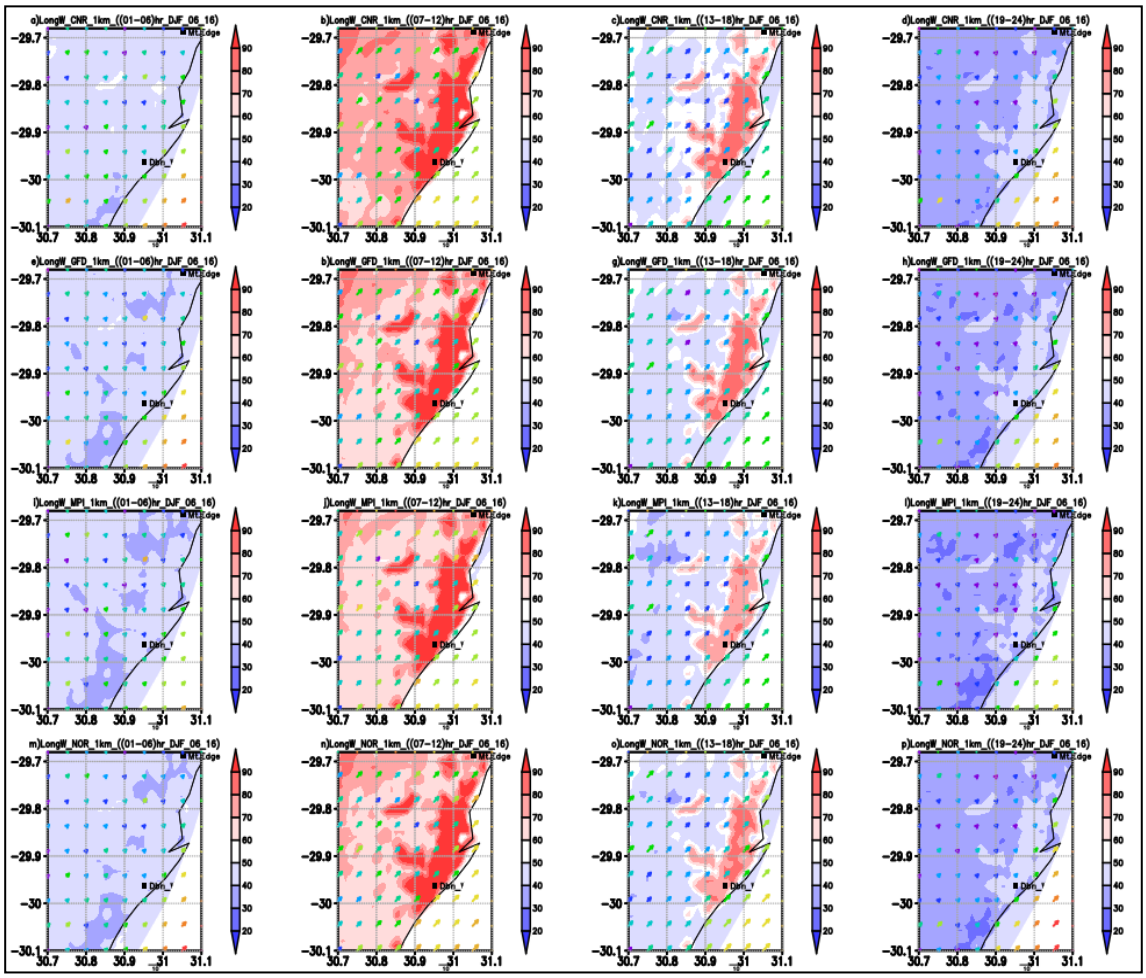

Figure 4.15: The spatial and temporal distribution of longwave radiation (positive values are upwards, and negative values are downwards) versus wind with CMIP5 driven simulations for DJF period 2005/6-2016. Left row (01h00-06h00); second row (07h00-12h00); third row (13h00-18h00); fourth row (19h00-24h00) UTC). First column: CNR simulations; second column: GFD simulations; third column: MPI simulations; fourth column: NOR simulations. Both Durban (to the south of the domain, 29.965°S; 30.946°E) and Mt. Edgecombe (to the northeast of the domain, 29.706°S; 31.046°E) stations are plotted.

UNIVERSITEIT VAN PRETORIA
UNIVERSITY OF PRETORIA
YUNIBESITHI YA PRETORIA

From 07h00 to 12h00 UTC, the highest values of longwave radiation are observed, with maxima exceeding 90 W/m^2 within the city and less than 70 W/m^2 in non-urban areas. This pattern is consistent across both ERAI and CMIP5 driven simulations and coincides with peak shortwave radiation (Figure C.1).

From 13h00 to 18h00 UTC, longwave radiation decreases, with maximum values dropping to below 80 W/m^2 within the city and falling to less than 40 W/m^2 in non-urban areas. From 19h00 to 24h00 UTC, the UHI effect is still evident, though the maximum longwave radiation values fall below 50 W/m^2 within the city and are reduced further in non-urban areas. The spatio-temporal distribution of longwave radiation resembles that of surface temperature for both ERAI and CMIP5 driven simulations.

c) Shortwave and net radiation

Since the UHI is influenced by the variation of radiation, both shortwave (Figure C.1), and net radiation (Figure C.2) have been examined for their temporal and spatial distribution. An analysis of downward shortwave radiation for both ERAI and CMIP5 driven simulations (Figure C.1) illustrates the spatio-temporal distribution of incoming shortwave radiation. Positive values indicate downward radiation towards the ground, while negative values represent upward radiation from the ground.

From 00h00 to 06h00 UTC, shortwave radiation is minimal, with a constant value of 120 W/m^2 in both ERAI and CMIP5 driven simulations, due to the low values of shortwave radiation during sunrise. From 07h00 to 12h00 UTC, radiation increases, reaching over 300 W/m^2 due to the sun's maximum solar inclination. From 13h00 to 18h00 UTC, shortwave radiation decreases to values of range of 200-220 W/m^2 within the city and drops below 200 W/m^2 in non-urban areas. Amongst the CMIP5 runs, MPI8.5 and NOR8.5 models show lower values compared to CNR8.5 and GFD8.5 runs. From 19h00 until 24h00, shortwave radiation reaches a minimum of 0 W/m^2, as no solar radiation is received during these hours.

The net radiation (Figure C.2), which is the difference between shortwave and longwave radiation, exhibits a spatial and temporal distribution almost similar to that

UNIVERSITEIT VAN PRETORIA
UNIVERSITY OF PRETORIA
YUNIBESITHI YA PRETORIA

of shortwave radiation (Figure C.1) over the 24-hour period. However, there are differences in the spatial pattern observed from 19h00 to 24h00 UTC. From 01h00 to 06h00 UTC, net radiation is less than 60 W/m^2 over most areas within the city and up to 80 W/m^2 in the surrounding areas. This pattern is consistent across both ERAI and CMIP5 driven simulations. Net radiation increases from 07h00 to 12h00 UTC, reaching a maximum and constant (steady) value exceeding 200 W/m^2 across the entire domain, as observed in all runs. Following this peak, net radiation decreases between 13h00 and 18h00 UTC, with values ranging from 80 to 100 W/m^2 within the UHI and exceeding 100 W/m^2 in non-urban areas. From 19h00 to 24h00 UTC, net radiation drops to an average less than 60 W/m^2 in all runs including CMIP5 and ERAI driven simulations, showing a pattern similar to the one during the early morning hours. These results indicate that the amount of radiation received at the surface and its storage contribute to the development of the UHI.

d) Planetary boundary layer

The diurnal range of the planetary boundary layer for the ERAI (Figure 4.13) and CMIP5 driven simulations (Figure 4.16) exhibit signs of the UHI effect. From 01h00 to 06h00 UTC, the boundary layer reaches its highest average value of 400 metres within the UHI, with slightly lower values observed in surrounding areas. Between 07h00 and13h00 UTC, the boundary layer height is at its maximum across the entire domain, exceeding 1000 metres on average and approaching the 1200 metres reported in Bastin *et al.,* (2006) and Pokhrel and Lee, (2011). Higher boundary layer values are also observed away from the city, indicating a disturbed convective boundary layer noted by Bozonnet *et al.,* (2007). From 14h00 to 18h00 UTC, the boundary layer begins to weaken but remains stronger over the UHI, with height less than 700 metres. In non-urban areas, the boundary layer diminishes to values below 400 metres. These maximum and minimum heights are consistent with those reported by Pokhrel and Lee, (2011) and Chen and Dipankar, (2022).

There are slight differences between the diurnal range of the boundary layer simulated by ERAI and those by CMIP5 driven simulations. The boundary layer from with ERAI driven simulation is slightly stronger than in CMIP5 driven simulations,

UNIVERSITEIT VAN PRETORIA
UNIVERSITY OF PRETORIA
YUNIBESITHI YA PRETORIA

particularly regarding the maximum values observed between 07h00 and 12h00 UTC. This discrepancy may be credited to variations in the forcing data applied to in model simulations.

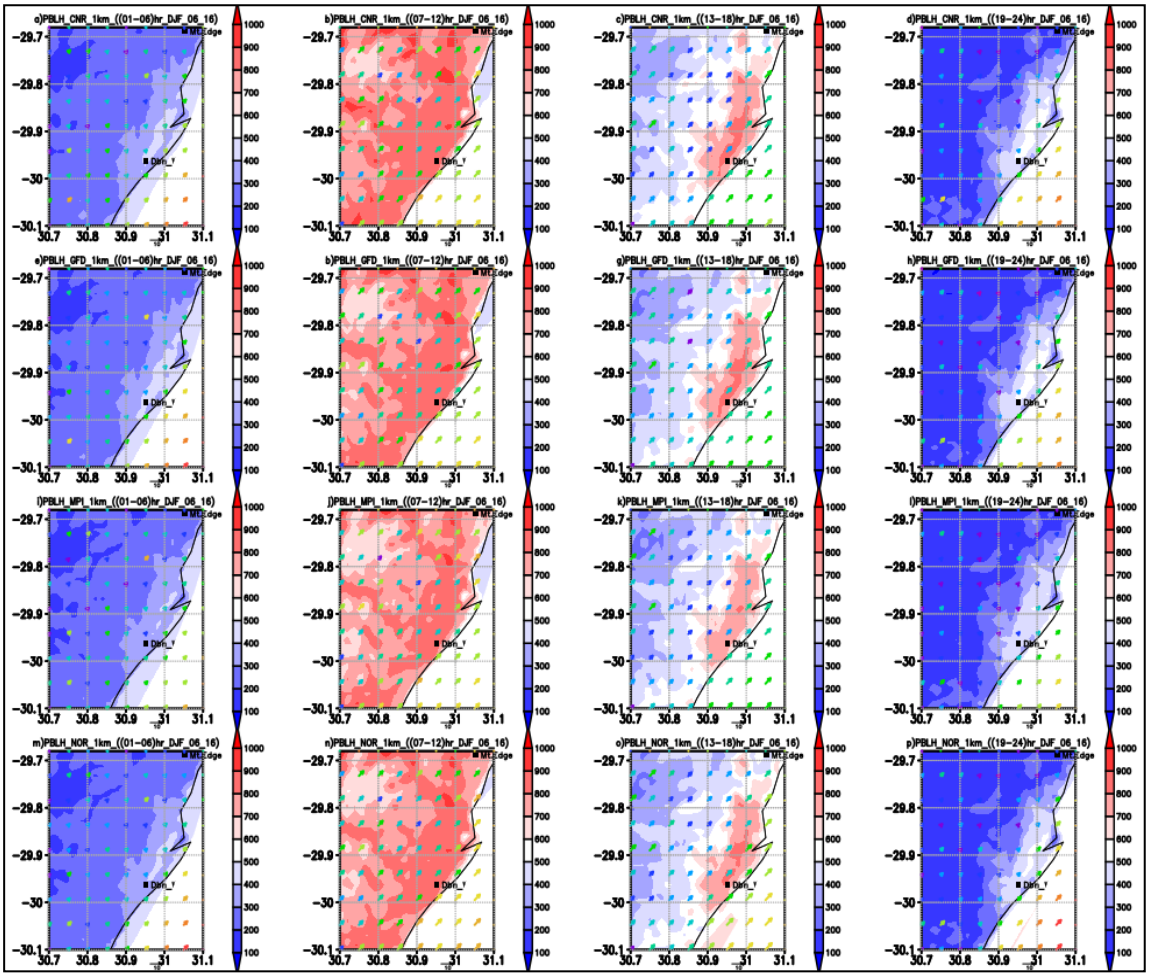

Figure 4.16: The spatial and temporal distribution of planetary boundary layer versus wind with ERAI driven simulations for DJF period 2005/6-2016. Left row (01h00-06h00); second row (07h00-12h00); third row (13h00-18h00); fourth row (19h00-24h00) UTC). First column: CNR simulations; second column: GFD simulations; third column: MPI simulations; fourth column: NOR simulations. Both Durban (to the south of the domain, 29.965°S; 30.946°E) and Mt. Edgecombe (to the northeast of the domain, 29.706°S; 31.046°E) stations are plotted.

These findings suggest that atmospheric flow patterns, including synoptic-scale systems and mesoscale scale systems such as land and sea breezes or mountain and valley winds, play a role in the destruction of the convective boundary layer during

UNIVERSITEIT VAN PRETORIA
UNIVERSITY OF PRETORIA
YUNIBESITHI YA PRETORIA

the day and the strengthening or mixing of the boundary layer at night (Parker, 2010; Grachev *et al.*, 2018).

The analysis of temperature and longwave radiation show that during the day, the UHI is observed from the early hours, strengthens in the afternoon, and hardly dissipates at night. Thus strong offshore winds (land breeze) can result in warmer air from the land moving over the ocean, which may potentially disrupt the UHI effect (Estoque, 1962).

e) Sensible heat flux

The spatial and temporal distribution of sensible heat flux for ERAI (Figure 4.13) and CMIP5 driven simulation (Figure C.3) is also illustrated. This flux is weak from 00h00 to 06h00 UTC, with a maximum value of 20 W/m^2, driven by radiation. From 07h00 to 12h00 UTC, the sensible heat flux increases and reaches a maximum of over 160 W/m^2 across the entire domain. This increase is due to greater release of sensible heat from urban surfaces and buildings during this period. Sensible heat is reduced from 13h00 to 18h00 UTC, demonstrating a clear UHI effect with a maximum value reaching up to 120 W/m^2 within the UHI area while values outside the UHI drop to less than 60 W/m^2. From 19h00 to 24h00 UTC, the sensible heat flux decreases to a constant value of less than 20 W/m^2, which is comparable to the 01h00 to 06h00 UTC.

There is a slight difference between ERAI and CMIP5 driven simulations, with ERAI driven simulation showing stronger values than CMIP5 driven simulations, particularly from 06h00 to18h00 UTC. The higher values in sensible heat flux in both ERAI and CMIP5 driven simulations are attributed to the presence of more artificial materials such as concrete, buildings and less water bodies in the city, which increases sensible heat fluxes compared to latent heat fluxes. The results of these simulations show that the UHI occurs over the city of eThekwini. They also show the temporal and spatial distribution of the UHI. Although the winds are complex to analyse at 1 km resolution, they provide evidence that winds are weak at night, strengthening the UHI and slightly strong during the day, it is evidence from observed winds that both synoptic scale and mesoscale systems influence the sustainability of the UHI.

UNIVERSITEIT VAN PRETORIA
UNIVERSITY OF PRETORIA
YUNIBESITHI YA PRETORIA

4.3.2.3 The longitudinal vertical cross-section of winds

An analysis of observed and simulated temperatures (surface and minimum) has indicated the presence of the UHI over the city of eThekwini (Chapters 2 and 3). Similarly, an analysis and verifications of observed and simulated wind speed and direction indicate that atmospheric circulation patterns, including synoptic-scale and mesoscale systems such land and sea breezes, as well as anabatic and katabatic winds, influence the UHI.

To understand the penetration depth of the circulation systems into the UHI simulation domain, a longitudinal vertical cross-section was conducted at three latitudinal points: (a)southern latitude: 30^{o}S, (b) middle latitude: 29.9^{o}S and (c) northern latitude: 29.8^{o}S, respectively. These points are marked as P1, P2 and P3 in Figure 4.1, and they are located ~0.1^{o} (10-12 km) apart. Vertical winds (omega, shaded) and horizontal winds (u,v, vectors) are plotted and analysed to help understand the role of atmospheric circulation including synoptic scale and mesoscale system in the development and evolution of the UHI.

a) Southern latitude: 30°S (P1)

(i) Wind pattern at 06h00 UTC

An analysis of winds was conducted at latitude 30°S, which is the southern point on the domain (see Figure 4.1 and Figure 4.17). At this latitude (Figures 4.17 and 4.18), the city starts at approximately 30.9°E and stretches eastward, ends around 30.93°E. Simulations at 06h00 UTC (the start of the sea breeze) using ERAI and CMIP5 driven simulations show positive vertical velocities ranging from 9 to 12 m/s between 1000 hPa and 900 hPa (Figure 4.17). Horizontal winds are strong at the surface up to 900 hPa. Between 900 hPa and 800 hPa, there is a large reduction in vertical winds, with wind speeds of range 3 to 6 m/s, separating the non-urban area to the west, from the urban area to the east of the 30.8°E longitude (Figure 4.17). This reduction is depicted in all the CMIP5 and ERAI simulations. In this area, the city is bounded by natural vegetation to the west (Figure 4.1), where forest and topography could have resulted in the reduction in wind speed.

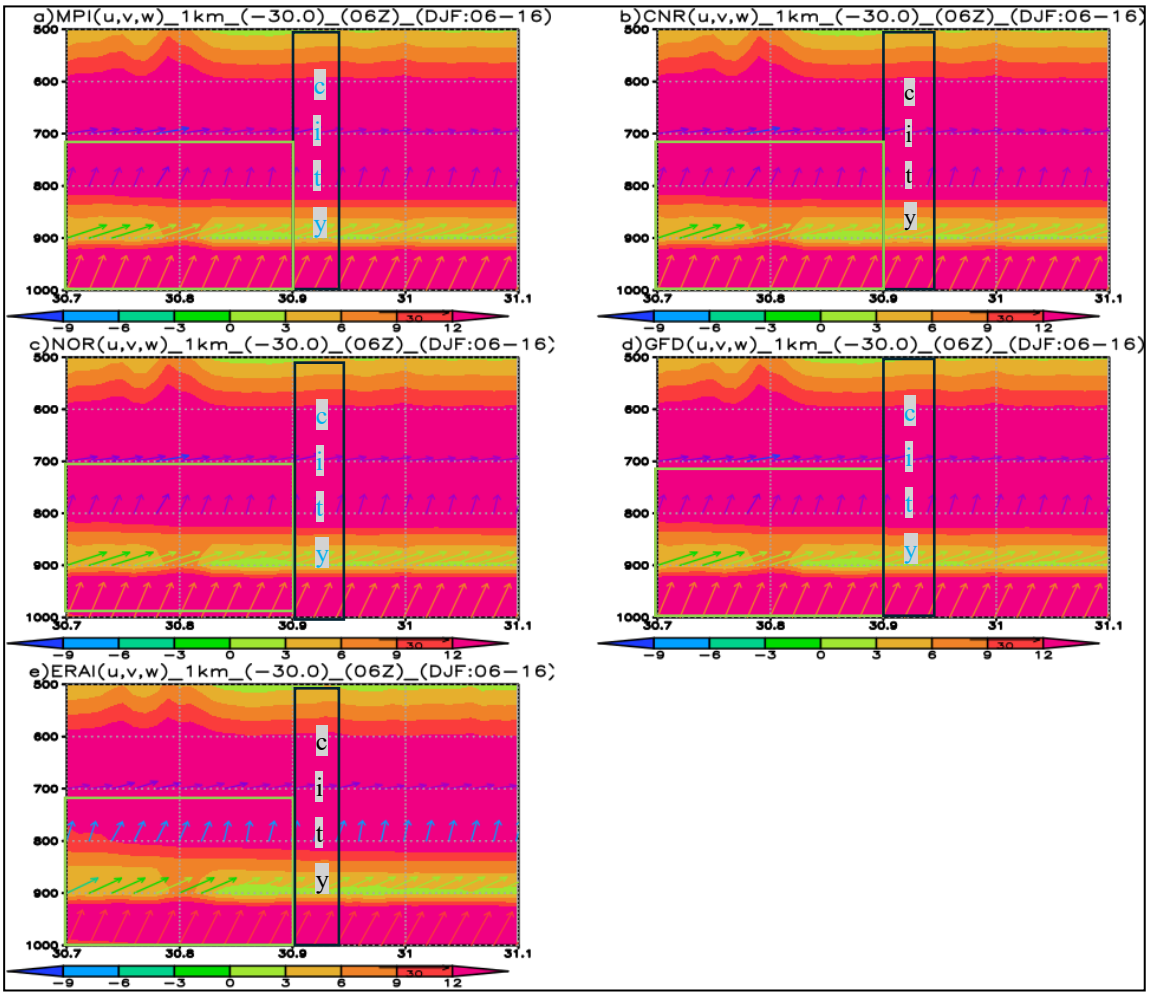

Figure 4.17: The DJF 06h00 UTC CCAM longitudinal cross-section of vertical winds (omega) and horizontal winds (u and v components from the surface (1000 hPa) to upper-air level (500 hPa) at latitude 30°S. The wind speed is measured in meters per second (m/s). At this latitude, the city starts at approximately 30.9°E and stretches eastward, ending at around 31.93°E (black box). To the east, the city is bounded by the Indian Ocean, and to the west it is bounded by natural vegetation (green box).

From 30.8°E to 31°E, the vertical velocity decreases from a range of 3-6 m/s to a range of 0-3 m/s, while horizontal winds remain almost constant. Between 800 hPa and 700 hPa, there is no longitudinal gradient in vertical winds, but horizontal winds shift from southerlies at lower level (800 hPa) to westerlies at 700 hPa. This pattern is consistent in both ERAI and CMIP5 driven simulations. This reduction could be due to buildings within the city as they obstruct wind flow over the city.

UNIVERSITEIT VAN PRETORIA
UNIVERSITY OF PRETORIA
YUNIBESITHI YA PRETORIA

(ii)Wind pattern at 18h00 UTC

At 18h00 UTC the vertical and horizontal wind patterns from the surface to 900 hPa are similar to those observed at 06h00 UTC (see Figure 4.17). However, from 900 hPa to 800 hPa, the pattern changes. While there is a vertical wind gradient at 30.8°E, to the west of this longitude, vertical wind speeds range from 6 to 9 m/s, decreasing to a range of 3 to 6 m/s as they enter the city. This is indicated by the south westerlies between these two levels.

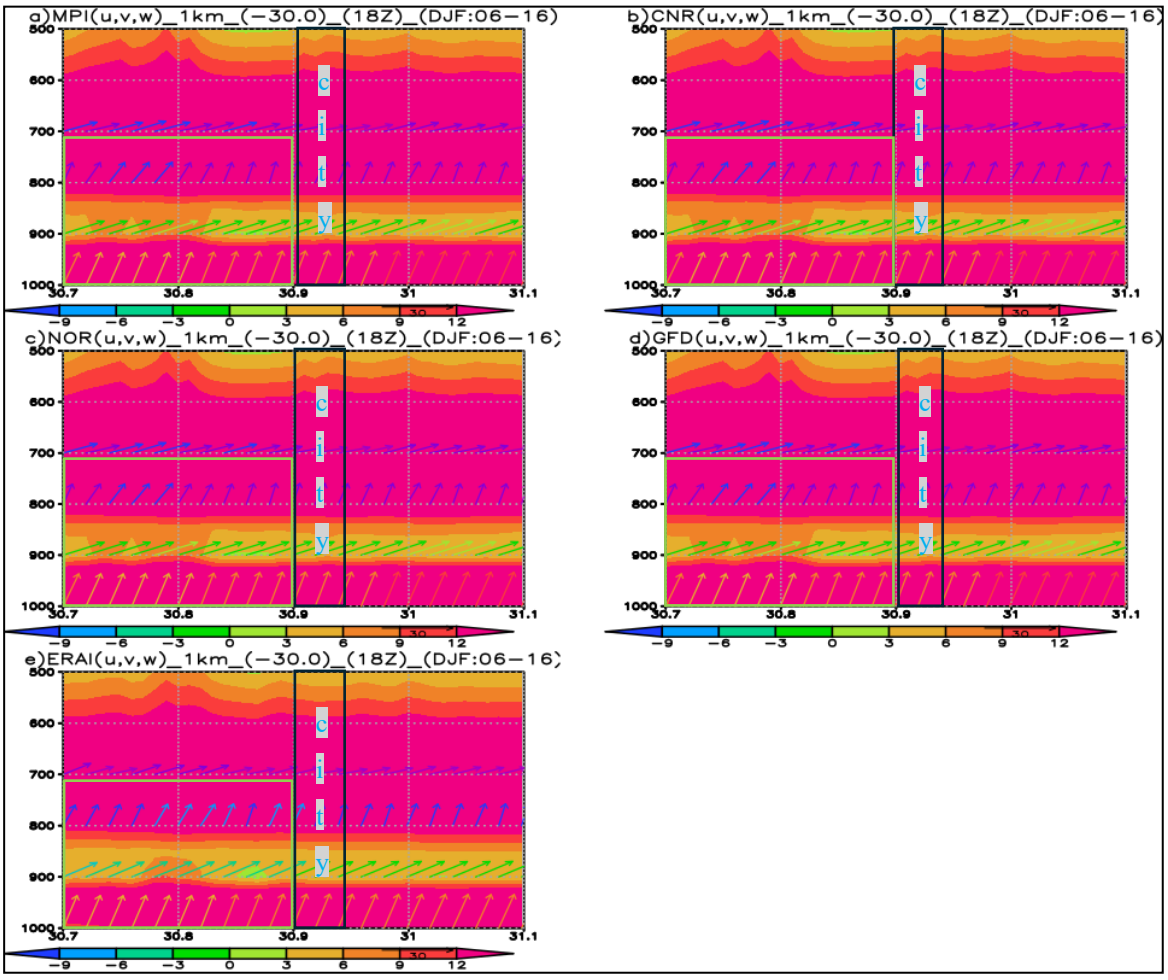

Figure 4.18: The DJF 18h00 UTC CCAM longitudinal cross-section of vertical winds (omega) and horizontal winds (u and v) components from the surface (1000 hPa) to upper-air level (500 hPa) at latitude 30°S. The wind speed is measured in meters per second (m/s). At this latitude, the city starts at approximately 30.9°E and stretches eastward, ending at around 31.93°E (black box). To the east, the city is bounded by the Indian Ocean, and to the west it is bounded by natural vegetation (green box).

UNIVERSITEIT VAN PRETORIA
UNIVERSITY OF PRETORIA
YUNIBESITHI YA PRETORIA

From 30.8°E to 31°E, wind speeds vary, light winds were simulated at the lower level and stronger winds were simulated at the higher level. From 800 to 600 hPa and above, the vertical wind speed exceeds 12m/s, with southerlies at 800 hPa changing to southwesterlies at 700 hPa. Interestingly, between 600 and 500 hPa, the vertical winds exhibit wave patterns, with wind speeds decreasing with height. This wind pattern is consistent in both ERAI and all the CMIP5 driven simulations (see Figure 4.18).

b) Middle latitude: 29.9 ^{o}S (P2)

(i) Wind pattern at 06h00 UTC

At latitude 29.9 ^{o}S (Figures 4.19 and 4.20), the city begins at approximately 30.85°E and stretches eastward, ending around 31.05°E (black box). To the east, the city is bounded by the Indian Ocean, and to the west, it is bounded by natural vegetation (green box). There is also some vegetation including grassland and savannah between 30.91°E and 30.93°E. The wind pattern observed at 06h00 UTC and 30°S (Figure 4.17) slightly differs from that at 29.90°S (Figure 4.19). At 1000 hPa, the wind pattern is similar to the one seen at the previous latitude, but between 900 and 800 hPa, there is a variable vertical wind pattern ranging from 3 to 9 m/s.

This could be due to the fact that this latitude is heavily dominated by urban areas (see Figure 4.1b), particularly to the east of 39.9°E, in contrast to 30.8°E and 30°S. The boundary layer at this latitude appears to be highly disturbed. However, the horizontal winds remain predominantly south-westerly and are comparable to those at 30^{0}S.

From 800 hPa to 600 hPa, the vertical wind speed remains constant at 12 m/s, while the horizontal wind shifts from southerly to westerly. Between 600 hPa and 500 hPa, the vertical wind exhibits a wave pattern. Although results vary between models, there is minimal difference between ERAI and CMIP5 driven simulations.

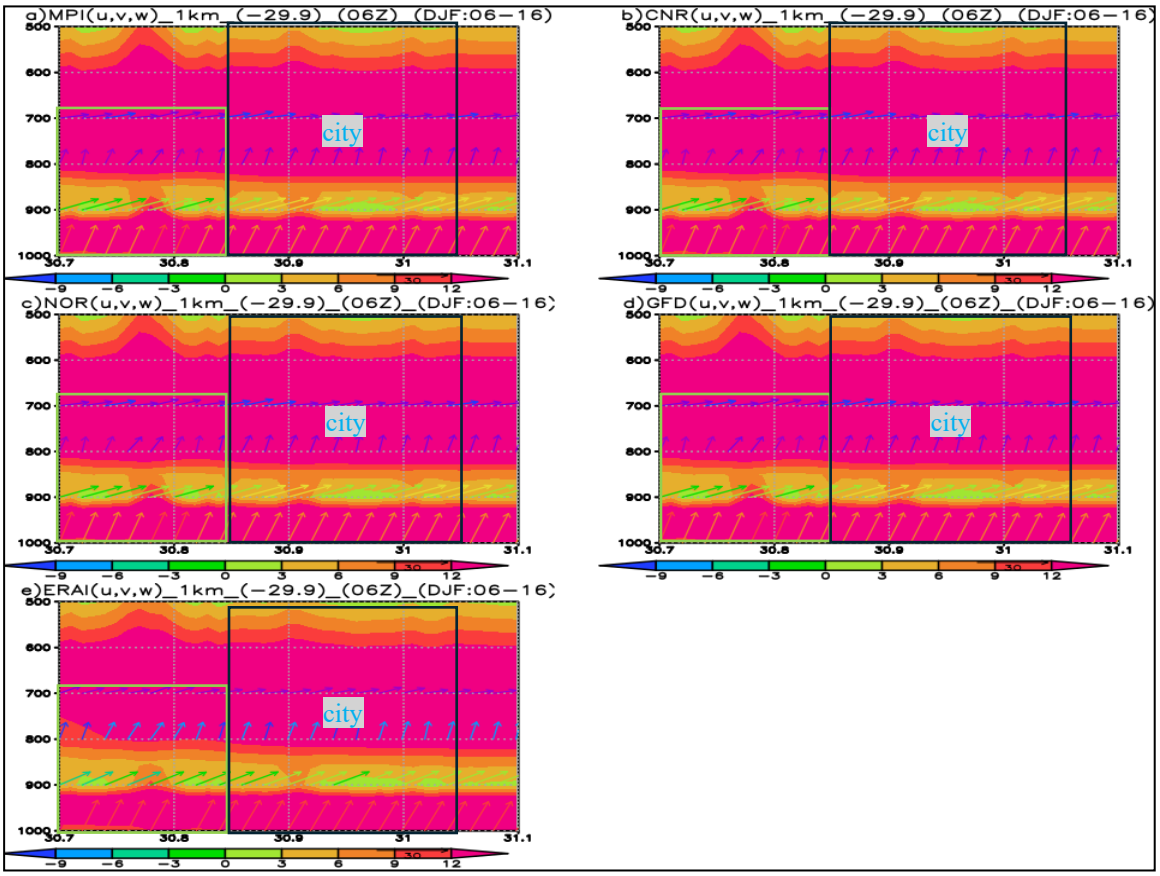

Figure 4.19: The DJF 06h00 UTC CCAM longitudinal cross-section of vertical winds (omega) and horizontal winds (u and v) components from the surface (1000 hPa) to upper-air level (500 hPa) at latitude 29.9°S. The wind speed is measured in meters per second (m/s). At this latitude, the city starts at a longitude of approximately 30.85°E and stretches eastward, ending at around 31.05°E (black box). To the east, the city is bounded by the Indian Ocean, and to the west it is bounded by natural vegetation (green box).

(ii) Wind pattern at 18h00 UTC

At 18h00 UTC (Figure 4.20), there are both similarities and differences when comparing winds at 06h00 UTC (Figure 4.19) and the simulation at 30°S (Figure 4.17). During the 18h00 UTC simulation, the wind patterns at 30°S (Figure 4.18) show a dominance of wind speeds higher than 6 m/s at longitude 30°E. In contrast, at this latitude, there is longitudinal variability in vertical wind. However, at levels above 800 hPa, both vertical and horizontal wind patterns are similar. When comparing winds at this latitude with those at 06h00 UTC (Figure 4.19), there is a slight difference between 900 and 800 hPa. The 06h00 UTC pattern shows a slightly weaker

UNIVERSITEIT VAN PRETORIA
UNIVERSITY OF PRETORIA
YUNIBESITHI YA PRETORIA

vertical wind gradient compared to the 18h00 UTC pattern. This difference is expected due to changes from sea to land breeze, which is characterised by intense winds. At this latitude, distinguishing between land and sea breeze influence on the UHI can be complex.

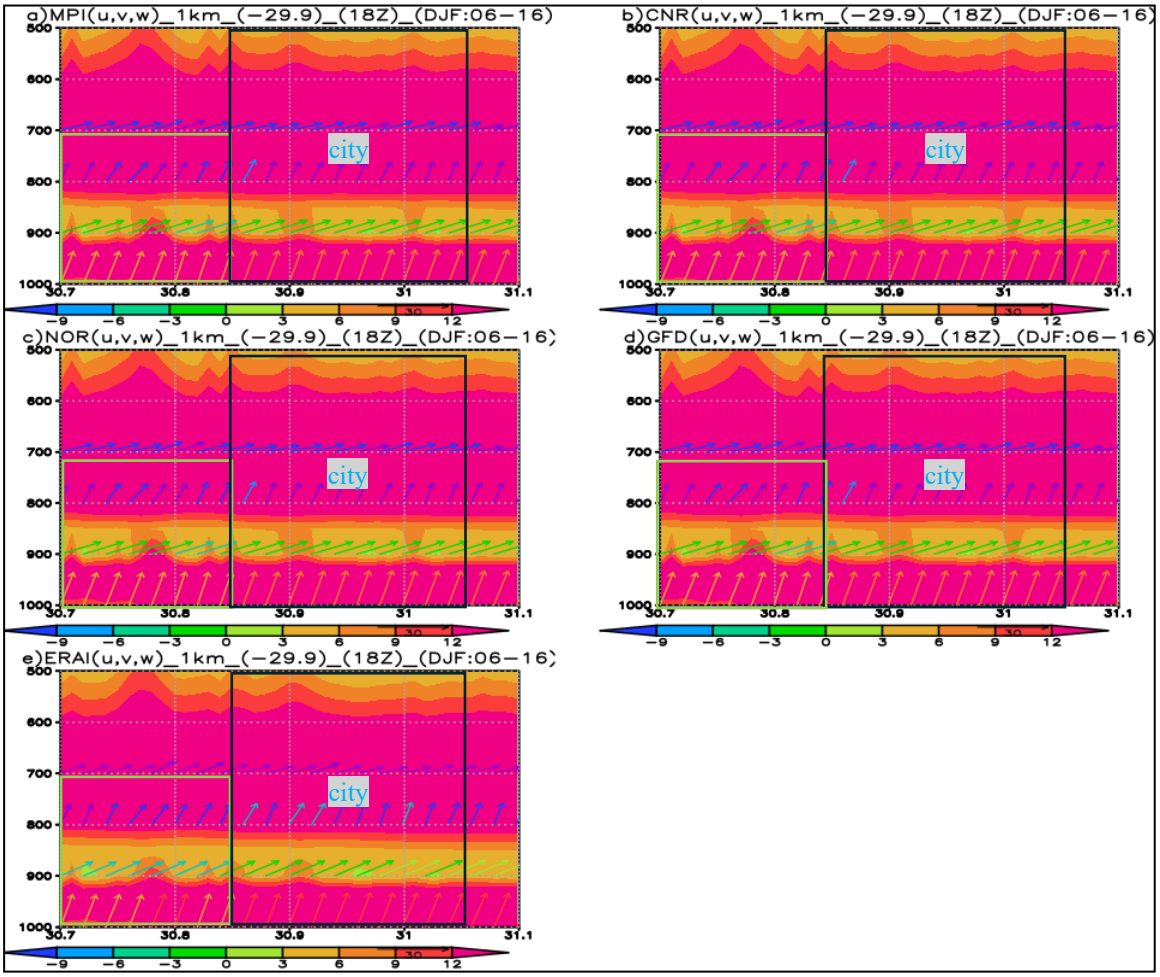

Figure 4.20: The DJF 18h00 UTC CCAM longitudinal cross-section of vertical winds (omega) and horizontal winds (u and v) components from the surface (1000 hPa) to upper-air level (500 hPa) at latitude 29.9°S. The wind speed is measured in meters per second (m/s). At this latitude, the city starts at a longitude of approximately 30.85°E and stretches eastward, ending at around 31.05°E (black box). To the east, the city is bounded by the Indian Ocean, and to the west it is bounded by natural vegetation (green box).

c) Northern latitude: 29.8°S (P3)

(i) Wind pattern at 06h00 UTC

Latitude 29.8°S is the northern point of the city and represents a latitude where both the land breeze and mountain and valley breeze could influence the UHI. At this

UNIVERSITEIT VAN PRETORIA
UNIVERSITY OF PRETORIA
YUNIBESITHI YA PRETORIA

latitude (Figures 4.21 and 4.22), the city begins at approximately 30.81°E and stretches eastward, ending around 31.05°E (black box). To the east, the city is bounded by the Indian Ocean, and to the west, it is bounded by natural vegetation (green box). However, some parts of the domain between 30.9°E and 30.95°E are covered by savannah and grasslands. At this latitude (Figure 4.21), there is no difference in wind patterns from the surface up to 900 hPa. Changes become apparent at levels between 900 and 800 hPa. Although there is a slight similarity with the 06h00 UTC wind patterns at latitude 29.9°S (Figure 4.19), the vertical wind gradient is more pronounced around 30.8°E. This is due to the dominance of non-urban areas at that latitude (see Figure 4.2 for urban distribution). At this longitude (30.8°E), vertical wind speeds increase to values greater than 6 m/s away from urban areas.

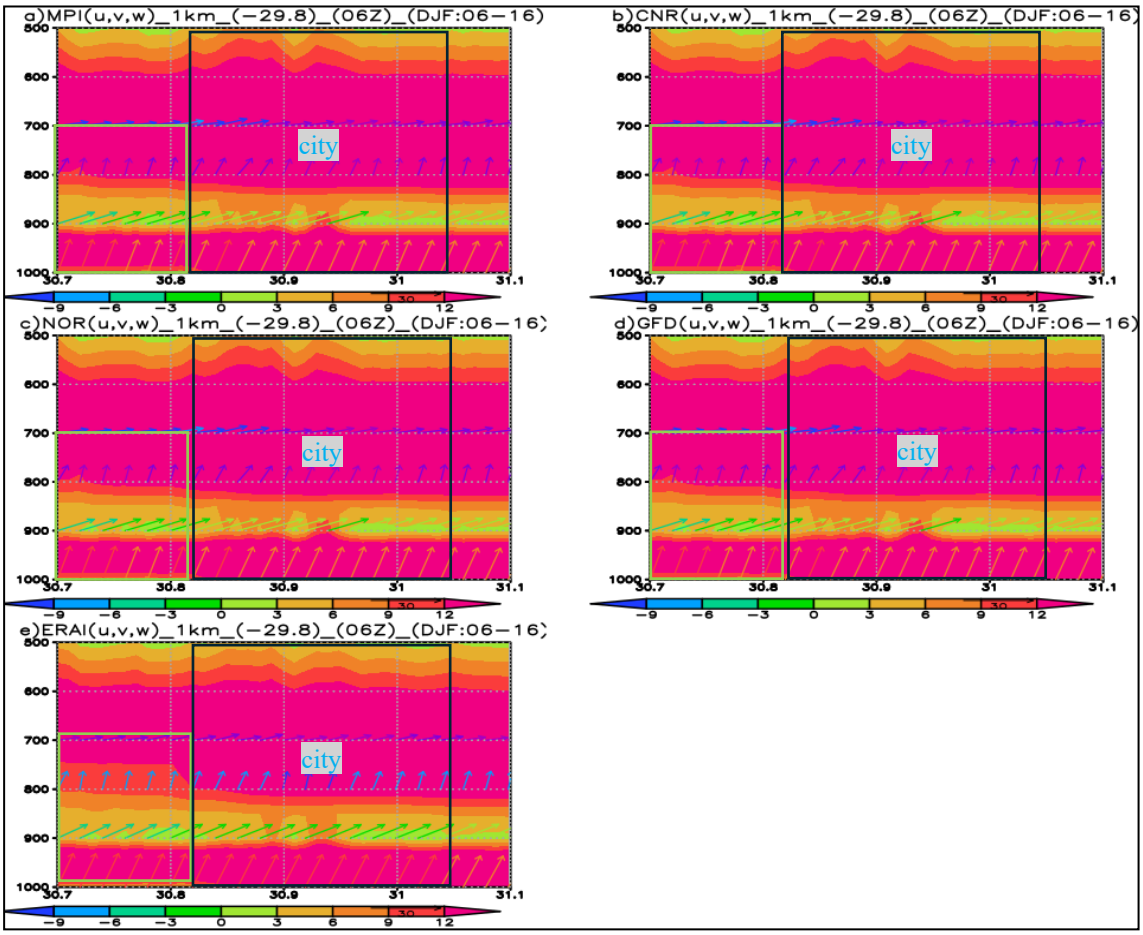

Figure 4.21: The DJF 06h00 UTC CCAM longitudinal cross-section of vertical winds (omega) and horizontal winds (u and v) components from the surface (1000 hPa) to upper-air level (500 hPa) at latitude 29.8°S. The wind speed is measured in meters per second (m/s). At this

UNIVERSITEIT VAN PRETORIA
UNIVERSITY OF PRETORIA
YUNIBESITHI YA PRETORIA

latitude, the city starts at a longitude of approximately 30.95°E and stretches eastward, ending at around 31.05°E (black box). To the east, the city is bounded by the Indian Ocean, and to the west it is bounded by natural vegetation (green box).

However, at levels higher than 800 hPa and up to 500 hPa, a similar pattern is observed, with higher vertical wind speeds up to 600 hPa, and a wave pattern up to 500 hPa. This figure provides clear evidence of the influence of land and sea breeze on the distribution of the UHI.

(ii) Wind pattern at 18h00 UTC

Comparing the wind patterns at 06h00 UTC (Figure 4.21) and 18h00 UTC (Figure 4.22) at this latitude, there are similarities at the surface. However, from 900 to 800 hPa, there are slight differences. The vertical wind gradient is observed at 30.9°E due to the dominance of non-urban areas, leading to an increase in wind speeds (Figure 4.20).

However, these changes are difficult to notice, possibly due to various factors. (i) All the simulations were performed using the same model (CCAM) and identical CABLE settings to produce similar boundary conditions, which yielded similar results. (ii) The boundary conditions applied for each CMIP5 (RCP8.5) scenario were generated at different global climate prediction centres but produced nearly identical results during the current climate. However, the differences became more apparent in the near and far future climates. This suggests that the initial and boundary conditions may not differ significantly. This trend was also observed in some of the current climate simulations in the previous chapters.

At higher levels, vertical wind speeds remain high but are moderated by a wave pattern at 500 hPa. When comparing the 18h00 UTC simulation at this latitude and the 30°S latitude (seen in Figure 4.18) and the previous latitude (29.9°S, see Figure 4.20), the vertical wind profiles from surface to 900 hPa are quite similar. At 900 hPa, the boundary layer at the latitude (30°S) is dominated by more convective activities, which is expected in the city centre at this time of the day. However, at the current latitude (29.8°S), such convective activities are reduced. This may be due to its

UNIVERSITEIT VAN PRETORIA
UNIVERSITY OF PRETORIA
YUNIBESITHI YA PRETORIA

location on the border with non-urban areas and the reduced strength of the land and sea breeze caused by varying land surface types and vegetation contrast.

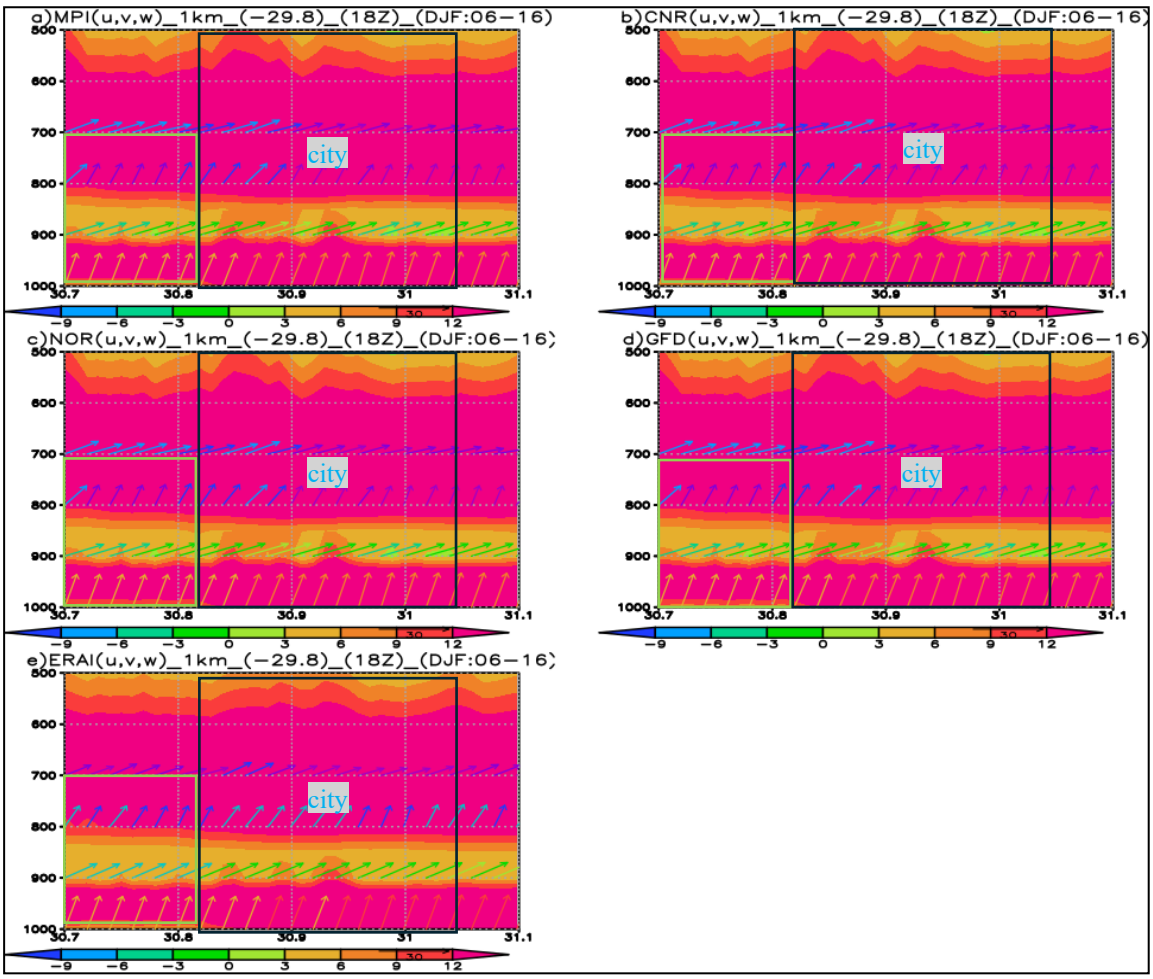

Figure 4.22: The DJF 18h00 UTC CCAM longitudinal cross-section of vertical winds (omega) and horizontal winds (u and v) components from the surface (1000 hPa) to upper-air level (500 hPa) at latitude 29.8°S. The wind speed is measured in meters per second (m/s). At this latitude, the city starts at a longitude of approximately 30.95°E and stretches eastward, ending at around 31.05°E (black box). To the east, the city is bounded by the Indian Ocean, and to the west it is bounded by natural vegetation (green box).

The current longitudinal vertical cross-section over the city of eThekwini analysed indicates that the UHI is influenced by atmospheric circulation at different latitudinal and longitudinal points. The 06h00 UTC winds are weaker due to nighttime land breeze, while the 18h00 UTC winds are stronger due to the dominant sea breeze. At the southern boundary of the urban area, stronger winds are observed at the western

UNIVERSITEIT VAN PRETORIA
UNIVERSITY OF PRETORIA
YUNIBESITHI YA PRETORIA

longitude (30.8°E). Moving northwards, stronger winds are observed at longitude 30.9°E, which agrees with the orientation of the city. From these results it could be deduced that the boundary layer within the city is highly disturbed, resulting in variable winds at this location.

4.4 Discussion

The study examines the interaction between atmospheric circulation patterns and the UHI effect over the city of eThekwini during the current climate (2006-2016). The CCAM was run at a horizontal resolution of 1 km to simulate the development and evolution of the UHI during the summer season. The CCAM was run with downscaling from CMIP5 and ERAI data.

An analysis of the monthly wind speeds was conducted at both Durban and Mt. Edgecombe weather stations (see Figure 4.2). The analysis reveals that during DJF, CMIP5 winds are slightly higher over the urban station (Durban) compared to a non-urban station (Mt. Edgecombe), which agrees (aligns) with observations. At Mt. Edgecombe, CMIP5 and ERAI driven simulations wind speeds are light (~0.9 m/s) and lower than observed. From April to July, CMIP5 and ERAI driven simulations wind speeds are stronger than observed, leading to (indicating) a positive bias. However, from August to November, CMIP5 and ERAI driven simulations winds are lighter than observed. This discrepancy could be due to the location of weather stations, with Durban station situated closer to the coast, and Mt. Edgecombe is located a little further inland.

The diurnal range of observed wind speed was compared between the weather stations in Durban and Mt. Edgecombe during DJF (see Figure 4.3). In Durban wind speeds from 00h00 to 04h00 UTC, and from 18h00 to 00h00 UTC are, on average, less than 3 m/s. Between 04h00 and 180h00 UTC, wind speed varies between 3 and 6 m/s. The wind rose for February (Figure 4.3a and c) indicates that from 04h00 and 18h00 UTC, the dominant winds from the north-north-east to south-south-west.

Given that Durban is 1.76 km from the coast, this suggests the occurrence of sea breeze during these hours. Conversely, from 00h00 to 04h00 UTC and from 18h00 to

UNIVERSITEIT VAN PRETORIA
UNIVERSITY OF PRETORIA
YUNIBESITHI YA PRETORIA

00h00 UTC, the dominant winds shift from the south-west to north-north-east, indicating the presence of land breeze. These observations are consistent with findings by Pokhrel and Lee (2011), although there is some variation in wind speed.

At Mt. Edgecombe station (Figure 4.3b), wind speed is on average 1 m/s from 00h00 to 04h00 UTC and from 18h00 to 00h00 UTC. However, between 04h00 and 18h00 UTC, the average wind speed reaches its highest value of 3.5 m/s, resulting in a diurnal range of 2.5 m/s. The windrose (Figure 4.4b and 4.4d) indicates that, between 04h00 and 18h00 UTC, the dominant winds are from east-north-easterly to south-westerly. Due to the station's location being 4.63 km from the coast, it can also be conclusively said that the station experiences sea breeze. Similarly, from 00h00 to 04h00 UTC and from 18h00 to 00h00 UTC, the wind direction is dominantly south-westerly and north-easterly, and this pattern confirms the presence of land breeze.

Validation statistics were performed for both Durban and Mt. Edgecombe stations respectively (see Table 4.1). During DJF, the bias was negative and, on average, less than 1 m/s, with the RMSE averaging less than 1.3 m/s over Durban for all CMIP5 and ERAI driven simulations. At Mt. Edgecombe, the DJF bias was also negative, but slightly higher than at Durban, with an average of -1.2 m/s for all CMIP5 runs, and even higher for ERAI. The RMSE was also higher at Mt.Edgecombe, with an average of 1.3 m/s. In all other seasons, both bias and RMSE scores were lower at Durban and higher at Mt. Edgecombe. These validation statistics suggest that land and sea breeze are more pronounced at both Durban and Mt. Edgecombe stations. This is due to (i) stations proximity to the coastline, making them more susceptible to sea breezes, and (ii) the urban setting applied when the urban scheme was activated, which assumed that the entire domain to be predominantly urban.

To investigate the relationship between observed winds and the UHI effect, the diurnal range of atmospheric variables was analysed at two stations: one in urban area (Durban) and the other one in non-urban area (Mt. Edgecombe). The analysis of surface temperature in the urban station displays a pattern similar to the observed diurnal range of winds at the same station, as demonstrated across all CMIP5 driven simulations. In contrast, the diurnal range of surface temperature in the non-urban

UNIVERSITEIT VAN PRETORIA
UNIVERSITY OF PRETORIA
YUNIBESITHI YA PRETORIA

station is weaker and lower compared to the urban station, with some variability between CMIP5 runs.

There is no difference in the diurnal range of shortwave and longwave radiation between urban and non-urban areas, as both stations receive similar amounts of radiation. However, there is a difference in net radiation between urban and non-urban areas. In urban areas, diurnal range of net radiation is stronger, and consistent across the CMIP5 driven simulations. In contrast, the diurnal range is weaker in non-urban areas, with slight variability between the CMIP5 driven simulations. This discrepancy may be attributed to the fact that urban surfaces, which are dominated by artificial materials and buildings, trap more heat, and release it less efficiently compared to non-urban areas with natural surfaces.

The boundary layer profile in urban areas differs slightly from the one in non-urban areas. It is stronger and convective in urban areas compared to non-urban areas. However, the boundary layer in urban areas is also more disturbed, leading to a stronger UHI effect compared to non-urban areas.

The diurnal range of sensible heat fluxes is higher in urban areas than in the non-urban areas. This increase is attributed to more artificial material in urban areas, which increases anthropogenic heating and thereby intensifying the UHI. In contrast, the UHI effect is weaker in non-urban areas due to less amount of artificial material, leading to reduced anthropogenic heating.

The distribution of latent heat fluxes is the inverse of that of sensible heat fluxes. In urban areas, there is less evaporation due to reduced natural surfaces, vegetation, and water bodies, thus increasing the UHI effect. Conversely, in non-urban areas, the presence of more vegetation, natural surfaces and water bodies promotes evaporation, thereby reducing the UHI effect.

An analysis of the 24-hour temporal and spatial distribution of the UHI during summer revealed some variability in surface temperatures. Higher values (above 32°C) were simulated during the day, and lower temperatures at night (less than

UNIVERSITEIT VAN PRETORIA
UNIVERSITY OF PRETORIA
YUNIBESITHI YA PRETORIA

26°C). The UHI was clearly visible along the coast. It is important to note that land breeze could mitigate the UHI during the early hours of the day.

There is strong agreement between the distribution of surface temperature and the planetary boundary layer. The planetary boundary layer exhibits higher values at night rather than during the day. Instead of having a strong convective boundary layer during the day and a stable boundary layer at night, the opposite is observed.

During the day, a sea breeze develops over the ocean, bringing in cold air from the ocean towards the land. This process cools the warmer land, resulting in a shallow boundary layer over the land, and a more disturbed boundary layer during the day (Bozonnet *et al.*, 2007). At night, a land breeze develops over the land, resulting in cooler air moving from the land towards the ocean. This causes the land to remain warmer and the ocean cooler, leading to a stronger and higher boundary layer height over the land.

Surface temperatures exceeding 32°C are observed from 07h00 UTC to 14h00 UTC. This period correlates with higher shortwave radiation values, which exceeds 280 W/m^2 from 05h00 UTC to 12h00 UTC. Longwave radiation displays a similar spatial and temporal distribution to shortwave radiation, but with higher values, exceeding 120 W/m^2 from 04h00 UTC to 14h00 UTC. However, both the net radiation and shortwave radiation do not show the spatio-temporal variation of the UHI that is observed in surface temperature.

However, net radiation confirms the presence of the UHI effect, which is clearly depicted during nighttime hours. Although signals of the UHI are present throughout the 24-hour period, it is not evident between 04h00 UTC and 15h00 UTC. The UHI becomes clearly visible from 16h00 UTC to 03h00 UTC the following day. Between 04h00 UTC to 15h00 UTC, higher shortwave radiation leads to an increased net radiation, with values exceeding 240 W/m^2 across the entire domain. The distribution of sensible heat flux exhibits the strongest UHI signal during the day, from 07h00 UTC to 13h00 UTC, with values exceeding 80W/m^2.

UNIVERSITEIT VAN PRETORIA
UNIVERSITY OF PRETORIA
YUNIBESITHI YA PRETORIA

The study also examined the profiles of vertical and horizontal winds at three latitudinal points to assess the changes in wind direction during land and sea breezes. Consequently, the vertical profiles at 06h00 UTC and 18h00 UTC were analysed at latitudes -30°S, 29.9°S and 29.8°S, respectively to study these wind changes.

At the southernmost part of the domain, at -30°S, the vertical profile for the 06h00 UTC simulation shows a slight increase and decrease in in wind speed between 900 and 800 hPa respectively at 30.8°E. At this longitude, the non-urban area is situated to the west and the urban area is located to the east.

Additionally, a strong wind wave is observed between 600 to 500 hPa at this longitude. Consequently, the land breeze leads to a less mixed nocturnal boundary layer. By 18h00 UTC, the boundary layer between 900 and 800 hPa becomes more mixed, and the wind wave between 600 to 500 hPa is present at all longitudinal points. This indicates that sea breezes lead to a strongly mixed boundary layer, which helps disperse the UHI effect, resulting in a less intense UHI (Parker, 2010) over the city of eThekwini.

At the middle latitude of -29.9°S, the vertical profiles at 06h00 UTC and 18h00 UTC differ from those -30°S. At this latitude, vertical winds exhibit wave patterns between 900 and 800 hPa and between 600 and 500 hPa, respectively. This latitude is predominantly urban across all longitudinal points. Consequently, the boundary layer is more unstable and experiences more vertical mixing.

At the northernmost part of the city, at latitude, -29.8°S, the areas at 30.98°E are non-urban, with urban areas to the west and east of this latitude. This results in increased wind speeds in the non-urban areas compared to the urban areas. Although the vertical wind profile is similar at the surface up to 900 hPa, there is strong vertical mixing between 900 and 800 hPa, as well as between 600 to 500 hPa. These observations indicate a clear rural-to-urban contrast and highlight the impact of land and sea breezes.

The analyses indicate that high daytime surface temperature correlates with shortwave, longwave and net radiation, and also both sensible and latent heat fluxes.

UNIVERSITEIT VAN PRETORIA
UNIVERSITY OF PRETORIA
YUNIBESITHI YA PRETORIA

In contrast, nighttime UHI effects are strongly correlated with net radiation. These findings suggest that the UHI is influenced by man-made factors, such as the expansion of the city, replacement of vegetation with concrete, leading to an increase in longwave radiation within cities and also anthropogenic heating. Additionally, the high sensible heat fluxes observed can be attributed to a higher percentage of artificial materials, such as concrete, and anthropogenic heating sources including emissions from vehicles and air-conditioners.

This study has demonstrated that modelling land and sea breeze is complex due to the complexity of the domain, and the study's resolution of 1 km. A study by Pokhrel and Lee, (2011) successfully captured land and sea breezes at a resolution of 2 km. Therefore, achieving an accurate representation of how the UHI interacts with land and sea breezes is more feasible at a sub-kilometer resolution than a kilometer-scale resolution. This is because, in urban-scale modelling, subgrid processes are better captured when parametrisation scheme is switched off. According to the IPCC (2023), improving the performance of the RCM can be achieved by refining the boundary conditions for dynamical downscaling, especially when the regional climate is influenced by large-scale circulations.

Mitigation studies demonstrate that effective urban planning is crucial for mitigating the UHI effect. Buildings should be oriented perpendicular to rivers, to create open spaces and circulation channels that allows for better air flow into the city (Pokhrel and Lee, 2011; Chen and Dipankar, 2022). This approach helps minimise the impacts on urban microclimate and the UHI (Yamamoto, 2005; Nuruzzaman, 2015). Increasing latent heat fluxes and reducing sensible heat fluxes can be achieved by incorporating more water bodies and replacing concrete surfaces with green areas. To further reduce anthropogenic heating in buildings, it is advisable to use highly reflective building materials and to install green and cool roofs (Estrada *et al.*, 2017), which help to reflect heat.

4.5 Summary and conclusion

The CCAM was set up at a horizontal resolution of 1 km over the city of eThekwini to simulate the UHI effect and link it with atmospheric circulations such as land and sea

UNIVERSITEIT VAN PRETORIA
UNIVERSITY OF PRETORIA
YUNIBESITHI YA PRETORIA

breezes. The 1 km downscaling in CCAM was initialised with CMIP5 and ERAI driven simulations. The CMIP5 and ERAI runs were first compared against observed variables, such as maximum, minimum, and surface temperature (Chapter 2) and wind speed at Durban and Mt. Edgecombe weather stations, respectively.

Monthly analysis reveals variability in wind speed between CMIP5 driven simulations and observations. At the two stations, CMIP5 driven simulations are comparable to observations, but vary monthly.

An analysis of the diurnal range in wind speeds was conducted over a 24-hour period at the two stations. At the two stations, wind speed was weaker at night and slightly stronger during the day. This pattern suggests the occurrence of land and sea breezes at the two stations, given their proximity to the coastline. These observations are consistent with previous studies by Pokhrel and Lee (2011), Grachev *et al*., (2018), and Khan *et al.,* (2018). The wind roses support this analysis, showing that during the day, winds are predominantly north-north-easterly to south-south-westerly, indicating the presence of sea breeze originating from the ocean. At night, these winds shift predominantly south-westerly to north-north-easterly, indicating the presence of land breeze.

A comparison of the diurnal temperature range at the two reveal that the surface temperatures are at most 2°C higher at the urban site than non-urban site. This confirms the presence of the UHI during DJF. This temperature difference is also evident in longwave and net radiation, as well as in sensible heat flux.

The temporal and spatial distribution of surface variables was analysed over a 24-hour period for the current climate period to determine the onset and dissipation times of the UHI. The analysis of temperature, longwave radiation, the boundary layer and sensible heat flux effectively reproduced the spatio-temporal distribution of the UHI. However, this was not observed in either shortwave or net radiation.

In the longitudinal cross section of horizontal and vertical winds, the penetration depth of the UHI in both the horizontal and vertical was assessed. Analysis shows winds transition from a land to a sea breeze at around 06h00 UTC, resulting in an

UNIVERSITEIT VAN PRETORIA
UNIVERSITY OF PRETORIA
YUNIBESITHI YA PRETORIA

increase in speed, whereas at 18h00 UTC, a similar pattern is observed, but the winds change direction from sea to land breeze due to changes in diurnal heating.

This study has demonstrated that the UHI over coastal area is influenced by atmospheric circulations including land and sea breezes as well as large-scale circulations.

This study has shown that, despite the extremely high resolution of 1 km, the application of the UCM struggles to capture land and sea breezes, as well as mountain and valley breezes, even though they all fall under the mesoscale atmospheric circulations. This limitation may be attributed to the relatively small number of vertical levels used during model integration (27), and the limited number of vertical levels included during post-processing, which did not cover enough vertical levels in the boundary layer, as it was meant to reduce computational costs. As a result, the model output indicates a boundary layer height averaging only 800 m in summer, leading to poor simulation of land and sea breezes and their impact on UHI evolution. This issue has been confirmed in the IPCC (2023) report, which states that improving boundary layer representation enhances the performance of the RCM, particularly in regions where the climate is influenced by large scale atmospheric circulations.

This study recommends that: (i) increasing air flow through enhanced ventilation in cities could help reduce the UHI effect, and (ii) designing structures parallel to prevailing air flow from the ocean could help maintain the land and sea breezes effects, which may further reduce the UHI.

UNIVERSITEIT VAN PRETORIA
UNIVERSITY OF PRETORIA
YUNIBESITHI YA PRETORIA

Postface

In this chapter, CCAM runs with CMIP5 and ERAI driven simulations from the current climate (2005/6–2016) were analysed to evaluate how atmospheric circulations influence the variability of the eThekwini heat island. The analysis of diurnal wind cycles and wind roses at the two stations revealed the presence of land and sea breezes. However, winds were weaker at the non-urban station compared to the urban station.

Monthly wind speed exhibited some seasonal variability, with weaker wind speed at the non-urban station than the urban station. This difference indicates the influence of land and sea breeze at a coastal station. The bias and RMSE at the two stations reflected this pattern, with a less negative bias at the urban station and a positive bias at the non-urban station.

Analysis of diurnal range at the urban and non-urban stations revealed a more pronounced UHI effect at the urban station compared to non-urban station. This was evident in surface temperature, longwave radiation, and sensible heat flux. The 24 hours spatial and temporal analysis of the UHI clearly showed its onset and cessation. The surface temperature indicated that the UHI began to develop in the late afternoon (after 14h00 UTC) and dissipated around (03h00 UTC), which was also reflected in net radiation (difference between shortwave and longwave radiation).

The latitudinal penetration of land and sea breezes into the interior of the domain varied with longitude and the distribution of the city. At a longitude of 30.9°E, where the city dominates most of the domain, the UHI penetrated up to 29.8°S. This chapter demonstrates that the UHI is influenced by the land and sea breeze.

UNIVERSITEIT VAN PRETORIA
UNIVERSITY OF PRETORIA
YUNIBESITHI YA PRETORIA

CHAPTER 5:

Summary, conclusions, and recommendations

5.1 Summary

In this study, the Conformal Cubic Atmospheric Model (CCAM) was employed to simulate the current climate and the future occurrence of the urban heat island (UHI) over the city of eThekwini, in Kwazulu-Natal. The simulations were performed at a high resolution with a 1 km grid length, covering an area of 200 km x 200 km centered over eThekwini Metropolitan Municipality. A stretched grid factor of 0.019 was applied to achieve the highest resolution possible in the middle of the domain. The Urban Canopy Model (UCM) called ATEB (Masson, 2000; Thatcher and Hurley, 2012; Luhar *et al.*, 2014; Garuma, 2018) was applied to provide the measured city boundary conditions, as well as topography and bathymetry datasets. The model was run continuously in a seamless manner, over a period of one decade (10 years) for three selected decades. The data was averaged into seasonal intervals namely, December to February (DJF), March to May (MAM), June to August (JJA) and September to November (SON), with particular attention given to the DJF season. All model outputs were analysed using UTC time (Greenwich meridian) and adjusted by +02 hours for South African Standard Time (SAST).

For the analysis described in the second chapter, the CCAM was initialised with the CCAM-ERAI driven simulations *(Dee et al.,* 2011; Balsamo *et al.,* 2015), whereas for the analysis described in the third and fourth chapters, the CCAM was initialized with the CMIP5, RCP8.5 driven simulations (Riahi *et al.*, 2011; van Vuuren *et al.*, 2011; Taylor *et al.*, 2012; Yan *et al.*, 2013; Thevakaran *et al.*, 2016) and compared with the CCAM-ERAI driven simulations output. The results of these experiments are summarised in section 5.1.1 through 5.1.3.

5.1.1 Simulation of eThekwini heat islands in South Africa

In this chapter (Chapter 2), CCAM simulations were conducted for the period from December 2005 to December 2016. Firstly, temperature output from CCAM was compared to observed temperature from SAWS stations at 24-hour intervals and also

UNIVERSITEIT VAN PRETORIA
UNIVERSITY OF PRETORIA
YUNIBESITHI YA PRETORIA

on a monthly time scale. Statistical analysis was performed using WMO methods as described by Gordon and Shaykewich, (2000). The comparisons demonstrated good agreement between model and observed data for daily, monthly, and averaged maximum and minimum temperatures. This result indicates that CCAM simulated observed monthly temperatures accurately, leading to high correlations between the model simulations and observations. However, monthly average errors between an urban and a non-urban station varied across the year, with comparable errors during DJF and large errors from April to August.

The diurnal range between the model and observed temperature shows a time lag. In summer, a stronger diurnal range was observed, with a temperature range averaging 4°C; this is the season when the city experiences the UHI. Spring followed, with an average diurnal range of about 5°C. In winter, the diurnal range was weaker, with a range close to 8°C due to enormous differences between maximum and minimum temperature. During autumn and spring, diurnal range was intermediate between the range observed in summer and winter. In autumn, the diurnal range was close to 6°C for the model and 8°C for the observations. In spring, diurnal range averaged 5°C, and the cycle was almost similar to that observed in summer.

Comparisons were also made between the CCAM and MODIS-LST data to assess whether CCAM could reproduce seasonal variations of the UHI over the city of eThekwini. It was found that the model accurately simulated the nighttime temperature distribution and the UHI effect. In summer, CCAM reproduced the distribution of the MODIS depiction of the UHI, with a correlation coefficient of 0.9. This correlation decreased during autumn (0.88), and winter (less than 0.7), but slightly increased during spring (0.62).

An analysis of CCAM simulations for variables such as maximum, minimum, and surface temperatures, radiation (both outgoing longwave and shortwave), heat fluxes (sensible and latent), and boundary layer profiles was conducted on a seasonal time scale. The UHI was well simulated during summer. During transitional seasons, such as autumn, the UHI weakened, and developed again in spring. In winter, the UHI diminished, and was well captured by CCAM. This could be due to the reduced amount

UNIVERSITEIT VAN PRETORIA
UNIVERSITY OF PRETORIA
YUNIBESITHI YA PRETORIA

of both shortwave and longwave radiation over the southern hemisphere during winter.

The UHI effect was well depicted in surface and minimum temperatures, but not in maximum temperature, since the UHI is a night-time phenomenon and is influenced by the resultant longwave radiation. It was also accurately represented in longwave and net radiation, but not in shortwave radiation. The net upward radiation is lower within the city because artificial materials and buildings trap more radiation than is released (Lipson *et al.*, 2017, 2018).

The UHI effect is observed in highly urbanised areas within the city of eThekwini, characterised by less vegetation, more artificial materials such as concrete and asphalt, and high energy demands for heating (Pokhrel and Lee, 2011; Ramamurthy *et al.*, 2014; Estrada *et al.*, 2017). In contrast, the UHI diminishes away from the city centre, where the environment is predominantly rural, with higher vegetation and fewer artificial materials.

The diurnal range of variables including temperature, boundary layer height, longwave and shortwave radiation, and sensible and latent heat fluxes was also analysed. In summer, the diurnal range of temperature was stronger, with a smaller variation between maximum and minimum values. This could be due to increased warming seen in minimum temperature resulting from anthropogenic heating.

During winter, the diurnal range of temperature weakened, as the UHI effect diminished. Similar patterns of strengthening and weakening were also observed in longwave radiation and boundary layer profile. However, the diurnal range in shortwave radiation was weaker and exhibited higher values.

The overall assessment of the UHI indicates the presence of the summer night-time phenomenon (Chen *et al.*, 2014; Gubler *et al.*, 2021; Chen and Dipankar, 2022) over the city of eThekwini. This effect is due to higher urbanisation, characterised by increased artificial structures and higher energy demands for heating and air-conditioning (Lipson *et al.*, 2018; Spinoni *et al.*, 2021).

UNIVERSITEIT VAN PRETORIA
UNIVERSITY OF PRETORIA
YUNIBESITHI YA PRETORIA

The UHI effect is due to man-made factors including city expansion, increased anthropogenic heating, and reduced net upward radiation within the city. Additionally, the city's proximity from the Indian ocean may weaken the UHI due to atmospheric circulations between the land and ocean, such as land and sea breezes (Lee and Shun, 2003; Parker, 2010; Pokhrel and Lee, 2011; Grachev *et al.*, 2018).

In the next section, changes in the UHI due to climate change forcing (CMIP5, RCP8.5) parameters are analysed. This analysis covers the current, near-future, and far-future climate periods.

5.1.2 The current and future projections of eThekwini heat islands

In this section (Chapter 3), CCAM was run at a resolution of 1 km over eThekwini for the climate periods 2005/6-2016, 2039/40-2050 and 2089/90-2099, respectively. During the period 2005/6-2016; CCAM simulations using ERAI and CMIP5 driven simulations (CNR8.5, GFD8.5, MPI8.5 and NOR8.5) (Riahi *et al.*, 2011; Taylor *et al.*, 2012; Yan *et al.*, 2013; Thevakaran *et al.*, 2016) were compared with both MODIS and SAWS observations.

During the current climate observed maximum and minimum temperatures were compared to CMIP5 and ERAI driven simulations. Monthly observed maximum temperatures were comparable to both CMIP5 and ERAI driven simulations at the two stations. However, the observed minimum temperature was on average 2°C less than both simulations at the Durban station, and in contrast, was on average 2°C higher than both simulations at Mt. Edgecombe station.

Additionally, diurnal range showed similar patterns between CMIP5, and ERAI driven simulations during summer. However, during all other seasons, ERAI run exhibited maximum temperatures that were nearly 2-4°C higher than CMIP5 driven simulations. Research has attributed these variations to differences in input data, assimilation models, parametrisation schemes and both spatial and temporal resolution of the downscaling output, leading to reanalysis data performing differently in different parts of the globe. However, ERAI has best overall

UNIVERSITEIT VAN PRETORIA
UNIVERSITY OF PRETORIA
YUNIBESITHI YA PRETORIA

performance when simulating both daily and monthly air temperature as well as rainfall (Smith *et al.*, 2001; Lan *et al.*, 2023).

The diurnal range during summer was stronger than in all other seasons, with an average range of 8°C. When comparing nighttime minimum temperature from MODIS, ERAI and the four CMIP5 driven simulations, MPI8.5 is in broad agreement with MODIS, particularly over the land. Both MPI8.5 and MODIS temperatures were at most 2°C higher than those from GFD8.5, CNR8.5, NOR8.5 and ERAI. However, GFD8.5, CNR8.5, NOR8.5 and ERAI driven simulations were highly comparable to each other.

The spatial correlations indicated that all the CMIP5 driven simulations were almost 90% correlated to both ERAI driven simulations and MODIS during summer. These correlations scores decreased during autumn, spring, and winter, respectively. When comparing ERAI and CMIP5 driven simulations against station observations, the observed maximum temperatures were slightly higher than model-simulated temperature during summer, autumn, and winter, but slightly lower during spring. Additionally, ERAI and CMIP5 driven simulations exhibited lower temperatures than CMIP5 runs during all other seasons.

During the period 2039/40-2050, only CMIP5 driven simulations were compared, because ERAI driven simulations are available only during the current climate period. The modelled maximum and minimum and surface temperatures from CMIP5 are comparable and show that temperatures are at most 2°C higher over the city compared to the surrounding areas. Further inland away from the UHI, surface temperature is reduced by nearly 6°C. Among the CMIP5 driven simulations, GFD8.5 run exhibits a larger spatial distribution of the UHI compared to all other CMIP5 driven simulations.

However, the diurnal ranges are comparable between summer and spring, with temperatures higher during these seasons compared to autumn and winter. These temperatures are nearly 2°C higher during the near-future climate (2039/40-2050) than during the current climate (2005/6-2015/6) period. This finding also applies to

UNIVERSITEIT VAN PRETORIA
UNIVERSITY OF PRETORIA
YUNIBESITHI YA PRETORIA

other variables, including longwave, shortwave, and net radiation, boundary layer, and heat fluxes (latent and sensible), respectively.

Comparisons were also made for the far-future climate period 2089/90-2099. Both maximum, minimum and surface temperatures are comparable between CMIP5 driven simulations. However, GFD8.5 shows a greater spatial increase in UHI area compared to all other CMIP5 driven simulations. The UHI simulated with GFD8.5 exhibits temperatures that are at most 2°C higher in areas away from the UHI. Notably, the UHI simulated by NOR8.5 is weaker compared to all other runs. Diurnal range seen in temperature differs among the CMIP5 driven simulations during all seasons, with summer showing most variation. As expected, GFD8.5 shows higher diurnal range, while NOR8.5 shows the least spread. These results indicate that the intensity of the UHI simulated has increased by at most 2°C during the near-future climate and an additional 2°C during the far-future climate period. This suggests that increased anthropogenic heating and emissions in CMIP5 driven simulations contributed to an increase in the intensity of the UHI.

5.1.3 The influence of atmospheric circulation on the variability of eThekwini heat islands

In Chapter 4, CCAM output for both ERAI and CMIP5 driven simulations that were analysed in Chapter 2 and Chapter 3 were further analysed. However, more attention was paid to wind patterns as they impact atmospheric circulations that influence the UHI. Additionally, the diurnal range of meteorological variables was examined over a 24-hour period during summer, contrasting an urban area and a non-urban area to assess how urbanisation influences the UHI effect. It was observed that the UHI is more pronounced when local-scale systems dominate, as opposed to periods dominated by large-scale systems (Khan *et al.*, 2018). The reason for this is because large-scale systems, such as cold frontal systems, coastal lows, cause the dispersion of the UHI due to strong winds associated with them (Bozonnet *et al.*, 2007). For the UHI to be dominant, there should be a weak onshore flow during the day, leading to higher temperatures over the land (Lengoasa, 1988). Additionally, at night, there should be a weak offshore flow over the land for the UHI to persist (Case, 2002).

UNIVERSITEIT VAN PRETORIA
UNIVERSITY OF PRETORIA
YUNIBESITHI YA PRETORIA

An analysis of station-observed wind speed and direction confirms the presence of the land and sea breezes. The minimum wind speed during land breeze was averaged around 2 m/s, while the maximum wind speed during sea breeze was 7 m/s, respectively. These observations align closely with the findings by Khan et al., (2018). During land breeze, the observed wind direction was from the north (0^{o}). In contrast, during sea breeze, the observed wind direction varied from 45 to 200°, shifting from north-easterlies to south-westerlies.

The diurnal range of meteorological variables (i.e. temperature, net radiation, and boundary layer) was examined at two stations: one located in urban (Durban) and another in non-urban (Mt. Edgecombe) areas. The comparisons revealed that temperatures are higher within the city, leading to a stronger diurnal range compared to the station away from the city. The diurnal range of net radiation also showed a strong variation within the city. This is an indication of the city's composition, which includes concrete surfaces and buildings, with fewer water bodies, leading to higher absorption of radiation, an enhanced UHI effect.

Cities also exhibit an unstable (disturbed) boundary layer profile compared to rural areas. The spatial distribution of surface temperature shows higher values throughout the domain during the day, with clear UHI signals at night. This pattern is also evident in net radiation. However, the boundary layer profile is highly disturbed in the afternoon and a bit stable during the night, which results in the formation of the UHI (Bozonnet *et al.*, 2007).

A vertical cross-section of winds was performed and analysed over three different latitudes, 30°S, 29.9°S and 29.8°S, respectively. The analysis was conducted for early hours (04-06 h00 UTC) for land breeze and late hours (16-20h00 UTC) for sea breeze. At the southern-most point (30°S), the vertical wind speed from the surface up to 900 hPa shows: (i) an increase in wind speed away from the city and a decrease when approaching the city during the early hours, and (ii) a spatial distribution of reduced winds which increases during late hours due to sea breeze that occurred during the day.

UNIVERSITEIT VAN PRETORIA
UNIVERSITY OF PRETORIA
YUNIBESITHI YA PRETORIA

At the northernmost parts of the city (29.8°S), there is a longitudinal increase in reduced vertical winds from the surface up to 900 hPa during early hours. However, this effect is confined to a longitude of 30.9°E during the late hours. This analysis indicates the presence of both the land and sea breezes over the eThekwini domain. Such atmospheric circulation patterns could contribute to the reduction or diminishing UHI over the coastal city of eThekwini.

5.2 Conclusions

In this study, the occurrence of the UHI over the city of eThekwini was analysed across three climate periods. During the current climate, the UHI was observed during summer, using the MODIS nighttime LST, and it was well simulated with the CCAM-ERAI driven downscaling. This simulation indicates that ERAI can effectively validate the model and identify UHI-dominated areas.

During the current climate period, CCAM simulations were conducted using ERAI and CMIP5 driven downscaling, specifically with CNR8.5, GFD8.5 MPI8.5 and NOR8.5 scenarios. The results from CMIP5 driven simulations were comparable to those from CCAM-ERAI driven simulations. In summer, the UHI was stronger in urban areas due to higher levels of urbanisation, reduced vegetation within the city, increased artificial materials, and greater anthropogenic heating requirements, such as the usage of air-conditioning. Conversely, the UHI was reduced or absent in rural areas during summer. In winter, the UHI diminished both within the city and in the surrounding areas.

For the near-future climate, CCAM simulations using the CNR8.5, GFD8.5, MPI8.5 and NOR8.5 scenarios show comparable results. The UHI intensity in summer has increased by at most 2°C compared to the current climate period. In the far-future climate, simulations with the same scenarios also yield comparable results, with the UHI intensifying by nearly 4°C in summer compared to both the current and near-future climate periods.

The investigation of the influence of the atmospheric circulations on the UHI variability show that land and sea breezes were pronounced at the two stations over

UNIVERSITEIT VAN PRETORIA
UNIVERSITY OF PRETORIA
YUNIBESITHI YA PRETORIA

the city of eThekwini. Additionally, the area also experienced katabatic winds. The study also shows that the area experiences large-scale atmospheric circulation.

This study clearly observed the UHI, evident in the diurnal range of meteorological variables such as surface and minimum temperatures, net radiation, and heat fluxes. The findings indicate that the UHI is influenced by human-made factors such as urbanisation, and an increase in anthropogenic heating within cities. The combination of these factors leads to the reduction of net upward radiation within the city and an increase in radiation in surrounding areas. Increased urbanisation, including more buildings, transportation, and artificial surfaces results in increased longwave radiation being stored within the city than is emitted. This absorption reduces latent heat fluxes and evaporation while increasing sensible heat fluxes, thereby enhancing the UHI.

This study has revealed that the global atmospheric model, the CCAM when applied at a high resolution of 1 km can be applied to any city to study urban climate. When the model is coupled to a land surface model, the ATEB, which incorporates realistically high resolution landcover and measured urban parameters, and the urban scheme activated can realistically simulate seasonal dynamical changes in landcover. This system setup is able to reproduce the realistic orientation of the city, as well as the surface variables such as minimum and surface temperatures, longwave radiation and sensible heat fluxes. This makes the system able to reproduce the MODIS observed surface UHI over the city of eThekwini as influenced by human induced factors. The system also provides an opportunity to simulate the future occurrence of the UHI until the end of the 21st century.

The system can be used to assess the role of atmospheric circulations such as land and sea breezes over the city of eThekwini and any city globally. However, due to their complexity, at this resolution, the system struggles to reproduce the observed winds in coastal areas, this could be due to the fact that the city is closer to the coast and is affected by both land and sea breezes and also large-scale circulations.

Additionally, at high resolution of 1 km, the UCM application struggles to capture land and sea breeze although they all fall under the mesoscale atmospheric circulations.

UNIVERSITEIT VAN PRETORIA
UNIVERSITY OF PRETORIA
YUNIBESITHI YA PRETORIA

This could have been influenced by smaller number of vertical levels applied (27) in model simulation, and post-processing which did not cover enough boundary layer height, as it was meant to reduce computational costs, thus leading to poor simulation of land and sea breeze and how it has impacted the UHI evolution. In the IPCC (2023) report it has been stated that improving the boundary layer conditions improves the performance of the RCM in regions where the climate is influenced by large-scale atmospheric circulations.

In this study, the three research problems were addressed as the three objectives were responded to successfully. The first research question: can the CCAM, together with the ATEB model with updated land surface features realistically simulate the development of the UHI over eThekwini under present-day climate. For this research question, CCAM was setup at 1 km to run with both ERAI and four CMIP5 (RCP8.5) downscaled data for the period 2006-2016. The study found that the UHI was realistically simulated as seen in minimum and surface temperatures as well as longwave radiation and sensible heat flux. This was also evident in verification statistics against a station in urban areas (Durban) and a station away from urban areas (Mt. Edgecombe). The temperature was on average 2°C higher in urban areas when compared to non-urban areas.

From the second research question: If so, how realistically can the CCAM and the ATEB, with updated land surface features, project the future attributes of the UHI over eThekwini will change under climate change? For this research question, CCAM was setup at 1 km, initialised with four CMIP5 (RCP8.5) downscaled data for the period 2039-2050 and 2089-2099. The study found that the UHI will continue to exist during the near-future climate as well as the far-future climate period. During the near-future climate, temperature will increase by at most 1°C and by nearly 2°C during the far-future climate. The UHI will also intensify, and this could be attributed to global climate change.

From the third research question: considering the updated land surface features within the ATEB model, how realistic can the CCAM simulate the dynamical interactions of the UHI and land and sea breezes and katabatic winds? To address this

UNIVERSITEIT VAN PRETORIA
UNIVERSITY OF PRETORIA
YUNIBESITHI YA PRETORIA

research question, the CCAM runs with ERAI and CMIP 5 (RCP8.5) at 1 km resolution over eThekwini. The results show that CCAM struggled to reproduce winds at both stations although all the model runs almost agree with each other. The simulations were however able to reproduce the 24 hours diurnal range of the UHI as observed in minimum and surface temperatures, longwave radiation, sensible heat and boundary layer. However, the latitudinal and longitudinal and vertical penetration of the winds over the simulation domain yielded complex results. It was shown that winds reduced speed when entering urban areas and increased speed when moving across non-urban areas due to the influence of surface roughness which blocks air flow in highly constructed areas and accelerates in free spaces between buildings (Pokhrel and Lee, 2011).

In concluding this study, considering that global climate change has an impact on the UHI in cities, failure to mitigate and adapt to the impacts of UHI, there will be an intensification of the UHI, resulting in more mortalities to a wide range of population age group, i.e. people less than 65 years and children older than 5 years. The spread of cities will result in an increase in sensible heat flux making it more unbearable to live in cities. Additionally, the spread of the city will lead to higher demand for cooling, making energy use more expensive.

5.3 Limitations of numerical weather and climate prediction models

Both numerical weather and climate prediction models are subjected to errors, especially when predicting near surface atmospheric variables such as temperatures and wind (speed and direction). Limitations of numerical models include data accuracy, uncertainty of meteorological prediction and emissions data, as well as the underestimation of surface sensible heat flux at night during stable boundary conditions (Pokhrel and Lee, 2011). These errors are due to three factors: (i) model's initialisation (ii) model formulations, which includes both physics and dynamics, and (iii) model's inability to resolve subgrid scale phenomena which are close to the model grid points. Details of the model's errors have also been outlined in Maisha (2014).

UNIVERSITEIT VAN PRETORIA
UNIVERSITY OF PRETORIA
YUNIBESITHI YA PRETORIA

This study has shown that there are limitations in reproducing winds at this resolution as the domain is located over the coastal region and the winds could be influenced by synoptic scale circulations, making it difficult to simulate and analyse at 1 km resolution.

5.4 Recommendations

From this study, various techniques could be used to mitigate the impacts of the UHI, they include:

- Reducing artificial materials such as pavements, asphalt, and increasing vegetation, water bodies and parks. This will lead to the reduction of sensible heat fluxes and increase in latent heat fluxes and reduces the surface temperatures.
- Revegetation within the city. By increasing vegetation within the city, vegetation will assist in absorbing carbon components from the city atmosphere, thereby reducing higher temperatures, and the UHI.
- Improving the transport system. By introducing solar battery cars, anthropogenic emissions will be reduced, therefore reducing anthropogenic heating and the UHI.
- Introduce higher reflective materials and paints for the buildings, green roof, and streets. This will reflect heat, reduce the absorption of solar radiation and result in higher albedo and therefore reduce higher temperatures and the UHI.
- Increase height to width ratio between buildings and streets, this will increase the canyons within the city leading to more undisturbed circulations within the city.
- Apply urban planning, reduce building heights to reduce friction and improve air circulations within the city. Also construct buildings perpendicular to the ocean, allow for free spaces to channel air into the city and reduce the impacts of the UHI.

Additionally, since urban climate modelling is performed using high resolution urban climate models, some few recommendations are as follows:

UNIVERSITEIT VAN PRETORIA
UNIVERSITY OF PRETORIA
YUNIBESITHI YA PRETORIA

- The global models used in the downscaling process can benefit more from global analysis from high quality surface observations, but these are very scarce over the African continent. However, datasets including ERA5 reanalysis have improved in temporal and spatial resolution as well as increased data availability.

- The downscaling process can also benefit more from locally and updated generated landcover as well as measured urban parameters.

- Dynamical downscaling is a stepwise process and climate models could benefit more by nesting processes as applied in numerical weather prediction models.

- An increase in surface observation stations in cities can assist in providing key information to enhance our understanding of urban micro-climates and improve urban parametrisation.

The above-mentioned adaptation and mitigation techniques, when properly implemented, can help to improve the UHI effect and help improve city lives. In conclusion, this study has proven that the UHI exists over the city of eThekwini as a result of increased urbanisation, removal of vegetation, and increased anthropogenic heating. The study shows that UHI will likely increase towards the end of the 21st century. If no meaningful mitigation factors are applied, the city will become an uncomfortable place to live, however, land and sea breeze dilutes the UHI, thus providing relief.

Appendix A

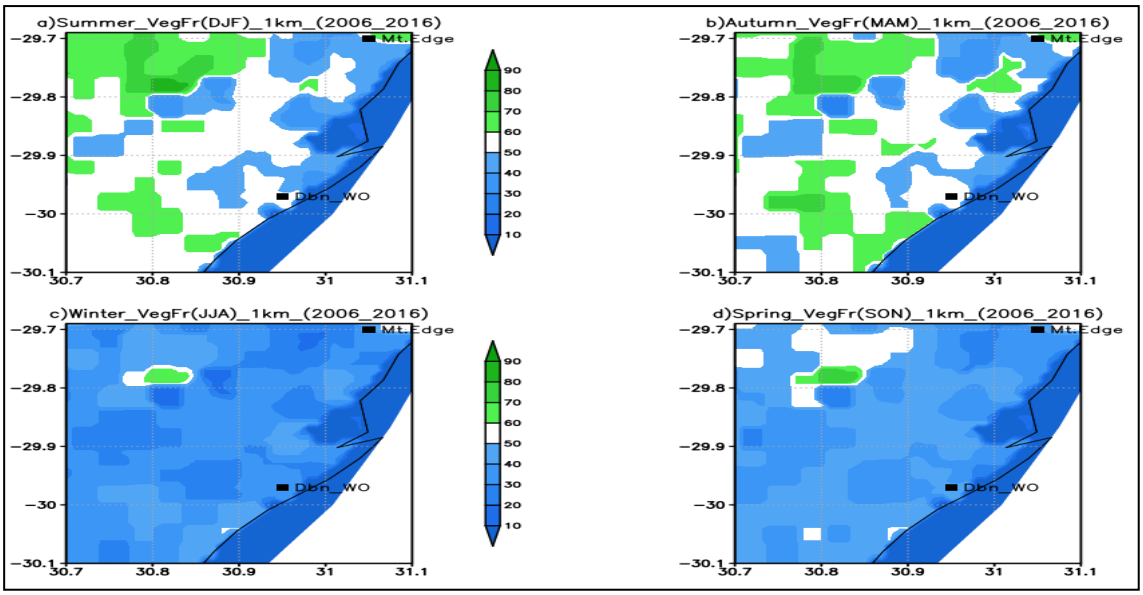

Figure A.1: The updated CCAM-ERAI driven 1 km simulated vegetation fraction over the city of eThekwini for the periods DJF, MAM, JJA and SON, 2005/6 to 2015/16. Both Durban (to the south of the domain, 29.965°S; 30.946°E) and Mt. Edgecombe (to the northeast of the domain, 29.706°S; 31.046°E) stations are plotted.

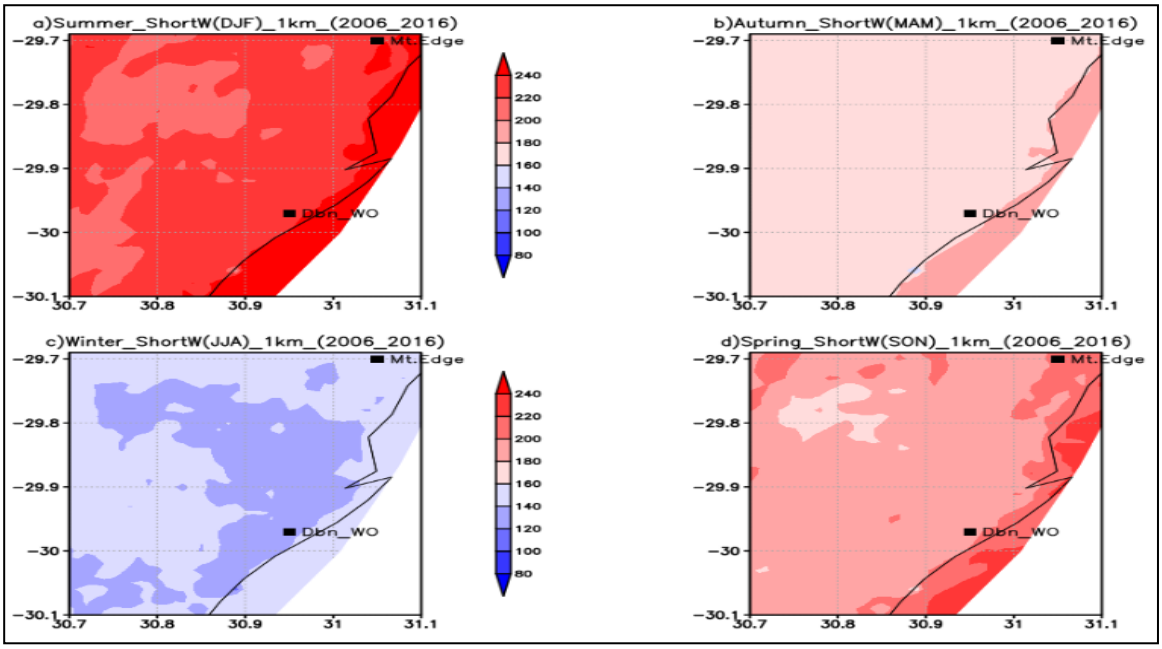

Figure A.2: The updated CCAM-ERAI driven 1 km simulated shortwave radiation over the city of eThekwini for the periods DJF, MAM, JJA and SON, 2005/6 to 2015/16. Both Durban (to the south of the domain, 29.965°S; 30.946°E) and Mt. Edgecombe (to the northeast of the domain, 29.706°S; 31.046°E) stations are plotted.

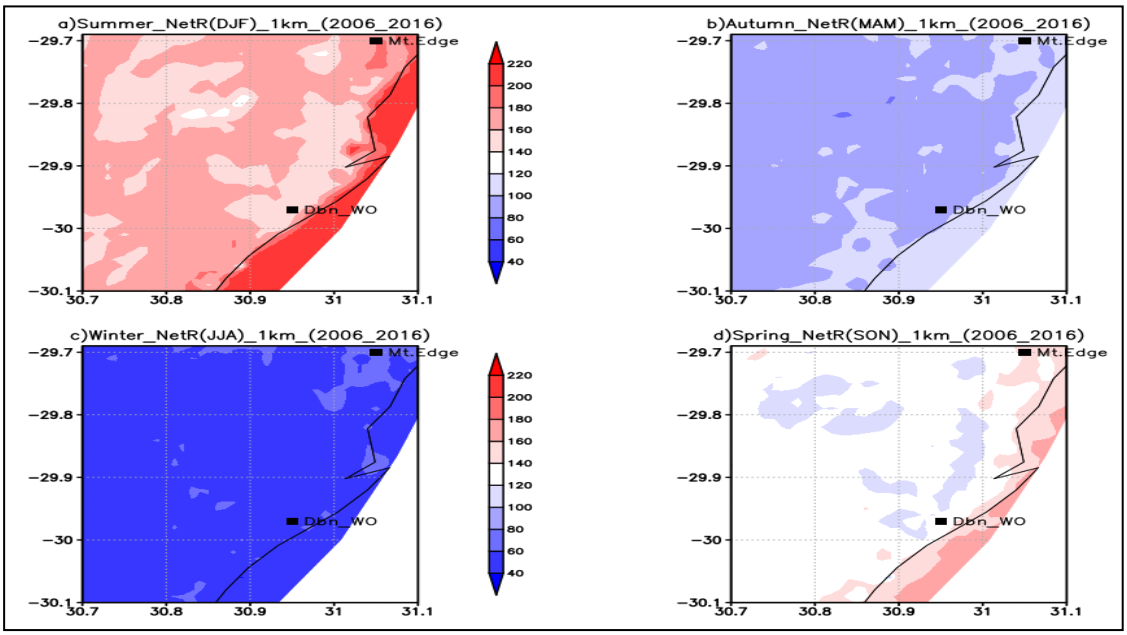

Figure A.3: The updated CCAM-ERAI driven 1 km simulated net radiation over the city of eThekwini for the periods DJF, MAM, JJA and SON, 2005/6 to 2015/16. Both Durban (to the south of the domain, 29.965°S; 30.946°E) and Mt. Edgecombe (to the northeast of the domain, 29.706°S; 31.046°E) stations are plotted.

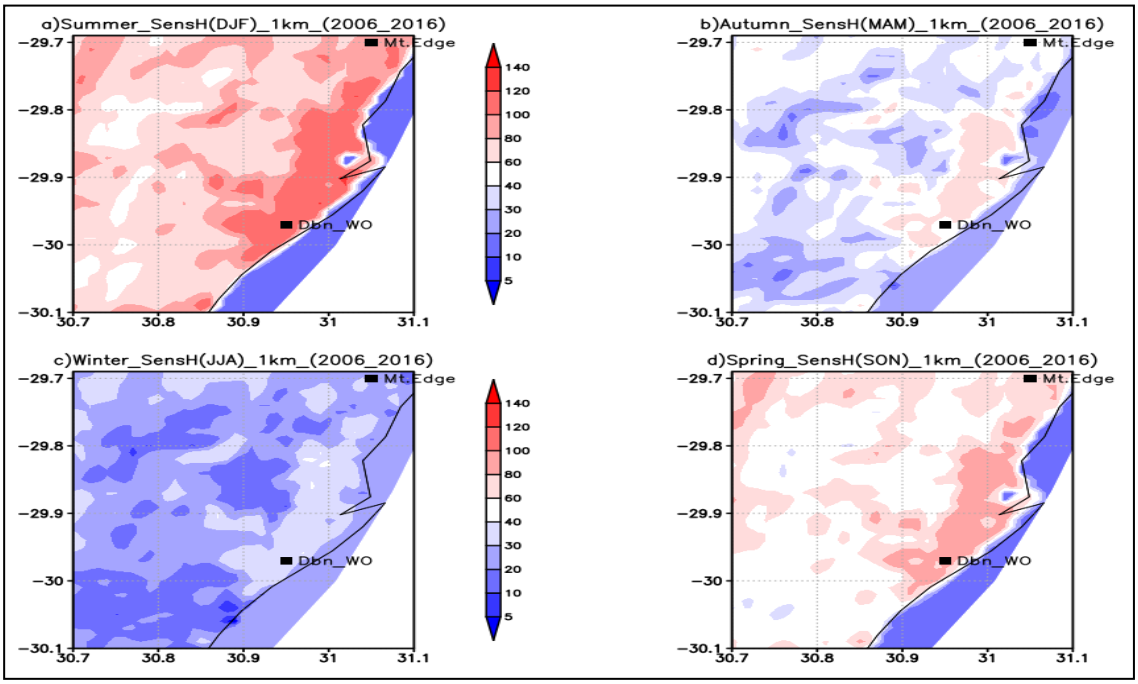

Figure A.4: The updated CCAM-ERAI driven 1 km simulated sensible heat flux over the city of eThekwini for the periods DJF, MAM, JJA and SON, 2005/6 to 2015/16. Both Durban (to the south of the domain, 29.965°S; 30.946°E) and Mt. Edgecombe (to the northeast of the domain, 29.706°S; 31.046°E) stations are plotted.

UNIVERSITEIT VAN PRETORIA
UNIVERSITY OF PRETORIA
YUNIBESITHI YA PRETORIA

Appendix B

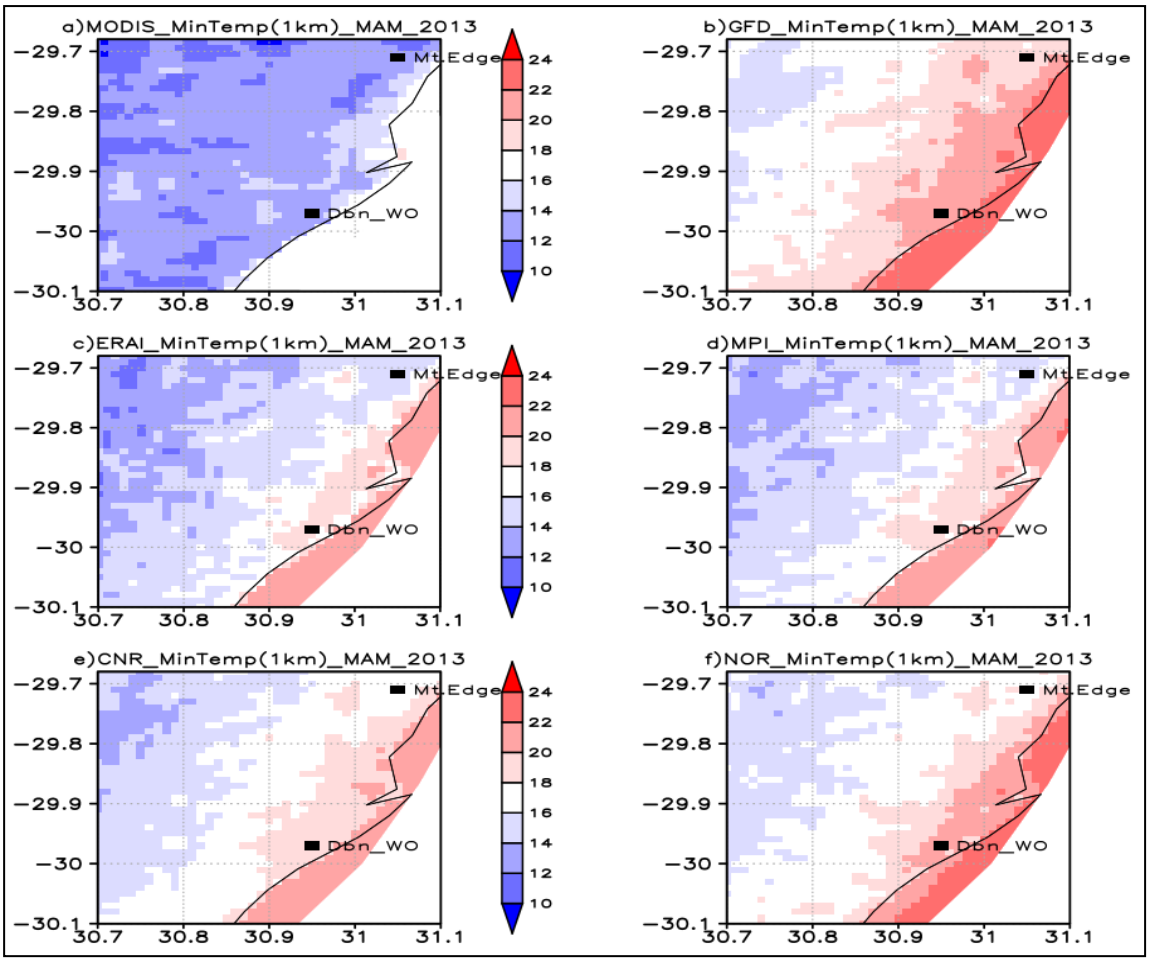

Figure B.1: The CCAM-CMIP5 driven minimum temperature versus MODIS nighttime LST over the City of eThekwini for the period MAM 2012/13. The panel represents MODIS (left-top), GFD8.5 (right-top), ERAI (middle- left), MPI8.5 (middle-right), CNR8.5 (bottom- left) and NOR8.5 (bottom-right). Both Durban (to the south of the domain, 29.965°S; 30.946°E) and Mt. Edgecombe (to the northeast of the domain, 29.706°S; 31.046°E) stations are plotted.

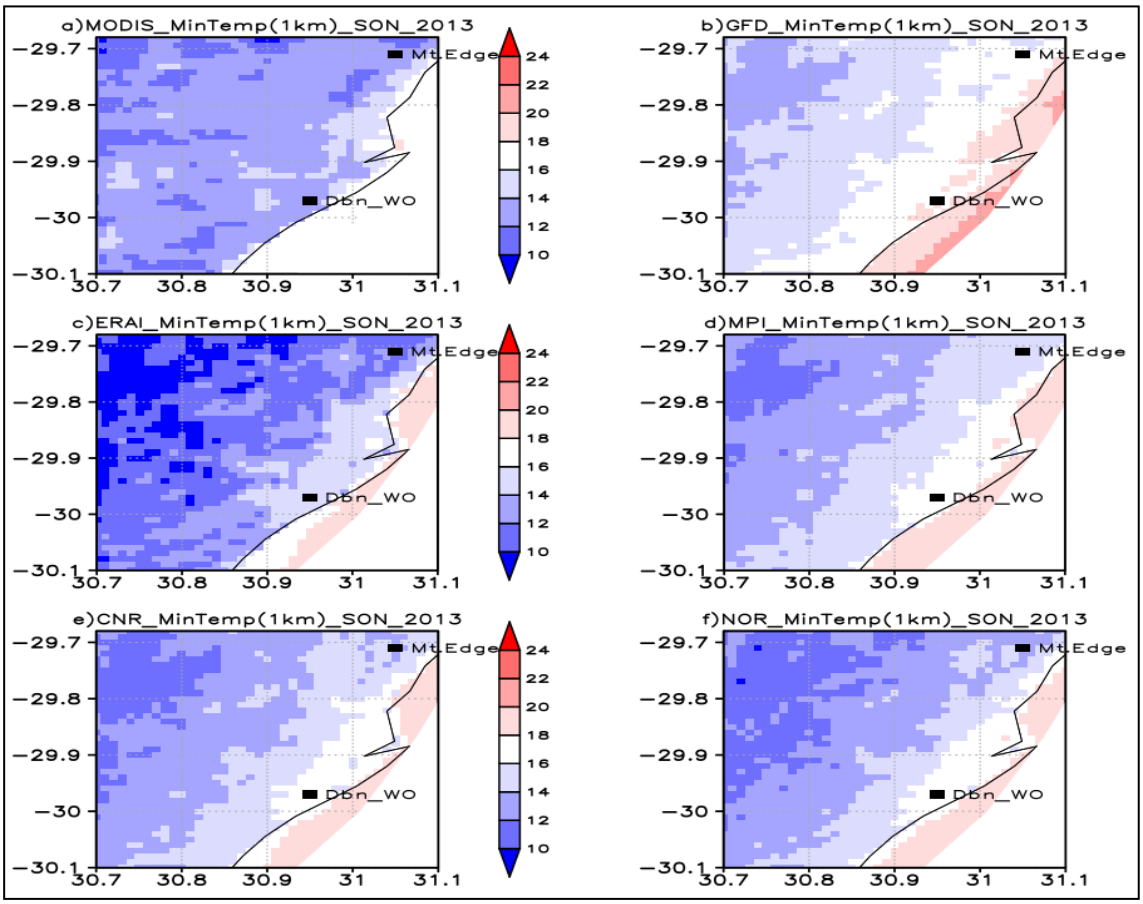

Figure B.2: The CCAM-CMIP5 driven minimum temperature versus MODIS nighttime LST over the city of eThekwini for the period SON 2012/13. The panel represents MODIS (left-top), GFD8.5 (right-top), ERAI (middle- left), MPI8.5 (middle-right), CNR8.5 (bottom- left) and NOR8.5 (bottom-right). Both Durban (to the south of the domain, 29.965°S; 30.946°E) and Mt. Edgecombe (to the northeast of the domain, 29.706°S; 31.046°E) stations are plotted.

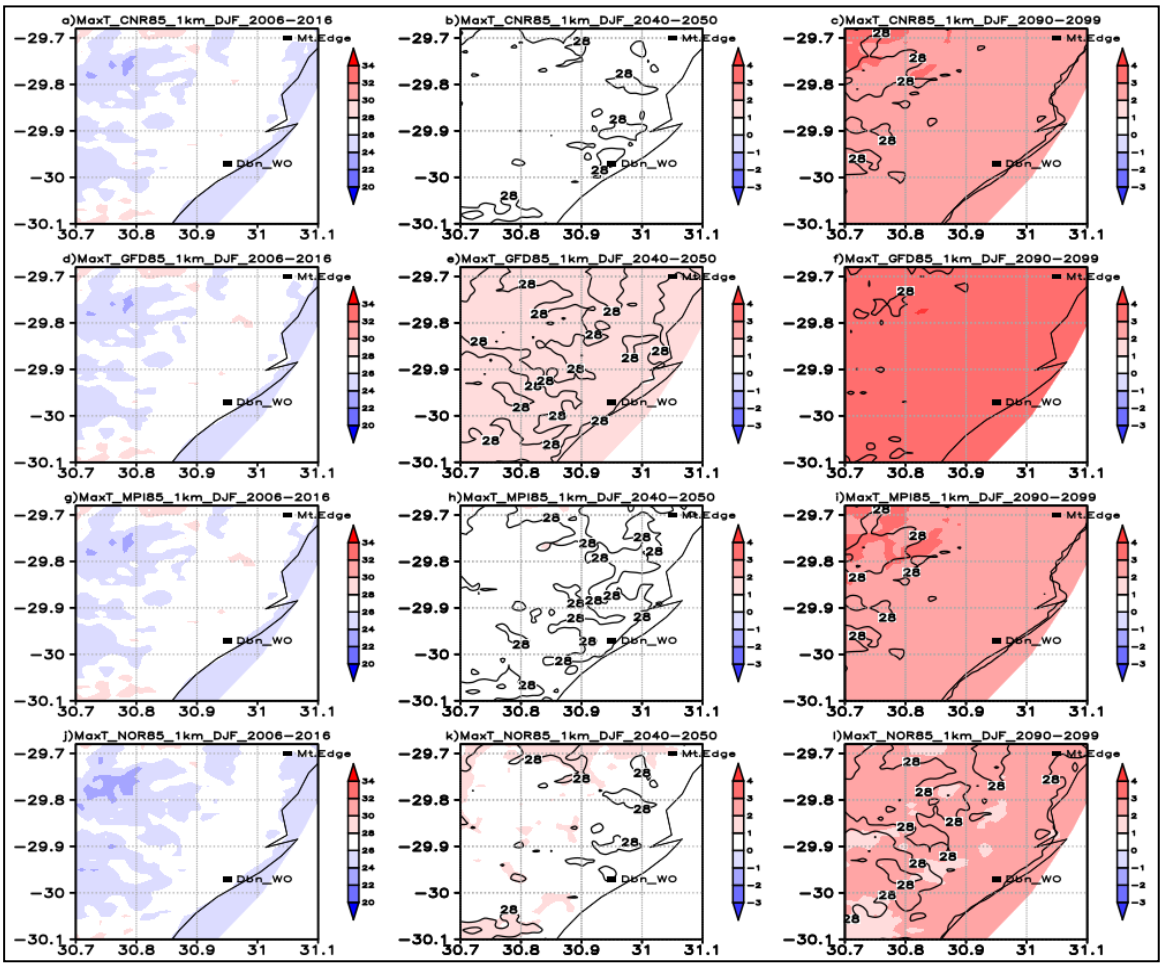

Figure B.3: The CCAM-CMIP5 driven simulation of maximum temperature with four RCP8.5 scenarios for the DJF period (2006-2016) and changes for the period (2040-2050) and (2090-2099) relative to (2006-2016) baseline. Changes from current to the near -future ((2040-2050) minus (2006-2016)) and from current to the far-future ((2090-2099) minus (2006-2016)) are shaded, whereas the near-future (2040-2050 and far-future (2090-2099) maximum temperature are contoured. Both Durban (to the south of the domain, 29.965°S; 30.946°E) and Mt. Edgecombe (to the northeast of the domain, 29.706°S; 31.046°E) stations are plotted.

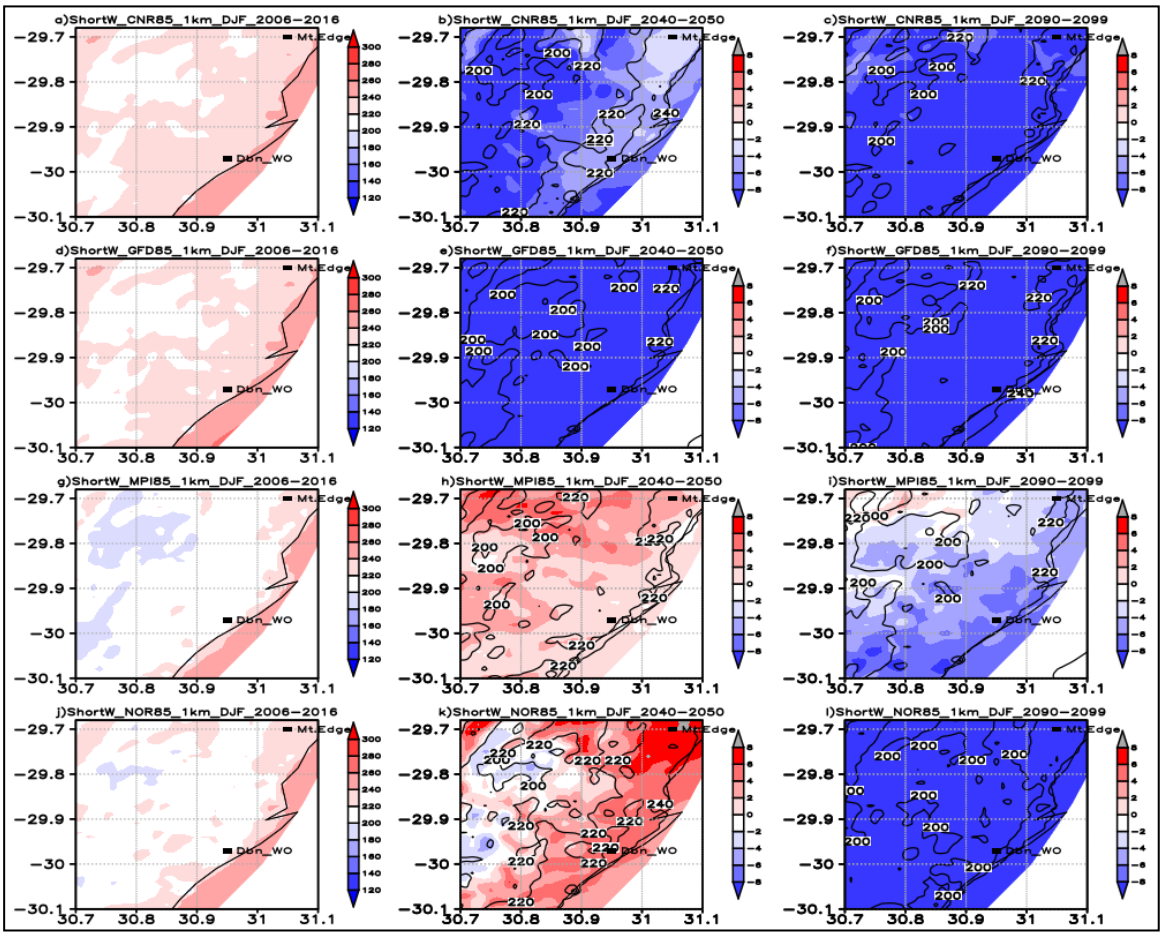

Figure B.4: The CCAM-CMIP5 driven simulation of shortwave radiation with four RCP8.5 scenarios for the DJF period (2006-2016) and changes for the period (2040-2050) and (2090-2099) relative to (2006-2016) baseline. Changes from current to the near -future ((2040-2050) minus (2006-2016)) and from current to the far-future ((2090-2099) minus (2006-2016)) are shaded, whereas the near-future (2040-2050 and far-future (2090-2099) shortwave radiation are contoured. Both Durban (to the south of the domain, 29.965°S; 30.946°E) and Mt. Edgecombe (to the northeast of the domain, 29.706°S; 31.046°E) stations are plotted.

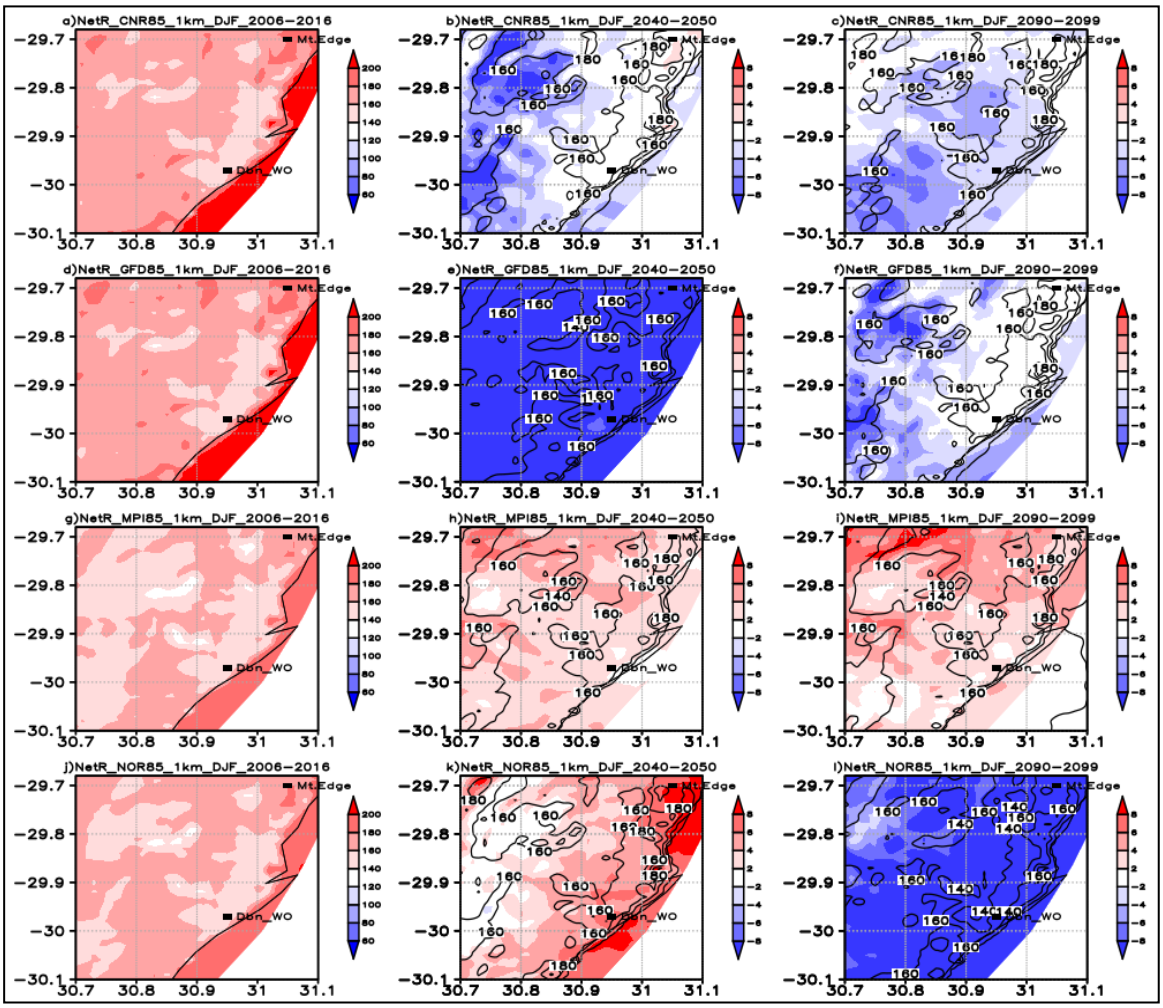

Figure B.5: The CCAM-CMIP5 driven simulation of net radiation (shortwave -longwave) with four RCP8.5 scenarios for the DJF period (2006-2016) and changes for the period (2040-2050) and (2090-2099) relative to (2006-2016) baseline. Changes from current to the near -future ((2040-2050) minus (2006-2016)) and from current to the far-future ((2090-2099) minus (2006-2016)) are shaded, whereas the near-future (2040-2050 and far-future (2090-2099) net radiation are contoured. Both Durban (to the south of the domain, 29.965°S; 30.946°E) and Mt. Edgecombe (to the northeast of the domain, 29.706°S; 31.046°E) stations are plotted.

UNIVERSITEIT VAN PRETORIA
UNIVERSITY OF PRETORIA
YUNIBESITHI YA PRETORIA

Appendix C

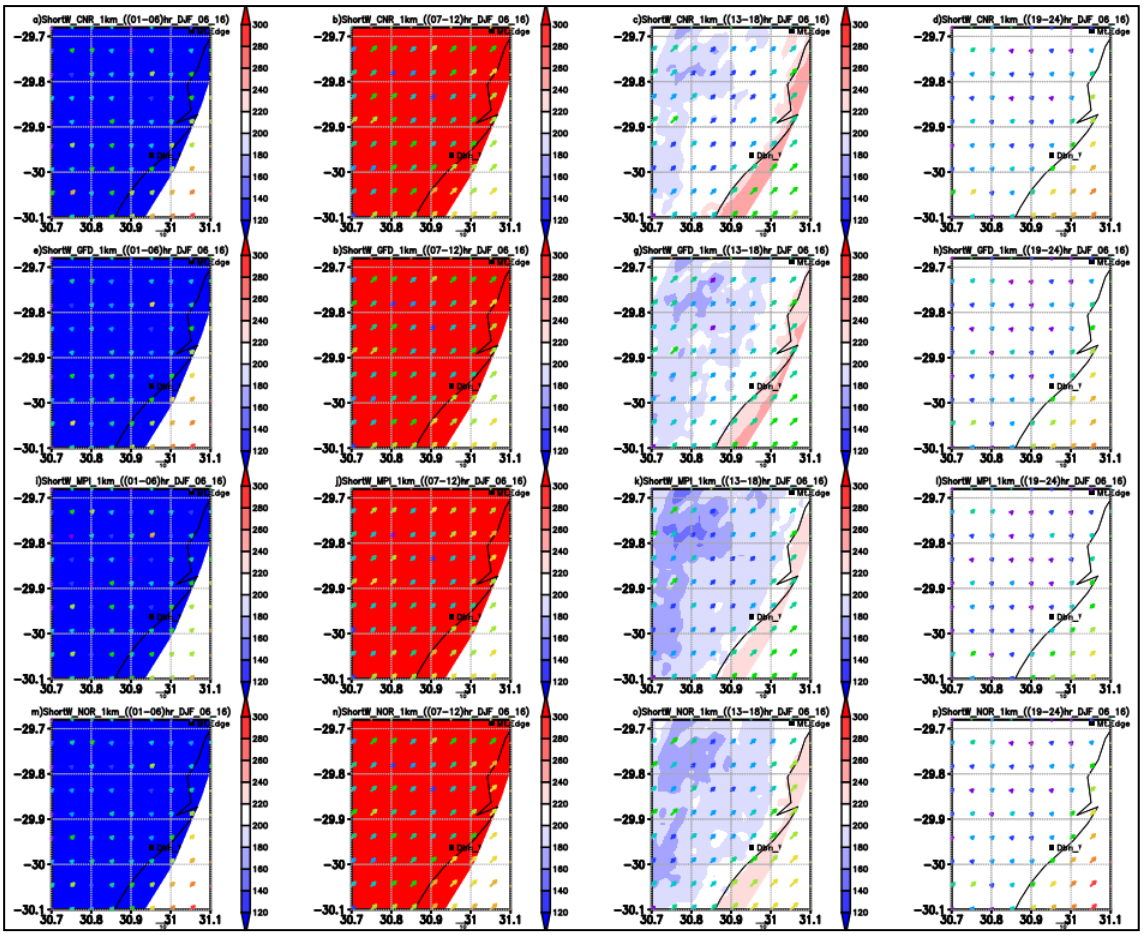

Figure C.1: The spatial and temporal distribution of shortwave radiation versus wind with CMIP5 driven simulations for DJF period 2005/6-2016. Left row (01h00-06h00); second row (07h00-12h00); third row (13h00-18h00); fourth row (19h00-24h00) UTC). First column: CNR8.5 simulations; second column: GFD8.5 simulations; third column: MPI8.5 simulations; fourth column: NOR8.5 simulations. Both Durban (to the south of the domain, 29.965°S; 30.946°E) and Mt. Edgecombe (to the northeast of the domain, 29.706°S; 31.046°E) stations are plotted.

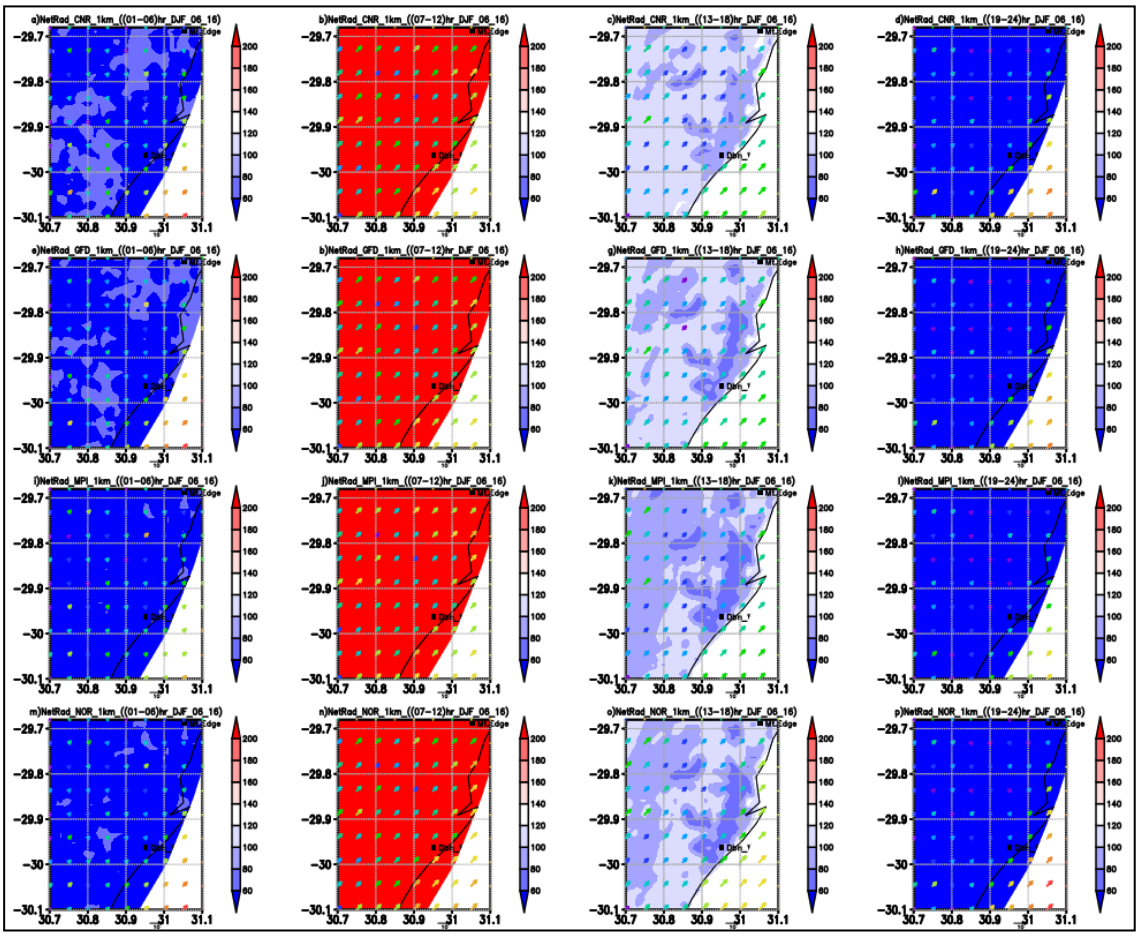

Figure C.2: The spatial and temporal distribution of net radiation versus wind with CMIP5 driven simulations for DJF period 2005/6-2016. Left row (01h00-06h00); second row (07h00-12h00); third row (13h00-18h00); fourth row (19h00-24h00) UTC). First column: CNR8.5 simulations; second column: GFD8.5 simulations; third column: MPI8.5 simulations; fourth column: NOR8.5 simulations. Both Durban (to the south of the domain, 29.965°S; 30.946°E) and Mt. Edgecombe (to the northeast of the domain, 29.706°S; 31.046°E) stations are plotted.

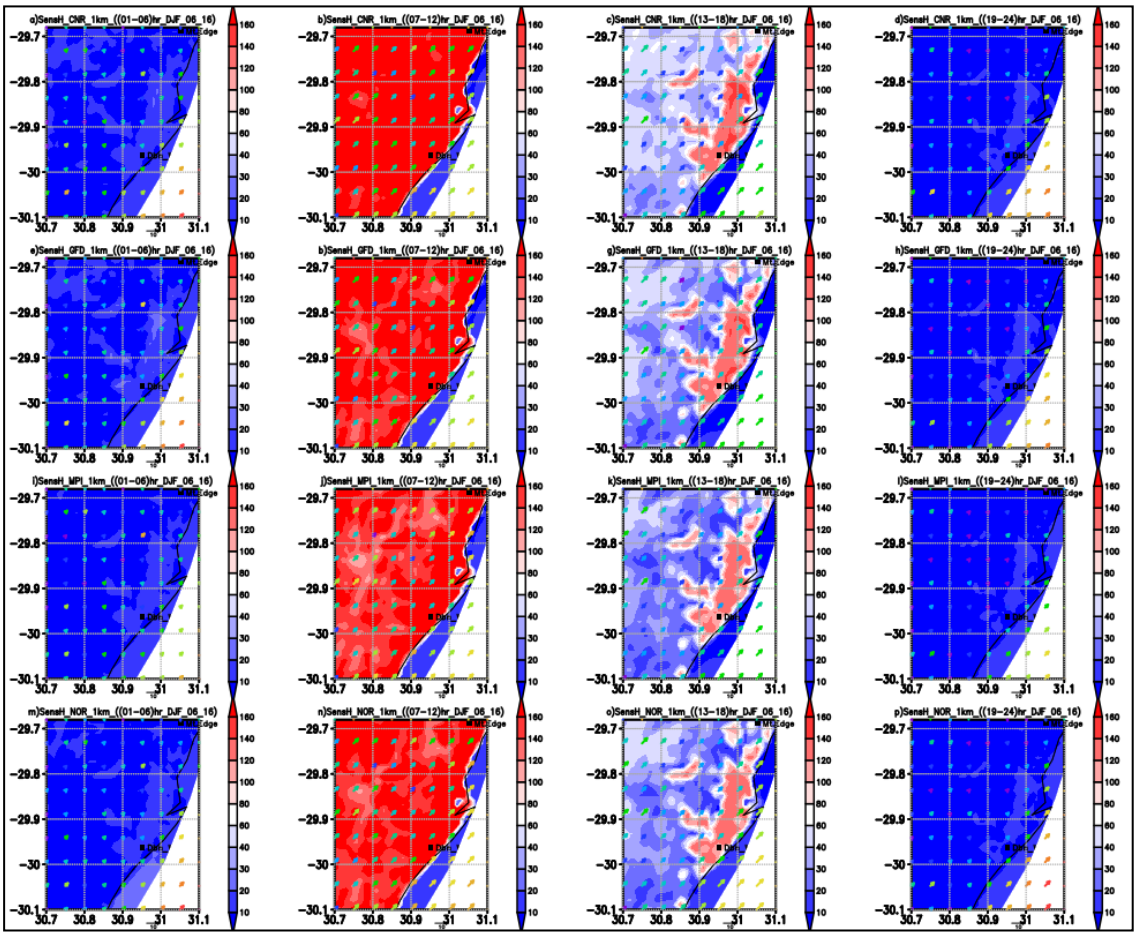

Figure C.3: The spatial and temporal distribution of sensible heat fluxes versus wind with CMIP5 driven simulations for DJF period 2005/6-2016. Left row (01h00-06h00); second row (07h00-12h00); third row (13h00-18h00); fourth row (19h00-24h00) UTC). First column: CNR8.5 simulations; second column: GFD8.5 simulations; third column: MPI8.5 simulations; fourth column: NOR8.5 simulations. Both Durban (to the south of the domain, 29.965°S; 30.946°E) and Mt. Edgecombe (to the northeast of the domain, 29.706°S; 31.046°E) stations are plotted.

UNIVERSITEIT VAN PRETORIA
UNIVERSITY OF PRETORIA
YUNIBESITHI YA PRETORIA

Appendix D

(a) Durban AWS

(b) Durban AWS distance to the east coast=1.76 km

Figure D.1: Location of the South African Weather Service (SAWS) automatic weather stations (AWS), (a) Durban South AWS (29.965°S; 30.946°E) and (b) the distance from Durban station to the east coast (Indian Ocean).

(a) Mt. Edgecombe AWS

(b) Mt. Edgecombe AWS distance to the east coast =4.63 km

Figure D.2: Location of the South African Weather Service (SAWS) automatic weather stations (AWS), (a) Mount Edgecombe (29.706°S; 31.046°E). b) the distance from Mt. Edgecombe station to the east coast (Indian Ocean).

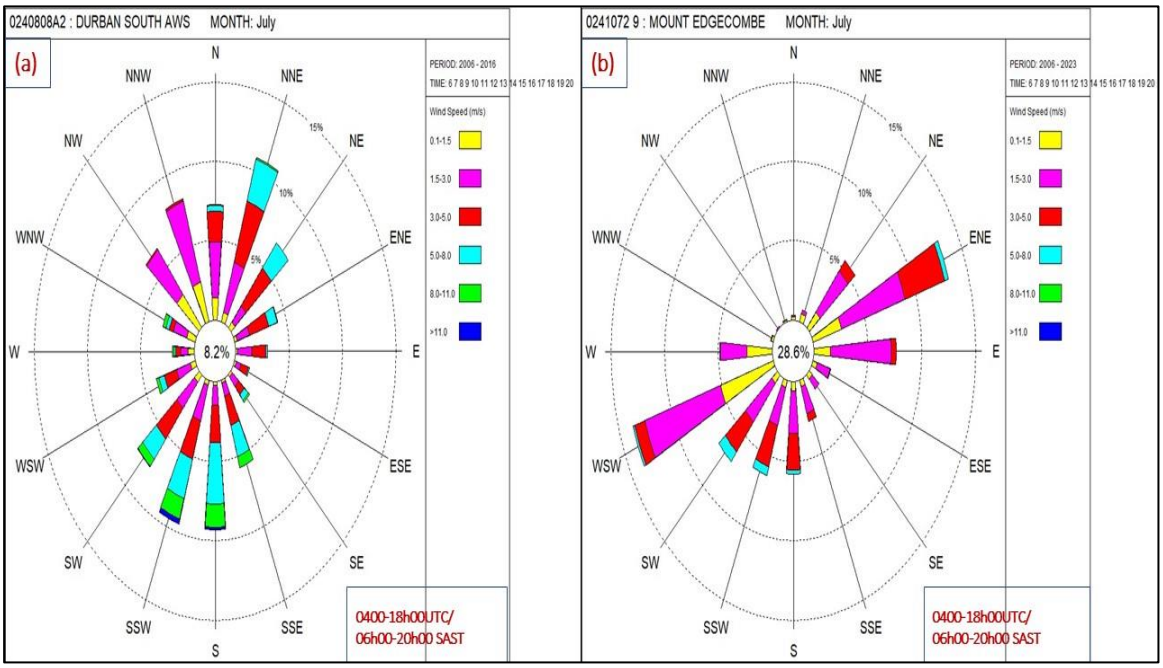

Figure D.3: The wind rose showing diurnal range of winds (speed and direction in metres per seconds (m/s) over (a) Durban and (b) Mt. Edgecombe weather stations during July (representing JJA) period 2006 -2016. The panels represent wind roses between 04h00 and 18h00 UTC (06h00 to 20h00 SAST). The percentage of the wind direction is categorised as 5%, 10%,15%, 20% and 25% respectively, and the average percentage is circled in the middle of each figure.

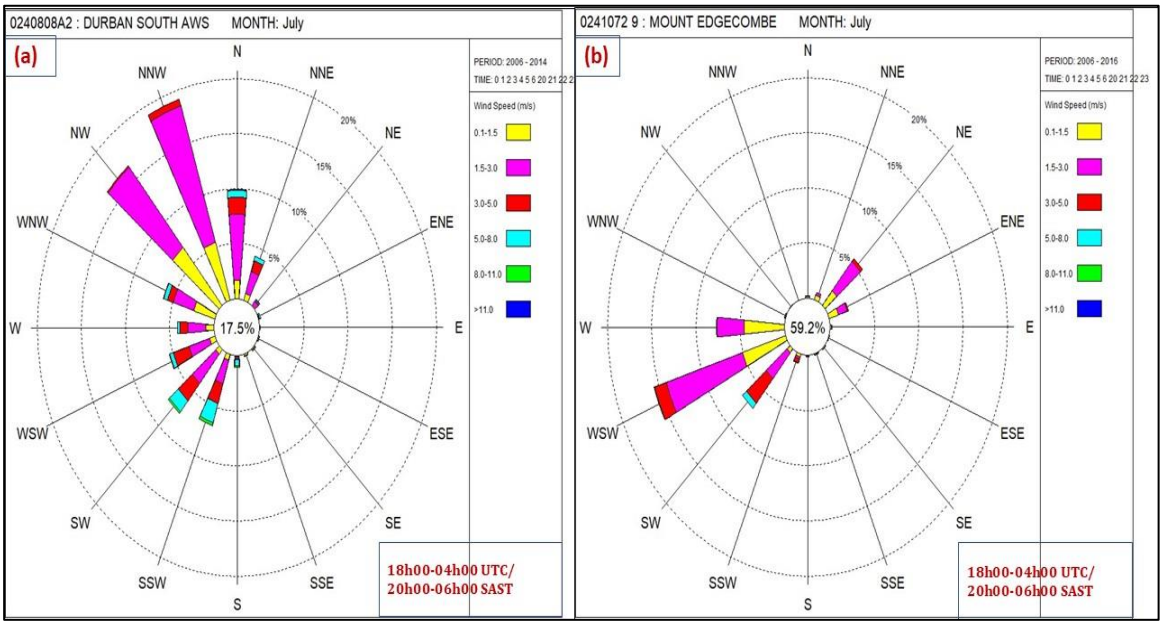

Figure D.4: The wind rose showing diurnal range of winds (speed and direction in metres per seconds (m/s) over (c) Durban and (d) Mt. Edgecombe weather stations during July

UNIVERSITEIT VAN PRETORIA
UNIVERSITY OF PRETORIA
YUNIBESITHI YA PRETORIA

(representing JJA) period 2006 -2016. The panels represent wind roses between 18h00 and 04h00 UTC (20h00 and 06h00 SAST). The percentage of the wind direction is categorised as 5%, 10%,15%, 20% and 25% respectively, and the average percentage is circled in the middle of each figure.

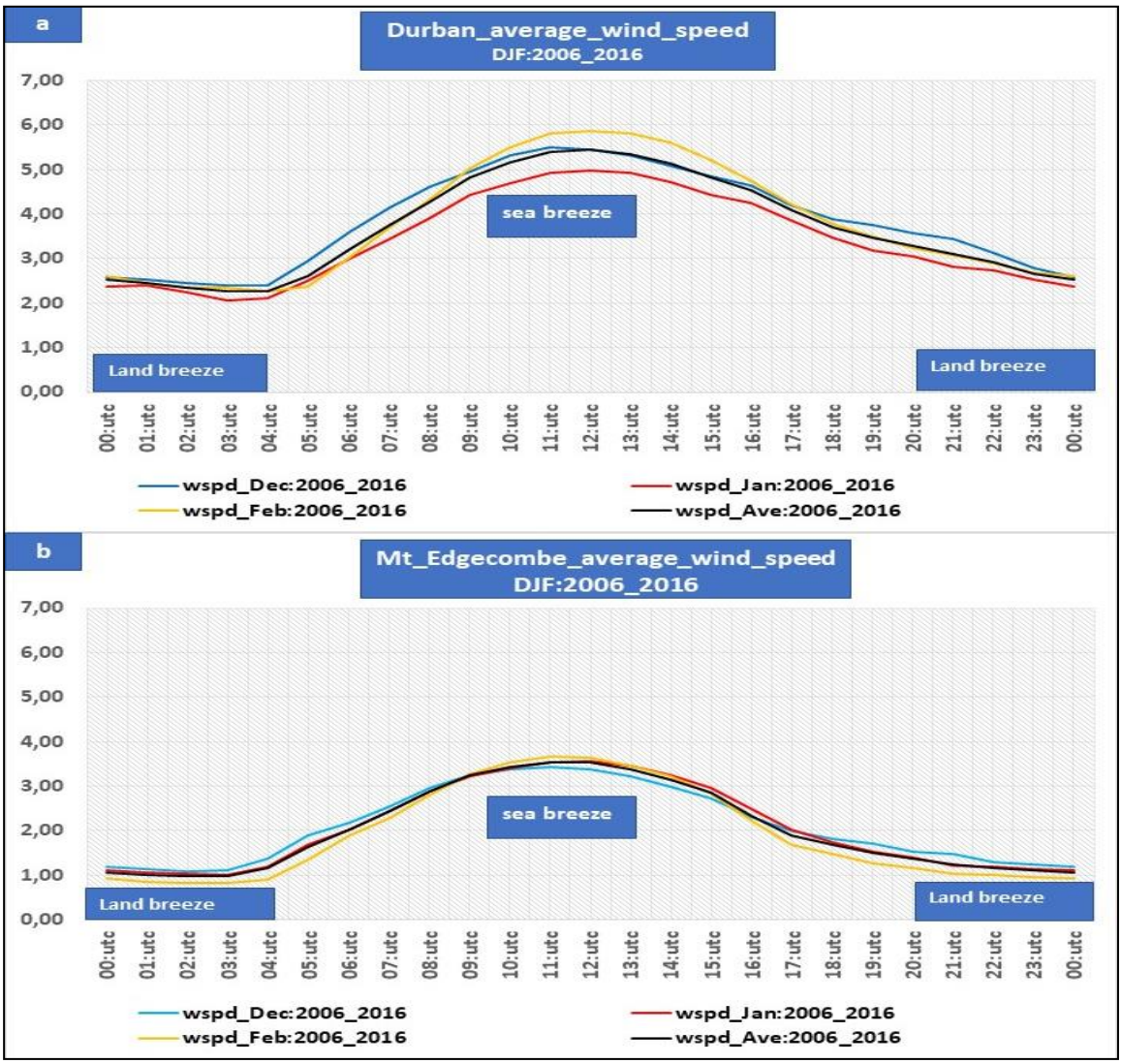

Figure D.5: The diurnal range of average wind speed over (a) Durban, (b) Mt. Edgecombe Weather stations during the period DJF 2006 -2016.

UNIVERSITEIT VAN PRETORIA
UNIVERSITY OF PRETORIA
YUNIBESITHI YA PRETORIA

REFERENCES

Akbari H, Pomerantz M, Taha H. 2001. Cool Surfaces and Shade Trees To Reduce Energy Use and Improve Air Quality in Urban Areas. , 70(3): 295–310.

Arakawa A. 2004. The cumulus parameterization problem: Past, present, and future. *Journal of Climate*, 17(13): 2493–2525. https://doi.org/10.1175/1520-0442(2004)017<2493:RATCPP>2.0.CO;2.

Arnfield AJ. 2003. Two decades of urban climate research: A review of turbulence, exchanges of energy and water, and the urban heat island. *International Journal of Climatology*, 23(1): 1–26. https://doi.org/10.1002/joc.859.

Arrillaga JA, de Arellano JVG, Bosveld F, Baltink HK, Yagüe C, Sastre M, Román-Cascón C. 2018. Impacts of afternoon and evening sea-breeze fronts on local turbulence, and on CO2and radon-222 transport. *Quarterly Journal of the Royal Meteorological Society*, 144(713): 990–1011. https://doi.org/10.1002/qj.3252.

Baklanov A, Grimmond CSB, Carlson D, Terblanche D, Tang X, Bouchet V, Lee B, Langendijk G, Kolli RK, Hovsepyan A. 2018. From urban meteorology, climate and environment research to integrated city services. *Urban Climate*. Elsevier B.V., 23: 330–341. https://doi.org/10.1016/j.uclim.2017.05.004.

Balsamo G, Albergel C, Beljaars A, Boussetta S, Brun E, Cloke H, Dee D, Dutra E, Munõz-Sabater J, Pappenberger F, De Rosnay P, Stockdale T, Vitart F. 2015. ERA-Interim/Land: A global land surface reanalysis data set. *Hydrology and Earth System Sciences*, 19(1): 389–407. https://doi.org/10.5194/hess-19-389-2015.

Barrao S, Serrano-Notivoli R, Cuadrat JM, Tejedor E, Saz Sánchez MA. 2022. Characterization of the UHI in Zaragoza (Spain) using a quality-controlled hourly sensor-based urban climate network. *Urban Climate*, 44. https://doi.org/10.1016/j.uclim.2022.101207.

Barriopedro D, Fischer EM, Luterbacher J, Trigo RM, García-Herrera R. 2011. The hot summer of 2010: Redrawing the temperature record map of Europe. *Science*, 332(6026): 220–224. https://doi.org/10.1126/science.1201224.

Bastin S, Drobinski P, Guénard V, Caccia JL, Campistron B, Dabas AM, Delville P, Reitebuch O, Werner C. 2006. On the interaction between sea breeze and summer mistral at the exit

UNIVERSITEIT VAN PRETORIA
UNIVERSITY OF PRETORIA
YUNIBESITHI YA PRETORIA

of the Rhône Valley. *Monthly Weather Review*, 134(6): 1647–1668. https://doi.org/10.1175/MWR3116.1.

Blake R, York N, Curitiba AG, Tokyo TI, Horton R, York N. 2011. Urban climate Coordinating Lead Authors : Lead Authors : , 43–81.

Blamey RC, Kolusu SR, Mahlalela P, Todd MC, Reason CJC. 2018. The role of regional circulation features in regulating El Niño climate impacts over southern Africa: A comparison of the 2015/2016 drought with previous events. *International Journal of Climatology*, (July 2017): 1–20. https://doi.org/10.1002/JOC.5668.

Bohnenstengel SI, Evans S, Clark PA, Belcher SE. 2011. Simulations of the London urban heat island. *Quarterly Journal of the Royal Meteorological Society*, 137(659): 1625–1640. https://doi.org/10.1002/qj.855.

Bopape MJM, Engelbrecht FA, Maisha R, Chikoore H, Ndarana T, Lekoloane L, Thatcher M, Mulovhedzi PT, Rambuwani GT, Barnes MA, Mkhwanazi M, Mphepya J. 2022. Rainfall Simulations of High-Impact Weather in South Africa with the Conformal Cubic Atmospheric Model (CCAM). *Atmosphere*, 13(12): 1–24. https://doi.org/10.3390/atmos13121987.

Bozonnet E, Belarbi R, Allard F. 2007. Thermal behaviour of buildings: Modelling the impact of urban heat island. *Journal of Harbin Institute of Technology (New Series)*, 14(SUPPL.): 19–22.

Bush M, Allen T, Bain C, Boutle I, Edwards J, Finnenkoetter A, Franklin C, Hanley K, Lean H, Lock A, Manners J, Mittermaier M, Morcrette C, North R, Petch J, Short C, Vosper S, Walters D, Webster S, Weeks M, Wilkinson J, Wood N, Zerroukat M. 2020. The first Met Office Unified Model-JULES Regional Atmosphere and Land configuration, RAL1. *Geoscientific Model Development*, 13(4): 1999–2029. https://doi.org/10.5194/gmd-13-1999-2020.

Caldwell P, Chin HNS, Bader DC, Bala G. 2009. Evaluation of a WRF dynamical downscaling simulation over California. *Climatic Change*, 95(3–4): 499–521. https://doi.org/10.1007/s10584-009-9583-5.

Canton J, Dipankar A. 2024. Climatological analysis of urban heat island effects in Swiss cities. *International Journal of Climatology*, (February): 1–17.

UNIVERSITEIT VAN PRETORIA
UNIVERSITY OF PRETORIA
YUNIBESITHI YA PRETORIA

https://doi.org/10.1002/joc.8398.

Case JL. 2002. Final Report on Land-Breeze Forecasting. .

Chapman S, Mcalpine CA. 2019. The impact of climate change and urban growth on urban climate and heat stress in a subtropical city. , (January): 1–18. https://doi.org/10.1002/joc.5998.

Chen D, Thatcher M, Wang X, Barnett G, Kachenko A, Prince R. 2015. Summer cooling potential of urban vegetation—a modeling study for Melbourne, Australia. *AIMS Environmental Science*, 2(3): 648–667. https://doi.org/10.3934/environsci.2015.3.648.

Chen F, Kusaka H, Bornstein R, Ching J, Grimmond CSB, Grossman-Clarke S, Loridan T, Manning KW, Martilli A, Miao S, Sailor D, Salamanca FP, Taha H, Tewari M, Wang X, Wyszogrodzki AA, Zhang C. 2011. The integrated WRF/urban modelling system: Development, evaluation, and applications to urban environmental problems. *International Journal of Climatology*, 31(2): 273–288. https://doi.org/10.1002/joc.2158.

Chen F, Yang X, Zhu W. 2014. WRF simulations of urban heat island under hot-weather synoptic conditions: The case study of Hangzhou City, China. *Atmospheric Research*. Elsevier B.V., 138: 364–377. https://doi.org/10.1016/j.atmosres.2013.12.005.

Chen J. 2010. Jan-Huey Chen. . https://doi.org/10.1175/WAF-D-10-05015.1.Reynolds.

Chen S, Dipankar A. 2022. On the applicability of urban canopy parametrization in building grey zone. *Quarterly Journal of the Royal Meteorological Society*, 148(745): 1644–1662. https://doi.org/10.1002/qj.4269.

Clelland AA, Marshall GJ, Baxter R. 2024. Evaluating the performance of key ERA-Interim, ERA5 and ERA5-Land climate variables across Siberia. *International Journal of Climatology*, 44(7): 2318–2342. https://doi.org/10.1002/joc.8456.

Cook C, Reason CJC, Hewitson BC. 2004. Wet and dry spells within particularly wet and dry summers in the South African summer rainfall region. *Climate Research*, 26(1): 17–31. https://doi.org/10.3354/cr026017.

Coutts AM, Beringer J, Tapper NJ. 2007. Impact of increasing urban density on local climate: Spatial and temporal variations in the surface energy balance in Melbourne, Australia. *Journal of Applied Meteorology and Climatology*, 46(4): 477–493.

UNIVERSITEIT VAN PRETORIA
UNIVERSITY OF PRETORIA
YUNIBESITHI YA PRETORIA

https://doi.org/10.1175/JAM2462.1.

Dedekind Z, Engelbrecht FA, Van Der Merwe J. 2016a. Model simulations of rainfall over southern africa and its eastern escarpment. *Water SA*, 42(1): 129–143. https://doi.org/10.4314/wsa.v42i1.13.

Dedekind Z, Engelbrecht FA, Van Der Merwe J. 2016b. Model simulations of rainfall over southern africa and its eastern escarpment. *Water SA*, 42(1): 129–143. https://doi.org/10.4314/wsa.v42i1.13.

Dee DP, Uppala SM, Simmons AJ, Berrisford P, Poli P, Kobayashi S, Andrae U, Balmaseda MA, Balsamo G, Bauer P, Bechtold P, Beljaars ACM, van de Berg L, Bidlot J, Bormann N, Delsol C, Dragani R, Fuentes M, Geer AJ, Haimberger L, Healy SB, Hersbach H, Hólm E V., Isaksen L, Kållberg P, Köhler M, Matricardi M, Mcnally AP, Monge-Sanz BM, Morcrette JJ, Park BK, Peubey C, de Rosnay P, Tavolato C, Thépaut JN, Vitart F. 2011. The ERA-Interim reanalysis: Configuration and performance of the data assimilation system. *Quarterly Journal of the Royal Meteorological Society*, 137(656): 553–597. https://doi.org/10.1002/qj.828.

Dirksen M, Knap WH, Steeneveld GJ, Holtslag AAM, Tank AMGK. 2020. Downscaling daily air-temperature measurements in the Netherlands. *Theoretical and Applied Climatology*. Theoretical and Applied Climatology, 142(1–2): 751–767. https://doi.org/10.1007/s00704-020-03313-1.

Easterling DR, Karl TR, Gallo KP, Robinson DA, Trenberth KE, Dai A. 2000. Observed climate variability and change of relevance to the biosphere. , 105: 101–114.

Efstathiou GA, Plant RS, Bopape MJM. 2018. Simulation of an evolving convective boundary layer using a scale-dependent dynamic smagorinsky model at near-gray-zone resolutions. *Journal of Applied Meteorology and Climatology*, 57(9): 2197–2214. https://doi.org/10.1175/JAMC-D-17-0318.1.

Engelbrecht CJ, Engelbrecht FA. 2016. Shifts in Köppen-Geiger climate zones over southern Africa in relation to key global temperature goals. *Theoretical and Applied Climatology*, 123(1–2): 247–261. https://doi.org/10.1007/s00704-014-1354-1.

Engelbrecht F, Adegoke J, Bopape MJ, Naidoo M, Garland R, Thatcher M, McGregor J, Katzfey J, Werner M, Ichoku C, Gatebe C. 2015a. Projections of rapidly rising surface

UNIVERSITEIT VAN PRETORIA
UNIVERSITY OF PRETORIA
YUNIBESITHI YA PRETORIA

temperatures over Africa under low mitigation. *Environmental Research Letters*. IOP Publishing, 10(8). https://doi.org/10.1088/1748-9326/10/8/085004.

Engelbrecht F, Adegoke J, Bopape MJ, Naidoo M, Garland R, Thatcher M, McGregor J, Katzfey J, Werner M, Ichoku C, Gatebe C. 2015b. Projections of rapidly rising surface temperatures over Africa under low mitigation. *Environmental Research Letters*. IOP Publishing, 10(8): 85004. https://doi.org/10.1088/1748-9326/10/8/085004.

Engelbrecht F, Adegoke J, Bopape MJ, Naidoo M, Garland R, Thatcher M, McGregor J, Katzfey J, Werner M, Ichoku C, Gatebe C. 2015c. Projections of rapidly rising surface temperatures over Africa under low mitigation. *Environmental Research Letters*. IOP Publishing, 10(8). https://doi.org/10.1088/1748-9326/10/8/085004.

Engelbrecht FA, Landman WA, Engelbrecht CJ, Landman S, Bopape MM, Roux B, McGregor JL, M T. 2011. Multi-scale climate modeling over Southern Africa using a variable-resolution global model. *Water SA*, 37(5): 647–658. https://doi.org/10.4314/wsa.v37i5.2.

Engelbrecht FA, Marean CW, Cowling RM, Engelbrecht CJ, Neumann FH, Scott L, Nkoana R, O'Neal D, Fisher E, Shook E, Franklin J, Thatcher M, McGregor JL, Van der Merwe J, Dedekind Z, Difford M. 2019. Downscaling Last Glacial Maximum climate over southern Africa. *Quaternary Science Reviews*. Elsevier Ltd, 226: 105879. https://doi.org/10.1016/j.quascirev.2019.105879.

Engelbrecht FA, McGregor JL, Rautenbach CJD. 2007a. On the development of a new nonhydrostatic atmospheric model in South Africa. *South African Journal of Science*, 103(3–4): 127–134.

Engelbrecht FA, McGregor JL, Rautenbach CJDW. 2007b. On the development of a new nonhydrostatic atmospheric model in South Africa. *South African Journal of Science*, 103(3–4): 127–134.

Estoque MA. 1962. The Sea Breeze as a Function of the Prevailing Synoptic Situation. *Journal of the Atmospheric Sciences*, 244–250.

Estrada F, Botzen WJW, Tol RSJ. 2017. A global economic assessment of city policies to reduce climate change impacts. *Nature Climate Change*, 7(6): 403–406. https://doi.org/10.1038/nclimate3301.

UNIVERSITEIT VAN PRETORIA
UNIVERSITY OF PRETORIA
YUNIBESITHI YA PRETORIA

Fischer EM, Oleson KW, Lawrence DM. 2012. Contrasting urban and rural heat stress responses to climate change. *Geophysical Research Letters*, 39(3): 1–8. https://doi.org/10.1029/2011GL050576.

Freidenreich SM, Ramaswamy V. 1999. A new multiple-band solar radiative parameterization for general circulation models. *Journal of Geophysical Research Atmospheres*, 104(D24): 31389–31409. https://doi.org/10.1029/1999JD900456.

Garl RM, Matooane M, Engelbrecht FA, Bopape MJM, Landman WA, Naidoo M, van der merwe J, Wright CY. 2015. Regional projections of extreme apparent temperature days in africa and the related potential risk to human health. *International Journal of Environmental Research and Public Health*, 12(10): 12577–12604. https://doi.org/10.3390/ijerph121012577.

Garuma GF. 2018. Review of urban surface parameterizations for numerical climate models. *Urban Climate*. Elsevier, 24(April): 830–851. https://doi.org/10.1016/j.uclim.2017.10.006.

Giugni M, Simonis I, Bucchignani E, Capuano P, Paola D, Engelbrecht F, Mercogliano P, Topa ME. 2015. *Urban Vulnerability and Climate Change in Africa*. .

Gordon N, Shaykewich J. 2000. On performance assessment of public weather services. *World Meteorological Organisation TD No. 1023*, (1023): 67.

Gordon N, Shaykewich J. 2009. Guidelines on Performance Assessment of Public Weather Services on Performance Assessment. *Technical Document*, (1023).

Grachev AA, Leo LS, Fernando HJS, Fairall CW, Creegan E, Blomquist BW, Christman AJ, Hocut CM. 2018. Air–Sea/Land Interaction in the Coastal Zone. *Boundary-Layer Meteorology*. Springer Netherlands, 167(2): 181–210. https://doi.org/10.1007/s10546-017-0326-2.

Grimmond CSB, Blackett M, Best MJ, Baik J-J, Belcher SE, Beringer J, Bohnenstengel SI, Calmet I, Chen F, Coutts A, Dandou A, Fortuniak K, Gouvea ML, Hamdi R, Hendry M, Kanda M, Kawai T, Kawamoto Y, Kondo H, Krayenhoff ES, Lee S-H, Loridan T, Martilli A, Masson V, Miao S, Oleson K, Ooka R, Pigeon G, Porson A, Ryu Y-H, Salamanca F, Steeneveld GJ, Tombrou M, Voogt JA, Young DT, Zhang N. 2011. Initial results from Phase 2 of the international urban energy balance model comparison. *International Journal of Climatology*, 31(2): 244–272. https://doi.org/10.1002/joc.2227.

UNIVERSITEIT VAN PRETORIA
UNIVERSITY OF PRETORIA
YUNIBESITHI YA PRETORIA

Grimmond CSB, Blackett M, Best MJ, Barlow J, Baik J-J, Belcher SE, Bohnenstengel SI, Calmet I, Chen F, Dandou A, Fortuniak K, Gouvea ML, Hamdi R, Hendry M, Kawai T, Kawamoto Y, Kondo H, Krayenhoff ES, Lee S-H, Loridan T, Martilli A, Masson V, Miao S, Oleson K, Pigeon G, Porson A, Ryu Y-H, Salamanca F, Shashua-Bar L, Steeneveld G-J, Tombrou M, Voogt J, Young D, Zhang N. 2010. The International Urban Energy Balance Models Comparison Project: First Results from Phase 1. *Journal of Applied Meteorology and Climatology*, 49(6): 1268–1292. https://doi.org/10.1175/2010JAMC2354.1.

Grimmond CSB, Oke TR. 1999. Heat Storage in Urban Areas: Local-Scale Observations and Evaluation of a Simple Model. *Journal of Applied Meteorology*, 38(7): 922–940. https://doi.org/10.1175/1520-0450(1999)038<0922:HSIUAL>2.0.CO;2.

Gubler M, Christen A, Remund J, Brönnimann S. 2021. Evaluation and application of a low-cost measurement network to study intra-urban temperature differences during summer 2018 in Bern, Switzerland. *Urban Climate*, 37(March). https://doi.org/10.1016/j.uclim.2021.100817.

Han JY, Baik JJ, Lee H. 2014. Urban impacts on precipitation. *Asia-Pacific Journal of Atmospheric Sciences*, 50(1): 17–30. https://doi.org/10.1007/s13143-014-0016-7.

Heaviside C, Macintyre H, Vardoulakis S. 2017. The Urban Heat Island: Implications for Health in a Changing Environment. *Current environmental health reports*. Current Environmental Health Reports, 4(3): 296–305. https://doi.org/10.1007/s40572-017-0150-3.

Horowitz HM, Garland RM, Thatcher M, Landman WA, Dedekind Z, Van Der Merwe J, Engelbrecht FA. 2017. Evaluation of climate model aerosol seasonal and spatial variability over Africa using AERONET. *Atmospheric Chemistry and Physics*, 17(22): 13999–14023. https://doi.org/10.5194/acp-17-13999-2017.

Hughes WS, Barling RC, 1996. Urban influences on south Africa temperature trends, *International Journal of Climatology*,16,935-940

Hurley P. 2007. Modelling mean and turbulence fields in the dry convective boundary layer with the eddy-diffusivity/mass-flux approach. *Boundary-Layer Meteorology*, 125(3): 525–536. https://doi.org/10.1007/s10546-007-9203-8.

Intergovernmental Panel on Climate Change (IPCC). 2023. *Linking Global to Regional Climate*

UNIVERSITEIT VAN PRETORIA
UNIVERSITY OF PRETORIA
YUNIBESITHI YA PRETORIA

Change. *Climate Change 2021 – The Physical Science Basis*.

Jones PD, Harpham C, Troccoli A, Gschwind B, Ranchin T, Wald L, Goodess CM, Dorling S. 2017. Using ERA-Interim reanalysis for creating datasets of energy-relevant climate variables. *Earth System Science Data*, 9(2): 471–495. https://doi.org/10.5194/essd-9-471-2017.

Jury MR. 2013. Climate trends in southern Africa. *South African Journal of Science*, 109(1–2): 1–11. https://doi.org/10.1590/sajs.2013/980.

Karl TR, Jones PD, Knight RW, Kukla G, Plummer N, Razuvayev V, Gallo KP, Lindseay J, Charlson RJ, Peterson TC. 1993. Asymmetric trends of daily maximum and minimum temperature. *Bulletin of the American Meteorological Society*, 74(6): 1007–1023.

Katzfey J, Schlünzen H, Hoffmann P, Thatcher M. 2020. How an urban parameterization affects a high-resolution global climate simulation. *Quarterly Journal of the Royal Meteorological Society*, 146(733): 3808–3829. https://doi.org/10.1002/qj.3874.

Khan B, Abualnaja Y, Al-Subhi AM, Nellayaputhenpeedika M, Nellikkattu Thody M, Sturman AP. 2018. Climatology of sea breezes along the Red Sea coast of Saudi Arabia. *International Journal of Climatology*, (March): 1–18. https://doi.org/10.1002/joc.5523.

King'uyu SM, Ogallo LA, Anyamba EK. 2000. Recent trends of minimum and maximum surface temperatures over Eastern Africa. *Journal of Climate*, 13(16): 2876–2886. https://doi.org/10.1175/1520-0442(2000)013<2876:RTOMAM>2.0.CO;2.

Kottek M, Grieser J, Beck C, Rudolf B, Rubel F. 2006. World map of the Köppen-Geiger climate classification updated. *Meteorologische Zeitschrift*, 15(3): 259–263. https://doi.org/10.1127/0941-2948/2006/0130.

Kowalczyk E, Wang Y, Law R. 2006. The general structure of CABLE. .

Kowalczyk EA, Garratt JR, Krummel PB. 1994. Implementation of a soil-canopy scheme into the CSIRO GCM: Regional aspects of the model response. *CSIRO Division of Atmospheric Research Technical Paper, no. 32*, 1–65.

Krishnamurthy R, Newsom RK, Chand D, Shaw WJ. 2021. Boundary Layer Climatology at ARM Southern Great Plains. , (January): 101.

Kruger AC, Rautenbach H, Mbatha S, Ngwenya S, Makgoale TE. 2019. Historical and projected trends in near-surface temperature indices for 22 locations in South Africa. *South African Journal of Science*, 115(5–6): 1–9. https://doi.org/10.17159/sajs.2019/4846.

Kruger AC, Sekele SS. 2013. Trends in extreme temperature indices in South Africa: 1962-2009. *International Journal of Climatology*, 33(3): 661–676. https://doi.org/10.1002/joc.3455.

Kruger AC, Shongwe S. 2004. Temperature trends in South Africa: 1960-2003. *International Journal of Climatology*, 24(15): 1929–1945. https://doi.org/10.1002/joc.1096.

Lan H, Guo D, Hua W, Pepin N, Sun J. 2023. Evaluation of reanalysis air temperature and precipitation in high-latitude Asia using ground-based observations. *International Journal of Climatology*, 43(3): 1621–1638. https://doi.org/10.1002/joc.7937.

Lee O, Shun CM. 2003. Observation of sea breeze interactions at and near Hong Kong International Airport. *Meteorological Applications*, 10(1): 1–9. https://doi.org/10.1017/S1350482703005012.

Lehoczky A, Sobrino J, Skoković D, Aguilar E. 2017. The Urban Heat Island Effect in the City of Valencia: A Case Study for Hot Summer Days. *Urban Science*, 1(1): 9. https://doi.org/10.3390/urbansci1010009.

Lemonsu A, Caillaud C, Alias A, Riette S, Seity Y, Le Roy B, Michau Y, Lucas-Picher P. 2023. What added value of CNRM-AROME convection-permitting regional climate model compared to CNRM-ALADIN regional climate model for urban climate studies ? Evaluation over Paris area (France). *Climate Dynamics*. Springer Berlin Heidelberg, (January). https://doi.org/10.1007/s00382-022-06647-w.

Lengoasa_1988_Note_on_Atmospheric.pdf. (n.d.). .

Lipson MJ, Hart MA, Thatcher M. 2017. Efficiently modelling urban heat storage : an interface conduction scheme in an urban land surface model (aTEB v2 . 0). , 991–1007. https://doi.org/10.5194/gmd-10-991-2017.

Lipson MJ, Thatcher M, Hart MA, Pitman A. 2018. A building energy demand and urban land surface model. , (April): 1–19. https://doi.org/10.1002/qj.3317.

Liu Z, Liu Y, Wang S, Yang X, Wang L, Baig MHA, Chi W, Wang Z. 2018. Evaluation of spatial

UNIVERSITEIT VAN PRETORIA
UNIVERSITY OF PRETORIA
YUNIBESITHI YA PRETORIA

and temporal performances of ERA-interim precipitation and temperature in Mainland China. *Journal of Climate*, 31(11): 4347–4365. https://doi.org/10.1175/JCLI-D-17-0212.1.

Luhar AK, Thatcher M, Hurley PJ. 2014. Evaluating a building-averaged urban surface scheme in an operational mesoscale model for fl ow and dispersion. *Atmospheric Environment*. Elsevier Ltd, 88: 47–58. https://doi.org/10.1016/j.atmosenv.2014.01.059.

Lyon B, Mason SJ. 2009. The 1997/98 summer rainfall season in southern Africa. Part II: Model simulations and coupled model forecasts. *Journal of Climate*, 22(13): 3802–3818. https://doi.org/10.1175/2009JCLI2600.1.

MacKellar N, New M, Jack C. 2014. Observed and modelled trends in rainfall and temperature for South Africa: 1960-2010. *South African Journal of Science*, 110(7–8): 1–13. https://doi.org/10.1590/sajs.2014/20130353.

Maisha RT, Ndarana T, Engelbrechf FA, Thatcher M. (n.d.). Simulation of the eThekwini Heat Island in South Africa. . https://doi.org/10.1175/JAMC-D-2.

Maisha TR. 2014. *The Influence of Topography and Model Grid Resolution on Extreme Weather Forecasts over South-Africa*. *Faculty of Natural and Agricultural Sciences University of Pretoria*.

Masson V. 2000. A physically-based scheme for the urban energy budget in atmospheric models. *Boundary-Layer Meteorology*, 94(3): 357–397. https://doi.org/10.1023/A:1002463829265.

Maure G, Pinto I, Ndebele-Murisa M, Lennard C, Nikulin G, Dosio A, Meque A. 2018a. The southern African Climate under 1.5 and 2 degree of global warming as simulated by CORDEX Regional Climate Models. *Environmental Research Letters*. https://doi.org/10.1088/1748-9326/aab190.

Maure G, Pinto I, Ndebele-Murisa M, Muthige M, Lennard C, Nikulin G, Dosio A, Meque A. 2018b. The southern African climate under 1.5 °c and 2 °c of global warming as simulated by CORDEX regional climate models. *Environmental Research Letters*, 13(6). https://doi.org/10.1088/1748-9326/aab190.

McGregor JL. 1996. Semi-Lagrangian Advection on Conformal-Cubic Grids. *Monthly Weather*

UNIVERSITEIT VAN PRETORIA
UNIVERSITY OF PRETORIA
YUNIBESITHI YA PRETORIA

Review, 1311–1322.

McGregor JL, Nguyen KC, Katzfey JJ. 2008. A variety of tropical climate simulations using CCAM. *High resolution modelling : extended abstracts of the second CAWCR Modelling Workshop, 25-28 November 2008, Melbourne, Australia, edited by A. J. Hollis. Bureau of Meteorology*, (January): 29–32.

Meehl GA, Tebaldi C. 2004. More intense, more frequent, and longer lasting heat waves in the 21st century. *Science*, 305(5686): 994–997. https://doi.org/10.1126/science.1098704.

Mirzaei PA. 2015. Recent challenges in modeling of urban heat island. *Sustainable Cities and Society*. Elsevier B.V., 19: 200–206. https://doi.org/10.1016/j.scs.2015.04.001.

Monerie PA, Wainwright CM, Sidibe M, Akinsanola AA. 2020. Model uncertainties in climate change impacts on Sahel precipitation in ensembles of CMIP5 and CMIP6 simulations. *Climate Dynamics*. Springer Berlin Heidelberg, 55(5–6): 1385–1401. https://doi.org/10.1007/s00382-020-05332-0.

Muthige MS, Malherbe J, Englebrecht FA, Grab S, Beraki A, Maisha TR, Van Der Merwe J. 2018. Projected changes in tropical cyclones over the South West Indian Ocean under different extents of global warming. *Environmental Research Letters*, 13(6). https://doi.org/10.1088/1748-9326/aabc60.

Ndarana T, Mpati S, Bopape MJ, Engelbrecht F, Chikoore H. 2021. The flow and moisture fluxes associated with ridging South Atlantic Ocean anticyclones during the subtropical southern African summer. *International Journal of Climatology*, 41(S1): E1000–E1017. https://doi.org/10.1002/joc.6745.

Nguyen KC, Katzfey JJ, McGregor JL. 2014. Downscaling over Vietnam using the stretched-grid CCAM: Verification of the mean and interannual variability of rainfall. *Climate Dynamics*, 43(3–4): 861–879. https://doi.org/10.1007/s00382-013-1976-5.

Nuruzzaman M. 2015. Urban Heat Island: Causes, Effects and Mitigation Measures - A Review. *International Journal of Environmental Monitoring and Analysis*, 3(2): 67. https://doi.org/10.11648/j.ijema.20150302.15.

Oleson KW, Bonan GB, Feddema J, Jackson T. 2011. An examination of urban heat island characteristics in a global climate model. *International Journal of Climatology*, 31(12):

UNIVERSITEIT VAN PRETORIA
UNIVERSITY OF PRETORIA
YUNIBESITHI YA PRETORIA

1848–1865. https://doi.org/10.1002/joc.2201.

Parker DE. 2010. Urban heat island effects on estimates of observed climate change. *Wiley Interdisciplinary Reviews: Climate Change*, 1(1): 123–133. https://doi.org/10.1002/wcc.21.

Pokhrel R, Lee H. 2011. Estimation of the effective zone of sea/land breeze in a coastal area. *Atmospheric Pollution Research*. Elsevier, 2(1): 106–115. https://doi.org/10.5094/APR.2011.013.

Ramamurthy P, Bou-Zeid E, Smith JA, Wang Z, Baeck ML, Saliendra NZ, Hom JL, Welty C. 2014. Influence of subfacet heterogeneity and material properties on the urban surface energy budget. *Journal of Applied Meteorology and Climatology*, 53(9): 2114–2129. https://doi.org/10.1175/JAMC-D-13-0286.1.

Reason CJC, Engelbrecht F, Landman WA, Lutjeharms JRE, Piketh S, Rautenbach CJ de W, Hewitson BC. 2006. A review of South African research in atmospheric science and physical oceanography during 2000-2005: review article. *South African journal of science*, 102(1 & 2): p--35.

Reichler T, Kim J. 2008. How well do coupled models simulate today's climate? *Bulletin of the American Meteorological Society*, 89(3): 303–311. https://doi.org/10.1175/BAMS-89-3-303.

Riahi K, Rao S, Krey V, Cho C, Chirkov V, Fischer G, Kindermann G, Nakicenovic N, Rafaj P. 2011. RCP 8.5-A scenario of comparatively high greenhouse gas emissions. *Climatic Change*, 109(1): 33–57. https://doi.org/10.1007/s10584-011-0149-y.

Rocklöv J, Ebi K, Forsberg B. 2011. Mortality related to temperature and persistent extreme temperatures: A study of cause-specific and age-stratified mortality. *Occupational and Environmental Medicine*, 68(7): 531–536. https://doi.org/10.1136/oem.2010.058818.

Rotstayn LD. 1997. A physically based scheme for the treatment of stratiform clouds and precipitation in large-scale models. I: Description and evaluation of the microphysical processes. *Quarterly Journal of the Royal Meteorological Society*, 123(541): 1227–1282. https://doi.org/10.1002/qj.49712354106.

Sannigrahi S, Bhatt S, Rahmat S, Uniyal B, Banerjee S, Chakraborti S, Jha S, Lahiri S, Santra K,

UNIVERSITEIT VAN PRETORIA
UNIVERSITY OF PRETORIA
YUNIBESITHI YA PRETORIA

Bhatt A. 2017. Analyzing the role of biophysical compositions in minimizing urban land surface temperature and urban heating. *Urban Climate*. Elsevier, (July): 0–1. https://doi.org/10.1016/j.uclim.2017.10.002.

Satterthwaite D. 2008. Cities' contribution to global warming: Notes on the allocation of greenhouse gas emissions. *Environment and Urbanization*, 20(2): 539–549. https://doi.org/10.1177/0956247808096127.

Sedlar J, Riihimaki LD, Turner DD, Duncan J, Adler B, Bianco L, Lantz K, Wilczak J, Hall E, Herrera C, Hodges GB. 2022. Investigating the Impacts of Daytime Boundary Layer Clouds on Surface Energy Fluxes and Boundary Layer Structure During CHEESEHEAD19. *Journal of Geophysical Research: Atmospheres*, 127(5): 1–24. https://doi.org/10.1029/2021JD036060.

Sharma A, Conry P, Fernando HJS, Hamlet AF, Hellmann JJ, Chen F. 2016. Green and cool roofs to mitigate urban heat island effects in the Chicago metropolitan area: Evaluation with a regional climate model. *Environmental Research Letters*. IOP Publishing, 11(6): 1–15. https://doi.org/10.1088/1748-9326/11/6/064004.

Smith SR, Legler DM, Verzone K V. 2001. Quantifying uncertainties in NCEP reanalyses using high-quality research vessel observations. *Journal of Climate*, 14(20): 4062–4072. https://doi.org/10.1175/1520-0442(2001)014<4062:QUINRU>2.0.CO;2.

Spinoni J, Barbosa P, Füssel HM, McCormick N, Vogt J V., Dosio A. 2021. Global population-weighted degree-day projections for a combination of climate and socio-economic scenarios. *International Journal of Climatology*, 41(11): 5447–5464. https://doi.org/10.1002/joc.7328.

Synnefa A, Santamouris M, Livada I. 2006. A study of the thermal performance of reflective coatings for the urban environment. *Solar Energy*, 80(8): 968–981. https://doi.org/10.1016/j.solener.2005.08.005.

Taha H. 1997. Urban climates and heat islands: albedo, evapotranspiration, and anthropogenic heat. *Energy and Buildings*, 25(2): 99–103. https://doi.org/10.1016/S0378-7788(96)00999-1.

Taylor KE, Stouffer RJ, Meehl GA. 2012. An overview of CMIP5 and the experiment design. *Bulletin of the American Meteorological Society*, 93(4): 485–498.

UNIVERSITEIT VAN PRETORIA
UNIVERSITY OF PRETORIA
YUNIBESITHI YA PRETORIA

https://doi.org/10.1175/BAMS-D-11-00094.1.

Thatcher M, Hurley P. 2012. Simulating Australian Urban Climate in a Mesoscale Atmospheric Numerical Model. *Boundary-Layer Meteorology*, 142(1): 149–175. https://doi.org/10.1007/s10546-011-9663-8.

Thatcher M, McGregor JL. 2009. Using a Scale-Selective Filter for Dynamical Downscaling with the Conformal Cubic Atmospheric Model. *Monthly Weather Review*, 137(6): 1742–1752. https://doi.org/10.1175/2008MWR2599.1.

Theeuwes NE, Steeneveld GJ, Heusinkveld RJRBG, Holtslag AAM. 2012. 197 : Mitigation of the urban heat island effect using vegetation and water bodies. , 2011–2013.

Thevakaran A, McGregor JL, Katzfey J, Hoffmann P, Suppiah R, Sonnadara DUJ. 2016. An assessment of CSIRO Conformal Cubic Atmospheric Model simulations over Sri Lanka. *Climate Dynamics*. Springer Berlin Heidelberg, 46(5–6): 1861–1875. https://doi.org/10.1007/s00382-015-2680-4.

Thomson AM, Calvin K V., Smith SJ, Kyle GP, Volke A, Patel P, Delgado-Arias S, Bond-Lamberty B, Wise MA, Clarke LE, Edmonds JA. 2011. RCP4.5: A pathway for stabilization of radiative forcing by 2100. *Climatic Change*, 109(1): 77–94. https://doi.org/10.1007/s10584-011-0151-4.

Uppala SM, Kållberg PW, Simmons AJ, Andrae U, da Costa Bechtold V, Fiorino M, Gibson JK, Haseler J, Hernandez A, Kelly GA, Li X, Onogi K, Saarinen S, Sokka N, Allan RP, Andersson E, Arpe K, Balmaseda MA, Beljaars ACM, van de Berg L, Bidlot J, Bormann N, Caires S, Chevallier F, Dethof A, Dragosavac M, Fisher M, Fuentes M, Hagemann S, Hólm E, Hoskins BJ, Isaksen L, Janssen PAEM, Jenne R, McNally AP, Mahfouf JF, Morcrette JJ, Rayner NA, Saunders RW, Simon P, Sterl A, Trenberth KE, Untch A, Vasiljevic D, Viterbo P, Woollen J. 2005. The ERA-40 re-analysis. *Quarterly Journal of the Royal Meteorological Society*, 131(612): 2961–3012. https://doi.org/10.1256/qj.04.176.

van Vuuren DP, Edmonds J, Kainuma M, Riahi K, Thomson A, Hibbard K, Hurtt GC, Kram T, Krey V, Lamarque JF, Masui T, Meinshausen M, Nakicenovic N, Smith SJ, Rose SK. 2011. The representative concentration pathways: An overview. *Climatic Change*, 109(1): 5–31. https://doi.org/10.1007/s10584-011-0148-z.

Walsh CL, Roberts D, Dawson RJ, Hall JW, Nickson A, Hounsome R. 2013. Experiences of

UNIVERSITEIT VAN PRETORIA
UNIVERSITY OF PRETORIA
YUNIBESITHI YA PRETORIA

integrated assessment of climate impacts, adaptation and mitigation modelling in London and Durban. *Environment and Urbanization*, 25(2): 361–380. https://doi.org/10.1177/0956247813501121.

Wan H, Zhong Z, Yang X, Li X. 2013. Impact of city belt in Yangtze River Delta in China on a precipitation process in summer: A case study. *Atmospheric Research*. Elsevier B.V., 125–126: 63–75. https://doi.org/10.1016/j.atmosres.2013.02.004.

Wang L, Li D. 2021. Urban heat islands during heat waves: A comparative study between Boston and Phoenix. *Journal of Applied Meteorology and Climatology*, 60(5): 621–641. https://doi.org/10.1175/JAMC-D-20-0132.1.

Wang Y, Kowalczyk E, Law R, Abramowitz G. 2006. The CSIRO Atmosphere Biosphere Land Exchange Model and future development for ACCESS. *BMRC Research Report*, No. 123, p(November).

Wang ZH, Li Q. 2017. Thermodynamic characterisation of urban nocturnal cooling. *Heliyon*, 3(4): 1–17. https://doi.org/10.1016/j.heliyon.2017.e00290.

Wilby RL. 2008. Constructing climate change scenarios of urban heat island intensity and air quality. *Environment and Planning B: Planning and Design*, 35(5): 902–919. https://doi.org/10.1068/b33066t.

Yamamoto Y. 2005. Measures to Mitigate Urban Heat Islands. *Environmental and Energy research Unit. Quaterly Review*, 18: 65–83.

Yan G, Wen-Jie D, Fu-Min R, Zong-Ci Z, Jian-Bin H. 2013. Surface Air Temperature Simulations over China with CMIP5 and CMIP3. *Advances in Climate Change Research*. Elsevier Masson SAS, 4(3): 145–152. https://doi.org/10.3724/SP.J.1248.2013.145.

Yang P, Ren G, Liu W. 2013. Spatial and temporal characteristics of Beijing urban heat island intensity. *Journal of Applied Meteorology and Climatology*, 52(8): 1803–1816. https://doi.org/10.1175/JAMC-D-12-0125.1.

Zhang J, Tian L, Lu J. 2022. Temporal Evolution of Urban Heat Island and Quantitative Relationship with Urbanization Development in Chongqing, China. *Atmosphere*, 13(10): 1594. https://doi.org/10.3390/atmos13101594.